AFRRI REPORTS

Second Quarter
1991

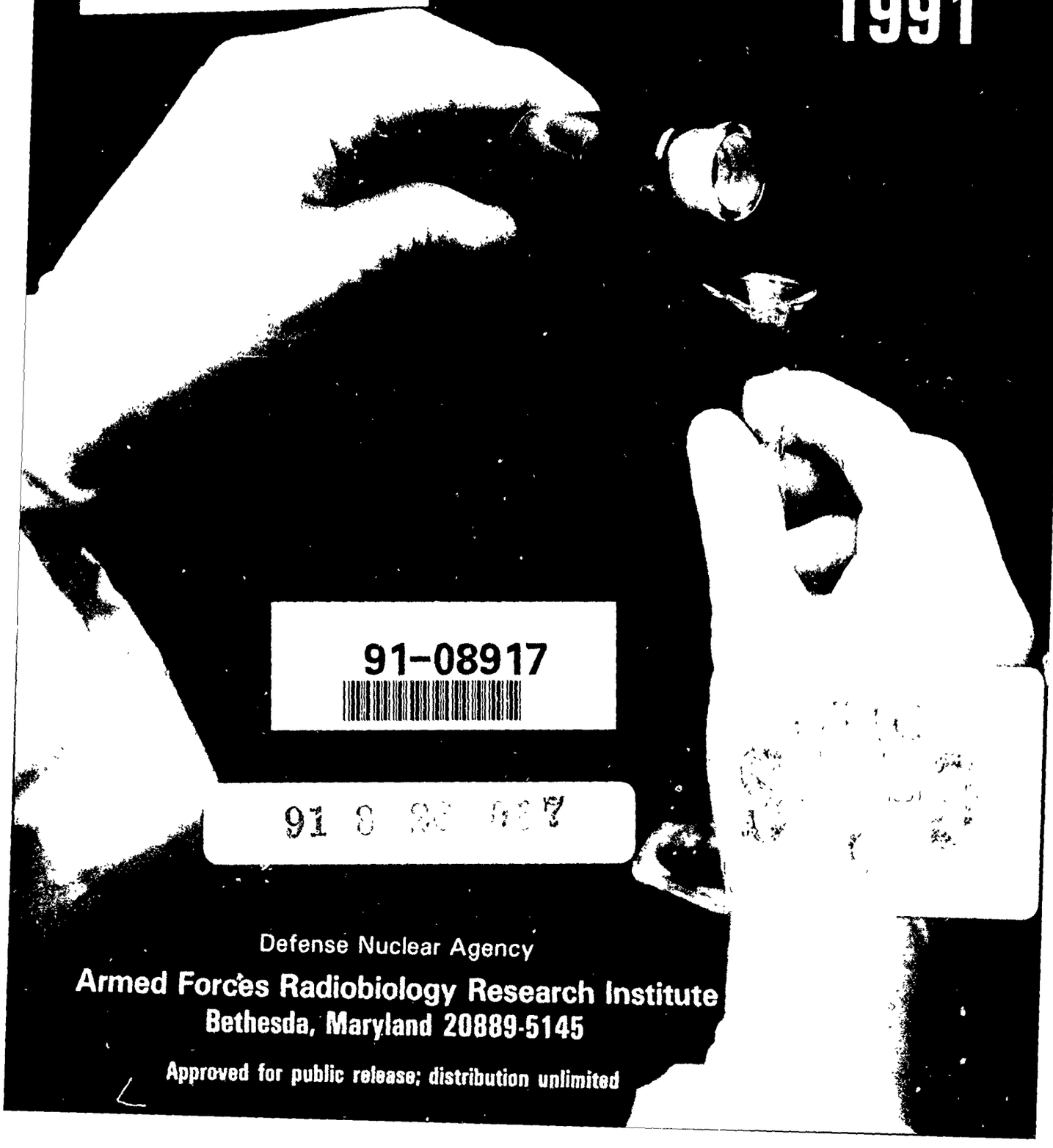

Defense Nuclear Agency
Armed Forces Radiobiology Research Institute
Bethesda, Maryland 20889-5145

REPORT DOCUMENTATION PAGE

Form Approved
OMB No. 0704-0188

1. AGENCY USE ONLY *(Leave blank)*	2. REPORT DATE	3. REPORT TYPE AND DATES COVERED
	1991 July	Reprints/Technical

4. TITLE AND SUBTITLE

Second Quarter
AFRRI Reports, Apr-Jun 1991.

5. FUNDING NUMBERS

PE: NWED QAXM

AFRRI-SR91-22,
AFRRI-SR91-23,
etc.

6. AUTHOR(S)

7. PERFORMING ORGANIZATION NAME(S) AND ADDRESS(ES)

Armed Forces Radiobiology Research Institute
Bethesda, MD 20889-5145

AFRRI

8. PERFORMING ORGANIZATION REPORT NUMBER

SR91-22, - SR91-35 and TR91-1

9. SPONSORING/MONITORING AGENCY NAME(S) AND ADDRESS(ES)

Defense Nuclear Agency
6801 Telegraph Road
Alexandria, VA 22310-3398

Includes Rept. nos. AFRRI-SR91-25 thru AFRRI-SR91-35 and AFRRI-TR91-1.

10. SPONSORING/MONITORING AGENCY REPORT NUMBER

11. SUPPLEMENTARY NOTES

12a. DISTRIBUTION/AVAILABILITY STATEMENT

Approved for public release; distribution unlimited.

12b. DISTRIBUTION CODE

13. ABSTRACT *(Maximum 200 words)*

This volume contains AFRRI Scientific Reports SR91-22 through SR91-35 and Technical Report TR91-1 for Apr-Jun 1991.

14. SUBJECT TERMS	15. NUMBER OF PAGES 147
	16. PRICE CODE

17. SECURITY CLASSIFICATION OF REPORT	18. SECURITY CLASSIFICATION OF THIS PAGE	19. SECURITY CLASSIFICATION OF ABSTRACT	20. LIMITATION OF ABSTRACT
UNCLASSIFIED	UNCLASSIFIED	UNCLASSIFIED	UL

CLASSIFIED BY:

DECLASSIFY ON:

Partial **CONTENTS**

Scientific Reports

SR91-35: Vaishnav, Y., Holwitt, E., Swenberg, C., Lee, H.-C., and Kan, L.-S. Synthesis and characterization of stereoisomers of 5,6-dihydro-5,6-dihydroxythymidine.

Technical Report

AFRRI TR91-1: Forsbacka, M., and Moore, M. Maximum temperature calculation and operational characteristics of fuel follower control rods for the AFRRI TRIGA reactor facility.

ANTIMICROBIAL AGENTS AND CHEMOTHERAPY, July 1990, p. 1387–1389
0066-4804/90/071387-03$02.00/0

Vol. 34, No. 7

Oral Ofloxacin Therapy of *Pseudomonas aeruginosa* Sepsis in Mice after Irradiation

ITZHAK BROOK* AND G. DAVID LEDNEY

Wound Infection Management Program, Experimental Hematology Department, Armed Forces Radiobiology Research Institute, Bethesda, Maryland 20814-5145

Received 24 January 1990/Accepted 8 May 1990

Death subsequent to whole-body irradiation is associated with gram-negative bacterial sepsis. The effect of oral therapy with the new quinolone ofloxacin for orally acquired *Pseudomonas aeruginosa* infection was tested in B6D2F1 mice exposed to 7.0 Gy of bilateral radiation from ^{60}Co. A dose of 10^7 organisms was given orally 2 days after irradiation, and therapy was started 1 day later. Only 4 of 20 untreated mice (20%) survived for at least 30 days compared with 19 of 20 mice (95%) treated with ofloxacin ($P < 0.005$). *P. aeruginosa* was isolated from the livers of 21 of 28 untreated mice (75%), compared with only 2 of 30 treated mice ($P < 0.005$). Ofloxacin reduced colonization of the ileum by *P. aeruginosa*; 24 of 28 untreated mice (86%) harbored the organisms, compared with only 5 of 30 (17%) with ofloxacin ($P < 0.005$). This experiment was replicated twice, and similar results were obtained. These data illustrate the efficacy of the quinolone ofloxacin for oral therapy of orally acquired *P. aeruginosa* infection in irradiated hosts.

Ionizing radiation enhances the susceptibility of the host to systemic infections due to endogenous and exogenous organisms (1, 7). *Pseudomonas aeruginosa* is one of the most frequent causes of gram-negative bacterial sepsis that develops in irradiated mice (5, 17) and is especially prevalent in immunocompromised patients (13, 19). This organism was found in patients that were therapeutically (11, 19) or accidentally (4) exposed to ionizing radiation.

Therapy of severe systemic infection due to gram-negative bacteria generally involves the use of aminoglycosides in combination with beta-lactam antibiotics (6). Such therapy reduces the mortality rate in irradiated animals (14). However, aminoglycosides are administered parenterally, and administration of such therapy requires close monitoring because of potential nephrotoxicity and ototoxicity. Simpler modes of therapy may be beneficial in situations that involve mass casualty exposure to ionizing radiation. The recently developed quinolone compounds have exhibited high in vivo bactericidal activity against most gram-negative bacteria, including *P. aeruginosa* (20). These agents can also be administered orally and are relatively free of serious side effects.

In this study, we evaluated the efficacy of oral therapy with the quinolone ofloxacin in a model of experimental septicemia due to orally administered *P. aeruginosa* in irradiated mice.

MATERIALS AND METHODS

Animals. Female B6D2F1 mice approximately 10 weeks of age were obtained from Jackson Laboratory, Bar Harbor, Maine. All animals were kept in quarantine for about 2 weeks. Representative organ samples were examined to ensure the absence of specific bacteria and common murine diseases. Animals were maintained on a 12-h light-dark cycle in a facility accredited by the American Association for Accreditation of Laboratory Animal Care in microisolator cages on hardwood chip bedding and were provided commercial rodent chow and acidified water (pH 2.5) that was changed to tap water 48 h before irradiation. This was done to facilitate colonization of the gastrointestinal tract with *P. aeruginosa* (18). All experimental procedures were performed in compliance with National Institutes of Health and Armed Forces Radiobiology Research Institute guidelines regarding animal use and care. We also followed the guidelines of the Institute of Laboratory Animal Resources, National Research Council (*Guide of the Care and Use of Laboratory Animals*).

Experimental design. Each mouse was fed 10^7 organisms 48 h after irradiation. The time of feeding was chosen after preliminary data showed that the animals became susceptible to *P. aeruginosa* sepsis following feeding with these gram-negative bacteria 48 h after irradiation (18). Antimicrobial therapy was initiated 24 h later and was administered for 15 days. A total of 100 mice were included in each of the first two experiments, and 40 were used in the third experiment; each experiment was performed three times. However, the microbial analysis of the ileal contents and livers was done only twice. Each experiment consisted of two groups: one antibiotic therapy group and one saline-treated control group. No other groups were included because preliminary work showed no recovery of *P. aeruginosa* from the livers or ileal contents of nonirradiated B6D2F1 mice. Each therapy or control group consisted of 50 mice as follows: 20 were observed for mortality, and 30 were used for cultures of liver and ileal content on the designated days.

^{60}Co irradiation. Mice were placed in Plexiglas restrainers (Rohm & Haas Co.) and given a whole-body dose of 7.0 Gy radiation at 0.4 Gy/min from bilaterally positioned ^{60}Co sources. Dose determinations were made by using a 50-ml tissue-equivalent ionization chamber (designed by the Armed Forces Radiobiology Research Institute) calibrated against a National Institute of Standards and Technology ionization chamber. The dose within the exposed field varied by 3%, as determined by thermal luminescence dosimetry conducted within tissue-equivalent mouse phantoms. The lethal dose for 50% of B6D2F1 female mice is 9.65 ± 0.36 (standard deviation) Gy 30 days after exposure in this laboratory. The dose of 7.0 Gy was, therefore, a sublethal dose and was chosen after previous studies showed that feeding the animals with *P. aeruginosa* produced mortality of 80 to 90% in 30 days (18). This dose produces significant

* Corresponding author.

neutropenia (1) but minimal translocation of enteric organisms.

Bacteria. The strain used in this study was a clinical isolate of *P. aeruginosa* PA220 that was isolated from a blood sample taken at the National Naval Medical Center, Bethesda, Md. The organism is serotype 1, exotoxin A and protease positive, sensitive to serum-mediated killing, and relatively virulent for normal mice. We have used this strain in previous animal studies (18). The organisms were harvested in the logarithmic phase of growth in brain heart infusion broth (BHIB). A concentration of 10^8 organisms per ml of saline was prepared, and a volume of 0.1 ml was fed to each animal by gavage by using a 20-gauge animal feeding tube fitted to a 1.0-ml syringe.

Antimicrobial agents. Ofloxacin was obtained from Ortho Pharmaceutical Corp., Raritan, N.J. A standard powder formulation with known potency was used for in vitro and in vivo studies. Ofloxacin was given every 24 h in a dose of 40 mg/kg. The antibiotic was administered in a volume of 0.1 ml of sterile distilled water by oral gavage with a 20-gauge feeding tube fitted to a 1.0-ml syringe. All control animals received 0.1 ml of sterile distilled water by oral gavage.

Antimicrobial concentrations in serum. Concentrations of the antimicrobial agents in serum were determined in six infected mice and six uninfected mice 1 and 23.5 h after oral administration of ofloxacin on day 5 of therapy. Antibiotic stock solutions were prepared volumetrically at a concentration of 50 μg/ml (5.0 mg/100 ml). Ofloxacin was solubilized by using 0.1 N NaOH followed by a sufficient quantity of H_2O. A 1:10 dilution of each stock solution was prepared by using 0.5 ml of sterile stock solution (filtered with a 0.2-μm-pore-size syringe filter) and 4.5 ml of mouse serum. Serial 1:2 dilutions were performed in mouse serum for each antibiotic tested (range, 5 to 0.3 μg/ml). The organism tested, *Escherichia coli* WYO02, was grown overnight in 50 ml of BHIB on a shaker at 100 rpm and 35°C. This was then diluted 1:10 with BHIB. At 580 nm, the 1:10 dilution gave a 36% transmission. A plate count confirmed the concentration to be 10^8 CFU/ml. One ml of the adjusted inoculum was added to 350 ml of Antibiotic Media 2 (10943, lot no. AQDRNE; BBL Microbiology Systems, Cockeysville, Md.). This was then poured into a square plate (12 by 12 cm). The agar was allowed to set at room temperature for 1 h. Wells were made in the agar with a no. 5 cork bore (diameter, ~8 mm). The wells were randomly numbered. For each number, there were four identical wells. An antibiotic solution of a differing concentration was placed in the first five sets of four wells to construct the standard curve. The remaining wells were used for the test samples (two wells per sample). The plate was then incubated at 35°C for 24 h. This procedure was repeated until all the samples could be tested.

Serum and tissue samples containing less than 0.2 μg of ofloxacin per sample were undetectable because of the limited sensitivity of the test system used. The laboratory daily correlation coefficient in determining ofloxacin levels was 0.99. All standard preparations were made in normal antibiotic-free mouse serum. The recovery of ofloxacin carboxylic acid was 99.7%.

In vitro susceptibility. MICs and MBCs were determined in Mueller-Hinton broth that was inoculated with 1.5×10^5 organisms per ml from an overnight culture.

Microbiological methods. Animals were observed for mortality and symptoms of disease. Five animals were selected at random from each group on days 4, 6, 8, 10, and 12 following irradiation. Animals were killed by cervical dislocation. Specimens of livers were processed for the presence of bacteria. No other organs were processed and no blood samples were obtained because previous studies showed that liver cultures correlated best with sepsis, whereas *P. aeruginosa* was concomitantly isolated in all animals that harbored the organisms in the liver (18). The livers were aseptically removed and immediately homogenized in sterile saline. The ileum was opened, and ileal content samples were obtained with swabs. The liver and stool specimens were swabbed onto blood and MacConkey agars, and the organisms were identified by conventional methods (12). The number of organisms was determined semiquantitatively.

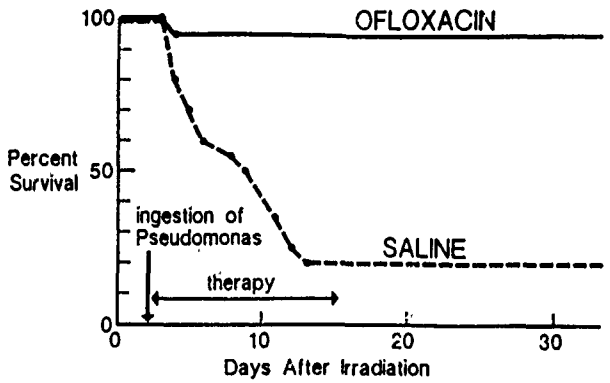

FIG. 1. Survival of 40 B6D2F1 mice irradiated with 7.0 Gy of ^{60}Co, fed with 10^7 *P. aeruginosa*, and treated orally with ofloxacin. Twenty mice were included in each group. (Data represent one experiment; two replicates of each experiment showed similar results.)

Statistical methods. Statistical analyses were done by using the Cox-Mantel test (10).

RESULTS

Mortality. Mortality in the groups that received ofloxacin was significantly lower from day 5 onward ($P < 0.05$ in all experiments) than that of the mice treated with water. In the first experiment (Fig. 1), only 4 of 20 mice treated with water (20%) survived, compared with 19 of 20 mice treated with ofloxacin (95%). In the second run of the experiment, 6 of the 20 mice treated with water (30%) survived whereas 18 of 20 mice treated with ofloxacin (90%) survived. In the third run, 5 of 20 mice treated with water (25%) survived, compared with 17 of 20 mice treated with ofloxacin (85%).

Isolation of organisms in liver. There was no correlation between the time following irradiation and the isolation of *P. aeruginosa*. More than 10 colonies of *P. aeruginosa* were isolated from each culture-positive liver sample. In the first experiment, *P. aeruginosa* was isolated in 21 of 28 randomly selected mice treated with water (75%) and in 2 of 30 mice treated with ofloxacin (7%). In the second experiment, *P. aeruginosa* was recovered in 14 of 26 mice treated with water (54%) and in no mice treated with ofloxacin. In the third experiment, *P. aeruginosa* was recovered in 17 of 25 mice treated with water (68%) and in no mice treated with the quinolone. ($P < 0.005$ in all experiments.)

Isolation of organisms in ileal contents. More than 10 colonies of *P. aeruginosa* were recovered from each culture-positive ileal content specimen. In the first experiment, *P. aeruginosa* was isolated in ileal content specimens of 24 of 28 mice treated with water (86%), compared with only 5 of 30 mice treated with ofloxacin (17%). In the second experiment, *P. aeruginosa* was recovered from the ileal contents of 19 of 26 mice treated with water (73%), compared with only 3 of 30 mice treated with quinolones (10%). ($P < 0.005$ in all experiments.)

Antibiotic concentrations in serum. The mean concentrations of ofloxacin were 2.6 ± 0.4 mg/liter at 1 h and 0.4 ± 0.2 mg/liter at 23.5 h. No difference was noted between infected and uninfected animals.

DISCUSSION

This study demonstrates that the quinolone ofloxacin can prolong survival and reduce colonization of the ileum and recovery of *P. aeruginosa* in the livers of irradiated mice.

We have developed a model of acquired *P. aeruginosa* infection in irradiated mice that may represent the mode of acquisition of external pathogens into an irradiated host (18). We also observed that the number of endogenous gastrointestinal tract aerobic and anaerobic bacteria declined 24 h after irradiation, and the decline was maximal at 7 days (2). The decrease in the number of endogenous bacterial flora may make the host more susceptible to the acquisition of external pathogens, such as *P. aeruginosa*.

The ability of *P. aeruginosa* to cause systemic infection in irradiated mice may be due to the following factors: (i) the bacterial void created in the gut following the decline in the number of other organisms (2), (ii) the increased permeability of the mucosal cells damaged by irradiation, and (iii) the decrease in local and systemic immune defenses.

The effectiveness of ofloxacin in the therapy of *P. aeruginosa* infection may be attributed to local inhibition of the growth of the organism within the gut lumen while the anaerobic gut flora was preserved (16) and to its systemic antibacterial activity to prevent the infection within the body.

The intraluminal concentration of ofloxacin achieved in our mouse model is estimated to be about 1,000 μg/ml, which is similar to that observed in humans (Ortho Pharmaceuticals, unpublished data). Although this initial concentration is reduced as the initial antimicrobial dose is absorbed, diluted, and excreted, it is probably capable of depressing the intraluminal growth of even resistant organisms, such as *Pseudomonas* species.

The optimal duration of quinolone therapy has not been determined. Although ofloxacin was administered for 15 days in the present study, a shorter course may be as efficacious. Further studies are under way to determine the optimal duration of therapy Although ofloxacin was administered twice a day in studies of humans (9), administration of this drug once a day was efficacious in our animal model and achieved concentrations in serum equal to those found in humans. Coprophagia, however, might have augmented the ingestion of ofloxacin. Further studies are warranted to evaluate the therapy of infection due to more resistant pathogens by using twice-daily administration of ofloxacin.

Selective decontamination of the gut with orally administered quinolones is used to prevent sepsis in immunocompromised hosts (3, 8, 9). These agents were also found to be effective in the management of septic episodes in neutropenic patients (11). The availability of an oral route of administration, the long half-life of ofloxacin that allows once-daily administration (15), the advantage of achieving selective inhibition of potential pathogens in the gut, and the ability to treat systemic infection make this quinolone a promising agent for oral therapy of orally acquired *P. aeruginosa* infection in irradiated hosts.

ACKNOWLEDGMENTS

We acknowledge the secretarial assistance of Gloria Contreras and Catherine Sund, and we thank K. P. Fu for performing the ofloxacin serum assays.

This research was supported by the Armed Forces Radiobiology Research Institute under work unit 4440-00129.

LITERATURE CITED

1. **Brook, I., T. J. MacVittie, and R. I. Walker.** 1984. Recovery of aerobic and anaerobic bacteria from irradiated mice. Infect. Immun. **46**:270–271.
2. **Brook, I., R. I. Walker, and T. J. MacVittie.** 1988. Effect of antimicrobial therapy on the gut flora and bacterial infection in irradiated mice. Int. J. Radiat. Biol. **53**:709–716.
3. **Dekker, A. W., M. Rozenberg-Arska, and J. Verhoef.** 1987. Infection prophylaxis in acute leukaemia: a comparison of ciprofloxacin with trimethoprim-sulfamethoxazole and colistin. Ann. Intern. Med. **106**:7–12.
4. **Gale, R. P.** 1987. Immediate medical consequences of nuclear accidents: lessons from Chernobyl. J. Am. Med. Assoc. **285**: 625–628.
5. **Hammond, C. V., D. Ruml, D. E. Cooper, and C. P. Miller.** 1955. Studies on susceptibility to infection following ionizing radiation. III. Susceptibility of the intestinal tract to oral inoculation with *Pseudomonas aeruginosa*. J. Exp. Med. **102**:403–411.
6. **Hathorn, J. W., M. Rubin, and P. A. Pizzo.** 1987. Empiric antibiotic therapy in the febrile neutropenic cancer patient: clinical efficacy and impact of monotherapy. Antimicrob. Agents Chemother. **31**:971–977.
7. **Kaplan, H. W., R. S. Speck, and F. Jawetz.** 1965. Impairment of antimicrobial defenses following total body irradiation of mice. J. Lab. Clin. Med. **40**:682–691.
8. **Karp, J. E., W. G. Merz, C. Hendricksen, B. Laughon, T. Redden, B. J. Bamberger, J. G. Bartlett, R. Saral, and P. J. Burke.** 1987. Oral norfloxacin for prevention of gram negative bacterial infections in patients with acute leukaemia and granulocytopenia. Ann. Intern. Med. **106**:1–7.
9. **Kern, W., E. Kyrrle, and E. Vanek.** 1987. Ofloxacin for prevention of bacterial infections in granulocytopenic patients. Infection **15**:427–433.
10. **Lee, T. E.** 1980. Statistical methods for survival data analysis, p. 127–129. Lifetime Learning Publication, Belmont, Calif.
11. **Leleux, A. R., J. Snoeck, J. Gerain, P. van der Auwera, D. Daneau, and F. Meunier.** 1989. Prevention par la perfloxacine des infections chez les malades cancereaux granulocytopenique. Presse Med. **18**:21–24.
12. **Lennette, E. H., A. Balows, W. J. Hausler, Jr., and H. J. Shadomy (ed.).** 1985. Manual of clinical microbiology, 4th ed. American Society for Microbiology, Washington, D.C.
13. **Maki, D. G.** 1981. Nosocomial bacteremia. An epidemiologic overview. Am. J. Med. **70**:719–732.
14. **Miller, C. P., C. W. Hammond, M. J. Tomkins, and G. Shorter.** 1952. The treatment of post irradiation infection with antibiotics, an experimental study on mice. J. Lab. Clin. Med. **39**: 462–479.
15. **Monk, J. P., and D. M. Campoli-Richards.** 1987. Ofloxacin: a review of its antimicrobial activity, pharmaceutical properties and therapeutic use. Drugs **33**:346–391.
16. **Pecquet, S., A. Andremont, and C. Tancrede.** 1987. Effect of oral ofloxacin on fecal bacteria in human volunteers. Antimicrob. Agents Chemother. **31**:124–125.
17. **Vincent, J. B., R. C. Veomett, and R. F. Riley.** 1955. Relation of the indigenous flora of the small intestine of the rat to post-irradiation bacteremia. J. Bacteriol. **69**:38–44.
18. **Walker, R. I., I. Brook, J. W. Costerton, T. J. MacVittie, and M. L. Myhal.** 1985. Possible association of mucous blanket integrity with post-irradiation colonization resistance Radiat Res. **104**:346–357.
19. **Weinstein, M. P., L. B. Reller, J. R. Murphy, and K. A. Lichtenstein.** 1983. The significance of positive blood cultures: a comprehensive analysis of 500 episodes of bacteremia and fungemia in adults. I. Laboratory and epidemiologic observations. Rev. Infect. Dis. **5**:35–53.
20. **Westland, M. P., and J. B. Cornett.** 1985 Quinolone antibacterial agents. Annu. Rev. Med. Chem. **20**:145–154.

Eur. J. Biochem. *195*, 707–713 (1991)

0014295691000085F

Linking phospholipase A_2 to phospholipid turnover and prostaglandin synthesis in mast cell granules

Stephen P. CHOCK[1], Sue Goo RHEE[2], Lily C. TANG[1] and Elsa A. SCHMAUDER-CHOCK[3]

[1] Division of Experimental Therapeutics, Walter Reed Army Institute of Research, Washington, DC, USA
[2] Laboratory of Biochemistry, National Heart, Lund and Blood Institute, National Institutes of Health, Bethesda, MD, USA
[3] Department of Experimental Hematology, Armed Forces Radiobiology Research Institute, Bethesda, MD, USA

(Received July 10, 1990) – EJB 90 0821

Rapid incorporation of exogenous arachidonic acid into phospholipid has been detected in conjunction with eicosanoid synthesis by purified mast cell granules [Chock, S. P. & Schmauder-Chock, E. A. (1988) *Biochem. Biophys. Res. Commun. 156*, 1308–1315]. The species of phospholipid formed has now been identified primarily as phosphatidylinositol. A calcium-dependent phospholipase A_2 has also been detected in the secretory granule. This enzyme, like the cyclooxygenase [Schmauder-Chock, E. A. & Chock, S. P. (1989) *J. Histochem. Cytochem. 37*, 1319–1328], appears to bind tightly to the granule matrix components. It is heat resistant and requires millimolar concentrations of calcium for optimal activity. It prefers phosphatidylinositol over phosphatidylcholine as substrate. Since the granule contains a large amount of phospholipid, the action of this phospholipase A_2 can provide the required substrate for the arachidonic acid cascade. These findings provide the basis for linking phospholipase A_2 to the production of eicosanoids during granule exocytosis. Since the granule also contains both an active acylating system that can rapidly reacylate lysophosphatidylinositol to form phosphatidylinositol, and an active phospholipase A_2 which hydrolyzes phosphatidylinositol, a rapid turnover involving the fatty acid at the *sn*-2 position of phosphatidylinositol may occur. These findings are consistent with our postulation that the secretory granule is the source and/or the cause of many of the early biochemical events associated with the process of stimulus-secretion coupling.

A rapid PtdIns turnover has been observed in many receptor-mediated secretory processes, including that of the mast cell [1–7]. Although extensive publications have implicated a possible role of phospholipid turnover in the mechanism of signal transduction, many basic questions remain unanswered [8, 9]. Much of the confusion may have stemmed from the lack of information concerning the origin of the phospholipid pool undergoing rapid turnover, and our inclination to attribute most, if not all, phospholipid-related events to the cell membrane. For receptor-related phospholipid changes, the plasma membrane has usually been assumed to be the source. Since most studies of phospholipid turnover have been based on analysis of the whole cell or tissue extracts, identification of the subcellular compartment responsible for phospholipid turnover has been impossible. Furthermore, many experiments were carried out using cells permeabilized with detergent. In our experience with mast cells, detergent treatment alone initiates the exocytotic process without the need of any additional agonist or secretagogue.

In conjunction with phospholipid turnover, many potent lipid-derived mediators of inflammation, such as prostaglandins, leukotrienes, thromboxanes and platelet-activating factors are also formed during secretion [3–5, 10–12]. Until recently, the enzymes responsible for their syntheses, and the phospholipid which provides the arachidonic acid substrate, have also been generally assumed to be associated with the plasma membrane. This assumption is based on the belief that most, if not all, cellular phospholipid existed only in the bilayer [13].

Recently we reported the presence of a large non-bilayer phospholipid store in the secretory granule of mast cells [14]. This phospholipid is needed to sustain the *de novo* membrane assembly process which occurs within the granule during granule activation [15–17]. Together with this matrix-bound phospholipid, we have also found enzymes of the arachidonic acid cascade [18, 19]. The coexistence of a phospholipid pool, to provide arachidonic acid, and the enzymes of the arachidonic acid cascade within the secretory granule, makes the link between granule activation and the synthesis of prostaglandins a physical possibility. However, the triggering of the arachidonic acid cascade during granule activation also requires the activation of a phospholipase A_2 (PLA_2) which liberates arachidonic acid from the phospholipid. Therefore, it is important to determine if the granule also contains a PLA_2 to provide the substrate for the cyclooxygenase, the lipoxygenase and other enzymes of the arachidonic acid cascade.

In this communication, we report that the mast cell granule not only has the enzymes to rapidly reacylate lyso-PtdIns and other lysophospholipids with arachidonic acid, but it also contains a matrix-bound PLA_2 to release arachidonic acid from PtdIns and other phospholipids. With the presence of a PLA_2 to provide the substrate, the granule can function as an independent eicosanoid-producing entity. These findings,

Correspondence to S. P. Chock, 203 Cedar Ave. Gaithersburg, MD 20877, USA

Abbreviations. PLC, phospholipase C; PLA_2, phospholipase A_2; PGE_2, prostaglandin E_2.

Enzymes. Phospholipase C (EC 3.1.4.10), phospholipase A_1 (EC 3.1.1.32); phospholipase A_2 (EC 3.1.1.4).

together with our previous published data, support our thesis that the secretory granule is not only able to actively facilitate its own extrusion from the cell via the process of perigranular membrane expansion, but it is also the source and/or the cause of the many early biochemical events which occur during the onset of exocytosis.

MATERIALS AND METHODS

Mast cell secretory granules were purified by peritoneal lavage of male Sprague-Dawley rats using Ca^{2+}-free Hank's balanced salt solution (Gibco Laboratories, Grand Island, NY) containing 0.4% fatty-acid-free bovine serum albumin (Sigma, St Louis, MO) and 10 units/ml heparin (Elkins-Sinn, Cherry Hill, NJ) according to previously published procedure [14]. The purified mast cells were suspended and sonicated in Ca^{2+}-free Hank's balanced salt solution containing 0.1 mg/ml leupeptin (Sigma) as described earlier [18]. To avoid contamination by cytosolic components, the purified membrane-bound granules obtained after the 15-min $960 \times g$ centrifugation [14], were routinely washed at least two more times in leupeptin-containing Ca^{2+}-free Hank's balanced salt solution before being used for cyclooxygenase or PLA_2 assay. The granule protein concentration was determined according to the modified Lowry procedure of Markwell et al. [20] using bovine serum albumin as standard.

Since the original wet volume of the purified mast cells used to prepare the granules was only about 100 µl, and the purified granules with its residual buffer was less than 30 µl, after repeated washes, the final dilution factor for the original cytosolic contents amounts to greater than 10^7-fold. Since the membrane-bound granules were sedimented at below $1000 \times g$, the contamination from membrane fragments (microsomes) is virtually nil. Electron micrographs which depict the purity of the typical granule preparation have been published [14, 18].

Assays for the synthesis of eicosanoids using [1-^{14}C]-arachidonic acid and purified granules were carried out according to [18]. The extraction of ^{14}C-labeled eicosanoids was according to Salmon and Flower [21]. TLC solvent A, for the separation of eicosanoids and arachidonic acid, was the organic phase of ethylacetate/2,2,4-trimethylpentane/acetic acid/water (44:20:8:40, by vol.) [21]. TLC solvent B, for the separation of phospholipids, was chloroform/methanol/acetic acid/water (50:30:8:4, by vol.) [22]. For separation and identification of eicosanoids and arachidonic acid in the reaction mixture, the chloroform extract of the Salmon and Flower procedure [21] was applied. To assess the arachidonic acid produced by PLA_2 hydrolysis, a hexane extract of the reaction sample was applied. HP-K high-performance TLC plates (Whatman) were used without heat activation. The radioactive reaction products were visualized by autoradiography. The eicosanoid standards were purchased from Cayman Chemical (Ann Arbor, MI) and all isotopes were purchased from Du Pont (Du Pont NEN Research Products, Wilmington, DE). The synthesis of PGE_2 from endogenous granule phospholipid arachidonic acid was analyzed using the radioimmunoassay kit procedure as described by the manufacturer (Du Pont NEN Research Products).

The digestion of ^{14}C-labeled PtdIns synthesized from exogenous [1-^{14}C]arachidonic acid [18] was carried out according to the procedure of Ryu et al. [23, 24] using a PtdIns-specific phospholipase C (PLC) purified from bovine brain. Briefly, the chloroform extract which also contained the eicosanoids was divided into two equal aliquots. One served as the control while the other was subjected to PLC digestion by the addition of 50 µl 4.6 mg/ml pure PLC and 100 µl assay medium. The mixture was sonicated and incubated in room temperature for 30 min before being extracted once with chloroform/methanol according to Bligh and Dyer [25] and twice with chloroform. The combined extracts were dried under nitrogen and dissolved in chloroform. Both the control and the digested sample were applied to separate TLC plates and developed using a two-dimensional chromatography. Solvent A was used to elute fatty acids, glycerides and eicosanoids while solvent B was used to separate phospholipids. Experiments using phospholipid standards were also carried out for the comparison of R_F values.

When 1-palmitoyl-2-[1-^{14}C]arachidonylglycerophosphocholine and 1-stearoyl-2-[1-^{14}C]arachidonylglycerophosphoinositol were purified, the silicic acid column procedure of Dittmer and Wells [26] was used. A rapid procedure for the assay of PLA_2 and cyclooxygenase using radioactive substrates, but without the use of TLC and autoradiography, has also been established. This method is based on the original extraction procedure of Salmon and Flower [21]. Briefly, ^{14}C-labeled substrate was dried under a stream of nitrogen to rid it of all organic solvent, then dispersed with the aid of sonication into an assay buffer containing 0.5 mg/ml digitonin (Fluka Bio Chemika), 0.1 mg/ml leupeptin, 2.5 mM $CaCl_2$ or an otherwise-specified amount of $CaCl_2$, and 20 mM Hepes at pH 6.8. The assay was started by adding a volume of the above substrate solution to a volume of purified granules which had just been disrupted and dispersed by sonication in the assay buffer. Rapid mixing was assured by a few brief sonication pulses. At the specified time, a 0.3-ml aliquot was removed and quenched in a 0.7 ml cold acetone. Parallel control experiments (without granules) were also run to assess the value of the blank for each experiment. Each quenched sample was vortexed thoroughly and clarified by centrifugation in an Eppendorf microfuge. 0.8 ml supernatant was transferred into a 1.5-ml polypropylene centrifuge tube followed by addition of 0.6 ml hexane to extract the fatty acid. The mixture was vortexed vigorously to assure complete extraction. After phase separation aided by brief centrifugation, aliquots of the upper hexane phase were counted. Using this procedure it was estimated that about 87% of the [1-^{14}C]arachidonic acid released by PLA_2 could be recovered in the hexane. For quantitation of the cyclooxygenase activity, the remaining bottom aqueous phase, after the hexane extraction step, was transferred into a polypropylene microfuge tube, acidified, and extracted with 0.6 ml chloroform. As much as 90% of the hydrophobic components (mainly eicosanoids and arachidonic acid) could be recovered in the chloroform phase [21]. Thus the amount of radioactivity in the chloroform phase is a reflection of the cyclooxygenase activity of the granules.

RESULTS

In our previous communications [18, 19], we reported the presence of the arachidonic acid cascade in the secretory granule of the mast cell. We also showed that as well as various prostaglandins and eicosanoids, the granule could also rapidly synthesize arachidonylated phospholipid from exogenous arachidonic acid. This synthesis occurs at the onset of mixing the contents of the purified granule with the [1-^{14}C]-arachidonic acid. We now identify the newly synthesized ^{14}C-labeled phospholipid of band 1 [18] as mainly PtdIns.

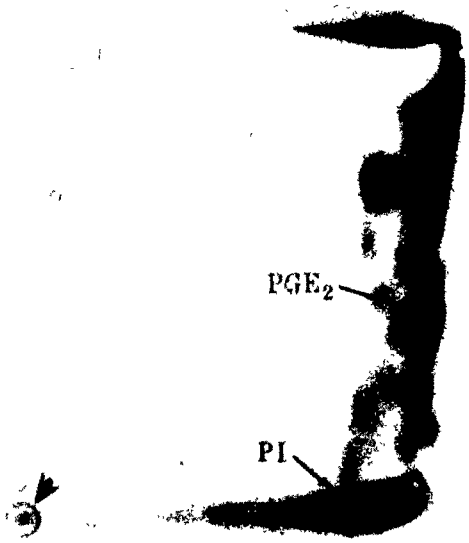

Fig. 1. *Synthesis of prostaglandins, eicosanoids and phospholipid from exogenous [1-^{14}C]arachidonic acid by purified mast cell granules.* Autoradiogram of two-dimensional TLC of ^{14}C-labeled products resulted from a 5-min 20 C incubation of disrupted granules with [1-^{14}C]arachidonic acid according to published procedure [18]. TLC solvent A was used to separate the eicosanoids vertically while solvent B resolved the ^{14}C-labeled phospholipid classes horizontally. The sample was applied at the lower left hand corner (arrowhead). The presence of prostaglandin E_2 and PtdIns (PI) were verified by parallel experiments using standards

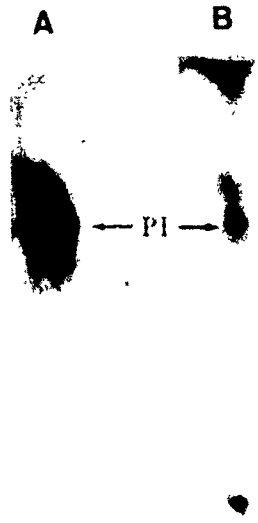

Fig. 2. *Phosphatidylinositol hydrolysis by phospholipase C.* The ^{14}C-labeled phospholipid from incubation of purified granules with [1-^{14}C]arachidonic acid was divided into two equal fractions. One fraction was run as a control and the other was subjected to hydrolysis with a PtdIns-specific PLC purified from bovine brain. The area of the two-dimensional chromatogram exhibiting separation of the phospholipid components are shown. Lane A (control) shows the phospholipid pattern of the sample before PLC incubation. Lane B (sample) shows the reduction in the intensity of the PtdIns (PI) band (arrow) after PLC digestion

By incubating disrupted purified granules in the presence of [1-^{14}C]arachidonic acid at pH 6.8 and separating the chloroform-extracted ^{14}C-labeled products using two-dimensional TLC, we could resolve the many arachidonic acid metabolites into distinct spots using autoradiography (Fig. 1). Since TLC solvent B, which was used in the horizontal direction, also separates phospholipids, we have been able to verify the major radioactive phospholipid (arrow) of band 1 as PtdIns by comparing its R_F with that of commercially prepared L-α-1-stearoyl-2-[1-^{14}C]arachidonylglycerophosphoinositol. The identity of the ^{14}C-labeled PtdIns was also confirmed by enzymatic digestion using the PtdIns-specific PLC purified from bovine brain. As seen in Fig. 2, the PtdIns band has largely disappeared following PLC digestion. Since mast cells contain very little lysophospholipid [27], the rapid synthesis of ^{14}C-labeled PtdIns from exogenous [1-^{14}C]-arachidonic acid not only suggests the presence of an active acylating enzyme, but it also indicates the presence of an active PLA_2, which supplies the lysophospholipid for the arachydonylation process.

It is also known that *in vivo*, it is the phospholipid which provides the arachidonic acid needed for the synthesis of eicosanoids [11]. By simply exposing the granule matrix to neutral buffer, we can demonstrate the rapid production of PGE_2 without the addition of exogenous arachidonic acid (Fig. 3). This must mean that the granule also contains a PLA_2 which can liberate arachidonic acid from phospholipid and render it available to the eicosanoid-synthesizing machinery. The presence of a PLA_2 in the secretory granule is evident in the results shown in Fig. 4. In these experiments, phospholipid with [1-^{14}C]arachidonic acid at its *sn*-2 position is used as substrate. In Fig. 4A, the release of arachidonic acid by PLA_2 is accompanied by its conversion into various eicosanoids via the cyclooxygenase and the lipooxygenase pathways. Some of

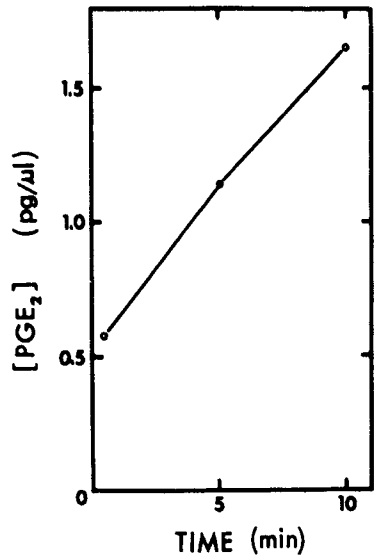

Fig. 3. *The production of prostaglandin E_2 from endogenous phospholipid arachidonic acid.* Purified granules were disrupted and dispersed by brief sonication in a buffer containing 1 mg/ml digitonin, 0.5 mM $CaCl_2$, 0.08 mg/ml leupeptin and 10 mM Hepes, pH 6.8, at 20 C. At the specified times, aliquots of samples were quenched with cold acetone and clarified, then prostaglandin E_2 content was determined by radioimmunoassay. The results represent an average of two separate determinations

these metabolites of [1-^{14}C]arachidonic acid have already been identified [18]. The rapid conversion of the newly released arachidonic acid into eicosanoids can be prevented by heat denaturation of the arachidonic-acid-metabolizing enzymes. Fig. 4B shows the result of heating the granule in a boiling

Fig. 4. *The ^{14}C-labeled products formed by incubating disrupted granules with 1-stearoyl-2-[1-^{14}C]arachidonylglycerophosphoinositol and developed in TLC solvent A.* (A) Lanes 1 and 2 represent the band patterns of chloroform extracts from a 30-s and a 10-min incubation of sonicated granules with 100 μM ^{14}C-labeled PtdIns, respectively. The appearance of prostaglandins bands are analogous to those already published. (B) Lane 1 is the control (no protein) and lane 2 is the result of a 2-min incubation of disrupted granules heated at 100°C for 5 min before being assayed with 36 μM ^{14}C-labeled PtdCho

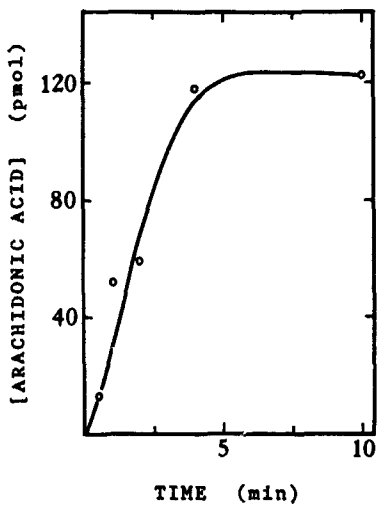

Fig. 5. *Time course of the release of arachidonic acid by phospholipase A_2.* Granules, after exposure to 100°C for 4 min, were assayed in the presence of 103 μM PtdIns (including 3 μM 1-stearoyl-2-[1-^{14}C]arachidonylglycerophosphoinositol, 2.75 mM $CaCl_2$, 0.1 mg/ml leupeptin, 0.5 mg/ml digitonin and 45 mM Hepes, pH 6.8, at 20°C. The concentration of the product, arachidonic acid, was calculated based on the specific activity of the substrate applied. A 120 pmol product is approximately equal to 6.7% hydrolysis of the PtdIns added. The granule protein content of each reaction sample was 75 μg

Table 1. *The resistance of phospholipase A_2 to heat denaturation*
Phospholipase A_2 activity was measured in granule samples heated at 100°C for 0 (control), 4 or 10 min before a 1-min 20°C assay using either PtdCho (8.6 μM) or PtdIns (7.7 μM) as substrate. Each sample also contained 2.75 mM $CaCl_2$, 0.5 mg/ml digitonin, 0.1 mg/ml leupeptin, 45 mM Hepes, pH 6.8, and 0.19 mg granule protein

Substrate	PLA_2 activity		
	control	4 min	10 min
	nmol/min		
PtdCho	0.041	0.031	0.022
PtdIns	0.13	0.13	0.096

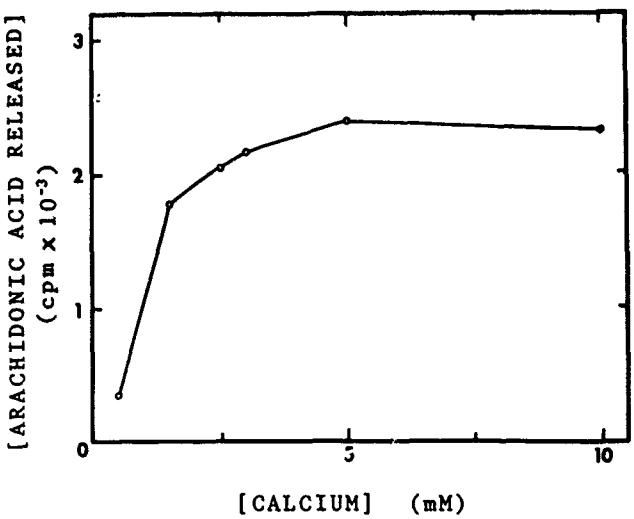

Fig. 6. *Calcium dependence of the hydrolysis of phosphatidylinositol by granule phospholipase A_2.* Granule samples heated to 100°C for 5 min were assayed for 2 min at pH 6.9, 20°C in the presence of 37 μM 1-stearoyl-2-[1-^{14}C]arachidonylglycerophosphoinositol, 0.5 mg/ml digitonin and 0.1 mg/ml leupeptin. Each reaction sample contained 0.45 mg/ml granule protein

water bath for 5 min prior to incubation with the phospholipid substrate. The heat resistance of the granule PLA_2 can be seen in the results listed in Table 1. This data indicates that the enzyme has a greater degree of heat resistance when assayed using PtdIns (a loss of 25%) than when assayed using PtdCho (a loss of 47% activity in 10 min) as substrate. The unusual heat resistance of PLA_2 from other sources has been reported previously [28, 29]. Many of these have a molecular mass of about 13 kDa and contain many disulfide bonds.

Fig. 5 shows a time course of the activity of granule PLA_2 using PtdIns as substrate. Under these conditions, the rate of hydrolysis is essentially linear for the first 5 min. Beyond that, the rate of hydrolysis tends to level off or become scattered. In this particular experiment, the maximum amount of substrate hydrolyzed equalled approximately 6.7%. This low level of substrate hydroylsis may be due to product inhibition [30, 31] and to the fact that mast cell granule PLA_2 tends to aggregate and sediment with the granule matrix during assay. The hydrophobic nature of the granule matrix may also exert some unexpected influence on the enzyme-substrate-product complex. The insoluble nature of granule PLA_2 was evident in the fact that about 84% of the PLA_2 activity can be sedimented at 2000 × *g* (10 min) following a 5-min 100°C incubation in the presence of 0.5 mg/ml digitonin and 2.5 mM Ca^{2+}. When the initial rate was obtained from a 1-min assay, the activity of PLA_2 was essentially proportional to granule concentration within a 10-fold range.

In Fig. 6, the calcium dependence of granule PLA_2 is plotted. The relative radioactivity as obtained from separate 2-min 20°C incubation assays. The result shows that granule PLA_2 has a strict requirement for calcium for its activity.

Table 2. *Synthesis of phospholipid from exogenous arachidonic acid by granule enzymes*

Each sample contained 33 μM [1-^{14}C]arachidonic acid, 0.5 mM $CaCl_2$, 0.05 mg/ml phenylmethylsulfonyl fluoride, 0.5 mg/ml digitonin, 0.1 mg/ml leupeptin, 20 mM Hepes, pH 6.8, and 1.3 mg granule protein. Each assay was carried out for 4 min at 20°C. The ^{14}C-labeled phospholipid synthesized was estimated by scraping and counting the radioactivity of the band 1 phospholipid spot of a TLC resolved using solvent A

Treatment	Phospholipid synthesized
	pmol (% control)
Control	44 (100)
100°C, 4 min	13(29)

When PtdIns is used as substrate, its rate of hydrolysis was optimal between 2.5 mM and 5 mM calcium at pH 6.8. The slight decrease in rate above 5 mM calcium might be due to precipitation of the substrate by calcium.

It is important to find out if an enzyme system exists in the secretory granule, which can account for the rapid formation of ^{14}C-labeled phospholipid from exogenous [1-^{14}C]arachidonic acid [18]. Since PLA_2 is heat stable, its contribution, if any, to the synthesis of ^{14}C-labeled PtdIns from [1-^{14}C]arachidonic acid and lyso-PtdIns should also be heat resistant. If the amount of heat-sensitive synthesis can be taken to represent the action of an acyltransferase system, then by comparing the amounts of phospholipid synthesized by regular and by heat-treated granules, the presence of an acyltransferase system may be elicited. The results (Table 2) suggest that the granule contains an acyltransferase system capable of rapidly synthesizing *sn*-2 arachidonyl phospholipid from exogenous arachidonic acid, and unlike PLA_2, this enzyme system is sensitive to heat denaturation.

DISCUSSION

By using purified secretory granules to study phospholipid metabolism implicated in the stimulus-secretion coupling process, we have avoided the ambiguity which plagues those studies which have based their interpretations solely on results obtained by analysis of whole cell extraction. In a previous report, we have shown that in conjunction with the synthesis of prostaglandins and other eicosanoids, the mast cell granule can also rapidly synthesize phospholipid from exogenous [1-^{14}C]arachidonic acid [18]. This newly synthesized phospholipid has now been identified as mainly PtdIns (Figs 1 and 2). The preferential incorporation of arachidonic acid into PtdIns was not a surprise to us, since most naturally occurring PtdIns contains arachidonic acid in the *sn*-2 position [32].

Since the unstimulated mast cell contains very little endogenous lysophospholipid [27, 33], the availability of lyso-PtdIns in the granule to support the rapid formation of PtdIns from exogenous arachidonic acid, suggests the simultaneous presence of both a phospholipid-acylating system and a phospholipid-deacylating system (PLA_2) in the mast cell granule. Since the rate of incorporation of [1-^{14}C]arachidonic acid into PtdIns by the granule acyltransferase system was very fast, and at the present time we do not know if acyl-CoA is also involved in this enzyme system, until proven otherwise, we will treat the granule acyltransferase as a unique system different from that involved in the biosynthesis of phospholipid. In contrast to the granule PLA_2 which is heat resistant (Table 1), the granule acyltransferase system is heat sensitive (Table 2). These two enzymes together, can effect the rapid turnover of the fatty acid moiety in the *sn*-2 position of the granule PtdIns and other phospholipid.

The granule PLA_2 appears to have higher affinity for PtdIns than for PtdCho. Under all experimental conditions used, PtdIns was consistently hydrolyzed much faster than PtdCho, sometimes as much as 10-fold. The catalysis with PtdIns also appeared to be more heat resistant than with PtdCho (Table 1). However, it should be borne in mind that our derivation of rates of hydrolysis did not take into consideration the amount of endogenous phospholipid present in the granule. We also did not consider the influence of the PtdIns-synthesizing system in the granule. The kinetic property of this enzyme can only be clarified by the use of purified PLA_2 in a defined assay system.

The presence of a PLA_2 which hydrolyzes PtdIns has been reported in other tissues including rat brain and porcine thyroid gland [34–36]. However, the deacylation of fatty acid from the *sn*-2 position of PtdIns could also be the result of the combined action of PLC and diglyceride lipase, or the combined action of PLA_1 and lysophospholipase [37, 38]. Since many experiments reported were carried out by using whole tissue extracts and with extended periods of assay incubation, it was virtually impossible to verify which enzymes were actually responsible for the net results observed. The elucidation of PLA_2 can also be complicated by the presence of acyltransferases in the assay media. Some of these enzymes can convert lyso-PtdIns into PtdIns via *sn*-2 acylation [39]. In the mast cell granule, the presence of the acylating enzymes must have been responsible for most of the ^{14}C found in band 1 phospholipid [18]. Another cellular enzyme, lysophospholipase, also utilizes lysophospholipid as substrate. The rapid consumption of lysophospholipid, the product of PLA_2, by other enzymes present in the milieu, has made it difficult to verify the presence of PLA_2 based on the recovery of lysophospholipid from the reaction media. Therefore the presence of PLA_2 can be easily overlooked in many unrefined systems. The elucidation of PLA_2 activity in whole cell or tissue extracts can be further aggravated by the domination of competing reactions, such as those of PLC and other phospholipases in the assay mixture.

Although PLC is a cytoplasmic enzyme [24, 40], its presence in the secretory granule has not been reported. To rule out the possibility that PLC might have contributed to our present result, we have attempted to detect PLC and its activity in the mast cell granule by using a monoclonal-antibody detection technique [41] and by an enzyme assay using [^{32}P]PtdIns as substrate [23]. So far, our results have been negative. This suggests the absence of PLC from the secretory granule. Therefore it is unlikely that PLC could have played a role in our results.

Both PLA_1 and lysophospholipase activities have been found in rat and human nervous tissues. These enzymes are heat sensitive. A 5-min 70°C incubation will completely destroy the lysophospholipase activity [35, 42]. Since we routinely heated our granules for 5 min at 100°C before performing the PLA_2 assays, it is unlikely that either of these enzymes, even if they were present in the granule, could have contributed to our current results. Furthermore, had PLA_1 been active during our assay, with [2-^{14}C]arachidonylglycerophosphoinositol as substrate in the 1-min or 2-min 20°C assay, the formation of lyso-PtdIns should have been observed prior to, or along with, the formation of [^{14}C]arachi-

donic acid. However, no radioactive band with relative mobility corresponding to that of lyso-PtdIns was detected on thin-layer chromatogram. Therefore, it appears that PLA_2 must have been responsible for hydrolysis of PtdIns in the secretory granule preparations.

The implication for the activation of a PLA_2 during mediator release has previously been suggested [32, 43–45]. Since it is the endogenous phospholipid which supplies the arachidonic acid required for eicosanoid synthesis [11], the fact that disrupted granules are able to produce PGE_2 without exogenous substrate (Fig. 3) further suggests the presence of a PLA_2 in the secretory granule. The simultaneous presence of the ability to reacylate (acyltransferase activity) and deacylate (PLA_2 activity) phospholipid suggests that the granule also has the capacity for rapid phospholipid turnover during exocytosis. This PLA_2-mediated phospholipid turnover is independent of that involving PLC which may occur in the cytoplasm. The simultaneous activation of PLA_2 and PLC during the stimulus-secretion coupling has been previously suggested [46, 47].

As well as the complication caused by the presence of a large amount of granule proteolytic enzymes, our initial study on PLA_2 was also hampered by the presence of enzymes of the arachidonic acid cascade (Fig. 4). The rapid conversion of the liberated arachidonic acid into various eicosanoids made the assessment of phospholipase activity inaccurate. This interference was mostly avoided by heating the granules. Therefore, in most of our experiments, we routinely heated the granules to deactivate the proteolytic enzyme and the enzymes of the arachidonic acid cascade before assaying PLA_2 activity.

Although the granule enzyme is very heat stable, prolonged heating at 100 °C decreases its specific activity (Table 1). Heating also did not cause the enzyme to dissociate from the insoluble granule matrix component. This allowed us to speculate whether, like the cyclooxygenase, the PLA_2 may also be tightly bound to the strands of proteoheparin granule matrix backbone material [19]. Since the granule also contains a high concentration of proteolytic enzymes which are assumed to be activated during granule activation, it is possible that some PLA_2 may be released by proteolysis during secretion. The presence of proteolytic enzymes might also have caused the appearance of the many PLA_2 isoforms in some snake venoms [29] and in the platelet [48]. For the mast cell granule, the packaging of PLA_2 with proteolytic enzyme might also result in the formation of various phospholipase isoforms of different molecular mass during granule activation. The presence of proteolytic enzyme may also give rise to a time-dependent deactivation of the granule enzymes following exocytosis.

The rate of substrate hydrolysis by PLA_2 is sensitive to the substrate concentration and to the presence of detergent [30, 49]. Although we have not determined the K_m for our granule enzyme, we have generally dervied the apparent rates from a 1-min 20 C incubation with about 20 μM substrate. Digitonin was used to disperse the granule matrix as in a previous granule cyclooxygenase assay [18]. Since the rates observed between 20 μM and 100 μM (Fig. 5) substrate did not vary greatly, it suggests that under our experimental conditions the enzyme was essentially saturated. This would mean that our granule enzyme might have a low K_m similar to that found in the macrophage-like cell line when assayed under a low substrate concentration [30]. However, at high substrate concentration the granule enzyme appears to be inhibited or unable to hydrolyze the substrate completely. As in Fig. 5, the rate of PtdIns hydrolysis began to level off at about 125 pmol, which represented only about 7% of the substrate hydrolyzed. We do not know if this is an artefact due to some non-specific inhibition, or if it reflects an inherent regulatory measure needed to prevent the uncontrolled hydrolysis of granule phospholipid. It is also possible that the granule matrix may provide an environment which predisposes the enzyme to product inhibition. Since the granule matrix is insoluble and also hydrophobic, it may adsorb and aggregate the substrate into some undefined complex which is not easily accessible to the enzymes which are themselves tightly bound to the matrix.

A striking similarity between the macrophage enzyme [50] and our granule enzyme can also be seen in their strict dependence on calcium for activity (Fig. 6). This millimolar-calcium dependence has also been observed in many other enzymes, such as those of the neutrophil [51] and the alveolar macrophage [52]. However, based on preliminary data, the mast cell granule PLA_2 appears to have a different pH requirement [50, 51]. In the pH range 4–8, it remained fully active (data not shown). This may imply that granule PLA_2 is active during granule activation, since the granule is thought to have an acidic environment [15, 53, 54]. A secreted PLA_2 from human neutrophils with optimal activity at pH 5.5 has also been reported [55]. This enzyme was localized to the azurophilic granule fractions of the cell extracts and was secreted along with β-glucuronidase.

It is interesting to note that for the mast cell, only phosphatidic acid, PtdCho and PtdIns showed rapid turnover as measured by ^{32}P incorporation during stimulated histamine release [56]. We now show that the secretory granule also contains a PLA_2 which can hydrolyze PtdIns and PtdCho. Consequently, arachidonic acid can be rapidly liberated from granule PtdIns and other phospholipid to serve as substrate for the arachidonic acid cascade which is initiated at the onset of granule activation [18]. Since mast cell granule can also rapidly synthesize PtdIns from fatty acid and lyso-PtdIns, a net flux toward PtdIns turnover may result. This may accentuate the rapid turnover of PtdIns during granule activation. A similar PLA_2 with high affinity towards PtdIns might have caused the selective release of arachidonic acid in the stimulated rat basophilic leukemic cells and in stimulated platelets [43–45].

Since the secretory granule contains both the phospholipid and the enzymes for eicosanoid synthesis and phospholipid turnover, this would provide the physical basis for linking exocytosis to the production of eicosanoids and rapid phospholipid turnover. This supports our thesis that the secretory granule may be responsible for many of the early biochemical events associated with secretion. Since granule activation also results in the extrusion of some granule matrix components into the cytoplasm of the activated cell according to our model [14], this may be partly responsible for activation of adenylate cyclase (or guanylate cyclase) [57, 58] and triggering of some unknown cellular responses. With the revelation that the secretory granule may actually be responsible for the many biochemical events associated with the stimulus-secretion coupling process [59], the role of the secretory granule in this important biological process must be reevaluated.

We are grateful to Dr Thomas L. Walden for help with the radioimmunoassay and to Mr Joe L. Parker and Miss Christine S. Cho for technical assistance. We are indebted to Drs Sang Yeol Lee, Jae Won Kim and Uh-Hyun Kim for help concerning phospholipase C. Special appreciation is due Dr Thomas Kim for performing the immunoblot experiments for the purpose of detecting phospholipase

C. We are also thankful to Drs Myra L. Patchen and Thomas J. MacVittie for kind support.

REFERENCES

1. Hokin, L. E. & Hokin, M. R. (1953) *J. Biol. Chem. 203*, 967–977.
2. Durell, J. T., Garland, J. T. & Friedel, R. D. (1969) *Science 165*, 862–866.
3. Michell, R. H. (1975) *Biochim. Biophys. Acta 415*, 81–147.
4. Berridge, M. J. (1984) *Biochem. J. 220*, 345–360.
5. Majerus, P. W., Connolly, T. M., Deckmyn, H., Ross, T. S., Bross, T. E., Ishii, H., Bansal, V.S. & Wilson, D. B. (1986) *Science 234*, 1519–1526.
6. Hokin, L. E. & Hokin, M. R. (1958) *J. Biol. Chem. 233*, 805–810.
7. Cockcroft, S. (1982) *Cell Calcium 3*, 337–359.
8. Gerber, D., Davies, M. & Hokin, L. E. (1973) *J. Cell. Biol. 56*, 736–745.
9. Exton, J. H. (1988) *FASEB J. 2*, 2670–2676.
10. Reichman, M., Nen, W. & Hokin, L. E. (1987) *Biochem. Biophys. Res. Commun. 146*, 1256–1261.
11. Samuelsson, B. (1982) *Biosci. Rep. 3*, 791–813.
12. Metcalfe, D. D., Kaliner, M. & Donlon, M. A. (1981) *CRC Crit. Rev. Immunol. 3*, 23–74.
13. Alberts, B., Bray, D., Lewis, J., Raff, M., Roberts, K. & Watson, J. D. (1983) *Molecular biology of the cell*, p. 350, Garland Publishing Inc., N.Y., London.
14. Chock, S. P. & Schmauder-Chock, E. A. (1989) *J. Biol. Chem. 264*, 2862–2868.
15. Chock, S. P. & Schmauder-Chock, E. A. (1985) *Biochem. Biophy. Res Commun. 132*, 134–139.
16. Schmauder-Chock, E. A. & Chock, S. P. (1987) *Histochem. J. 19*, 413–418.
17. Schmauder-Chock, E. A. & Chock, S. P. (1987) in *Proceedings of the 45th annual meeting of the electron microscopy society* of America, (Bailey, G. W. ed.) pp. 782–783, San Francisco Press.
18. Chock, S. P. & Schmauder-Chock, E. A. (1988) *Biochem. Biophys. Res. Commun. 156*, 1308–1315.
19. Schmauder-Chock, E. A. & Chock, S. P. (1989) *J. Histochem. Cytochem. 37*, 1319–1328.
20. Markwell, M. A. K., Haas, S. M., Bieber, L. L. & Tolbert, N. E. (1978) *Anal. Biochem. 87*, 206–210.
21. Salmon, J. A. & Flower, R. J. (1982) *Methods Enzymol. 86*, 477–493.
22. Skipski, V. P., Peterson, R. F. & Barclay, M. (1964) *Biochm. J. 90*, 374–378.
23. Ryu, S. H., Suh, P. G., Cho, K. S., Lee, K. Y. & Rhee, S. G. (1987) *Proc. Natl Acad. Sci. USA 84*, 6649–6653.
24. Rhee, S. G., Suh, P. G., Ryu, S. H. & Lee, S. Y. (1989) *Science 244*, 546–550.
25. Bligh, E. G. & Dyer, W. J. (1959) *Can. J. Biochem. Physiol. 37*, 911–917.
26. Dittmer, J. C. & Wells, M. A. (1969) *Methods Enzymol. 14*, 482–530.
27. Strandberg, K. & Westerberg, S. (1976) *Mol. Cell. Biochem. 11*, 103–107.
28. Dennis, E. A. (1987) *Drug Dev. Res. 10*, 205–220.
29. Sannanaik Vishwanath, B., Manjunatha Kini, R. & Veerabasappa, G. (1988) *Toxicon 26*, 713–720.
30. Lister, M. D., Deems, R. A., Watanabe, Y., Ulevitch, R. J. & Dennis, E. A. (1988) *J. Biol. Chem. 263*, 7506–7513.
31. Ballou, L. R. & Cheung, W. Y. (1985) *Proc. Natl Acad. Sci. USA 82*, 371–375.
32. Holub, B. J., Kuksis, A. & Thompson, W. (1970) *J. Lipid Res. 11*, 558–564.
33. Keller, R. (1962) *Helv. Physiol. Pharmacol. Acta 20*, c66.
34. Shum, T. Y. P., Gray, N. C. C. & Strickland, K. P. (1979) *Can. J. Biochem. 57*, 1359–1367.
35. Cooper, M. F. & Webster, G. R. (1970) *J. Neurochem. 17*, 1543–1554.
36. Hayc, B. & Jacquemin, C. (1977) *Biochim. Biophys. Acta 487*, 231–242.
37. Irvine, R. F., Letcher, A. J. & Dawson, R. M. C. (1980) *FEBS Lett. 119*, 287–289.
38. Hirasawa, K., Irvine, R. F. & Dawson, R. M. C. (1981) *Eur. J. Biochem. 120*, 53–58.
39. Hill, E. E. & Lands, W. E. M. (1970) in *Lipid metabolism* (Wakil, S. J., ed.), pp. 185–277, Academic Press, N.Y.
40. Irvine, R. F. & Dawson, R. M. C. (1978) *J. Neurochem. 31*, 1427–1434.
41. Suh, P. G., Ryu, S. H., Choi, W. C., Lee, K. Y. & Rhee, S. G. (1988) *J. Biol. Chem. 263*, 14497–14504.
42. Cooper, M. F. & Webster, G. R. (1972) *J. Neurochem. 19*, 333–340.
43. Strandberg, K., Sydbom, A. & Uvnas, B. (1975) *Acta Physiol. Scand. 94*, 54–62.
44. Garcia-Gil, M. & Siraganian, R. P. (1986) *J. Immunol. 136*, 3825–3828.
45. Mahadevappa, V. G. & Holub, B. J. (1983) *J. Biol. Chem. 258*, 5337–5339.
46. Kaya, H., Patton, G. M. & Hong, S. L. (1989) *J. Biol. Chem. 264*, 4972–4977.
47. Slivka, S. R. & Insel, P. A. (1987) *J. Biol. Chem. 262*, 4200–4207.
48. Loeb, L. A. & Gross, R. W. (1986) *J. Biol. Chem. 261*, 10467–10470.
49. Lombardo, D. & Dennis, E. A. (1985) *J. Biol. Chem. 260*, 16114–16121.
50. Ulevitch, R. J., Watanabe, Y., Sano, M., Lister, M. D., Deems, R. A. & Dennis, E. A. (1988) *J. Biol. Chem. 263*, 3079–3085.
51. Lanni, C. & Becker, E. L. (1983) *Am. J. Pathol. 113*, 90–94.
52. Lanni, C. & Franson, R. C. (1981) *Biochim. Biophys. Acta 658*, 54–63.
53. Chock, S. P. & Chock, E. S. (1985) *Fed. Proc. 44*, 1324.
54. Lagunoff, D. & Rickard, A. (1983) *Exp. Cell Res. 144*, 353–360.
55. Balsinde, J., Diez, E., Schuller, A. & Mollinedo, F. (1988) *J. Biol. Chem. 263*, 1929–1936.
56. Kennerly, D. A., Sullivan, T. J. & Parker, C. W. (1979) *J. Immunol. 122*, 152–159.
57. Peach, M. J. (1981) *Biochem. Pharmacol. 30*, 2745–2751.
58. Gerzer, R., Hamet, P., Ross, A. H., Lawson, J. A. & Hardman, J. G. (1983) *J. Pharmacol. Exp. Ther. 226*, 180–186.
59. Chock, S. P. & Schmauder-Chock, E. A. (1990) *Biofactors 2*, 133–146.

Agents and Actions, vol. 32, 3/4 (1991)

0065-4299/91/040237-08 $ 1.50+0.20/0

Effects of aminoguanidine on pre- and post-irradiation regional cerebral blood flow, systemic blood pressure and plasma histamine levels in the primate [1]

L.G. Cockerham [2], G.D. Prell [3], T.J. Cerveny [2], M. O'Brien [3] and J.D. Hampton [2]

[2] Physiology Department, Armed Forces Radiobiology Research Institute, Bethesda, Maryland 20814-5145
[3] Department of Pharmacology, Mount Sinai School of Medicine, of the City University of New York, New York, NY 10029

Abstract

Exposure to ionizing radiation causes hypotension, cerebral ischemia and release of histamine (HA). To investigate the relationship among these three responses, rhesus monkeys (*Macaca mulatta*) received aminoguanidine (AG) (1 mg/kg), then were given either 50 Gy whole-body irradiation or sham-irradiation. Monkeys receiving AG had lower mean arterial blood pressure (MABP) than saline-treated controls. Compared to controls, rCBF was lower in irradiated monkeys but pre-treatment with AG did not influence this effect. Among untreated, irradiated monkeys, HA levels were increased only at two minutes post-irradiation, but among AG-treated, irradiated monkeys, HA levels were higher at all times postirradiation. Radiation-induced release of HA may be associated with radiation-induced hypotension and reduced rCBF, but failure of AG to alter rCBF suggests that released HA may not be the sole mediator of these effects. Because elevations in plasma HA are probably due to HA derived from degranulation of mast cells, release of other bioactive substances from mast cells may also influence these cardiovascular effects. Surprisingly, in sham-irradiated monkeys, AG alone had a slight but significant hypotensive effect.

Introduction

Studies have shown elevated levels of circulating blood histamine (HA) in humans undergoing radiation therapy [1] and increased levels of HA in plasma of nonhuman primates [2–5] following irradiation. HA is implicated in radiation-induced hypotension [2] and in postirradiation reduced cerebral blood flow [3, 4]. Antihistamines attenuated the effects of HA released after irradiation and the concomitant early transient incapacitation (ETI) in the monkey [5, 6]. ETI, the complete, transient cessation of motor performance, occurs within the first 30 min after exposure to supralethal doses of ionizing radiation [7].

The metabolic pathways of HA in nonhuman primates have been studied less extensively than those in humans. In primates, as in rodents, HA is methylated, forming *tele*-methylhistamine (t-MH), which in turn is oxidized to *tele*-methylimidazoleacetic acid. HA is also deaminated by diamine oxidase (DAO), forming imidazoleacetaldehyde, which is converted to imidazoleacetic acid [8–10]. The pattern of labeled HA metabolites recovered in urine following slow infusion of small amounts of labeled HA into healthy humans suggests that, under these conditions, the contributions of each

[1] Address all correspondence to: Dr. Lorris G. Cockerham Biotechnical Services, Inc. 4700 West Commercial Dr., Suite B North Little Rock, AR 72116.
Supported by the Armed Forces Radiobiology Research Institute, Defense Nuclear Agency, under work unit 00105. Views presented in this paper are those of the authors; no endorsement by the Defense Nuclear Agency has been given or should be inferred. Research was conducted according to the principles enunciated in the "Guide for the Care and Use of Laboratory Animals" prepared by the Institute of Laboratory Animal Resources, National Research Council.

pathways to HA degradation are nearly equal [11]. Oral administration of 1 mg/kg of aminoguanidine (AG) (1 mg/kg) nearly abolished the amounts of oxidative metabolites, and enhanced the quantities of methylated metabolites and unmetabolized HA recovered in urine [11].

To facilitate measurements of HA in the plasma of rhesus monkeys, DAO is often inhibited, because its concentration in plasma is much higher in this species than in most other animals [12]. For example, one group (using a method with less sensitivity to HA than the one described below) reported that levels of HA in plasma from rhesus monkeys ranged from nondetectable to about 0.2 ng/ml [13]. Therefore, it is often useful to use a carbonyl reagent, such as AG, to inhibit enzymatic degradation of HA. Also, such inhibition would reduce the rates at which HA is metabolized after its levels are elevated [8, 14]. Although AG facilitated the measurement of HA levels in plasma, this agent had little effect on the hypotension of irradiation [unpublished data]. The effect of AG on cerebral blood flow in monkeys has not been previously investigated.

Because a relationship probably exists between release of HA, reduced mean arterial blood pressure (MABP), and decreased regional cerebral blood flow (rCBF) following irradiation [3, 4], we hypothesized that AG would alter these radiation-induced physiological responses. To test this hypothesis, we investigated the effects of AG treatment on these three parameters in irradiated and sham-irradiated monkeys.

Materials and methods

In this study, we used 23 rhesus monkeys (*Macaca mulatta*), weighing between 2.3 kg and 4.9 kg (3.3 ± 0.1 SEM). The animals were divided randomly into four groups: (1) six given saline (i.v.) 60 minutes before sham-irradiation, (2) five given AG (10 mg/kg, i.v.) in saline 60 minutes before sham-irradiation, (3) six given saline (i.v.) 60 minutes before irradiation, and (4) six given aminoguanidine (10 mg/kg, i.v.) in saline 60 minutes before irradiation. Food was withheld from all animals for 18 hours before the experiment, but water was available *ad libitum*. Research was conducted according to the principles enunciated in the *Guide for the Care and Use of Laboratory Animals* prepared by the Institute of Laboratory Animal Resources, National Research Council (USA). Monkeys were initially anesthetized in their cages with ketamine hydrochloride (20 mg/kg, i.m.) supplemented with 0.015 mg/kg atropine sulfate, and were then moved to the laboratory for the remainder of the experiment.

A systemic venous catheter was used to administer physiological saline and the principal anesthetic, α-Chloralose (100 mg), and supplemental infusions were provided as needed, based on heart rate, blood pressure, respiration rate, blood pH, and peripheral reflexes. A femoral arterial catheter was used to withdraw blood for blood chemistry and blood gas determinations and to measure systemic arterial blood pressure.

Approximately 2 hours before irradiation or sham-irradiation, the animals were intubated with a cuffed endotracheal tube and ventilated using a forced volume respirator to maintain stable blood pH and oxygen tension. After insertion of the endotracheal tube, each animal was placed on a circulating water blanket to maintain body temperature between 36 °C and 38 °C. A rectal probe monitored body temperature.

Using a technique previously described [3, 4, 15, 16], platinum-iridium wire electrodes were placed in the left and right hippocampi (CA1 region) in order to measure rCBF by hydrogen clearance. Measurements were taken for 30 minutes before irradiation or sham-irradiation and for 60 minutes thereafter. This technique is essentially an amperometric method that has been successfully employed in similar studies [3, 4, 15, 16].

After recording for 30 minutes, the animals were disconnected from the respirator and recording apparatus and irradiated in a separate room, using a bilateral, whole-body exposure to gamma ray photons from a ^{60}Co source located at the Armed Forces Radiobiology Research Institute. Exposure was limited to a mean dose of 46.8 seconds at 62.4 Gy/minutes steady state, free-in-air. Dose-rate measurements at depth were made with an ionization chamber placed in a tissue equivalent model. The measured midline tissue dose rate was 58.0 Gy/minutes, producing a calculated total dose of 50 Gy, taking into account the rise and fall of the radiation source. (The Gray (Gy), the Systeme International (SI) unit for absorbed dose, corresponds to an energy absorption of 1 J/kg or 100 rad.)

The animals were reconnected to the respirator and recording apparatus at 4 minutes postirradia-

tion or sham-irradiation and measurements were continued for a minimum of 60 minutes. At 30 and 10 minutes before irradiation or sham-irradiation, and at 2, 4 and 6 minutes after irradiation or sham-irradiation, blood samples were taken via the arterial catheter to determine plasma HA levels. Blood samples were taken to monitor stability of blood pH and oxygen tension, and respiration was adjusted to maintain pre-irradiation levels. MABP was determined via the arterial catheter during the experiment. After the experiment, the animals were humanely euthanized with an i.v. injection of saturated $MgSO_4$ while still under anesthesia. Brains were removed and dissected for visual verification of electrode placement.

Blood samples were drawn from the arterial catheter with plastic syringes and transferred to prelabeled, chilled collection tubes containing EDTA. The blood was then centrifuged (5°C) and the plasma was transferred to polypropylene tubes, rapidly frozen, and stored at −80°C until analyzed.

For measurements of plasma levels of HA, plasma was thawed, and 300 µl were transferred to 400-µl polypropylene tubes containing 100 µl of 100 m*M* sodium phosphate (NaP) buffer (pH 7.9). The mixture was vortexed, boiled for 10 minutes, cooled, and centrifuged at 50000 × *g* for 20 minutes. The supernatant (25 µl) was analyzed for HA. Quantitation of HA in samples collected 2, 4, or 15 minutes after irradiation often exceeded linear segments of the standard curve for HA content (2.5–250 pg base). Therefore, aliquots from these samples were diluted with 25-m*M* NaP buffer to 400 µl; 25 µl of this diluted mixture were analyzed for HA.

HA was methylated by tritiated S-adenosyl-L-methionine (SAM) in the presence of exogenous histamine N-methyltransferase (HMT) to form tritiated t-MH by modifications (in preparation) of the single isotope method of Salberg et al. [17] such that 2.5 pg (about fmol) of HA could be reliably measured.

Supernatants were transferred to 400-µl polypropylene tubes containing 5 µl of 50-m*M* NaP. HA standard solutions (5 µl of 2.5–250 pg base in 50-m*M* NaP) were added to tubes containing 25 µl of 25-m*M* NaP (pH 7.9). Methylation began after addition of a cocktail (10 µl) containing unlabeled SAM (Sigma Chemicals), [methyl-^{3}H]SAM (New England Nuclear), and HMT prepared from rat kidney, in 50-m*M* NaP buffer (pH 7.9). Final incubation concentrations were 1.03 µ*M* (13.4 Ci/mmol) and 14.8 µg protein (256 µmol/g protein/hr) for SAM and HMT, respectively. Blanks were identical to standard preparations but devoid of HA. To determine HA recovery, 5 µl of a solution containing 25 pg of HA in 50-m*M* NaP were added to aliquots of each assayed sample, and were processed in parallel.

The 40-µl mixture was incubated for 60 minutes in ice water, then quenched with 12.5 µl of 0.4-N $HClO_4$ containing unlabeled t-MH (50 µg/ml). After vortexing, 10 µl of 10-N NaOH and 200 µl of chloroform were added sequentially, vortexed, and centrifuged (2000 × *g*) for 2 minutes. The aqueous layer was aspirated away, and 50 µl of 3-N NaOH was added. The mixture was vortexed, re-centrifuged, and the aqueous layer was removed. Aliquots (100 µl) of the organic phase were transferred to scintillation counting vials. After the chloroform evaporated, scintillant (NEN-963, New England Nuclear) was added, and each vial was counted in a Beckman LS-3801 spectrophotometer. Standards and blanks were determined in quadruplicate, and the unspiked supernatant samples and those used for recovery, were analyzed in triplicate.

Blood pressure and blood flow data were grouped into 10 minute intervals, measured in relation to midtime of radiation. Data from each interval were averaged and plotted at the middle of the interval. The Shapiro-Wilk Test was used to assess normality of values of the various sample groups [18]. The Wilcoxon Rank Sum Test was used for the statistical analysis of the blood pressure, blood flow and HA data. A 95% level of confidence was employed to determine significance. Because all animals were treated identically before irradiation or sham-irradiation, and because the data for control and test animals showed no significant difference among monkeys at 30 minutes and 10 minutes before irradiation, pre-irradiation data for irradiated and sham-irradiated animals were combined for each monkey.

Results

The Shapiro-Wilk test, which assesses the composite hypothesis of normality [18], indicated that data from many samples were sufficiently inconsistent ($p<0.05$) with a normal distribution. This

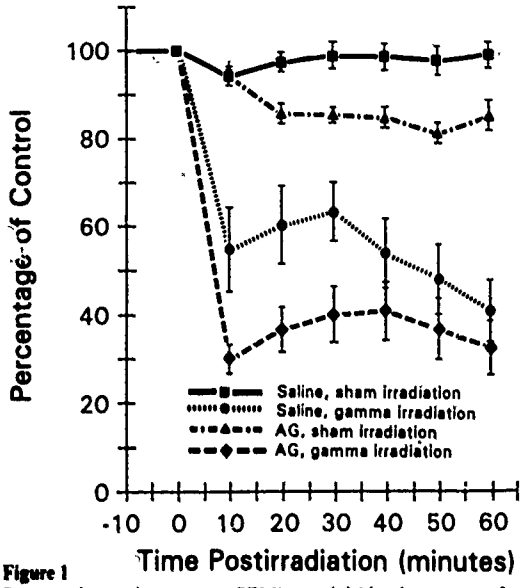

Figure 1
Percent change in mean (±SEM) arterial blood pressure after exposure to 50 Gy, whole-body, gamma irradiation, compared to a calculated pre-irradiation mean (99.8±1.8 mm Hg) determined from observations taken 30 min and 10 min before exposure. Changes in each monkey were based on their individual pre-irradiation mean arterial blood pressure. Twelve monkeys were pre-treated with saline 60 min before sham or gamma irradiation and eleven monkeys were pre-treated with aminoguanidine (AG) (10 mg/Kg, i.v.) 60 min before sham or gamma irradiation.

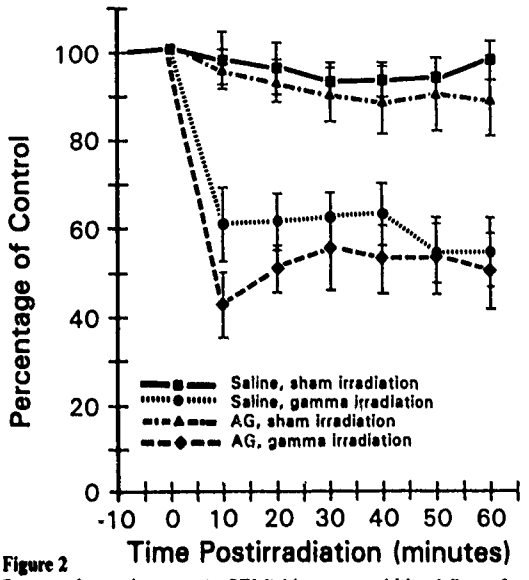

Figure 2
Percent change in mean (±SEM) hippocampal blood flow after exposure to 50 Gy, whole-body, gamma irradiation, compared to a calculated pre-irradiation mean (63.4±3.0 ml/g of tissue/min) determined from observations taken 30 min and 10 min before exposure. Changes in each monkey were based on their individual pre-irradiation hippocampal blood flow. Twelve monkeys were pre-treated with saline 60 min before sham or gamma irradiation and eleven monkeys were pre-treated with aminoguanidine (AG) (10 mg/Kg, i.v.) 60 min before sham or gamma irradiation.

finding encouraged us to use alternate methods, such as distribution-free techniques or non-parametric statistical procedures [18]. Therefore, the Wilcoxon Rank Sum Test was used for the final statistical analysis.

The MABP of both groups of irradiated animals decreased from the pre-irradiation mean of 99.8±1.8 mm Hg within 10 minutes after irradiation (Fig. 1). The irradiated group not treated with AG showed a drop to the 10 minutes postirradiation level that was 52% of the pre-irradiation value. The irradiated group treated with AG showed blood pressure levels that dropped to 30% of the pre-irradiation levels. These two levels were also significantly different for the remaining five observations in the two groups. The two control, sham-irradiated groups (one with AG and one without AG) were significantly different from each other at 20, 30, 50 and 60 minutes after sham-irradiation. However, these two groups were not significantly different from each other after 10 minutes and 40 minutes. The two groups of animals not treated with AG, one irradiated and one sham-irradiated, showed blood pressure levels that were always significantly different from each other after irradiation. Likewise, the two AG-treated groups of animals were significantly different after irradiation. In each of the four groups, the respiration of each subject was maintained at pre-irradiation levels, and the blood gas data revealed a general stability of blood pH and oxygen tension throughout the experiment (data not shown).

Fig. 2 displays a pre-irradiation mean blood flow of 63.4±3.0 ml per 100 g of tissue per minute in the hippocampus. Compared with sham-irradiated monkey, postirradiation blood flow values for both groups of irradiated animals showed a rapid ($p<0.01$) significant decline within 10 minutes after irradiation. The rCBF for the irradiated group treated with AG dropped markedly to 42% of the pre-irradiation level, while for the untreated, irradiated animals it only dropped to 60%. Although at most times after irradiation, rCBF of AG-treated monkeys was less than those given saline,

there was no significant difference between hippocampal blood flow levels of the two irradiated groups at any time after irradiation. Similarly, the two control, sham irradiated groups were not significantly different from each other or from pre-irradiation levels at any time after irradiation. The two groups of animals that were not treated with AG (one irradiated and one sham-irradiated) were significantly different ($p<0.01$) at each postirradiation time. Comparison of the two groups treated with AG also showed a significant difference ($p<0.01$) at all times after irradiation.

The mean (±SEM) pre-irradiation plasma HA level, averaged from 30 minute and 10 minute pre-irradiation levels of all monkeys, was 1.38 ng/ml ± 0.26 ng/ml (Fig. 3). Levels of HA for both sham-irradiated groups of monkeys showed no significant changes at any time during the experiment. After irradiation, HA levels for both irradiated groups showed abrupt increases within 2 minutes to levels that were significantly higher than the pre-irradiation levels. HA levels in Plasma of the AG-treated, irradiated group were also significantly higher than those in the sham-irradiated monkeys and in untreated, irradiated monkeys for all postirradiation observations. However, among monkeys that were not pretreated with AG, plasma levels of HA in irradiated monkeys significantly exceeded plasma levels in sham-irradiated monkeys after 2 minutes ($p<0.01$), but were not significantly higher after 4 or 6 minutes.

For all monkeys ($n=23$), the mean (±SEM) of the HA levels in samples of plasma collected 30 minutes before (−30 minutes) irradiation or sham-irradiation (1.46 ng/ml ± 0.49 ng/ml) exceeded those of samples collected 10 minutes before (−10 minutes) irradiation (1.30 ng/ml ± 0.23 ng/ml). Although this difference was not statistically significant, levels of HA were more often (16 of 23) higher in samples taken at −30 minutes. For all sham-irradiated monkeys ($n=11$), there were no correlations ($p<0.2$) between levels of HA in plasma collected at −30 minutes or at −10 minutes versus levels in samples taken 2, 4, or 6 minutes after sham-irradiation. There was a correlation (Spearman's rho = 0.66, $p<0.05$), however, between samples collected at −30 minutes and −10 minutes. For sham-irradiated monkeys, the mean (±SEM) levels (ng/ml) of HA in plasma collected at −30 minutes and −10 minutes, averaged together (1.66 ± 0.58), slightly but significantly (Wilcoxon test) exceeded

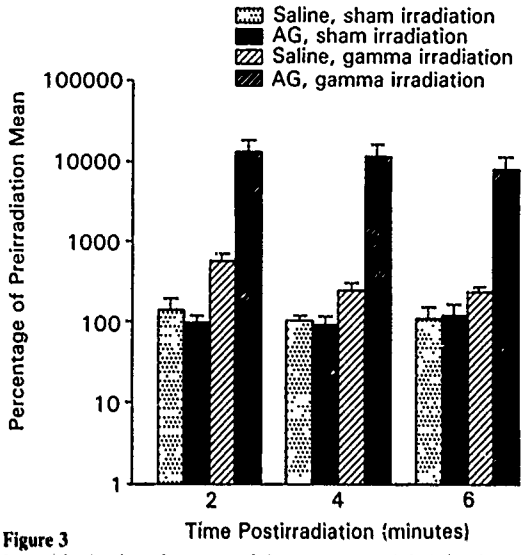

Figure 3
Logarithmic plot of percent of change (mean ± SEM) in plasma HA concentration after exposure to 50 Gy, whole body, gamma irradiation. Differences in concentration were calculated from the mean of levels (1.38 ± 0.26 ng/ml) determined from all monkeys 30 min and 10 min before exposure. Changes in each monkey were based on their individual pre-irradiation levels of HA. Twelve monkeys were pre-treated with saline 60 min before sham or gamma irradiation and eleven monkeys were pre-treated with aminoguanidine (AG) (10 mg/Kg, i.v.) 60 min before sham or gamma irradiation.

mean levels of samples collected 2 minutes (1.14 ± 0.34, $p<0.01$), 4 minutes (0.99 ± 0.24, $p<0.05$), or 6 minutes (0.78 ± 0.09, $p<0.05$) after sham-irradiation; however, none of the mean levels from 2, 4, or 6 minutes after sham-irradiation different significantly from any other. No significant differences (each $p<0.3$) existed among sham-irradiated monkeys in levels of HA for drug-treated or drug-free monkeys at any time during the study.

Discussion

The initial precipitous decline in postirradiation rCBF in the rhesus monkey reported here (Fig. 2) has been observed previously [3, 4, 15, 16, 19]. This decline previously has been associated consistently with an immediate fall in MABP. In primates, a critical MABP of 50% to 60% of normal is necessary for adequate autoregulation of cerebral circulation [6, 19, 20].

The measurements of blood flow in the hippocampus of monkeys exposed to 50 Gy of gamma radiation, when plotted at postirradiation times

(Fig. 2), presents a graph strikingly similar to the MABP graph of the monkey (Fig. 1). The abrupt increase in plasma HA levels 2 minutes after irradiation (Fig. 3) coincides with the initial depression in MABP (Fig. 1) and rCBF (Fig. 2). The involvement of HA is further supported by investigators who have reported the attenuation of radiation-induced ETI by the administration of antihistamines [6].

The levels of HA we found corroborate results from previous studies [2–5] by showing an immediate rise within 2 minutes after irradiation in nonhuman primates. Our results also demonstrate that AG has a pronounced effect on the postirradiation levels of HA. Irradiated monkeys given AG had levels of HA in plasma that were at least ten fold higher than those that were not treated with AG (Fig. 3). No significant differences were noted in the plasma HA levels of the two groups of sham-irradiated monkeys at any time. Additionally, the plasma HA levels in the saline-treated, irradiated monkeys were not significantly different from the levels in the control animals 4 minutes and 6 minutes post-irradiation. This is indicative of the primate's rapid metabolism through the oxidative pathway of the extremely high levels of HA in plasma that follow exposure to gamma radiation. Before development of techniques with sufficient sensitivity to measure plasma levels of HA in primates, like the one used here, investigators often pretreated primates with a DAO inhibitor to facilitate measurement of plasma HA. We measured plasma HA levels even in sham-irradiated monkeys that were not treated with AG. It seemed logical that, in primates, further studies of the effects of the radiation-induced release of HA (such as hypotension, induction of other intermediate agents, and central nervous system effects) might show a clearer, more accurate picture without a DAO inhibitor. The presence of a DAO inhibitor clearly affects the metabolism of newly released HA, elevating its peak concentrations and retarding its rate of disappearance (Fig. 3). Thus, using a paradigm that provoked a massive release of endogenous HA, we confirmed the observations of others [21] who showed that AG augmented the levels of HA given to dogs. In dogs and other species, AG shortened survival times following induction of intestinal ischemia [22, 23], presumably by extending the duration of histamine's deleterious effects.

In the absence or presence of a DAO inhibitor, we observed subtle, time-related differences in plasma levels of HA, findings that may extend beyond studies of the effects of radiation. The levels of HA in plasma collected before sham-irradiation of the monkeys showed a general decline with time, from about 1.5 ng/ml (at −30 minutes) to about 0.8 ng/ml in sham-irradiated monkeys. We attribute this small but statistically significant reduction to anesthetic-induced release of HA and its subsequent metabolism. The correlation between levels in samples taken at −30 minutes and −10 minutes, and lack of correlation or significant differences among samples collected after −10 minutes, suggests that the slightly elevated levels of HA may have been declining up until the time of sham-irradiation. At about this time, levels tended to stabilize; random differences among these lower levels probably abolished any relationship between levels in samples collected from the same animals. Conversely, among the same AG-treated, sham-irradiated monkeys, there was a significant relationship between the rank order of levels at −30 minutes and −10 minutes, a sequelae that we anticipated, based on the incomplete metabolism of HA, whose levels were almost certainly elevated after pretreatment with anesthetic. The phenomenon of anesthetic-induced release of HA during the course of surgical manipulation has been seen clinically [24–26]. In addition, the stress of surgery alone has been linked to the release of HA in humans [27]. This experiment shows that without additional doses of anesthetic, such as α-chloralose or atropine (which stimulate release of HA), as much as 2 hours may be required for plasma HA levels to return to near basal levels. This seems to be true whether or not AG is present.

AG pretreatment had a pronounced effect on postirradiation blood pressure. There was a significant difference between the treated and untreated groups of animals 10 minutes after irradiation. This corresponded with the postirradiation levels of plasma HA in the irradiated groups. Therefore, using AG to inhibit the enzymatic deamination of HA caused a significant difference in the postirradiation level of plasma HA and in the postirradiation hypotension. However, changes associated with AG may not be related exclusively to alterations in HA levels in plasma. For example, when comparing the two nonirradiated groups of animals, one can see that treatment with AG alone

had a significant effect on blood pressure (Fig. 1) although there were no significant differences in levels of HA between these groups in the first few minutes of the study (Fig. 3). The reason(s) for this minor, but statistically significant, 10-percent reduction in MABP is unclear. Also, we cannot explain why HA metabolism was altered in these unconscious monkeys more than 10 minutes after sham-irradiation. The simplest hypothesis to account for these changes is that AG, at the doses used, exerts hypotensive effects independent of its influence on HA metabolism in primates.

Unlike the changes observed in HA levels and blood pressure, rCBF responses in the sham-irradiated groups and irradiated groups were not significantly altered by the administration of AG. Although the two irradiated groups were significantly different from the two sham-irradiated groups, the irradiated groups were not significantly different from each other, nor were the sham-irradiated groups significantly different from each other (Fig. 2).

The drug-related differences in the level of HA (Fig. 3) cannot be reconciled immediately with the lack of a significant difference in rCBF (Fig. 2). Several possibilities may account for this. The postirradiation release of HA may not be directly responsible for reductions in rCBF. Instead, another intermediate agent(s) may be involved. For example, it is established that neurotensin (NT) is rapidly released in response to radiation [4]. Rioux et al. [28] showed in rats that the NT-induced release of HA was associated with cerebral edema, and that the increased resistance to blood flow in the brain was attributed to NT-induced release of serotonin (5-HT). Certainly, HA may affect rCBF through its effect on systemic arterial blood pressure. However, if the continued presence of HA produced a significant difference in blood pressure, it would follow that a significant change in cerebral blood flow would occur if HA were the sole regulator of rCBF.

Conversely, the enormous surge in levels of HA suggests that HA may achieve "ceiling-effects" within minutes. Such levels could trigger a sequela of responses that persist long after the removal of HA (by metabolism or diffusion) has occurred. Because correlations could not be made between several intermediate concentrations of HA and degrees of rCBF, our findings cannot resolve these possibilities. Under less severe provocations of HA release, or after administration of HA or HA agonists, HA alone may be a sufficient trigger to alter rCBF [29].

Besides the potential for HA to alter rCBF through its hypotensive actions, HA is also a direct acting cerebral vasodilator when applied *in vitro* or topically [29]. Furthermore, infusing HA into humans resulted in decreased MABP and altered rCBF [30, 31]. However, in another study, similar treatment altered neither MABP nor rCBF [32]. Therefore, the net effect of small concentrations or higher levels (Fig. 3) of HA on rCBF is unclear.

For these reasons, a unitary hypothesis that attempts to explain radiation-induced effects solely through either intra- or extra-cranial histaminergic mechanisms may be misguided. Mast cells, the likely origin of HA after irradiation-induced degranulation [33], will release other bioactive substances along with HA, including leukotrienes, prostaglandins, 5-HT, and heparin. Radiation-induced release of free radicals also influences mast cell degranulation [33, 34]. However, the administration of disodium cromoglycate [15], an efficient hydrated electron scavenger [35], did not decrease the radiation-induced release of HA in nonhuman primates.

This experiment showed that pretreatment of primates with the DAO inhibitor, AG, altered the postirradiation levels of plasma HA and the hypotensive response to radiation, but did not alter postirradiation rCBF response. It also showed that AG alone produced a small but significant hypotensive effect. The experimental conclusions further suggest that the radiation-induced release of HA may not be directly or solely responsible for the radiation-induced decrease in rCBF. Perhaps the radiation-induced release of another intermediate(s), such as serotonin, may better account for the profound reduction in rCBF [36].

Acknowledgements

The authors thank Mr. E. J. Golightly for technical assistance.

Received 20 May 1990; accepted by W. Lorenz, 27 September 1990

References

[1] E. C. Lasser and K. W. Stenstrom, *Elevation of circulating blood histamine in patients undergoing deep roentgen therapy.* Am. J. Roentgenol. *72*, 985–988 (1954).

[2] W. A. Alter, III, R. N. Hawkins, G. N. Catravas, T. F. Doyle and J. K. Takenaga, *Possible role of histamine in radiation*

induced hypotension in the rhesus monkey. Radiat. Res. *94,* 654 (1983).

[3] L. G. Cockerham, T. J. Cerveny and J. D. Hampton, *Postradiation regional cerebral blood flow in primates.* Aviat. Space Environ. Med. *57,* 578–582 (1986).

[4] L. G. Cockerham, E. L. Pautler, R. E. Carraway, D. E. Cochrane and J. D. Hampton, *Effect of disodium cromoglycate (DSCG) and antihistamines on postirradiation cerebral blood flow and plasma levels of histamine and neurotensin.* Fundam. Appl. Toxicol. *10(2),* 233–242 (1988).

[5] T. F. Doyle and T. A. Strike, *Radiation-released histamine in the rhesus monkey as modified by mast-cell depletion and antihistamine.* Experientia *33,* 1047–1048 (1977).

[6] T. F. Doyle, C. R. Curran and J. E. Turns, *The prevention of radiation-induced, early transient incapacitation of monkeys by an antihistamine.* Proc. Soc. Exper. Biol. Med. *145,* 1018–1024 (1974).

[7] D. J. Kimeldorf and E. L. Hunt, *Neurophysiological effects of ionizing radiation.* In *Ionizing radiation: neural function and behavior.* pp. 59–108 (Eds. D. J. Kimeldorf and E. L. Hunt) Academic, New York 1985.

[8] C. Maslinski, *Histamine and its metabolism in mammals. Part II: Catabolism of histamine and histamine liberation.* Agents and Actions *5,* 183–225 (1975).

[9] M. A. Beaven, *Factors regulating availability of histamine at tissue receptors.* In *Pharmacology of histamine receptors.* pp. 103–145 (Eds. C. R. Ganellin and M. E. Parsons) Wright, Bristol 1982.

[10] J. P. Green, G. D. Prell, J. K. Khandelwal and P. Blandina, *Aspects of histamine metabolism.* Agents and Actions *22,* 1–15 (1987).

[11] J. Bergmark and G. Granerus, *Ion exchange chromatography for quantitative analysis of radioactive histamine metabolites in human urine.* Scand. J. Clin. Lab. Invest. *34,* 365–373 (1974).

[12] G. R. Gordon and J. H. Peters, *Plasma histaminase activity in various mammalian species, a rapid method of assay.* Proc. Soc. Exp. Biol. Med. *124,* 339–404 (1967).

[13] A. P. Almeida, W. Flye, D. Deveraux, Z. Horakova and M. A. Beaven, *Distribution of histamine and histaminase (diamine oxidase) in blood of various species.* Comp. Biochem. Physiol. *67C,* 187–190 (1980).

[14] T. L. Sourkes and K. Missala, *Putrescine metabolism and the study of diamine oxidase activity in vivo.* Agents and Actions *11,* 20–27 (1981).

[15] L. G. Cockerham, T. F. Doyle, E. L. Pautler and J. D. Hampton, *Disodium cromoglycate, a mast cell stabilizer, alters postradiation regional cerebral blood flow in primates.* J. Toxicol. Environ. Health *18,* 91–101 (1986).

[16] L. G. Cockerham, C. M. Arroyo and J. D. Hampton, *Effects of 4-hydroxypyrazolo (3,4-d) pyrimidine (Allopurinol) on postirradiation cerebral blood flow: Implications of free radical involvement.* Free Radic. Biol. Med. *4(5),* 279–284 (1988).

[17] D. J. Salberg, L. B. Hough, D. E. Kaplan and E. F. Domino, *A reverse double-isotope enzymatic histamine assay: advantages over single-isotope methods.* Life Sci. *21,* 1439–1446 (1977).

[18] S. S. Shapiro and M. B. Wilk, *An analysis of variance test for normality.* Biometrika *52,* 591–611 (1965).

[19] P. H. Chapman and R. J. Young, *Effect of cobalt-60 gamma irradiation on blood pressure and cerebral blood flow in the Macaca mulatta.* Radiat. Res. *35,* 78–85 (1968).

[20] J. K. Farrar, F. W. Gamache, Jr., G. G. Ferguson, J. Barker, G. P. Varkey and C. G. Drake, *Effects of profound hypotension on cerebral blood flow during surgery for intracranial aneurysms.* J. Neurosurg. *55,* 857–864 (1981).

[21] J. Sattler, R. Hesterberg, W. Lorenz, U. Schmidt, M. Crombach and C.-D. Stahlknecht, *Inhibition of human and canine diamine oxidase by drugs used in an intensive care unit: relevance for clinical side effects?* Agents and Actions *16,* 91–94 (1985).

[22] J. Kusche, C.-D Stahlknecht, W. Lorenz, G. Reichert and W. Dietz, *Comparison of alterations in the histamine-diamine oxidase system during acute intestinal ischemia in pigs, dogs and rabbits: Evidence for a uniform pathophysiological mechanism?* Agents and Actions *9,* 49–52 (1979).

[23] J. Kusche, W. Lorenz and R. Hesterberg, *The relevance of the diamine oxidase-histamine system for shock development following intestinal ischemia.* In *Animal models for intestinal disease.* pp. 255–280 (Ed. C. J. Pfeiffer) CRC Press, Inc., Baca Raton, Florida, 1985.

[24] W. Lorenz and A. Doenicke, *Anaphylactoid reactions and histamine release by barbiturate induction agents: clinical relevance and pathomechanisms.* J. Anesth. *63,* 351–352 (1985).

[25] W. Lorenz, H. D. Roher, A. Doenicke and Ch. Obmann, *Histamine release in anaesthesia and surgery: a new method to evaluate its clinical significance with several types of causal relationship.* Clin. Anesth. *2,* 403–426 (1984).

[26] J. Moss and C. E. Rosow, *Histamine release by narcotics and muscle relaxants in humans.* Anesthesiology *59,* 330–338 (1983).

[27] W. Lorenz, W. Seidel, A. Doenicke, R. Tauber, H.-J. Reimann, R. Uhlig, G. Mann, P. Dormann, A. Schmal, G. Hafner and H. Hamelmann, *Elevated plasma histamine concentrations in surgery: Causes and clinical significance.* Klin. Wschr. *52,* 419–425 (1974).

[28] F. Rioux, R. Kerouac and S. St-Pierre, *Release of mast cell mediators, vasoconstriction and edema in the isolated, perfused head of the rat following intracarotid infusion of neurotensin. Neuropeptides 6,* 1–12 (1985).

[29] P. M. Gross, *Cerebral histamine: Indications for neuronal and vascular regulations.* J. Cereb. Blood Flow Metabol. *2,* 3–23 (1982).

[30] R. W. Alman, M. Rosenberg and J. F. Fazekas, *Effects of histamine on cerebral hemodynamics and metabolism.* A. M. A. Arch. Neurol. Psychiat. *67,* 354–356 (1952).

[31] H. A. Shenkin, *Effects of various drugs upon cerebral circulation and metabolism of man.* J. Appl. Physiol. *3,* 465–471 (1951).

[32] A. A. Krabbe and J. Olesen, *Effect of histamine on regional cerebral blood flow in man.* Cephalalgia *2,* 15–18 (1982).

[33] M. A. Donlon and T. L. Walden, Jr., *The release of biologic mediators in response to acute radiation injury.* Comments Toxicol. *2,* 205–216 (1988).

[34] P. F. Mannaioni and E. Masini, *The release of histamine by free radicals.* Free Radic. Biol. Med. *5,* 177–197 (1988).

[35] A. J. Carmichael, C. M. Arroyo and L. G. Cockerham, *Reaction of disodium cromoglycate with hydrated electrons.* Free Radic. Biol. Med. *4,* 215–218 (1988).

[36] L. G. Cockerham, C. D. Forcino, T. C. Pellmar and S. W. Smart, *Effect of methysergide on postirradiation hypotension and cerebral ischemia.* Proceedings of the Cerebral Hypoxia and Stroke Symposium, Budapest, Hungary, August 22–24, 1987.

GASTROENTEROLOGY 1991;100:884–891

Gastric Injury and Invasion of Parietal Cells by Spiral Bacteria in Rhesus Monkeys

Are Gastritis and Hyperchlorhydria Infectious Diseases?

ANDRE DUBOIS, ANDRZEJ TARNAWSKI, DIANE G. NEWELL, NANCY FIALA, WOJCIECH DABROS, JERSEY STACHURA, HOWARD KRIVAN, and LILLIE M. HEMAN-ACKAH

Laboratory of Gastrointestinal and Liver Studies, Digestive Diseases Division, Department of Medicine, Uniformed Services University of the Health Sciences, and Departments of Physiology and Veterinary Medicine, Armed Forces Radiobiology Research Institute, Bethesda, Maryland; V.A. Medical Center and University of California at Irvine, Long Beach and Irvine, California; Public Health Laboratory Service, Center for Applied Microbiology & Research, Salisbury, Wiltshire, England; Laboratory of Structural Biology, National Institutes of Health, Bethesda, Maryland; and Biocarb, Inc., Gaithersburg, Maryland

The possibility of using the rhesus monkey as a model for studying gastric function in the presence of infection with spiral bacteria was studied. Endoscopic evaluation of the gastric mucosa was performed under general anesthesia in 29 colony-bred rhesus monkeys, and gastric pinch biopsy specimens were obtained from each animal. On a separate day, gastric emptying and acid output were determined using a ^{99m}Tc dilution technique. Biopsy samples were fixed for light microscopy (H&E, Gram, and Warthin–Starry stains) and for transmission electron microscopy. The presence of spiral bacteria and gastritis was assessed and rated on coded slides. In 8 of 29 monkeys, *Helicobacter pylori*–like organisms were observed in close proximity to the mucosal epithelial cells or in the lumen of the gastric pits. In 14 other monkeys, "*Gastrospirillum hominis*"–like organisms were observed in the mucus covering the surface of epithelial cells, in the lumina of the gastric glands, and overlying parietal cells. Gastritis was present in 8 of 8 animals positive for *H. pylori*–like organisms, in 2 of 14 animals positive for "*G. hominis*"–like organisms, and in none of the uninfected monkeys, and the mean gastritis index was significantly greater in animals positive for *H. pylori*–like organisms. Moreover, acid output was significantly higher in monkeys positive for "*G. hominis*"–like organisms than in controls or animals positive for *H. pylori*–like organisms. Gastric emptying was not significantly different in the three groups. In conclusion, (a) *H. pylori*–like, but not "*G. hominis*"–like, organisms cause gastritis while not modifying acid output; (b) "*G. hominis*"–like, but not *H. pylori*–like organisms, invade and on occasion damage parietal cells while apparently causing hyperchlorhydria; and (c) the rhesus monkey appears to be a good model for the study of gastric infection with spiral bacteria.

The cause of gastritis and of gastric ulcer is unknown, but gastric acid secretion is believed to play an important role in the pathogenesis of these conditions. Epidemiological data have suggested that histological gastritis may be caused by *Helicobacter pylori* (previously named *Campylobacter pylori*) and that the increased prevalence of this disease in older individuals is associated with a greater frequency of

Abbreviations used in this paper: BAO, basal acid output; CFU, colony forming units; DTPA, diethylene triamine pentacetic acid; GHLO, "*Gastrospirilium hominis*"–like organisms; HPLO, *Helicobacter pylori*–like organisms; PAO, postload acid output; SDS, sodium dodecyl sulfate.

0016-5085/91/$3.00

infection with this organism (1). Experimental transmission of *H. pylori* to two healthy volunteers has resulted in acute clinical illnesses characterized by epigastric pain, histological gastritis, and hypochlorhydria (2,3). Both subjects were treated with antimicrobial agents, and one of them recovered rapidly and completely. However, the other subject developed chronic gastritis which was only partly healed 103 days after ingestion of the bacteria. No duodenal ulcer developed in either subject. Although these observations suggest that chronic gastritis may be provoked by gastric mucosal infection with spiral bacteria, direct proof of a causal relationship is still lacking. Recently, another spiral organism, "*Gastrospirillum hominis*," has been observed in patients suffering from upper gastrointestinal symptoms (4–7), but the pathogenicity of this bacterium is presently unclear. Because ethical considerations preclude experimental infection of humans until a completely effective treatment against gastric infection with spiral bacteria becomes available, the evaluation of this question requires the development and validation of animal models.

Several animal species have been studied. Early investigators recognized the presence of spiral organisms (spirilla, spirochetes) in the stomachs of cats, dogs, and monkeys (8–10). More recently, spirilla isolated from the cat stomach were cultured (11), and intragastric administration of 10^9–10^{10} colony-forming units (CFU) of these isolates to mice resulted in gastric colonization in 80% of the animals (12). Like *H. pylori*, this spirillum is urease positive and morphologically resembles "*G. hominis*," although its ultrastructure is markedly different. *H. mustelae* has been isolated from both normal and inflamed gastric mucosae of ferrets (13), but this subspecies is morphologically and immunologically different from human *H. pylori*. Oral challenge of gnotobiotic piglets with 10^8 CFU of human *H. pylori* isolates was followed by colonization of the gastric mucosa and chronic gastric inflammation, and *H. pylori* were recovered from gastric mucosal samples obtained at necropsy up to 24 days after infection (14,15). However, only one of the challenge strains could be recovered from piglets' stomachs (16) and there was no prolonged accumulation of polynuclear leukocytes (14,15). Therefore, to date, these animal models do not appear to adequately mimic human diseases.

Other studies demonstrated that the gastric mucosa of rhesus monkeys may be spontaneously infected with organisms that closely resemble human strains of *H. pylori* (17–19). To evaluate and characterize this potentially useful model, we determined the prevalence of spiral bacteria in 29 domestic colony born rhesus monkeys, and concurrently measured the degree of gastritis, as well as the rates of gastric acid secretion and of gastric emptying.

Materials and Methods

Twenty-nine male rhesus monkeys, *Macaca mulatta* (age, 2–3 years; weight, 3.1 ± 0.2 kg; means ± SEM), were housed in individual stainless steel cages in conventional holding rooms of an American Association for Accreditation of Laboratory Animal Care–accredited animal facility where they were quarantined for 90 days. Monkeys were provided with tap water ad libitum, commercial primate chow, and fruits. After testing negative for tuberculosis three times at 2-week intervals, the monkeys were adapted to a primate restraining chair and were subsequently studied between 8 AM and noon after an overnight fast.

Each monkey underwent gastric endoscopic examination under general anesthesia (ketamine HCl, 10 mg/kg) using an 81200 Welch–Allyn videogastroscope with an outer diameter of 9.8 mm (Welch–Allyn, Skaneateles Falls, NY). The macroscopic appearance of fundic and antral mucosae was assessed qualitatively. Multiple pinch biopsy specimens (average number, 3) of the gastric mucosa were obtained from both the distal corpus and the antrum of each animal. The specimens were fixed in neutral buffered formalin and routinely processed for light microscopy. Five-micrometer paraffin sections were stained using H&E, the Warthin–Starry method, or Gram method and viewed under magnification ranging from ×100 to ×1,000 (oil immersion). After familiarization of one of us (N.F.) with the appearance of the bacteria present in uncoded slides stained with Warthin–Starry, Gram, or H&E (see below in Results), H&E–stained slides were coded and scored at 1,000× using a scale of 0 to 3 (index 0, no bacteria; 1, 1–3 aggregates seen in 1 to 2 of 10 fields of view; 2, 1–3 aggregates seen in 3 to 7 of 10 fields; 3, 3–5 aggregates seen in 8 to 10 of 10 fields). The presence and extent of gastritis was rated independently from the scoring for infection on coded H&E slides using a scale of 0 to 3 (index 0, intact mucosal lining and minimal infiltration of the lamina propria with lymphocytes and plasma cells; 1, mild increase of mononuclear infiltration, localized in upper half of the mucosa; 2, marked mononuclear infiltration extending from the surface to the muscularis mucosae, superficial erosions; 3, presence of polymorphonuclear leukocytes in glands, associated with marked mononuclear infiltration, and erosions).

Other pinch biopsy specimens obtained in 10 of these monkeys were fixed in Karnovsky's solution and processed routinely for transmission electron microscopy (20). Coded ultrathin sections were evaluated blindly by two independent investigators (A.T. and W.D.) to determine the presence of spiral bacteria using a Philips 400 transmission electron microscope at 80 kV (Bethesda, MD).

In addition, biopsy specimens obtained in 14 of these monkeys were immediately placed in sterile 0.9% NaCl, kept on ice, vortexed within 1 hour of sampling, and grown on blood agar plates under microaerophilic conditions. The growth that was observed in three of these biopsy samples was tested for urease activity (21). Furthermore, a 10%–25% linear gradient sodium dodecyl sulfate (SDS)-polyacrila-

mide gel electrophoresis (PAGE) system (22) was used to determine the total protein profiles of these three cultures. Electroblots of the SDS-PAGE gels were then incubated with either hyperimmune rabbit anti-*H. pylori* antisera or mouse monoclonal antibody (CP11) directed against *H. pylori* urease (22–24).

The same 29 colony-bred rhesus monkeys were studied on a separate day using a previously described marker dilution technique (25,26) to concurrently measure gastric acid secretion and emptying. A size 12F double-lumen nasogastric Ventrol Levine tube (National Catheter, Mallinckrodt, Argyle, NY) was placed in the stomach, and samples of the mixed gastric contents were aspirated just before and immediately after intragastric administration of 5–20 mL of a ^{99m}Tc–diethylene triamine pentacetic acid (DTPA) test solution (30 μCi/100 mL distilled water; pH 7.4; 37°C) and centrifuged. The clear supernatant of each sample was assayed for ^{99m}Tc and acid concentrations using an autogamma counter (1282 Compugamma; LKB Instruments Inc., Gaithersburg, MD) and a titration assembly (Radiometer, Oberlin, OH). These determinations were repeated at 10-minute intervals during a 40-minute fasting period and for 60 minutes after intragastric instillation of an 80-mL water meal containing ^{99m}Tc-DTPA (3 μCi/100 mL; pH 7.4; 37°C) (postmeal period). Fractional gastric emptying rate and acid output were then calculated as previously described (25,26).

Statistical Analysis

Results were expressed as means ± SEM. A two-way analysis of variance with repeated measures (27) was used to determine the effects due to type of infection, time, or an interaction among these two factors. This statistical method takes into account the fact that multiple measurements are repeated in the same animals over time by establishing a distinction between a factor that classifies the subjects into groups (grouping factor) and a factor for which each subject is measured at all levels (within subject factor). Computer implementation of this statistical method was performed using locally developed programs.

Results

At gastroscopy, patches of erythema and localized pallor was observed in 5 of 29 animals suggesting the presence of superficial gastritis in 17% of animals. However, as in humans, this appearance correlated poorly with infection and microscopic gastritis.

No evidence of microscopic gastritis or mucosal infection was observed in the biopsy specimens of seven of the monkeys with no endoscopic symptoms of gastritis. In the remaining 22 animals, two morphologically distinct types of bacteria were observed in the pinch biopsy specimens that were harvested, but only one of these was identified in any individual animal.

In 8 of 29 monkeys, curved, rod shaped bacteria measuring 3–4 μm × 0.5–1.0 μm were observed under light microscopy in close proximity to the mucosal epithelial cells (Figure 1*A*) or in the lumina of the gastric pits (Figure 1*C*), and the infection index was 2.2 ± 0.2 (means ± SE; Figure 2). These organisms were associated with superficial erosions as well as marked mononuclear and polynuclear infiltration (Figure 1*A*), but they were never observed within gastric mucosal cells. As a result, a gastritis index of 2.4 ± 0.2 was calculated for this group of monkeys (Figure 2). Urease-positive growth was obtained under microaerophilic conditions from three of the four biopsy specimens harvested in four of these animals, and these cultures were macroscopically and microscopically identical to those obtained with human *H. pylori* strains. The total protein profiles of these bacterial strains were identical to those of human strains of *H. pylori* (Figure 3). Incubation of electroblots of the SDS-PAGE gels with either hyperimmune rabbit anti-*H. pylori* antisera or mouse monoclonal antibody (CP11) directed against *H. pylori* urease demonstrated identical antigenic profiles of the monkey isolates compared with human *H. pylori* strains (Figure 4). Thus, because no morphological, biochemical, or antigenic differences were found between these monkey spiral bacteria and human *H. pylori*, they are termed *H. pylori*–like organisms (HPLO).

In 14 other monkeys, tightly coiled spiral-shaped bacteria measuring 4–7.5 μm × 0.5–1.0 μm were found in the mucus covering the surface of epithelial cells (Figure 1*B*), in the lumina of the gastric pits and deeper glands (Figure 1*D*), and overlying parietal cells (Figure 1*D*, *insert*). Although these bacteria were found in close proximity to healthy superficial epithelial cells (Figure 1*B*) and damaged crypt cells (Figure 1*D*) as well as within intact parietal cells (Figure 1*D*, *insert*), mononuclear and/or polynuclear infiltration was observed in only 2 animals. Therefore, gastritis index was significantly lower in these monkeys than in HPLO-positive animals (0.6 ± 0.2 vs. 2.4 ± 0.2; $P < 0.05$) and was not different from the index of uninfected animals (Figure 2). No urease-positive bacterial growth was observed in microaerophilic culture of any of the biopsy samples obtained in 10 of these monkeys. Ultrastructural examination of biopsy samples obtained in 5 of these 14 monkeys showed that these bacteria were present in intact parietal cell canaliculi (Figure 5*A*) and within the cytoplasm of parietal cells undergoing different stages of injury (Figure 5*B* and *C*). In addition, some of the bacteria appeared to be partly digested (Figure 5*D*). These bacteria more closely resembled human "*C. hominis*" (4) than those observed in cats and in dogs (9–11) and are therefore termed "*C. hominis*" like organisms (GHLO).

Neither basal acid output (BAO) nor peak postload acid output (PAO) were significantly different in HPLO-positive monkeys compared with uninfected

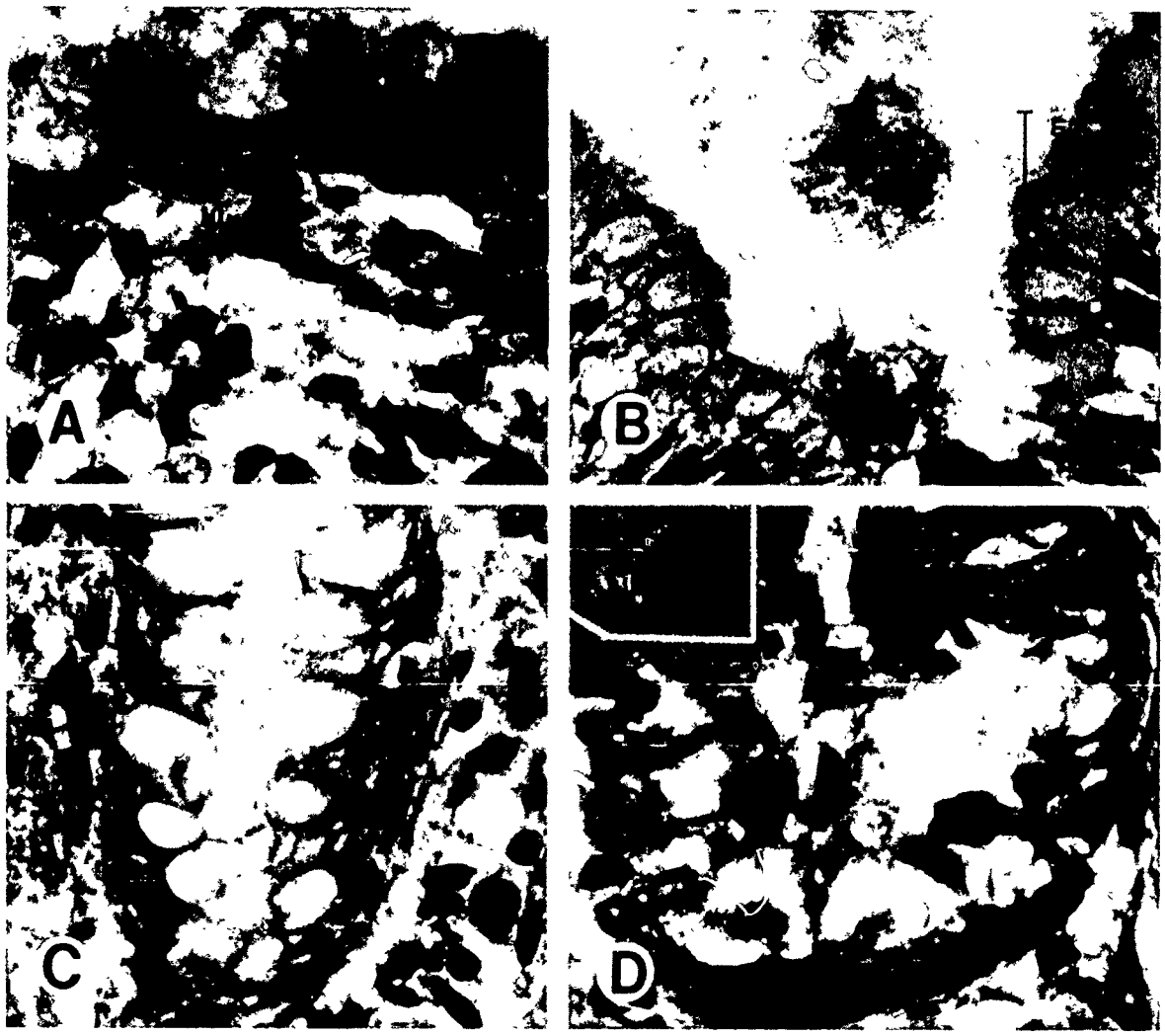

Figure 1. Effect of infection with spiral bacteria on rhesus monkey superficial gastric mucosa (H&E; original magnification ×1000).

A. H. pylori like organisms (HPLO) associated with superficial antral erosions and with superficial mononuclear infiltration.

B. Superficial epithelial cells do not appear to be affected by the presence of "*C. hominis*"-like organisms (GHLO).

C. Healthy crypt cells lined by HPLO.

D. Marked cytolysis associated with GHLO at the bottom of a gastric gland, *inset* (original magnification ×2000), apparently healthy parietal cell containing four GHLO.

monkeys (Figure 6). In contrast, both BAO and PAO were significantly increased in GHLO-positive monkeys compared with uninfected animals as well as compared with HPLO positive monkeys (Figure 6). Gastric fractional emptying rates tended to be slower in both HPLO-positive and GHLO positive animals, but the difference was not statistically significant (2.4% ± 0.2% per minute and 2.2% ± 0.4% per minute, respectively, vs. 3.4% ± 0.8% per minute).

Discussion

Gastritis and hypochlorhydria have been considered to be inexorable signs of aging and may predispose to cancer of the stomach. Early investigators postulated an infectious origin for these syndromes, but it is only during the last decade that *H. pylori* was implicated as a possible causative agent (1). The concept of a possible infectious origin of ill defined gastric diseases was broadened by the discovery that other spiral bacteria such as "*G. hominis*" may be found in the gastric mucosa of patients complaining of gastric symptoms (4–7). The present study illustrates that, as in humans, the stomach of rhesus monkeys may be spontaneously infected with these two spiral organisms. In 14 of the animals, the observed GHLO were similar to the spirilla that have been described by others in monkeys (13,28) and baboons (29). Similarly, the rod-shaped bacteria measuring 3–4 μm × 0.5–1.0 μm

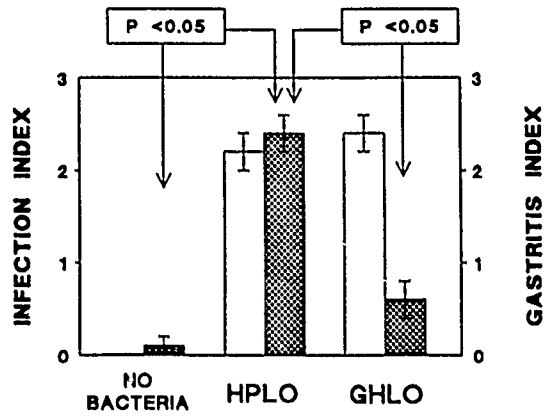

Figure 2. Infection index and gastritis index in rhesus monkeys infected with HPLO and GHLO. Note that although infection index is similar in both groups of animals, the gastritis index is elevated only in HPLO monkeys. □, infection; ⊠, gastritis (means ± SEM).

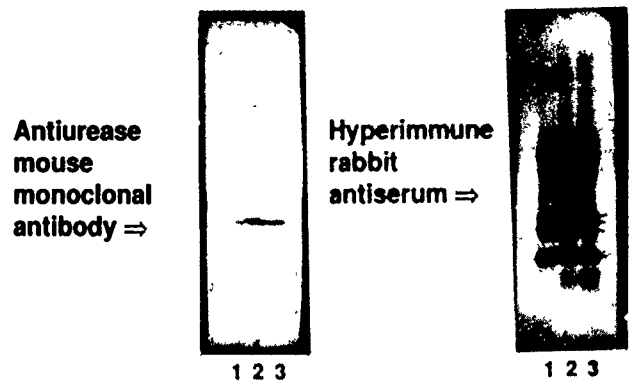

Figure 4. Antigenic profile of rhesus monkey HPLO and human *H. pylori* using a 10%–25% linear gradient SDS-PAGE system. Note the close similarity between the strains. Tracks 1 and 2, rhesus monkeys strains; track 3, human strains.

closely resembled human *H. pylori* as well as those previously described in the stomachs of monkeys (17–19) and baboons (29). An excellent agreement between histological and cultural detection of HPLO was observed in the 19 animals in which biopsies were cultured: no urease-positive growth was detected in any of 10 GHLO-positive animals or 4 uninfected monkeys, whereas typical *H. pylori* colonies were grown from biopsy specimens obtained in 3 of 4 HPLO-positive monkeys. Furthermore, the bacteria grown from HPLO-positive animals were immunologically and antigenically identical to human strains of *H. pylori*, as was previously reported for cultures grown from autopsy material obtained in rhesus monkeys in England (30). Finally, stomach infection with these two spiral organisms is associated with gastric mucosal lesions and acid hypersecretion, which are often associated with gastroduodenal symptoms in humans.

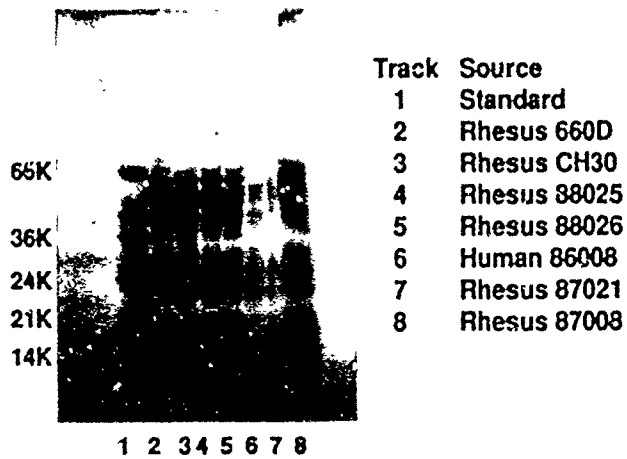

Figure 3. Total protein profile of rhesus monkey HPLO (tracks 2–5 and 7–8) and human *H. pylori* (track 6). Note the close similarity between these strains. Sample is 10%–25% linear gradient SDS PAGE gel stained with kenacid blue.

These observations confirm that both HPLO and GHLO are frequently present in the stomach of rhesus monkeys (17–19,28). In our colony, the prevalence of these bacteria in domestic born animals was 27% and 48%, respectively. The HPLO were associated with superficial erosions, but no apparent cellular damage was observed when these bacteria were in close proximity to the surface of mucosal cells lining the gastric glands. As in humans, HPLO were commonly associated with gastritis. In contrast, GHLO were observed in close association with intact superficial mucosa and with cellular injury of gastric glands and crypts, although no infiltration was observed in these biopsy specimens. Previous studies have shown that GHLO may be observed in gastric glands and parietal cells of monkeys (28) and of patients with upper gastrointestinal complaints (31,32). Our novel finding that intact and partly digested GHLO were present in the cytoplasm of healthy and partly disintegrated parietal cells suggests that, contrary to the opinion presented by others (19), GHLO could be invasive pathogens rather than commensal saprophytes. The apparent invasion of parietal cells by GHLO was associated with a significant increase of acid output, albeit no gastritis. This observation is important because, to our knowledge, it provides the first experimental evidence that gastric hyperacidity may be of infectious nature. In contrast, animals infected with HPLO had gastritis but no significant changes of acid output. This latter finding is in agreement with the absence of a consistent relationship between infection with *H. pylori* and gastric acid secretion in humans (33,34). In the present series, none of 29 monkeys studied showed evidence of infection with both HPLO and GHLO, although we cannot exclude that the 2 GHLO positive animals with gastritis were not harbor-

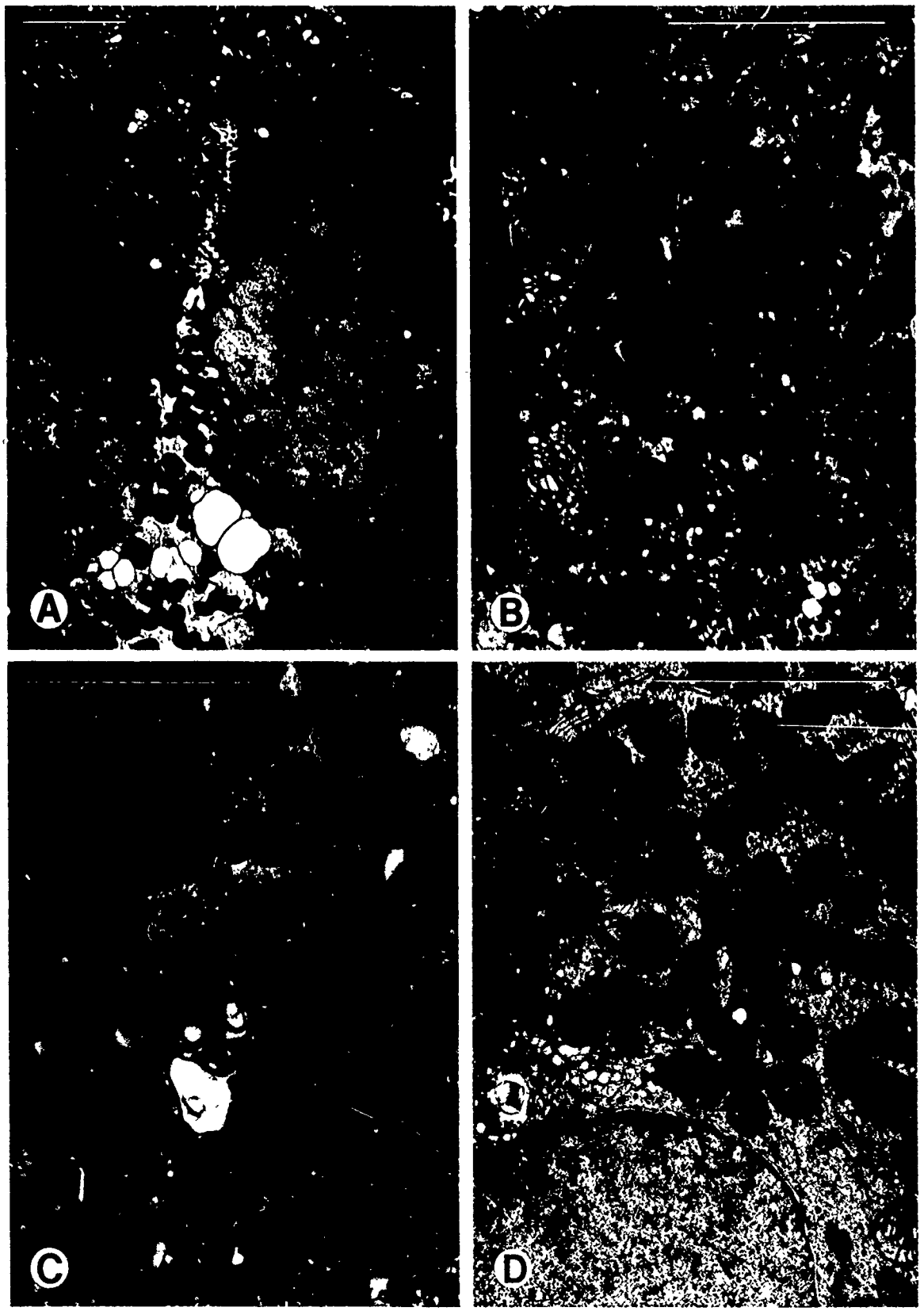

Figure 5. Electron micrograph of gastric parietal cells associated with GHLO (*bar* = 10 μm).

A. "*G. hominis*"-like organisms in the lumen of a gastric gland, one of them within the canaliculus of a parietal cell.

B. "*G. hominis*"-like organisms within the cytoplasm of parietal cells either intact (*single arrow*) or injured (*double arrow*).

C. The GHLO partly surrounded by membrane within healthy parietal cell.

D. Partly digested intracellular GHLO.

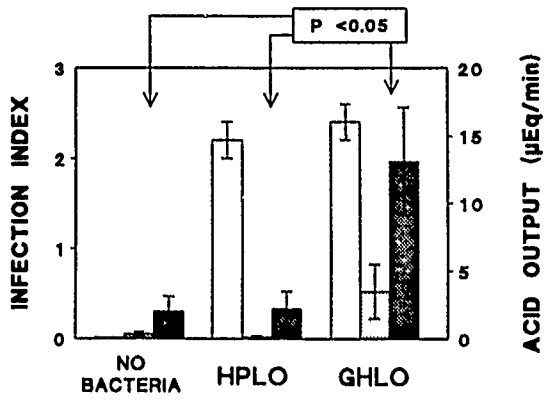

Figure 6. Infection index, BAO, and PAO in rhesus monkeys infected with HPLO and GHLO compared with uninfected animals. Note that infection index is similar in HPLO and GHLO, and that both BAO and PAO are significantly elevated in GHLO-positive monkeys compared with both uninfected and HPLO-positive animals. □, infection; ▨, BAO; □, PAO (means ± SEM).

ing HPLO in areas that were not biopsied. If such a concurrent infection was present, these animals could be at added risk for mucosal injury; HPLO would interfere with mucosal protection and GHLO would stimulate gastric secretion.

These findings are potentially important because spontaneous gastric ulcers were found at autopsy in 2 monkeys of a series of 42 animals, although the presence of spiral bacteria was not determined at the time (35). In addition, endoscopies performed in monkeys subjected to stress resulted in various lesions of the gastric mucosa (36). Together, these observations demonstrate that monkeys are naturally prone to both gastroduodenal infection with spiral bacteria and gastric mucosal disease, suggesting that this animal model is potentially useful for the study of human infection. Further evidence of the importance of this infection in primates would be provided if gastritis was to disappear upon eradication of the HPLO and to reappear following administration of human strains of these bacteria to healthy animals.

References

1. Marshall BJ. *Campylobacter pylorids* and gastritis. J Infect Dis 1986;153:650–657.
2. Marshall BJ, Armstrong J, McGechie DB, Glancey RJ. Attempts to fulfill Koch's postulates for pyloric Campylobacter. Med J Aust 1985;142:436–439.
3. Morris A, Nicholson G. Ingestion of *Campylobacter pylorids* causes gastritis and raised fasting gastric pH. Am J Gastroenterol 1987;82:192–199.
4. Dent JC, McNulty CAM, Uff JC, Wilkinson SP, Gear MWL. Spiral organisms in the gastric antrum. Lancet 1987;1:96.
5. Lee A, Dent J, Hazell S, McNulty C. Origin of spiral organisms in human gastric antrum. Lancet 1988,1.300–301.
6. McNulty CAM, Dent JC, Curry A, Uff JS, Ford GA, Gear MWL, Wilkinson SP. New spiral bacterium in gastric mucosa. J Clin Pathol 1989;42:585–591.
7. Lee A, Dick E, Eckstein RP, Kellow JE, Fevre DI. Non *Campylobacter pylori* organisms in the gastric antrum. Aust N Z J Med 1989;19:156–158.
8. Rappin J. Contribution à l'étude de bactéries de la bouche à l'état normal. 1881;68. Quoted by Breed RS, Murray EGD, Hitchens AP, in: Bergey's manual of determinative bacteriology. 6th ed. Baltimore: Williams & Wilkins, 1948:217.
9. Salomon H. Ueber das Spirillum des Säugetiermagens und sein Verhalten zu den Belegzellen. Zentralbl f Bakt 1896;19:433–442.
10. Bizzozero G. Ueber die schlauchförmigen Drüsen des Magendarmkanals und die Beziehungen ihres Epithels zu dem Oberflächenepithel der Schleimhaut. Archiv f. Mikrosk Anatomie 1893;42:82–152.
11. Lee A, Hazell SL, O'Rourke J, Kouprach SJ. Isolation of a spiral-shaped bacterium from the cat stomach. Infect Immun 1988;56:2843–2850.
12. Dick E, Lee A, Watson G, O'Rourke J. Use of the mouse for the isolation and investigation of stomach-associated, spiral-helical shaped bacteria from man and other animals. J Med Microbiol 1989;29:55–62.
13. Fox JG, Cabot EB, Taylor NS, Laraway R. Gastric colonization by *Campylobacter pylori* subsp. *mustelae* in ferrets. Infect Immun 1988;56:2994–2996.
14. Krakowa S, Morgan DR, Kraft WG, Leunk RD. Establishment of gastric *Campylobacter pylori* infection in the neonatal gnotobiotic piglet. Infect Immun 1987;55:2789–2796.
15. Lambert JR, Borromeo M, Pinkard KJ, Turner H, Chapman CB, Smith ML. Colonization of gnotobiotic pigleis with *Campylobacter pyloridis*—an animal model? J Infect Dis 1987;155:1344.
16. Eaton KA, Morgan DR, Krakowka S. *Campylobacter pylori* virulence factors in gnotobiotic piglets. Infect Immun 1989;57:1119–1125.
17. Newell DG, Hudson MJ, Baskerville A. Naturally occurring gastritis associated with *Campylobacter pylori* infection in the Rhesus monkey. Lancet 1987;2:1338.
18. Baskerville A, Newell DG. Naturally occurring chronic gastritis and *C. pylori* infection in the Rhesus monkey: a potential model for gastritis in man. Gut 1988;29:465–472.
19. Reed KD, Berridge BR. Campylobacter-like organisms in the gastric mucosa of Rhesus monkeys. Lab Anim Sci 1988;38:329–331.
20. Tarnawski A, Hollander D, Cummings D, Krause WJ, Stachura J, Zipser RD, Gergely H. Does sucralfate affect the normal gastric mucosa? Histologic, ultrastructural and functional assessment in the rat. Gastroenterology 1986;90:893–905.
21. Fishbein WN. Formamide, the minimum structure for urease. Biochim Biophys Acta 1977;484:433–442.
22. Newell DG. Identification of the outer membrane proteins of *Campylobacter pyloridis*. J Gen Microbiol 1987;133:163–170.
23. Kyhse-Andersen J. Electroblotting of multiple gels: a simple apparatus without buffer tank for rapid transfer of protein from polyacryiamide to nitrocellulose. J Biophys Biochem Methods 1984;10:203–209.
24. Newell DG, Lee A, Hawtin PR, Hudson MJ, Stacey AR, Fox J. Antigenic conservation of the ureases of spiral- and helical-shaped bacteria colonising the stomachs of man and animals. FEMS Microbiol Letts 1989;65.183–189.
25. Dubois A, Van Eerdewegh P, Gardner JD. Gastric emptying and secretion in Zollinger Ellison syndrome. J Clin Invest 1977,59.255–263.
26. Dorval ED, Mueller CP, Durakovic A, Conklin JJ, Dubois A. Effect of ionizing radiation on gastric secretion and gastric motility in monkeys. Gastroenterology 1985,89.374–380.
27. Winer BJ. Statistical Principles in Experimental Design. (2nd ed). New York: McGraw-Hill, 1971.

28. Sato T, Takeuchi TA. Infection by spirilla in the stomach of the Rhesus monkey. Vet Pathol 1982;19(Suppl 7):17–25.
29. Curry A, Jones DM, Eldridge J. Spiral organisms in the baboon stomach. Lancet 1987;2:634–635.
30. Newell DG, Hudson MJ, Baskerville A. Isolation of a gastric campylobacter-like organism from the stomach of four Rhesus monkeys, and identification as *Campylobacter pylori*. J Med Microbiol 1988;27:41–44.
31. Rollason TP, Stone J, Rhodes JM. Spiral organisms in endoscopic biopsies of the human stomach. J Clin Pathol 1984;37: 23–26.
32. Dye KR, Marshall BJ, Frierson HF, Guerrant RL, McCallum RW. Ultrastructure of another spiral organism associated with human gastritis. Dig Dis Sci 1989;34:1787–1791.
33. Brady CE III, Hadfield TL, Hyatt JR, Utts SJ. Acid secretion and serum gastrin levels in individuals with *Campylobacter pylori*. Gastroenterology 1988;94:923–927.
34. Wagner S, Freise J, Beholz S, Schmidt FW. Gastric acid secretion and *Campylobacter pylori*. Gastroenterology 1988;95: 1695–1696.
35. Parker GA, Gilmore CJ, Dubois A. Spontaneous gastric ulcer in a Rhesus monkey. Brain Res Bull 1981;6:445–447.
36. Natelson BJ, Dubois A, Sodetz FJ. Effect of multiple stress procedures on monkey gastroduodenal mucosa, serum gastrin and hydrogen ion kinetics. Am J Dig Dis 1977;22:888–897.

Received June 11, 1990. Accepted September 26, 1990.

Address requests for reprints to: Andre Dubois, M.D., Ph.D., Department of Medicine, Uniformed Services University, 4301 Jones Bridge Road, Bethesda, Maryland 20814-4799.

The experiments reported herein were conducted according to the principles set forth in the "Guide for the Care and Use of Laboratory Animals," Institute of Laboratory Animal Resources, National Research Council, HHS/NIH Publ. No. 85-23. The opinions and assertions contained herein are the private ones of the authors and are not to be construed as official or reflecting the views of the Department of Defense, the Uniformed Services University of the Health Sciences, or the Defense Nuclear Agency.

INT. J. RADIAT. BIOL., 1990, VOL. 58, NO. 2, 341–350

Quantitative study of wound infection in irradiated mice

T. B. ELLIOTT†, I. BROOK‡ and S. M. STIEFEL‡

Immunology Division, Department of Experimental Hematology, and ‡Department of Veterinary Sciences, Armed Forces Radiobiology Research Institute, Bethesda, Maryland 20814-5145, USA

(Received 4 August 1989; second revision received 20 February 1990; accepted 1 March 1990)

Bacterial infection of simple wounds was studied directly and quantitatively in adult mice given 6·5 Gy ^{60}Co. Three days later, when neutropenia was evident, the skin and the medial gluteus muscle of anaesthetized mice were incised. A suspension of *Staphylococcus aureus*, *Escherichia coli*, *Klebsiella pneumoniae* or *Streptococcus pyogenes* was inoculated into the wound. Bacteria per mg muscle were enumerated 3, 4 or 7 days later. The geometric means of bacteria per mg were greater in irradiated than in non-irradiated mice. Phagocytic cells were present in the wounded tissue. Hence sublethal ionizing radiation enhanced the susceptibility of mice to infections of wounds by these four bacterial species.

1. Introduction

Sublethal ionizing γ-irradiation enhances susceptibility of animals to endogenous and exogenous bacterial infections by depressing normal haematopoiesis and host defences (Schechmeister and Bond 1951, Kaplan *et al.* 1952, Schechmeister *et al.* 1953, Clapper *et al.* 1954, Schechmeister 1954, Taliaferro *et al.* 1964, Anderson and Warner 1976). Neutropenia is a particularly important factor that predisposes to infection (Bodey 1985). Trauma, when superimposed on the consequences of irradiation, increases the chance of mortality (Ledney *et al.* 1985, Lindop *et al.* 1985, Rotblat 1986). Mice that were wounded 2 days after 9·0 Gy γ-radiation died sooner than those wounded immediately before or after irradiation (Ledney *et al.* 1985). Nuclear accidents may expose many persons to whole-body radiation with complex biomedical consequences, including infections (Finch 1987, Gale 1987 1988). Wounds that occur after exposure to radiation are likely to become infected in a neutropenic host. Enumeration of bacteria in a biopsy of infected wound tissue indicated severity of the infection and improved clinical judgement (Robson and Heggers 1969). Knowledge of the variety of bacteria that can cause enhanced post-irradiation wound infections is necessary to develop sound strategies for effective treatment of such combined injuries.

We developed a model to study bacteria directly and quantitatively at the site of infection after irradiation in order to study the efficacy of therapeutic agents in combined injured animals. After exposure of mice to a sublethal dose of γ-radiation we induced bacterial infections in simple wounds during neutropenia with minimal mortality for 7 days. The model was used to evaluate combined antibacterial therapies for infections by *Staphylococcus aureus* in irradiated mice (Brook and Elliott 1989). We present studies of four species of bacteria in this model, which

†To whom correspondence should be addressed.

show that wound infections by these bacteria were enhanced by prior sublethal ionizing radiation even when phagocytic cells were present near the wound.

2. Materials and methods

2.1. *Animals*

Approximately 400 female, B6D2F1/J mice (Jackson Laboratories, Bar Harbor, ME), 20–25 g, 8–19 weeks of age, were held in quarantine for 2 weeks. Representative samples were examined to assure the absence of specific intestinal bacteria and common murine diseases by microbiology, serology and histopathology. Up to nine mice were housed in sanitized 46 cm × 24 cm × 15 cm polycarbonate boxes with a filter cover (MicroIsolator, Lab Products, Inc., Maywood, NJ) on hardwood-chip bedding in a facility accredited by the American Association for Accreditation of Laboratory Animal Care. Mice were given feed (Wayne Lab Blox, Continental Grain Co., Chicago, IL) and acidified (pH 2·5) water freely. The animal holding room was maintained with conditioned fresh air that was changed at least 10 times per hour at approximately 21°C and 50% (±10%) relative humidity and with a 12-h light/dark full-spectrum lighting cycle.

2.2. *Radiation*

The hair on the rear dorsal quarter of mice was shaved. Mice were exposed in perforated Plexiglas restrainers, which permitted normal exchange of air, to bilateral radiation from the AFRRI ^{60}Co source at a rate of 0·4 Gy/min at ambient temperature. The mid-line absorbed dose was 6·5 Gy. This sublethal dose was chosen to minimize mortality in infected mice. The lethal dose for 50% of uninfected B6D2F1/J female mice 30 days after exposure ($LD_{50/[30]}$) to this source is 9·65±0·30 Gy.

2.3. *Leukocyte and thrombocyte counts*

Tail blood was drawn immediately before and daily after irradiation from five 15-week-old mice, selected randomly from a group of 10. Leukocytes and thrombocytes were counted microscopically by haemocytometer. The minimum number of detectable leukocytes was 110/μl.

2.4. *Bacteria*

Species of bacteria were selected because of their relative importance as causes of wound infections in human patients, because of their different effects on muscle tissue, and to provide diversity of the challenge. *S. aureus* and *Escherichia coli* are facultative species that are commonly isolated from wounds. *Klebsiella pneumoniae* provides a strong challenge because of its large polysaccharide capsule, whereas *Streptococcus pyogenes* causes necrosis of tissue, which may inhibit effective systemic treatment of the local infection.

S. aureus ATCC 25923, *S. pyogenes* AFRRI 4, *K. pneumoniae* AFRRI 7, and *E. coli* AFRRI 6 were transferred from stock suspensions in skimmed milk frozen at −20°C onto Columbia Sheep Blood (5%) Agar (SBA; BBL 21263, Cockeysville, MD). Cultures of *S. pyogenes* were incubated for 24 h in 5% CO_2 at 35°C, whereas the other species were incubated at 30°C for 24 h.

The highest number of bacteria of each species was used in inocula that would cause a serious infection but minimal mortality. These numbers were determined empirically. Preparation of inocula and counting of bacteria were previously described (Brook and Elliott 1989).

2.5. *Trauma*

Three days after irradiation, mice were anaesthetized by inhalation of methoxyflurane (Metofane™, Pitman-Moore, Washington Crossing, NJ). In initial experiments, shaved skin was wiped with a gauze sponge that was moistened with 70% ethanol and the skin over the right medial gluteus muscle was incised with a sterile no.15 scalpel. The incision was approximately 12 mm long and approximately 30° to the spine caudally. The exposed medial gluteus was then incised three times about 3 mm deep with the blade at different angles along the same stroke as the initial incision. To induce a specific infection, a 0·1 ml volume of a bacterial suspension in 0·9% NaCl was inoculated onto the incised muscle. The mice were placed in sanitized cages and observed until they recovered from the anaesthesia. Similar incisions were made in two irradiated and unirradiated mice without inoculation of bacteria. These mice were used to evaluate aseptic technique during removal of muscles.

Some inoculum occasionally leaked from the open wound, so the model was modified by injecting the inoculum s.c. to form a bleb over the right medial gluteus muscle. After the liquid was absorbed, in 20–30 min, the skin and muscle of anaesthetized mice were incised.

2.6. *Quantitation of bacteria in infected muscle*

Three mice from each experimental group were randomly selected and euthanized by cervical dislocation. The backs of the mice were wiped with 70% ethanol. The entire dorsal skin was removed and the entire medial gluteus, including abscess and necrotic tissue, was excised aseptically, weighed and homogenized. Homogenate and 100-fold dilutions were spread onto duplicate Columbia SBA plates.

After incubation, the number of bacteria per mg muscle was calculated (Brook and Elliott 1989). The mass of excised muscles in these experiments varied from 89 to 241 mg in unirradiated mice and from 114 to 300 mg in irradiated mice.

2.7. *Qualitative cultures of spleens and livers*

This was done as previously described (Brook and Elliott, 1989). The spleens and livers were removed aseptically and macerated with sterile cotton swabs in sterile Petri dishes. The tissues on the swabs were then spread onto SBA and incubated. Growth of bacteria was noted and identified presumptively.

2.8. *Histology*

We wanted to determine the local response of cellular defences in irradiated mice to a normally pyogenic infection. Strain ATCC 25923 of *S. aureus* is sensitive to penicillin, but is difficult to eradicate in wounded muscle (Brook and Elliott 1989). Ten mice were given 7·0 Gy γ-radiation, followed 3 days later with *S. aureus* and wounding. Three and 5 days later the wounded legs of five mice were dissected and fixed in formalin. Sections of wounds were examined microscopically.

2.9. *Experimental design*

This study focused on severity of wound infection in irradiated and unirradiated mice with minimum mortality. Because some mice died, however, a sufficient number from one birth-date were included in each experiment to assure survivors for culture of bacteria. Tweny-four were irradiated, of which eight were held for measuring survival. Sixteen irradiated and 16 unirradiated mice were wounded and

bacteria were inoculated 3 days after irradiation. The mice were observed daily for general appearance, signs of local infection and signs of healing. Bacteria in the wounded muscle of three mice in each group were enumerated on the third or fourth and seventh days after bacteria were inoculated directly onto the wound, and on the fourth day in the modified procedure.

3. Results

3.1. *Leukocytes and thrombocytes in blood*

The ($\log_{10}$) number of leukocytes decreased immediately after irradiation from nearly $4{\cdot}0 \pm 3{\cdot}3\,\mu l^{-1}$ to daily averages between 2·3 and $2{\cdot}7\,\mu l^{-1}$ ($p < 0{\cdot}0001$), a reduction of 95–98%, between 3 and 13 days after irradiation (Figure 1). Recovery of the number of leukocytes began approximately 15 days after irradiation.

The ($\log_{10}$) number of thrombocytes remained stable (standard errors overlapped) for 5 days after irradiation at about $6{\cdot}2 \pm 5{\cdot}4\,\mu l^{-1}$, then decreased rapidly to $5{\cdot}9 \pm 4{\cdot}6\,\mu l^{-1}$, a reduction of 50% ($p = 0{\cdot}002$), on the sixth day after irradiation; the level was minimal between the eighth and tenth days (Figure 1), when the average was between $5{\cdot}1 \pm 4{\cdot}1\,\mu l^{-1}$ and $5{\cdot}3 \pm 4{\cdot}5\,\mu l^{-1}$, a reduction of 88–92%. Recovery of the number of thrombocytes began by the thirteenth day.

3.2. *Number of bacteria in infected muscles*

3.2.1. *Inoculation directly onto wounded muscle.* The number of the inoculated species increased by the third or fourth day above the number that was inoculated, except when *K. pneumoniae* was inoculated into unirradiated mice (Table 1). The number of all three species of bacteria in infected muscles was greater in irradiated mice than in non-irradiated mice 3 or 4 and 7 days after inoculation of bacteria and incision, but differences (d) on the seventh day between sets of irradiated versus non-irradiated mice infected by *S. pyogenes* ($\log_{10} d = 3{\cdot}61$) and *K. pneumoniae*

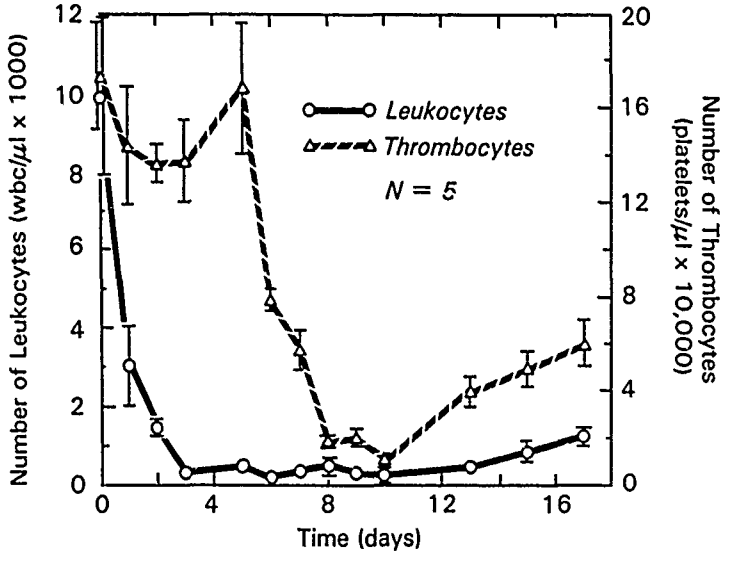

Figure 1. Numbers of leukocytes and thrombocytes in blood of mice exposed to 6 5 Gy ^{60}Co γ-rays. Blood was drawn from tail veins of five 15-week-old, female, B6D2F1/J mice that were chosen randomly from a group of 10.

Table 1. Numbers of bacteria in wounded muscles of unirradiated and irradiated mice.

Site of inoculation	Inoculum		Days after challenge	Log GM-CFU/mg (SEM)[a]			
	Species	CFU/mouse		Irradiated	Unirradiated	Difference[b]	p
Directly onto wound	*S. aureus*	$3{\cdot}7\times10^{6}$	4	6·68 (0·23)	5·45 (0·35)	1·23	0·042
	S. pyogenes	$9{\cdot}5\times10^{2}$	3	5·47 (0·14)	2·95 (0·68)	2·52	0·022
	K. pneumoniae	$1{\cdot}3\times10^{2}$	3	3·96 (1·69)	−1·63 (0·33)	5·59	0·032
Directly onto wound	*S. aureus*	$3{\cdot}7\times10^{6}$	7	7·34 (0·06)	3·31 (1·04)	4·03	0·061
	S. pyogenes	$9{\cdot}5\times10^{2}$	7	5·36 (0·36)	1·75 (1·99)	3·61	0·148
	K. pneumoniae	$1{\cdot}3\times10^{2}$	7	0·88 (1·67)	−1·97 (0·01)	2·85	0·230
Subcutaneous before wound	*S. aureus*	$3{\cdot}6\times10^{6}$	4	6·95 (0·05)	3·78 (0·97)	3·17	0·083
	S. pyogenes	$1{\cdot}1\times10^{2}$	4	5·70 (0·49)	4·31 (0·40)	1·39	0·093
	E. coli	$2{\cdot}0\times10^{6}$	4	6·91 (0·08)	1·26 (0·23)	5·65	0·000

[a] Logarithm, base 10, of geometric mean of CFU bacteria/mg muscle (standard error of the mean), $n=3$.
[b] Irradiated − unirradiated.

($\log_{10}d=2{\cdot}85$) were not statistically significant because of high standard errors ($p>0{\cdot}1$, Table 1). In unirradiated controls, the concentration of inoculated species in wounded muscle decreased between 3 or 4 and 7 days after inoculation. In irradiated mice the concentration of *S. aureus* increased, *S. pyogenes* remained steady, and *K. pneumoniae* decreased between 4, 3 or 3 days, respectively, and 7 days. A species of *Micrococcaceae* was also isolated from muscles from six of six irradiated mice that were infected by *S. pyogenes*, but not from corresponding unirradiated mice or from irradiated mice infected by the other species. Inocula were not contaminated. Complete identification of this micro-organism was not performed. Experiments were repeated with similar results three times with *S. aureus*, once with *S. pyogenes* and once with *K. pneumoniae*.

3.2.2. *Subcutaneous inoculaton before wounding.* As in the previous experiments, when inocula of *E. coli*, *S. aureus*, or *S. pyogenes* were injected s.c. before the muscles were incised, the number of bacteria in wounded muscle was greater 4 days later in irradiated mice than in unirradiated mice ($p<0{\cdot}1$, Table 1). Experiments were repeated twice with *S. aureus* and once with *E. coli* with similar results at 7 days after challenge. A presumptive species of *Micrococcaceae* again was isolated (perhaps a species of *Staphylococcus* based on subsequent unpublished studies) together with *S. pyogenes* as occurred when bacteria were inoculated into the open wound. This consistent finding suggests that this stray species is a natural inhabitant of the skin and that there is a symbiotic affinity between these two species.

When the number of bacteria in muscles of irradiated versus unirradiated mice are compared, $p<0{\cdot}10$ at 3 or 4 days after challenge for all sets of data and at 7 days only for *S. aureus* that was inoculated directly onto the wounded muscle (Table 1). Variability in a set is evident from the standard errors of the means, which were smaller for irradiated than unirradiated mice in four of six sets.

Although the difference between numbers of *K. pneumoniae* in muscles of irradiated and unirradiated mice was the least statistically significant among the species ($p=0{\cdot}23$), the numbers of this species in muscles of irradiated mice 7 days after challenge were, nevertheless, higher than in those of unirradiated mice. In addition, although this study was designed to minimize mortality, a non-lethal infectious dose of *K. pneumoniae* in irradiated mice was difficult to achieve. Six of 12 irradiated mice that were challenged with *K. pneumoniae*, but not used for cultures, died during the 7 days after challenge, compared with two of nine challenged with *S. aureus* and none of those challenged with *S. pyogenes*. All mice that were only irradiated survived for 21 days of observation.

3.3. *Cultures of spleens and livers*

The inoculated bacterial species were detected in 9 of 18 spleens and 12 of 18 livers of irradiated mice, but not in those of unirradiated mice (Table 2). Only *K. pneumoniae* was not isolated from livers or spleens.

3.4. *Histology*

Lesions in mice that were irradiated, wounded and challenged with *S. aureus* showed focal loss of superficial epithelium and focally extensive coagulative necrosis from the dermis through the subcutis into underlying muscle. Bacteria colonized the area of necrosis and, in 5 of 10 specimens, along the fascial planes of

Table 2. Number of mice from which challenge bacteria were recovered from spleens and livers after combined injury.

Inoculum		Days after challenge	Irradiated : Unirradiated[a]	
Species	CFU/mouse		Spleen	Liver
S. aureus	$3{\cdot}7\times10^6$	7	2:0	3:0
S. aureus	$3{\cdot}6\times10^6$	4	2:0	3:0
S. pyogenes	$9{\cdot}5\times10^2$	7	2:0	2:0
S. pyogenes	$1{\cdot}1\times10^2$	4	1:0	2:0
K. pneumoniae	$1{\cdot}3\times10^2$	7	0:0	0:0
E. coli	$2{\cdot}0\times10^6$	4	2:0	2:0

[a] Three irradiated and three unirradiated mice were examined in each experiment.

the perimysial connective tissue. Inflammatory infiltrations of the subcutis or perimysium were adjacent to the areas of necrosis. Minimum to moderate numbers of degenerating neutrophils surrounded the zones of necrosis. Occasional healthy neutrophils penetrated into perimysium or endomysium. Macrophages were occasionally associated with areas of necrosis and often in nodular accumulations within the subcutis or perimysium adjacent to focal necrosis. Normal numbers of mast cells were within the subcutis, but occasionally in increased numbers within the areas of granulomatous inflammation. Mild to moderate proliferation of fibroblasts, multifocally in subcutis or randomly in perimysium, were seen adjacent to the area of necrosis, more on the fifth day after challenge and wounding than the third day.

3.5. *Observations of wound infections*

Although severity of muscle infections varied in irradiated mice, infections were generally more severe than those in unirradiated mice. Signs of infection, including swelling and excretion of pus, often remained in irradiated mice more than 7 days after bacterial challenge, longer than in unirradiated mice. However, spontaneous closing of the incision occurred in irradiated mice as well as in unirradiated mice between 7 and 14 days after challenge; however, muscles did not heal in irradiated mice.

Infection by each bacterial species caused a different effect on the muscle in irradiated mice. Infection is a process which includes effects of the host repsonses as well as effects of the micro-organism. A remarkable hardened and blanched disc of swollen muscle was often observed after inoculation of *S. pyogenes*; an abscess often formed after inoculation of *S. aureus*; dryness and erythema were observed after inoculation of *E. coli*; whereas clean serous lesions, sometimes with haemorrhage and oedema, and occasionally an abscess followed inoculation of *K. pneumoniae*. These effects were not noticeable in the unirradiated mice.

4. Discussion

This model demonstrated that a bacterial infection of a wound was more severe and persistent in an irradiated mouse than in an unirradiated mouse by quantitative measurement of the infecting bacteria even when neutrophils and macrophages were present; however, the neutrophils were degenerating and phagocytosis was not

observed. The numbers of bacteria that were recovered from muscles of irradiated mice were consistently higher than in unirradiated mice, although the differences between CFU in irradiated and unirradiated mice were more significant at 3 or 4 days than at 7 days after bacterial inoculation.

Although infection is a major complication in contaminated traumatic wounds (Gilbert *et al.* 1973, Pollock, 1988), septicaemia can overwhelm irradiated persons (LeRoy 1947), and surgery in irradiated tissue increases complications of wound healing (Luce 1984), clinical experience with bacterial infections in traumatic wounds in whole-body irradiated persons is limited and has received little attention. It is necessary to understand the mechanisms in order to manage effectively the infectious complications of combined injury (Walker and Conklin 1987). We are aware of no other experimental model used recently to study bacteria in wound infections in irradiated animals.

Kaplan *et al.* (1952) established that mice were most susceptible to bacterial infection of thighs by injection of a β-haemolytic streptococcus between 3 and 7 days after whole-body exposure of about 4·5 or 4·85 Gy X-irradiation. Histology showed liquefaction necrosis, avascularity and leukopenia in their irradiated mice. The bacteria disseminated into tissues sooner in irradiated than in unirradiated, infected controls; however, pressure induced by initial injection may have forced some bacteria into perimysial spaces.

The fact that the bacterial species in the inoculum, except *K. pneumoniae*, was detected in spleens and livers of most irradiated mice, but not at all in those of unirradiated mice, indicated bacteraemia and emphasized the decreased resistance and consequential systemic threat of wound infections in these irradiated animals, as was also shown by Kaplan *et al.* (1952). We have noticed that *K. pneumoniae* is often not isolated from livers and spleens of active mice after inoculation, but is always found in moribund mice. This observation indicates a rapid onset and course of septicaemia by this organism.

A satisfactory, complete explanation of changes that account for increased susceptibility to infections in irradiated animals (Kaplan *et al.* 1952, Schechmeister *et al.* 1952, Miller 1956) remains a challenge. Schechmeister *et al.* (1952) found that mice were susceptible to infection by an aerosol of *Streptococcus zooepidemicus*, and that leukopenia occurred between 3 and 21 days after a dose of about 3·5 Gy X-irradiation, but suggested that the increase in susceptibility could not be attributed to any one factor.

The local inflammatory process is important for control of infections, but radiation alters numbers and functions of phagocytic cells (Schechmeister 1954, Smith *et al.* 1963). Depression of this process probably contributes to mortality from septicaemia. Although neutrophils were attracted to the zones of necrosis and infection, they were degenerating and not noticeably phagocytic. Evidently, they can respond to chemotactic agents, but their phagocytic and cidal functions are deficient.

We selected the time of bacterial challenge to coincide with the precipitous decrease in the number of leukocytes 3 days after irradiation. When bacteria were inoculated into wounds 1 or 2 days after irradiation, infections were not as severe (Elliott and Brook unpublished data). Because granulocytopenia is similar in several mammalian species after 5–6 Gy X-irradiation (Patt and Maloney 1963), other mammalian species, e.g. humans, might be expected to show similar increased susceptibility to bacterial infections of wounds after sublethal irradiation.

Thrombocytopenia that occurred in our mice between the sixth and thirteenth days after irradiation is similar to observations in other animals (Cronkite 1946, Rosenthal and Benedek 1950, Cronkite *et al.* 1952). This depletion is caused by their response to deterioration of the vascular endothelium and exposure of collagen and by injury to bone marrow stem cells (Monroy 1987). Although all thrombocytopenic animals do not become purpuric (Cronkite *et al.* 1952), small local haemorrhages can occur in tissues during thrombocytopenia, which enable infecting bacteria to penetrate the tissue (Bond *et al.* 1954). The extravascular blood may also provide nutrients for bacterial growth, and thus enhance infection.

This model provides a practical means to study bacteria directly and quantitatively in irradiated, neutropenic animals, and is being used to determine the effect of combined antimicrobial therapies directly on bacteria *in vivo*.

Acknowledgements

We are grateful to David Funckes for technical assistance; E. J. Golightly and W. E. Wilson for their co-operation and operation of the cobalt radiation facility; William E. Jackson III for programs to calculate geometric means and *t*-tests; Brenda W. Bell for performing counts of leukocytes and thrombocytes in blood; and Dr G. Heisey and staff for their veterinary services and animal care. This work was supported by Work Unit 4420-00129 of the Armed Forces Radiobiology Research Institute, Defense Nuclear Agency. Views presented in this paper are those of the authors; no endorsement by the Defense Nuclear Agency has been given or should be inferred. Research was conducted according to the principles enunciated in the Guide for the Care and Use of Laboratory Animals, prepared by the Institute of Laboratory Animal Resources, National Research Council.

References

ANDERSON, R. E. and WARNER, N. L., 1976, Ionizing radiation and the immune response. *Advances in Immunology*, edited by F. J. Dixon and H. G. Kunkel, (Academic Press, New York), Vol. 24, pp. 215–335.

BODEY, G. P., 1985, Overview of the problem of infections in the immunocompromised host. *American Journal of Medicine*, **79**, (Suppl. 5B), 56–60

BOND, V. P., SILVERMAN, M. S. and CRONKITE, E. P., 1954, Pathogenesis and pathology of post-irradiation infection. *Radiation Research*, **1**, 389–400.

BROOK, I. and ELLIOTT, T. B., 1989, Treatment of wound sepsis in irradiated mice. *International Journal of Radiation Biology*, **56**, 75–82.

CLAPPER, W. E., ROBERTS, J. E. and MEAD, G. H., 1954, Radiation effects on pneumococcal infection produced by subcutaneous injections into white mice. *Proceedings of the Society for Experimental Biology and Medicine*, **86**, 420–422.

CRONKITE, E. P., 1946, The hemorrhagic syndrome of acute ionizing radiation illness produced in goats and swine by exposure to the atomic bomb at Bikini, 1946. *Blood*, **5**, 32–45.

CRONKITE, E. P., JACOBS, G. J., BRECKER, G. and DILLARD, G., 1952, The hemorrhagic phase of the acute radiation syndrome due to exposure of the whole body to penetrating ionizing radiation. *American Journal of Roentgenology, Radium Therapy and Nuclear Medicine*, **67**, 796–804.

FINCH, S. C., 1987, Acute radiation syndrome. *Journal of the American Medical Association*, **258**, 664–667.

GALE, R. P.,1987, Immediate medical consequences of nuclear accidents: lessons from Chernobyl. *Journal of the American Medical Association*, **258**, 625–628.

GALE, R. P., 1988, Perspective–medical response to radiation and nuclear accidents: lessons for the future. *Journal of the National Cancer Institute*, **80**, 995–998.

GILBERT, D. N., SANFORD, J. P., KUTSCHER, E., SANDERS, JR, C. V., LUBY, J. P. and BARNETT, J. A., 1973, Microbiologic study of wound infections in tornado casualties. *Archives of Environmental Health*, **26**, 125–130.

KAPLAN, H. S., SPECK, R. S. and JAWETZ, E., 1952, Impairment of antimicrobial defenses following total body irradiation of mice. *Journal of Laboratory and Clinical Medicine*, **40**, 682–691.

LEDNEY, G. D., EXUM, E. D. and JACKSON, III, W. E., 1985, Wound-induced alterations in survival of ^{60}Co irradiated mice: importance of wound timing. *Experientia*, **41**, 614–616.

LEROY, G. V., 1947, The medical sequelae of the atomic bomb explosion. *Journal of the American Medical Association*, **134**, 1143–1148.

LINDOP, P., ROTBLAT, J. and WEBBER, P., 1985, Radiation casualties in a nuclear war. *Nature*, **313**, 345–346.

LUCE, E. A., 1984, The irradiated wound. *Surgical Clinics of North America*, **64**, 821–829.

MILLER, C. P., 1956, The effect of irradiation on natural resistance to infection. *Annals of the New York Academy of Sciences*, **66**, 280–291.

MONROY, R. L., 1987, Radiation effects on the lymphohematopoietic system: a compromise in immune competency. *Military Radiobiology*, edited by J. J. Conklin and R. I. Walker (Academic Press, Orlando), pp. 111–134.

PATT, H. M. and MALONEY, M. A., 1963, A comparison of radiation-induced granulocytopenia in several mammalian species. *Radiation Research*, **18**, 231–235.

POLLOCK, A. V., 1988, Surgical prophylaxis—the emerging picture. *Lancet*, **i**, 225–230.

ROBSON, M. C. and HEGGERS, J. P., 1969, Bacterial quantification of open wounds. *Military Medicine*, **134**, 19–24.

ROSENTHAL, R. L. and BENEDEK, A. L., 1950, Blood coagulation and hemorrhage following total body X-irradiation in the rabbit. *American Journal of Physiology*, **161**, 505–514.

ROTBLAT, J., 1986, Acute radiation mortality in a nuclear war. *The Medical Implications of Nuclear War*, edited by F. Solomon and R. Q. Marston (National Academy Press, Washington), pp. 233–250.

SCHECHMEISTER, I. L., 1954, Susceptibility of irradiated animals to infection. *Radiation Research*, **1**, 401–409.

SCHECHMEISTER, I. L., BOND, V. P. and SWIFT, M. N., 1952, The susceptibility of irradiated mice to infection as a function of post-irradiation time. *Journal of Immunology*, **68**, 87–95.

SCHECHMEISTER, I. L. and BOND, V. P., 1951, Response of mice to certain avirulent bacteria after exposure to sublethal total body X-irradiation. *Proceedings of the Society for Experimental Biology and Medicine*, **77**, 77–80.

SCHECHMEISTER, I. L., PAULISSEN, L. J. and FISHMAN, M., 1953, Sublethal total body X-radiation and susceptibility of mice to *Salmonella enteritidis* and *Escherichia coli*. *Proceedings of the Society for Experimental Biology and Medicine*, **83**, 205–209.

SMITH, M. R., FLEMING, D. O. and WOOD, JR, W. B., 1963, The effect of acute radiation injury on phagocytic mechanisms of antibacterial defense. *Journal of Immunology*, **90**, 914–924.

TALIAFERRO, W. H., TALIAFERRO, L. G. and JAROSLOW, B. N., 1964, *Radiation and Immune Mechanisms* (Academic Press, New York)

WALKER, R. I. and CONKLIN, J. J., 1987, Mechanisms and management of infectious complications of combined injury. *Military Radiobiology*, edited by J. J. Conklin and R. I. Walker (Academic Press, Orlando), pp. 219–230.

INTERACTION OF LEUKOTRIENE C_4 AND CHINESE HAMSTER LUNG FIBROBLASTS (V79A03 CELLS). 2. SUBCELLULAR DISTRIBUTION OF BINDING AND UNLIKELY ROLE OF GLUTATHIONE-S-TRANSFERASE

Y.X. Liu[1], D.F.Contois[1], D.S. Watt[2], T.L. Walden, Jr.[3] and T.A. Fitz[1,4]

[1]Department of Obstetrics and Gynecology, Uniformed Services University of the Health Sciences, Bethesda, Maryland 20889-4799, [2] Department of Chemistry and Division of Medicinal Chemistry, Lucille Parker Markey Cancer Research Center, University of Kentucky, Lexington, Kentucky 40506-0055, [3]Radiation Biochemistry Department, Armed Forces Radiobiology Research Institute, Bethesda, Maryland 20889-5145, [4]Correspondence

Abstract

It was reported previously that radiation-induced cytotoxicity in V79A03 (V79) cells was attenuated by pretreatment of cells with leukotriene C_4 (LTC_4), leading us to determine that V79 cells possessed specific binding sites, with characteristics of receptors, for LTC_4 (see the preceding, companion communication). Additional studies were conducted to determine the subcellular distribution and the chemical nature of the LTC_4 binding site in V79 cells. Trypsin treatment of cells before LTC_4 binding assays resulted in a 74% reduction in high-affinity binding. In tests to examine the subcellular location of LTC_4 binding, plasma membrane and nuclear fractions were obtained from V79 cells. In contrast to Scatchard analyses of LTC_4 binding to intact cells which were curvilinear, Scatchard analyses of nuclear and plasma membrane fractions were linear, indicative of the presence in these cellular substituents of low and high-affinity binding, respectively. To examine the nature of the high-affinity LTC_4 binding sites, intact V79 cells were photolyzed with [^{3}H]-LTC_4 rendered photoactive by preincubation with N-hydroxysuccinimidyl-4-azidobenzoate. The cell-bound radioactivity migrated during sodium dodecyl sulfate-polyacrylamide gel electrophoresis (SDS-PAGE) with an apparent molecular weight of approximately 40 kdal. Five different commercial preparations of glutathione-S-transferase (GST), which has been implicated as a source of LTC_4 "specific binding" in other cells, migrated in the same SDS-PAGE system with an apparent molecular weight of 20-24 kdal. Furthermore, preincubations of V79 cells with three antisera generated against GST had minimal effects upon subsequent LTC_4 binding to intact cells. These data, taken together with the data from the preceding companion communication, suggest that the radioprotective effect of LTC_4 upon V79 cells may be attributable to a receptor-mediated phenomenon which appears distinct from leukotriene binding to GST.

Introduction

The cytotoxic effects of γ-irradiation from a ^{60}Co source were attenuated in V79A03 (V79) cells that were pretreated with leukotriene C_4 (LTC_4) (1), which induced us to demonstrate that V79 cells contained binding sites for [^{3}H]-LTC_4 (2). Interaction of LTC_4 with V79 cells was reminiscent of a ligand-receptor interaction, because LTC_4 bound to V79 cells in a manner that was specific, reversible, and with both a high- and low-affinity component. However, specific binding of LTC_4, without a demonstrable biological role for the leukotriene, has been reported for several cells,

cell lines, and tissues (reviewed in 3), leading to questions of the biological significance of widespread LTC_4 binding phenomena. The widely distributed detoxicating enzyme glutathione-S-transferase (GST) has been implicated in LTC_4-binding phenomena, following the demonstration by Sun et al. (4) that LTC_4 bound with high-affinity to GST in rat liver.

To further characterize the interaction of LTC_4 with V79 cells, we examined the leukotriene-binding characteristics of plasma membrane and nuclei fractions from V79 cells. To examine the possibility that binding of LTC_4 to V79 cells could be attributed to GST, we examined the mobilities on sodium dodecyl sulfate-polyacrylamide gel electrophoresis (SDS-PAGE) of the photolytic product of V79 cells and [^{3}H]-LTC_4 derivatized with the bifunctional reagent N-hydroxysuccinimidyl-4-azidobenzoate (HSAB), and monitored the effect of antibodies against GST upon LTC_4 binding to V79 cells.

Methods

Materials. [14,15-^{3}H] Leukotriene C_4 ([^{3}H]-LTC_4, 38.4 Ci/mmol) and ^{125}I-Na were purchased from Dupont-NEN (Boston, MA). Nonradioactive LTC_4 was obtained from by Cayman Chemical (Ann Arbor, MI). HSAB and bicinchoninic acid protein assay kit were purchased from Pierce Chemical (Rockford IL). Supplies for SDS-PAGE were purchased from Bio-Rad (Richmond, CA). GST, protein molecular weight standards, L-serine and 5'-nucleotidase kit were obtained from Sigma (St. Louis, MO). Antisera against GST were a gift from Dr. W. Jakoby (National Institutes of Health, Bethesda, MD).

LTC_4 Binding Assay. Binding of [^{3}H]-LTC_4 to preparations of V79 cells was assessed using the methodology described in the preceding companion communication (2), with modifications as described. Aliquots of plasma membrane, cells or isolated nuclei were incubated for 30 min on ice in Hank's buffered salt solution (HBSS) containing 25 mM HEPES, pH 7.35, and 20-70 fmol of [^{3}H]-LTC_4. Nonspecific binding was determined in triplicate by the addition of 16 μM unlabeled LTC_4 to a parallel set of assay tubes. Displacement curves were generated using incubations in graded levels of LTC_4 from 0 to 16 μM. Binding assays were terminated by dilution with 3 ml of ice-cold HBSS and the bound radioactivity was recovered by filtration through Whatman GF/B filters on a Yeda filtration manifold. Bound radioactivity was assessed on a Tracor Analytic Mark III scintillation counter. All binding assays were conducted in duplicate or triplicat , and all experiments were repeated at least once. To assess LTC_4 binding by preparations of plasma membranes or nuclei, preliminary experiments were conducted to demonstrate that radioactivity retention by Whatman GF/B filters was equivalent to retention following filtration on Millipore HAWP, EHWP or GSWP disks, or following centrifugation at approximately 14,000 x g in a microfuge (Eppendorf; Brinkman Instruments; Westbury, NY).

Enzymatic Modification of Glycoproteins. Lots of 40-60 x 10^6 V79 cells were harvested by exposure to PBS-EDTA, divided into equal fractions, and pelleted by centrifugation at 1000 x g. The pelleted cells were resuspended in 10 ml PBS-EDTA containing (a) no enzymes (control), (b) 10 mg hyaluronidase, (c) 1 mg neuraminidase, or (d) 2.5 μg trypsin. The cells were incubated in these solutions for 5 min at 22°C, repelleted, resuspended in IMDM containing 5% fetal bovine serum (FBS) and cooled to

4°C. This medium was replaced with the assay buffer; then Scatchard analyses were conducted using control cells and cells from each enzyme treatment.

Preparation of Nuclei and Plasma Membranes. Fractions highly enriched in nuclei and plasma membranes were prepared by the aqueous two-phase polymer system of Lesko (5). Briefly, harvested cells were resuspended in swelling buffer which consisted of 0.5 mM $CaCl_2$ and 1.0 mM $NaHCO_3$, at pH 7.5 to which 1 mg/l of deoxyribonuclease was added. The cells were allowed to equilibrate in swelling buffer for approximately 30 min during which time the nuclei became swollen. The plasma membranes were lysed using a Dounce homogenizer. The homogenate was centrifuged at 10,000 x g to pellet the plasma membrane and nuclear fractions. The pellet was resuspended and the nuclei separated from the plasma membrane using the aqueous two-phase polymer system. Plasma membranes were retained at the polymer interface while the nuclei were isolated in the pellet. Both fractions were washed twice in HBSS to remove the polymer mixture, prior to use of the fractions in binding assays. Binding assays were conducted using approximately 1-5 x 10^6 nuclei or 10-50 μg of membrane protein per assay tube.

Cell Surface Iodination. To monitor the possible contamination of isolated nuclei with cell surface components, nuclei were prepared from cells in which a portion was cell-surface radioiodinated. Intact viable V79 cells harvested by incubation with 0.002% EDTA were labeled with ^{125}I using lactoperoxidase catalysis modified from the procedure of Miyachi et al. (6). Briefly, ten million cells were suspended in HBSS-HEPES (pH 7.4, 200 μl volume), to which 1 mCi Na-^{125}I, 8 μg lactoperoxidase and 800 ng H_2O_2 were added. Iodination was allowed to proceed for 5 min at 22°C, then cells were washed twice to remove free iodine. Cell-bound radioactivity was assessed by solid scintillation counting. The iodinated cells were added to 10^{10} unlabeled V79 cells and the nuclei isolated as described above.

5'-Nucleotidase Assay. 5'-Nucleotidase activity was assayed by the method of Arkesteijn (7). Whole cells, nuclei, and purified plasma membrane were resuspended in distilled water and homogenized using a Brinkman Polytron. The protein content of each fraction was determined with a bicinchoninic acid protein assay kit, and each solution was diluted with water to a concentration of 1 mg/ml. 5'-Nucleotidase activity was assayed in quadruplicate using approximately 70 μg of protein per assay tube.

Preparation of (Azidobenzoyl) [^3H]-LTC_4. The ethanol in 180 μl of stock [^3H]-LTC_4 (1.8 μCi, 46.8 pmol) was evaporated under a stream of nitrogen gas and 1 M K_2HPO_4, pH 8.0 was added to the remaining aqueous solution to produce a final concentration of approximately 0.52 μM LTC_4. Two hundred nmol HSAB in 10 μl of dimethyl sulfoxide was added to the [^3H]-LTC_4 solution, mixed and incubated in the dark at 22°C for 60 min.

Crosslinking of (Azidobenzoyl) [^3H]-LTC_4 to V79 Cells. Freshly harvested V79 cells ($5x10^5$) were washed twice and incubated in 10 mM serine-borate/HBSS, pH 7.4 with 26 nM (azidobenzoyl) [^3H]-LTC_4 in a final volume of 900 μl. After incubation at room temperature for 90 min in a dark room, the mixture was pelleted by centrifugation at 1500 x g for 2 min, followed by aspiration of the supernatant. The cell pellet was irradiated

using a 254 nm UV lamp (Spectroline, Model ENP-26, Spectronics Corporation, NY) at 1.5-2.0 cm distance at 22°C for 6 min. The cells were suspended in 1 ml of 10 mM serine-borate/HBSS, pH 7.4, and centrifuged at 1500 x g for 5 min. The resulting pellet was collected for electrophoresis. The crosslinking protocol was also replicated using one of two modifications to assess nonspecific binding; addition of 14 μM unlabeled LTC_4 or omission of the UV irradiation step.

SDS-PAGE. The cell pellet was solubilized in 200 μl of SDS-PAGE sample buffer (2% SDS, 10% glycerol, 0.001% bromphenol blue, 50 mM Tris-HCl, 8 M urea with reducing agents 50 mM dithiothreitol and 2% β-mercaptoethanol), by boiling for 5 min. The soluble material was obtained by centrifugation in a Beckman Type 75TI rotor at 100,000 x g for 45 min at 20°C. 130-150 μl sample was loaded onto the gel. A 5-20% linear gradient acrylamide gel was prepared using the procedure of Laemmli (3). Gels contained individual lanes of non-irradiated sample, samples incubated in the absence or presence of 14 μM LTC_4, and molecular weight markers. After electrophoresis, the gel was cut into lanes, and selected lanes were cut into 0.5 cm sections. Each section was immersed in 10 ml of Hydrofluor, then homogenized by polytron (Beckman Instruments, NY; setting 10) for 10 sec. Radioactivity in homogenized sections was quantified by β-scintillation detection. Proteins were visualized in selected lanes using Comassie blue stain. This experiment was replicated three times with equivalent results. The same electrophoretic methodology was utilized to assess the electrophoretic mobility of commercially available preparations of GST obtained from human placentas and liver of bovine, equine, rabbit, and rat.

Incubations with Anti-GST Antisera. LTC_4 binding assays were conducted in the presence of antisera against isoforms of GST (anti-B, anti-C, and anti-E; kindly provided by Dr. W. Jakoby). Binding assays were conducted as described earlier, except that cells in assay tubes were preincubated for 10 min at 22°C in assay buffer containing 10% (v/v) antiserum before addition of [^{3}H]-LTC_4. Each antiserum was evaluated at full strength, at 1:10 and 1:100 dilutions, and compared with simultaneous, control incubations conducted in the absence of antiserum.

GST Assay. GST activity was determined using homogenates of V79 cells prepared by sonication, and using plasma membranes that were purified according to the procedure described by Lesko et al. (5). GST activity was measured using 1-chlor-2,4-dinitrobenzene as a substrate (4). Assays were performed in quadruplicate.

Results

Enzyme Treatments. V79 cells were incubated with enzymes capable of modifying glycoproteins. No treatment significantly influenced binding to the low-affinity binding site. However, treatment with trypsin reduced LTC_4 binding to the high-affinity binding site to 26% that of controls (Table 1). Treatment with neuraminidase slightly enhanced LTC_4 binding, while treatment with hyaluronidase caused increased, but variable LTC_4 binding. Examination of the cells under a light microscope revealed that the cells treated with the hyaluronidase were swollen and partially lysed. Extended periods of trypsinization also resulted in cell lysis and a partial restoration of binding (data not shown). It is possible that the

Table 1. Effect of Enzymes on [^{3}H]-LTC_4 Binding.[a]

Enzyme Treatment	% Control Binding[b]
None (EDTA)	100
Hyaluronidase (N=3)[c]	131 ± 54
Neuraminidase (N=3)	134 ± 8[d]
Trypsin (N=5)	26 ± 10[d]

[a] V79 cells were incubated with enzymes as described in Methods. After enzyme treatment, binding of [^{3}H]-LTC_4 was assessed by Scatchard analyses, and high affinity sites were quantified using LIGAND

[b] ($\bar{x}$ ± SEM)

[c] N represents the number of separate experiments

[d] $P<0.01$ by t-test

increases observed after treatment with several enzymes were due to the release of intracellular binding sites rather than to enzymatic modification of the cell surface binding sites. No effect of enzyme treatment upon binding affinities was apparent.

Preparations of V79 Nuclei and Plasma Membranes. Preparations of nuclei were assessed by determination of 5'-nucleotidase and by monitoring retention of cell-surface radioiodine. Preliminary experiments with iodination using nonradioactive iodine indicated a negligible effect of the iodination procedure upon cellular integrity and viability, as assessed by exclusion of trypan blue. Using the commercial kit for 5'-nucleotidase, we could not detect this enzyme in nuclear preparations. By monitoring radioactivity in nuclei isolated from radioiodinated cells, up to 12% of the radioiodine present on intact cells was detected in the nuclear preparation. The plasma membrane fraction used in these studies was that remaining at the polymer interface during final pelleting of nuclei in the two-phase polymer system. Plasma membranes appeared free of nuclei by microscopic examination, but other assessments of plasma membrane purity were not attempted.

LTC_4 Binding to V79 Subcellular Fractions. Scatchard analyses were conducted of LTC_4 binding to plasma membrane and nuclear fractions from V79 cells. A representative plot of LTC_4 binding to plasma membranes is depicted in Fig. 1. Using LIGAND, the data were best fit by a straight line, suggestive of a single class of binding sites having a Kd ≈ 43 nM. A depiction of LTC_4 binding to two concentrations of nuclei is presented in Fig. 2. The binding of LTC_4 to nuclei were best fit by a straight line indicating a Kd ≈ 240 nM. Scatchard analyses of LTC_4 binding to both plasma membranes and nuclei were repeated twice with equivalent results.

Association and dissociation kinetics of LTC_4 binding to isolated nuclei were compared to that obtained using intact cells (Fig. 3). The association of LTC_4 to 10^6 nuclei proceeded rapidly but attained a lower magnitude than LTC_4 binding to an equivalent number of intact cells, while dissociation of LTC_4 from nuclei followed a similar time course as dissociation from intact cells.

Crosslinking of LTC_4 to V79 Cells. The reaction product of [^{3}H]-LTC_4 and HSAB retained the capacity to bind to V79 cells (Fig. 4). The electrophoretic mobility of radioactive photoreaction products is depicted in Fig. 5, which was representative of three replicated experiments. A major radioactive peak was demonstrable which corresponded to a molecular mass of 40 kDa. When cells were incubated with [^{3}H]-LTC_4 in the presence

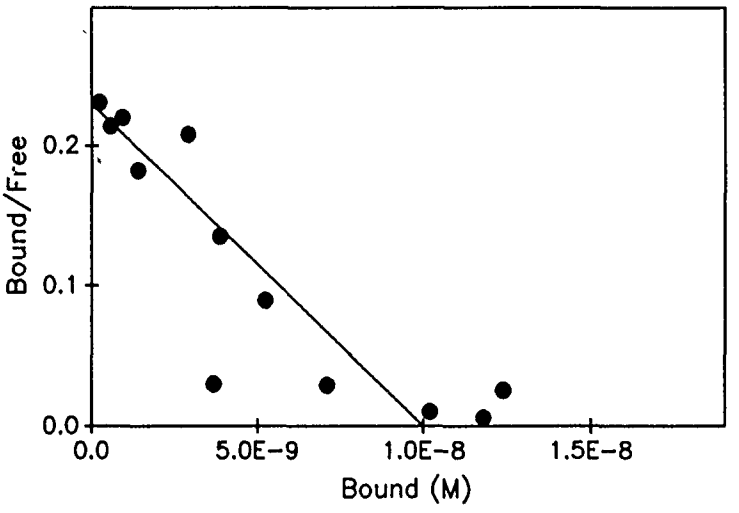

Fig. 1. Scatchard Plot of LTC_4 Binding to V79 Cell Plasma Membranes. Membranes were prepared as described in Methods. Scatchard analyses of LTC_4 binding to approximately 1 mg membrane protein/tube were conducted as described in Methods.

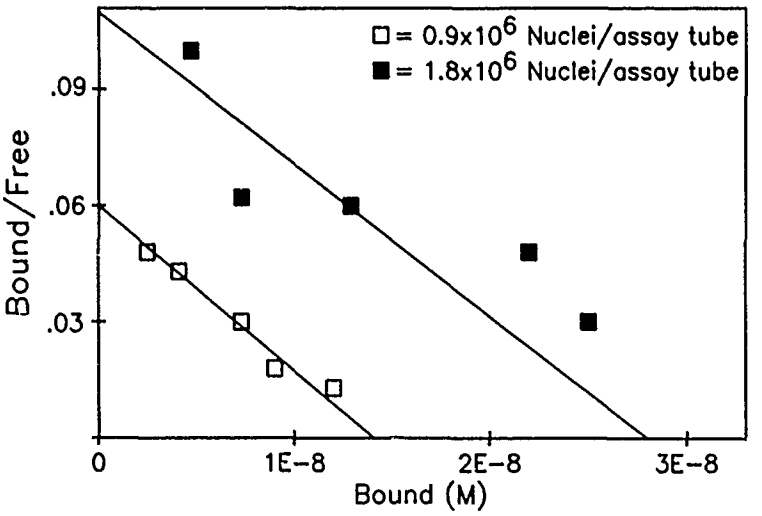

Fig. 2. Scatchard Plots of Leukotriene C_4 (LTC_4) Binding to V79 Nuclei. Nuclei preparation and Scatchard analyses were performed as described in Methods. Binding assays were conducted at two concentrations of nuclei.

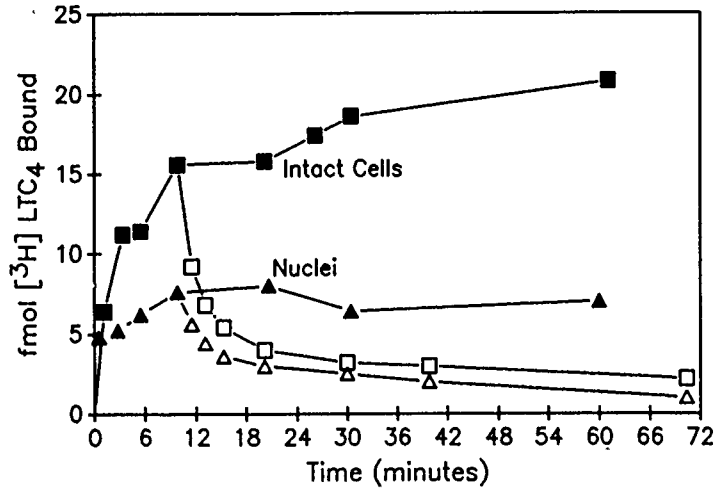

Fig. 3. Association and Dissociation of LTC_4 to V79 Intact Cells and Nuclei. Tubes containing 10^6 cells (■) or 10^6 nuclei (▲) per tube were incubated at 4°C with 1.3 nM [^{3}H]-LTC_4 in 50 µl assay buffer for the indicated times. Dissociation was monitored (open symbols) in tubes to which LTC_4 (16 µM final concentration) was added at 10 min. Incubations were terminated by filtration.

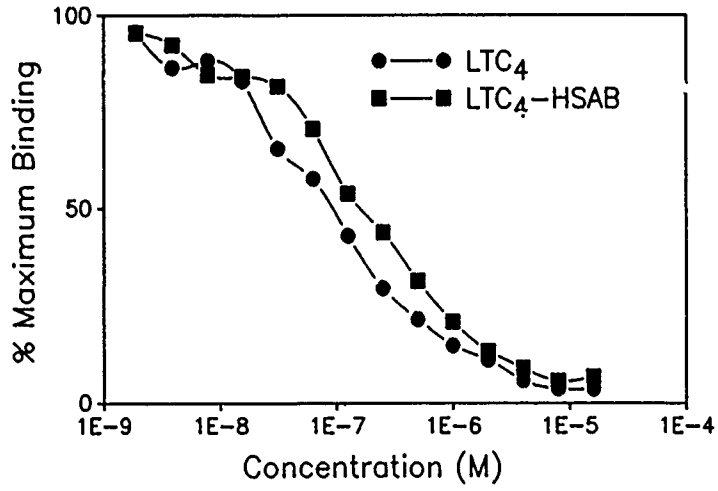

Fig. 4. Displacement of [^{3}H]-LTC_4 Binding to V79 Cells by LTC_4 and LTC_4 Derivatized with HSAB. Binding assays were conducted as described in Methods. In one set of tubes (•), indicated doses of LTC_4 were added. In the other set (■), indicated doses of LTC_4 obtained after derivatization were added.

of 14 μM nonradioactive LTC_4, radioactivity in the gel was greatly reduced (Fig. 5). When samples were not irradiated, radiation in gel fractions was also reduced to levels similar to nonspecific binding (data not shown).

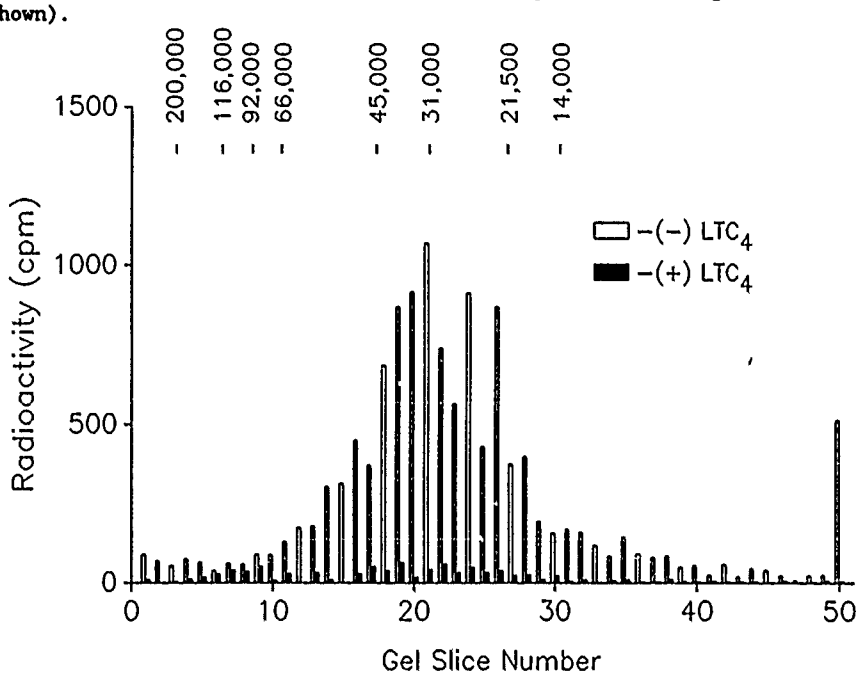

Fig. 5. Radioactivity in SDS-PAGE Slices Following Crosslinking of [^{3}H]-LTC_4 to V79 Cells. [^{3}H]-LTC_4 was crosslinked to cells as described in Methods, in the absence (open bars) and presence (solid bars) of excess unlabeled LTC_4. Gel lanes were sectioned, homogenized, and subjected to β-scintillation counting. The migration positions of the molecular weight markers are indicated.

Using electrophoretic conditions identical to those used to identify photoreaction products, the mobility of five different commercial preparations of GST corresponded to approximately 22-25 kDa (Fig. 6). The data of Figs. 5 and 6, taken together, are suggestive that the major binding product resulting from LTC_4 crosslinking is not GST.

GST Activity in V79 Cell Fractions. As another avenue to assess the possibility that GST could account for LTC_4 binding to V79 cells, GST activity was examined in homogenates prepared by sonication and in plasma membranes. Summarizing data from three different determinations (each determination in triplicate), enzyme activity in sonicated V79 cell preparations was 2.91 ± 0.61 mIU/mg protein, and enzyme activity in the plasma membrane fraction was undetectable (lower limit of detection approximately 0.04 mIU/mg protein). Homogenized cells bound 26 ± 0.9 fmol LTC_4/mg protein and plasma membranes bound 31.4 ± 2.07 fmol LTC_4/mg protein. In comparison, a commercially obtained standard of GST from bovine liver bound approximately 5 fmol LTC_4 per unit of enzyme activity.

Accordingly, GST appeared to be a possible source of a small amount of LTC_4 binding to V79 cells, but appeared unlikely to account for the magnitude of LTC_4 binding observed.

Fig. 6. SDS-PAGE of Five Different Sources of GST. Preparations of GST were solubilized and eluted using the same conditions described for Fig. 5. Sources of GST were Lane 1-rat liver; Lane 2-equine liver, Lane 3-rabbit liver, Lane 4-bovine liver, Lane 5-human placenta.

Further evidence indicating that GST was not the major binding site in intact V79 cells was obtained using binding assays in the presence of antisera against GST. When LTC_4 binding assays were conducted in the presence of 0.1, 1, or 10% dilutions of anti-B, anti-D or anti-E antisera, no influence upon [^{3}H]-LTC_4 binding was detected (data not shown).

Discussion

We conducted experiments to characterize LTC_4 binding to V79 cells. In the report which precedes this communication (2), information was provided relative to the binding characteristics of LTC_4 and viable V79 cells. In this communication, we evaluated the subcellular distribution of LTC_4 binding to V79 cells and examined the possibility that GST was the principal source of LTC_4 binding to V79 cells.

Scatchard analyses of LTC_4 binding to intact V79 cells resulted in concave plots (2), suggesting either that the cells contained multiple classes of binding sites, or that the binding sites displayed negative binding cooperativity. The former possibility appears more likely because curvilinear Scatchard plots resulted from assays of LTC_4 binding to intact cells but linear plots were obtained in assays using preparations of plasma membrane or nuclei, and Hill plots of LTC_4 binding to V79 cells or subcellular components were consistently equal to or less than unity (data not shown). Consequently, it appears probable that V79 cells contain both high-affinity and low-affinity binding sites.

The LTC_4 binding sites appeared proteinaceous in nature because preincubations of V79 cells with trypsin greatly attenuated subsequent LTC_4 binding (Table 1). The reaction product of a photoactive derivative of LTC_4 and intact V79 cells exhibited mobility on SDS-PAGE of approximately 40 kDa (Fig. 5). The high-affinity LTC_4 binding site appeared to be localized largely to the V79 cell surface, because intact, viable cells contained abundant binding and no increase in high-affinity binding was detected when cells were homogenized before LTC_4 binding assays (data not shown). Preparations enriched in plasma membranes also possessed high-affinity binding without a demonstrable low-affinity component (Fig. 1). Conversely, only low-affinity LTC_4 binding was detected using isolated V79 cell nuclei (Fig. 2). Preparations of nuclei had no detectable 5'-

nucleotidase activity, but contained up to approximately 12% of the radioiodine incorporated onto intact cells, suggesting that nuclei might have been contaminated with a small but demonstrable amount of the cell surface.

Interaction of LTC_4 with V79 cells was previously correlated with a quantifiable biological response, namely protection against γ-irradiation (1). Thus, V79 cells that were pretreated with LTC_4 proved resistant to subsequent γ-irradiation. Our studies of LTC_4 binding to V79 cell preparations suggest that the radioprotective effect of LTC_4 can be attributed to a receptor-mediated event. LTC_4 is a thiol-ether and thiols are known to act as radioprotectants through several mechanisms including free-radical scavenging. However, the concentrations of LTC_4 that induce radioprotection are much lower than necessary for the most effective thiol radioprotections (9). As demonstrated in the companion communication (2), LTC_4 binding to V79 cells is of high-affinity, specific, saturable, and reversible. We report studies in this communication demonstrating that LTC_4 binding appears to be attributable to a $\approx$40,000 molecular weight protein which is localized at least in part on the plasma membrane of V79 cells. Finally, the concentrations of LTC_4 that conferred radioprotection (1) correlated with the high-affinity binding of LTC_4 to V79 cells.

The mechanism by which LTC_4 influences the function of its target tissues presumably proceeds by a receptor-mediated process (10); accordingly, specific binding sites for LTC_4 have been reported on several putative target tissues, including guinea pig lung (11), brain and uterus (12), myocardial membranes (13), human lung (14,15), rat lung (16), rat renal glomeruli (17), and on several smooth muscle cell lines (18,19). However, many of these studies did not describe the observed specific binding as a receptor because correlations between LTC_4 binding and target tissue response were not established.

V79 cells are derived from Chinese hamster lung fibroblasts. A LTC_4 receptor was also described in lung fibroblasts from rats (20). The rat fibroblast receptor had many similarities to the binding site which we report in V79 cells, although some differences in the two systems were apparent (such as cyclic nucleotide dependence, and activity of the leukotriene antagonist FPL 55712) which might be attributable to species differences, degree of cell passage, or methodological differences. However, it is most interesting that LTC_4 binding to the rat receptor was correlated with stimulation of collagen synthesis, leading Phan *et al.* (20) to speculate that LTC_4 might serve a cytoprotective or wound healing function. Thus, it is possible that the conferrence of radioprotection to V79 cells by LTC_4 treatment proceeds via a receptor-mediated effect upon protein synthesis. However, we did not address this possible pathway.

We examined the possibility that GST was the source of LTC_4 binding in V79 cells. The glutathione transferases are a multigene family of isoenzymes that catalyze the conjugation of glutathione to electrophilic compounds as the first step in a detoxification pathway (21). Sun *et al.* (4) provided convincing evidence that GST was a major source of LTC_4 binding to rat liver cells, but later urged caution in ascribing physiological significance to LTC_4 binding by tissues and cells for which a physiological role of LTC_4 has not been described (3).

The family of enzymes which are collectively designated GST has been detected in a variety of tissues including lung, kidney, and testis, but is most abundant in liver, where it may constitute 10% of the total soluble protein (22). The glutathione transferases serve in detoxication and have the capacity to bind an enormous number of compounds that have a hydrophobic character (22). It is interesting to speculate that LTC_4 may bind V79 cells (and possibly other cells and tissues) by binding to GST. LTC_4 binding to GST might also account for the inhibition by PGA_2 of LTC_4 binding to V79 cells (4), because GST has been reported to catalyze the conjugation of PGA_1 and glutathione (23).

One interpretation of the data for the two LTC_4 binding sites on V79 cells is that one site represents GST and the other represents γ-glutamyl transpeptidase. γ-Glutamyl transpeptidase, which catalyses the conversion of LTC_4 to leukotriene D_4 (LTD_4), seems an unlikely candidate for a major site of LTC_4 binding to V79 cells: (a) Serine-borate was routinely added to incubates to inhibit the activity of this enzyme. (b) Conversion of LTC_4 to LTD_4 by V79 cells incubated under standard assay conditions could not be detected (Fig. 5 in reference 2). (c) The reported molecular weights (46,000 and 22,000 for two subunits) and binding affinity (Kd = 5-10 μM) of γ-glutamyl transpeptidase (24) are at variance with the values obtained for the interaction of LTC_4 with V79 cells (2, this report). We also think it unlikely that GST is a major source of LTC_4 binding in V79 cells: (a) Intact cells were used for LTC_4 binding studies. GST is predominantly intracellular, and was detectable in homogenates of V79 cells (see Results) but not in plasma membrane preparations, although plasma membranes serve as an effective source of LTC_4 binding. Passive cellular internalization of LTC_4 (which is water soluble) to provide access to intracellular GST would be unexpected, and an active process of LTC_4 internalization seems unlikely during our incubations at 4°C. (b) In the event that LTC_4 traversed the V79A03 cell membrane and bound to intracellular GST, the magnitude of detectable GST activity in homogenized cells appeared insufficient to account for all LTC_4 binding (see Results). (c) Preincubations of intact V79 cells with antisera against GST isozymes B, C and E had no effect upon binding of LTC_4 (data not shown). (d) Photolysis of a photoreactive derivative of LTC_4 and V79 cells resulted in a product that migrated on SDS-PAGE with an apparent molecular weight of 40 kDa, while several commercial preparations of GST migrated in the same gel system with an apparent molecular weight of 20-24 kDa. (e) Given the capacity of GST to bind a multitude of molecules having some degree of hydrophobicity, no mechanism has been advanced by which binding of LTC_4 by GST would confer radioprotection. Ligands bound by GST serve to inhibit enzymic activity (25), thus it is difficult to propose a mechanism by which occupancy (and inactivation) of the detoxicating enzyme GST by LTC_4 would promote radioprotection.

Acknowledgements

The contributions of Dr. W.B. Jakoby for donation of antisera against GST, Mrs. Margaret Marr for expert cell culture, Ms. Yvonne Caicedo for technical manipulations, and Mrs. Jane Koeser for secretarial help, are gratefully acknowledged. This work was supported by NIH HD20780, USUHS Protocol C08517, and Defense Nuclear Agency Work Unit #B2152. The views presented in this paper are those of the authors. No endorsement by the Defense Nuclear Agency or the Department of Defense has been given or

should be inferred.

References

1. Walden, T.L., E.V. Holahan, and G.N. Catravas. Development of a Model System to Study Leukotriene-Induced Modification of Radiation Sensitivity in Mammalian Cells. *Prog. Lipid Res.* 25:587. 1986.
2. Fitz, T.A., D.F. Contois, D.S. Watt, and T.L. Walden Jr. Interaction of Leukotriene C_4 (LTC_4) and Chinese Hamster Lung Fibroblasts (V79A03 Cells). 1. Characterization of Binding. *Prostaglandins*, this issue.
3. Sun, F.F., L.Y. Chau, and K.F. Austen. Binding of Leukotriene C_4 by Glutathione Transferase: A Reassessment of Biochemical and Functional Criteria for Leukotriene Receptors. *Fed. Proc.* 46:204. 1987.
4. Sun, F.F., L.-Y. Chau, B. Spur, E.J. Corey, R.A. Lewis, and K.F. Austin. Identification of a High Affinity Leukotriene C_4-Binding Protein in Rat Liver Cytosol as Glutathione-S-Transferase. *J. Biol. Chem.* 261:8540. 1986.
5. Lesko, L., M. Donlon, G.V. Marinetti, and J.D. Hare. A Rapid Method for the Isolation of Rat Liver Plasma Membranes Using an Aqueous Two-Phase Polymer System. *Biochim. Biophys. Acta* 311:173. 1973.
6. Miyachi, Y., J.L. Vaitukaitis, E. Nieschlag, and M.B. Lipsett. Enzymatic Radioiodination of Gonadotropins. *J. Clin. Endocrinol. Metab.* 34:23. 1972.
7. Arkesteijn, C.L.M. A Kinetic Method for Serum 5'-Nucleotidase Using Stabilized Glutamate Dehydrogenase. *J. Clin. Chem. Clin. Biochem.* 14:155. 1976.
8. Laemmli, U.K. Cleavage of Structural Proteins During the Assembly of the Head of Bacteriophage T4. *Nature* 227:680. 1970.
9. Walden Jr, T.L., M.L. Patchen, and T.J. MacVittie. Leukotriene-Induced Radioprotection of Hematopoietic Stem Cells in Mice. *Radiat. Res.* 113:388. 1988.
10. Fleisch, J.H., L.E. Rinkema, and W.S. Marshall. Commentary: Pharmacological Receptors for the Leukotrienes. *Biochem. Pharmacol.* 33:3919, 1984.
11. Hogaboom, G.K., S. Mong, H.-L. Wu, and S.T. Crooke. Peptidoleukotrienes: Distinct Receptors for Leukotriene C_4 and D_4 in the Guinea Pig Lung. *Biochem. Biophys. Res. Commun.* 116:1136. 1983.
12. Cheng, J.B., D. Lang, A. Bewtra, and R.G. Townley. Tissue Distribution and Functional Correlation of [^{3}H] Leukotriene C_4 and [^{3}H] Leukotriene D_4 Binding Sites in Guinea Pig Uterus and Lung Preparations. *J. Pharmacol. Exp. Ther.* 232:80. 1985.
13. Hogaboom, G.K., S. Mong, J.M. Stadel, and S.T. Crooke. Characterization of Guinea Pig Myocardial Leukotriene C_4 Binding Sites: Regulation by Cations and Sulfhydryl-Directed Reagents. *Mol. Pharmacol.* 27:236. 1985.
14. Rovati, G.E., D. Oliva, L. Sautebin, G.C. Folco, A.F. Welton, and S. Nicosia. Identification of Specific Binding Sites for Leukotriene C_4 in Membranes from Human Lung. *Biochem. Pharmacol.* 34:2831. 1985.
15. Lewis, M., S. Mong, R.L. Vesella, G.K. Hogaboom, H.-L. Wu, and S.T. Crooke. Identification of Specific Binding Sites for Leukotriene C_4 in Human Fetal Lung. *Prostaglandins* 27:961. 1984.
16. Pong, S-S., R.N. DeHaven, F.A. Kuehl Jr. and R.W. Egan. Leukotriene C_4 Binding to Rat Lung Membranes. *J. Biol. Chem.* 258:9616. 1983.

17. Ballerman, B.J., R.A. Lewis, E.J. Corey, K.F. Austin, and B.M. Brenner. Identification and Characterization of Leukotriene C_4 Receptors in Isolated Rat Renal Glomeruli. *Circ. Res.* 56:324. 1985.
18. Clark, M.A., M. Cook, S. Mong, G.K. Hogaboom, R. Shorr, J. Stadel, and S.T. Crooke. Leukotriene C_4 ($[^3H]LTC_4$) Binding to Membranes Isolated From a Hamster Smooth Muscle Cell Line (DDT1MF2). *Life Sci.* 35:441. 1984.
19. Krillis, S., R.A. Lewis, E.J. Corey, and K.F. Austen. Specific Receptors for Leukotriene C_4 on a Smooth Muscle Cell Line. *J. Clin. Invest.* 72:1516. 1983.
20. Phan, S.H., B.M. McGarry, K.M. Loeffler, and S.L. Kunkel. Binding of Leukotriene C4 to Rat Lung Fibroblasts and Stimulation of Collagen Synthesis In Vitro. *Biochemistry* 27:2846. 1988.
21. Kramer, R.A., J. Zakher, and G. Kim. Role of the Glutathione Redox Cycle in Acquired and De Novo Multidrug Resistance. *Science* 241:694. 1988.
22. Jakoby, W.B. The Glutathione-S-Transferases: A Group of Multifunctional Detoxification Proteins. *Adv. Enzymol.* 46:383. 1978.
23. Cagen, L.M., J.J. Pisano, J.N. Ketley, W.H. Habig, and W.B. Jakoby. The Conjugation of Prostaglandin A_1 and Glutathione Catalyzed by Homogeneous Glutathione S-Transferases From Human and Rat Liver. *Biochim. Biophys. Acta* 398:205. 1975.
24. Meister, A., S.S. Tate, and O.W. Griffith. In: *Methods in Enzymology* (W.B. Jakoby, ed.) Vol. 77, Academic Press, New York, 1981, p. 237.
25. Ketley, J.N., W.H. Habig, and W.B. Jakoby. Binding of Nonsubstrate Ligands to the Glutathione S-Transferases. *J. Biol. Chem.* 250:8670. 1975.

Editor: P. Ramwell Received 5-18-87 Accepted 8-16-90

0022-5282/91/3103-0316$03.00/0
THE JOURNAL OF TRAUMA

Vol. 31, No. 3
Printed in U.S.A.

Treatment of Mice with Sepsis Following Irradiation and Trauma with Antibiotics and Synthetic Trehalose Dicorynomycolate (S-TDCM)

GARY S. MADONNA, PH.D., G. DAVID LEDNEY, PH.D., MARY M. MOORE, B.S., THOMAS B. ELLIOTT, PH.D., AND ITZHAK BROOK, M.D.

Compromise of antimicrobial defenses by irradiation can result in sepsis and death. Additional trauma can further predispose patients to infection and thus increase mortality. We recently showed that injection of synthetic trehalose dicorynomycolate (S-TDCM) significantly augments resistance to infection and increases survival of mice compromised either by whole-body irradiation with gamma radiation or equal mixtures of fission neutron and gamma radiation. In this study, C3H/HeN mice were given a lethal dose of gamma radiation (8.0 Gy) and an open wound (15% total body surface area [TBSA]) 1 hr later while anesthetized. Irradiated/wounded mice became more severely leukopenic and thrombocytopenic than mice exposed to radiation alone, and died from natural wound infection and sepsis within 7 days. S-TDCM given 1 hr postirradiation increased survival of mice exposed to radiation alone. However, this treatment did not increase survival of the irradiated/wounded mice. Systemic antibiotic therapy with gentamicin or ofloxacin for 10 days significantly increased survival time compared with untreated irradiated/wounded mice ($p < 0.01$). Combination therapy with topical gentamicin cream and systemic oxacillin increased survival from 0% to 100%. Treatment with S-TDCM combined with the suboptimal treatment of topical and systemic gentamicin increased survival compared with antibiotic treatment alone. These studies demonstrate that post-trauma therapy with S-TDCM and antibiotics augments resistance to infection in immunocompromised mice. The data suggest that therapies which combine stimulation of nonspecific host defense mechanisms with antibiotics may increase survival of irradiated patients inflicted with accidental or surgical trauma.

Leukopenia in compromised patients can result in life-threatening sepsis caused by bacteria (6, 37). Current therapeutic regimens used to treat infections in immunocompromised patients do not ensure survival (9, 28). Present antimicrobial therapies need to be augmented with new approaches to stimulate impaired nonspecific host defenses.

From the Wound and Infection Management Program, Experimental Hematology Department, Armed Forces Radiobiology Research Institute, Bethesda, Maryland.

Some of the data were presented at the XIV International Symposium on Microbial Ecology and Disease, San Antonio, Texas, September 21-23, 1989, and the Immunocompromised Surgical Patient: Mechanisms and Therapy in Trauma and Burns, Snowbird, Utah, January 24-28, 1990.

Supported by the Armed Forces Radiobiology Research Institute, Defense Nuclear Agency, under Research Work Unit 4440 00129. The views presented in this paper are those of the authors. No endorsement by the Defense Nuclear Agency has been given or should be inferred. Research was conducted according to the principles enunciated in the *Guide for the Care and Use of Laboratory Animals* prepared by the Institute of Laboratory Animal Resources, National Research Council.

Address for reprints: Gary S. Madonna, Ph.D., Experimental Hematology Department, Armed Forces Radiobiology Research Institute, Bethesda, MD 20814-5145.

Sublethal exposure of mice to ionizing radiation causes prolonged leukopenia (8). Animals given lethal doses of ionizing radiation die with sepsis within 2 weeks (36). Sepsis can result from the passage of bacteria from the gastrointestinal tract, i.e., bacterial translocation, or from exogenously acquired bacteria (10). Increased susceptibility to infection following irradiation results from hematopoietic stem cell depletion, severe and prolonged leukopenia, depressed antimicrobial resistance, and disruption of cellular barriers to infection, e.g., the gastrointestinal tract (2, 36) and the skin (15, 16). Antibiotic therapy alone in irradiated animals (3, 4) and immunocompromised patients (9, 28) does not prevent death.

Recent work with mice in our laboratory showed that intraperitoneal (IP) injection of purified trehalose dimycolate (TDM), a glycolipid extracted from the cell walls of *Mycobacterium phlei*, mitigated the lethal effects of ionizing radiation (19). TDM or synthetically prepared trehalose dicorynomycolate (S-TDCM) stimulated hematopoiesis, decreased sepsis, and increased survival when given either 1 day before or 1 hr after gamma (19)

or fission neutron irradiation (23). S-TDCM increased host resistance to lethal *Klebsiella pneumoniae* infection in gamma- (19) or fission-neutron-irradiated mice (23), and acted in synergy with ceftriaxone to augment resistance to supralethal doses of *K. pneumoniae* in gamma-irradiated mice (19). We also showed that TDM derived from *M. phlei* increased the resistance of sublethally irradiated mice more effectively than monophosphoryl lipid A derived from *Salmonella minnesota* (20). Macrophages from irradiated mice were able to kill *K. pneumoniae* more effectively when stimulated in vitro with TDM than were untreated macrophages from irradiated mice (Ledney, G. D., Madonna, G. S., Chock, S. P.: Abstr. Ann. Meet. Am. Soc. Microbiol., 1988, E71, p.120). Further, evidence showing that TDM is active against intracellular organisms (18) and protection of mice against influenza virus is abrogated by silica, dextran sulfate, or carrageenan (22) clearly points to the macrophage as the main effector cell of TDM in vivo. S-TDCM caused no apparent toxic effects (ruffled fur, diarrhea, eye exudate) in unirradiated or irradiated animals (19). The synthesis, biologic properties, and mechanisms of action of TDM were reviewed by Lemaire et al. (18) and Lederer (12).

These results suggest that S-TDCM might augment resistance and increase survival under a more severe condition of lethal radiation and trauma. In this study, we focused on the ability of S-TDCM to increase survival when given immediately after trauma occurring 1 hr postirradiation. We also explored the use of systemic antibiotic therapies with oxacillin, gentamicin, and ofloxacin (2-fluoro-quinolone) for their respective spectra of activity, and topical antibiotic therapy for its effect on wound-infecting bacteria, to help us differentiate which bacteria caused death. Finally, these therapies were combined in order to achieve maximal survival.

MATERIALS AND METHODS

Mice. C3H/HeN female mice, 8 to 12 weeks old and weighing 19 to 24 gm, were obtained from the National Cancer Institute Animal Breeding Facility (Frederick, MD). All mice were quarantined upon arrival for 1 week and screened for evidence of disease before being released from quarantine. They were maintained in plastic Micro-Isolator cages (Lab Products, Inc., Maywood, NJ) on hardwood chip contact bedding and provided commercial rodent chow and acidified (pH 2.5 by addition of HCl) tap water ad libitum. Animal holding rooms were maintained at 70°F ± 2°F (ca 21.1°C) and 50% ± 10% relative humidity, with at least ten air changes per hr with 100% conditioned fresh air. The mice were on a 6 A.M. to 6 P.M. 12 hr light dark full spectrum lighting cycle with no twilight. Research was conducted in an American Association for Accreditation of Laboratory Animal Care accredited facility and reviewed by an Institutional Animal Care and Use Committee.

Immunomodulator and Antimicrobial Agents. i) *S TDCM.* S TDCM was generously provided by Ribi Immuno Chem Research, Inc. (Hamilton, MT). S TDCM was prepared essentially by the method of Numata et al. (24). Potassium mycolate used in the preparation of S TDCM was obtained by Claisen condensation of methyl palmitate as described by Polonsky and Lederer (29). Before injection of mice, S-TDCM was prepared as an aqueous suspension as described previously (19), with modification. Briefly, 10 mg of S-TDCM were solubilized in 1 ml of hexane (HPLC grade (Optima) (Fisher Scientific, Fairlawn NJ), placed in a smooth-walled glass 30-ml Potter-Elvehjem tissue homogenizer (Wheaton, Millville, NJ), and dried under nitrogen with rotation. S-TDCM was then homogenized using a Teflon pestle for 5 min at 1,000 r.p.m. in 10 ml of cold pyrogen-free 0.2% Tween 80, 0.9% NaCl (saline). The suspension was then sonicated (five 10-sec bursts) using a Sonicator Cell Disrupter (200 watts, 50/60 Hz, frequency 20 KHz; Heat Systems-Ultrasonics, Inc., Plainview, NY). All glassware used to prepare S-TDCM was depyrogenated by heating in air at 180°C for 4 hr. Aqueous stock preparations of S-TDCM (1 mg/ml) were tested for endotoxin using the limulus amebocyte lysate assay (Associates of Cape Cod, Inc., Woods Hole, MA) and found to contain <0.03 endotoxin units (EU)/ml (<0.006 ng/ml).

ii) *Drugs:* Oxacillin sodium (Bactocill, Beecham Laboratories, Division of Beecham, Inc., Bristol, TN), gentamicin sulfate (Elkins-Sinn, Inc., Cherry Hill, NJ), and ofloxacin, generously provided by R. W. Johnson (Pharmaceutical Research Institute, Raritan, NJ), were reconstituted with sterile distilled pyrogen-free water. A 0.1-ml dose was injected subcutaneously (SC) above the right or left (alternated daily) gluteus medius of each restrained mouse once per day for 10 days. The daily dose of oxacillin was 150 mg/kg, gentamicin 7.5 mg/kg, and ofloxacin 40 mg/kg. Doses were adjusted according to weight at approximately 4-day intervals. A 0.1 ml amount of pyrogen-free water was injected daily SC into each control mouse.

The following creams, ointment, and solutions were tested: Garamycin cream (0.1% gentamicin sulfate, Schering Corp., Kenilworth, NJ), Pharmadine ointment (10% povidone-iodine, Sherwood Pharmaceutical Co., Mahwah, NJ), Operand Aerosol Spray (povidone-iodine [0.5% available iodine], Redi-Products, Prichard, WV), Silvadene cream (1% silver sulfadiazine, Marion Laboratories Inc., Kansas City, MO), Bactroban ointment (2% mupirocin, Beecham Laboratories, Bristol, TN), and Dakin's solution (0.25% and 0.125% sodium hypochlorite, The Clorox Co., Oakland, CA). Each preparation was applied once daily in sufficient amounts to cover the entire wounded area.

Serum Concentration of Antibiotics. On the fourth day of therapy following irradiation, cardiac blood was collected from mice anesthetized by inhalation of methoxyflurane (Metofane; Pitman-Moore, Inc., Washington Crossing, NJ) 1 hr and 6 hr after administration of each antibiotic. The concentration of gentamicin was detectable at 0.3 μg/ml by fluorescence polarization immunoassay (TDX, Abbott Laboratories, Irving, TX). Oxacillin was detectable at 0.5 μg/ml by the agar diffusion bioassay with *Bacillus subtilis* ATCC 6633 and *Staphylococcus aureus* ATCC 6538P (1). Ofloxacin levels were not determined.

Radiation and Trauma Model. Mice were placed in aerated Plexiglas containers and bilaterally irradiated with a ^{60}Co gamma source at 0.4 Gy/min. The midline absorbed dose was 8.0 Gy. The techniques of irradiation and dosimetric determination were previously described (33). At approximately 1 hr postirradiation mice were wounded as previously described (14). Briefly, mice were anesthetized by inhalation of methoxyflurane and subjected to wound trauma by punching out a double layer of dorsal surface skin between the shoulders. The panniculus carnosus muscle and overlying skin was removed by sliding the loose dorsal skin away from the body and by striking a steel punch with a hammer. The procedure was done on a clean, Teflon covered operation board. The size of the open wound was 2.5 × 3.75 cm, which was approximately 15% of the total body surface area (TBSA) of the mouse. Computation of

body surface area was based on

$$BSA = \frac{W^{213}\ K}{104}$$

(K = 9 for mice) (31). Experimental controls included groups of mice exposed to radiation alone (8.0 Gy), and wounded alone (15% TBSA). Mice were housed four to a cage with daily changes of bedding for the first 10 days after irradiation and injury. Thereafter, fresh bedding was provided thrice weekly. Food was changed every other day and water was changed weekly.

Bacteriology and Hematology. Culture of wounds, blood, and liver samples and hematology of whole blood were determined in a separate experiment using the following procedure. On days 1, 2, 3, 4, 7, 10, and 14 postirradiation, the wounds of four mice from irradiated/wounded or wounded (control) groups were cultured for bacteria using a sterile cotton-tipped applicator (Citmed Corp., Citronelle, AL), moistened in sterile saline, and rolled over the wound surface. The sample was then inoculated to one plate of 5% defibrinated sheep blood in soybean casein digest agar with phenyl ethanol and one plate of MacConkey agar (BBL, Cockeysville, MD) for isolation of facultative bacteria. Culture plates were incubated in 5% carbon dioxide and air at 35°C for 48 hr.

Following wound culture, irradiated/wounded mice and controls (normal, irradiated, and wounded mice) were anesthetized by inhalation of methoxyflurane and exsanguinated by cardiac puncture using a syringe containing 10 μl of heparin. A 50-μl quantity of heparinized blood from each mouse was inoculated to one tube of thioglycollate medium (BBL, Cockeysville, MD) with added glucose and incubated for 48 hr. Remaining blood was transferred to tubes (Sarstedt, W. Germany) that contained 3 mg EDTA. The numbers of white blood cells and platelets per mm^3 of blood were determined on individual blood samples using a System 9000 Automated Cell Counter (Serono-Baker Diagnostics, Inc., Allentown, PA). White blood cell differentials were determined from blood smears stained with Modified Wright's stain (Hema-Tek II Stain Pak, Miles Inc., Elkhart, IN).

The liver from each mouse was aseptically removed, weighed, and homogenized in cold sterile 0.9% NaCl solution at a dilution of 1:5 (w/v). One-tenth ml of each homogenate was inoculated into thioglycollate medium. After 48 hr of incubation at 35°C, blood and liver cultures in thioglycollate were inoculated to 5% defibrinated sheep blood agar with phenyl ethanol, MacConkey agar, and CDC anaerobic blood agar with kanamycin and vancomycin (BBL, Becton-Dickinson Microbiology Systems, Cockeysville, MD). Blood agar and MacConkey agar plates were incubated in 5% carbon dioxide and air for an additional 48 hr. Plates for anaerobic culture were incubated in a GasPak Anaerobic System (BBL, Microbiology Systems, Cockeysville, MD). Staphylococci, Streptococci, and Gram-negative bacteria were identified using Staph Trac, 20S Streptococcus System, and API 20E (Analytab Products, Division of Sherwood Medical, Plainview, NY), respectively. Liver homogenates were further diluted 1:20 with pyrogen-free water, heat treated for 10 min in a 75°C water bath, and tested for endotoxin using the limulus amebocyte lysate assay. The endotoxin levels of liver homogenates from irradiated/wounded mice were similar to control levels, and were found to contain <0.03 EU/ml.

Survival Measurements and Statistical Evaluation. Data for survival of mice in experimental groups during 30 day periods after irradiation were compared by the generalized Savage (Mantel-Cox) procedure (Program 1L; BMD Statistical Software, Inc., Los Angeles, CA). Statistical significance of hematology values obtained from cardiac blood was determined by one-way analysis of variance and Student's *t*-test. Mean survival times (MST) during the 30-day period of observation were calculated using the following equation: $\sum$[(# of deaths on day N) (N)]/total dead.

RESULTS

Effect of Trauma on Mortality, Hematology, Wound Infection, and Sepsis following Lethal Irradiation. i) *Mortality:* Previous studies in B6D2F1 mice showed that a 15%–30% TBSA wound given 1 hr postirradiation causes a higher rate of mortality than irradiation alone (13). To assess the effect of wounding in irradiated C3H/HeN mice, groups of mice were given various doses of radiation and wounded 1 hr later. Mice irradiated only or wounded only served as controls. Mortality was accelerated by trauma and was dependent upon the dose of radiation (Fig. 1). For example, mice given 8.0 Gy radiation and wounded died earlier in a 30-day period (MST = 9 days) than mice that received radiation alone (MST = 16 days) ($p < 0.001$). Early death was accompanied by severe lethargy and wasting. A 15% TBSA wound was not lethal in unirradiated mice.

ii) *Hematology:* To assess leukopenia following trauma, groups of mice were given 8.0 Gy and wounded 1 hour later. On days 1, 2, 3, 4, 7, 10, and 14 following irradiation, the numbers of white blood cells and platelets from blood samples were determined. Groups of mice that received either radiation, wounding, or no treatment served as controls. Postirradiation trauma significantly decreased the number of white blood cells by day 1 as observed in animals which received irradiation only (Fig. 2A). Postirradiation trauma significantly decreased the number of platelets by day 2, earlier than irradiation alone (Fig. 2B). The numbers of both leukocytes and platelets continued to decline until death. In contrast, trauma in normal mice was followed by significantly increased numbers of white blood cells and platelets by day 10 and day 7, respectively. Postirradiation trauma or irradiation alone also caused a progressive decline in the number of red blood cells starting 2 days postirradiation that was accompanied by a decline in both hemoglobin and hematocrit (data not shown).

iii) *Wound infection and sepsis. Staphylococcus aureus* was the predominant organism recovered from the wounds of irradiated/wounded mice and wounded mice. *Escherichia coli* was only isolated from the wounds of irradiated/wounded mice. Other bacteria that were isolated from wounds included *Staphylococcus xylosus*, *Staphylococcus epidermidis*, and *Streptococcus faecium*. No bacteria were cultured from the skin or hair of normal mice. Only *S. aureus* was isolated from blood culture of irradiated/wounded mice on days 3, 4, and 7. No bacteria grew in blood cultures from control, irradiated, and wounded mice throughout the 14 day period. Only *S. aureus* was isolated from liver cultures from irradiated/wounded mice on days 2, 3, 4, and 7. *S. aureus* was isolated from liver cultures of irradiated mice, but not until day 10 postirradiation. No anaerobic bacteria were cultured from blood or liver.

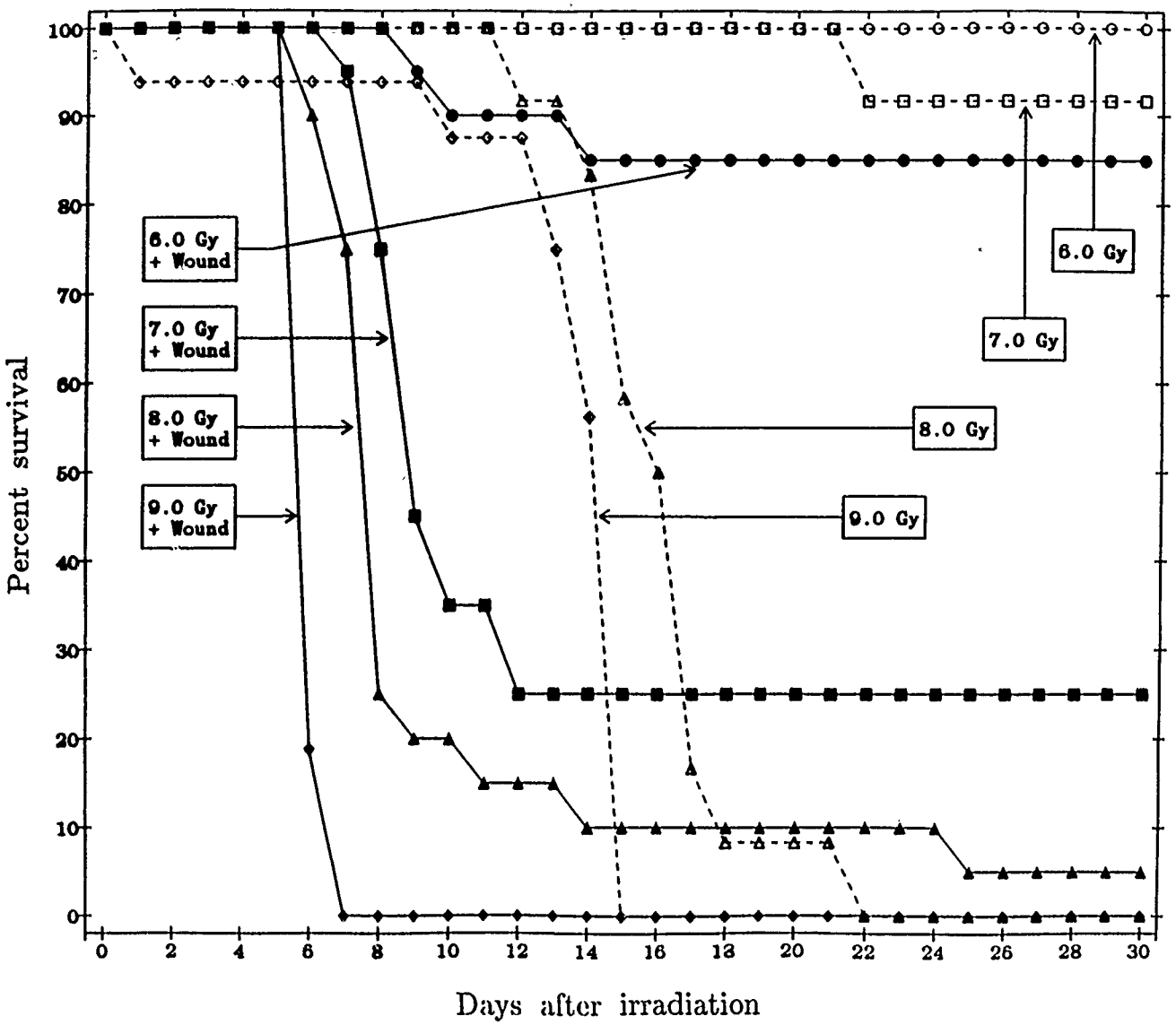

FIG. 1. Survival following ^{60}Co irradiation and trauma of C3H/HeN mice given 6.0, 7.0, 8.0, or 9.0 Gy. At 1 hr postirradiation, mice given each radiation dose were given either a 15% total body surface area wound and saline, 0.5 ml, IP (R + W, $n = 20$) or saline alone (R, $n = 12$).

Changes in the MST after S-TDCM or Systemic Antibiotic Therapy in Irradiated/Wounded Mice. Previous work showed that S-TDCM increased both resistance to bacterial infection and survival of mice following irradiation (19). We tested the possibility that S-TDCM might raise resistance and increase survival of irradiated mice following trauma. Mice were irradiated and wounded, and S-TDCM (200 μg/mouse, IP) was injected 1 hr postirradiation. Control mice received saline. Mice that received radiation alone were also given either S-TDCM or saline 1 hr postirradiation. S-TDCM increased survival of irradiated mice, however, it did not increase survival of irradiated/wounded mice (Fig. 3). *S. aureus*, *S. faecium*, *E. coli*, and *Proteus mirabilis* grew in cultures of the wound sites of both saline and S TDCM treated mice 4 days postirradiation.

Because of these findings, we postulated that additional therapy with antibiotics would be necessary to reduce infection in these mice. To select a suitable antibiotic, groups of irradiated/wounded mice ($N = 20$) initially received a 10-day course of therapy with either oxacillin, gentamicin, or ofloxacin SC, beginning on day 2. Control mice were given water SC. Survival times of mice that were treated with gentamicin or ofloxacin increased significantly (8.8 days and 9.2 days, respectively) compared with water-treated mice (5.5 days; $p < 0.01$). Oxacillin did not significantly increase the MST (6.6 days; $p > 0.05$).

In a separate experiment, the wounds of antibiotic-treated mice were cultured for 5 successive days postirradiation to evaluate any differences in the incidence of bacterial species. The recovery of *S. aureus* was decreased in oxacillin treated mice, although oxacillin did not increase survival time. Recovery of both Gram positive and Gram-negative bacteria was reduced in ofloxacin-treated mice, whereas systemic gentamicin had no apparent effect on the recovery of bacteria from the wound site (data not shown).

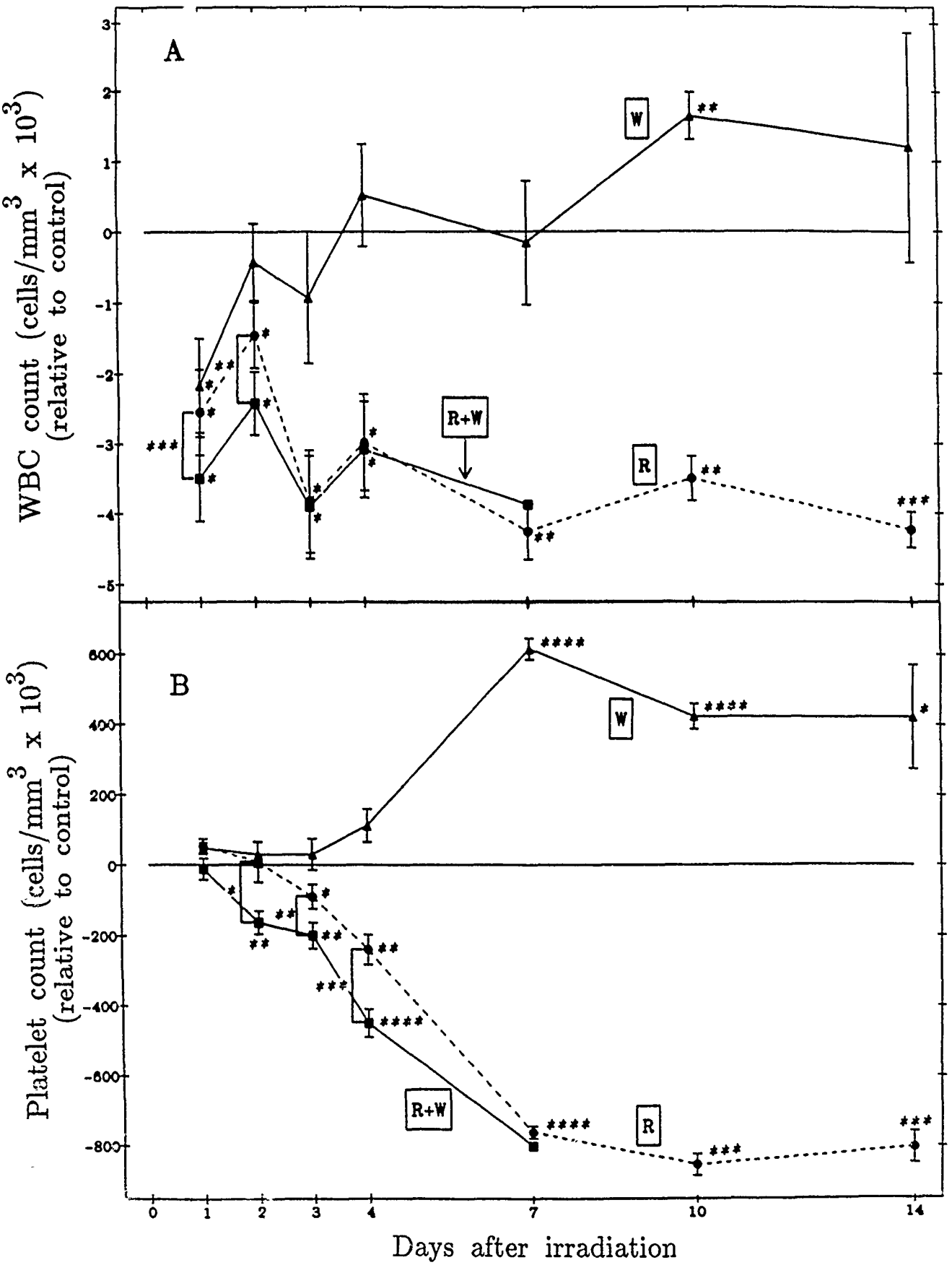

FIG 2 White blood cell and platelet numbers in peripheral whole blood following lethal irradiation and trauma of C3H/HeN mice given 8.0 Gy ^{60}Co At 1 hr postirradiation, mice received either a 15% total body surface area wound and saline (R + W), or saline alone (R). Normal unirradiated mice received either a 15% TBSA wound and saline (W), or saline alone (control). On days 1, 2, 3, 4, 7, 10, and 14, the number of

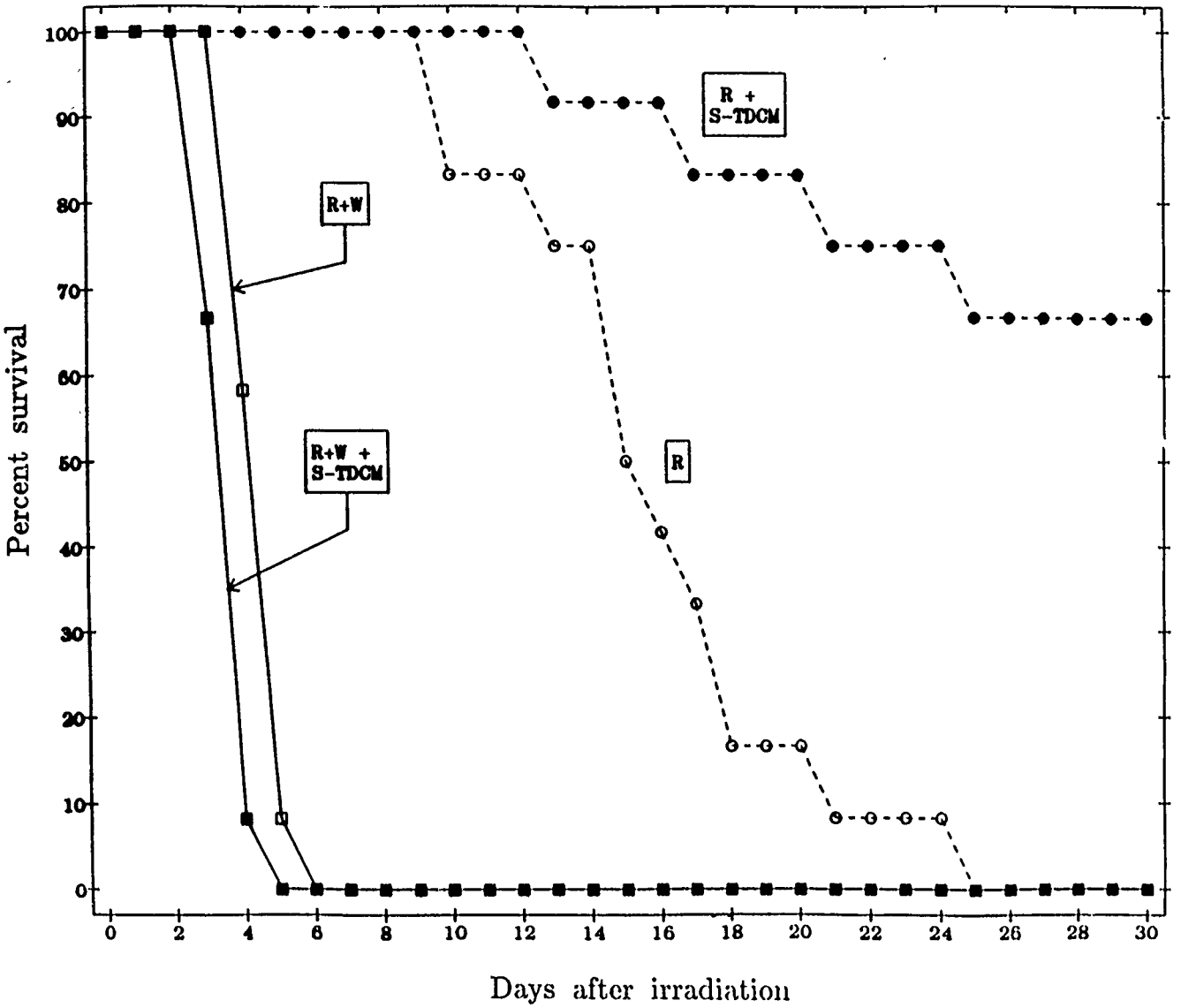

FIG. 3. Survival of irradiated/wounded C3H/HeN mice treated with synthetic trehalose dicorynomycolate and given 8.0 Gy ^{60}Co. At 1 hr postirradiation, mice received a 15% total body surface area wound and injection with either 200 μg S-TDCM/mouse, IP (R + W + S-TDCM), or 0.5 ml saline/mouse, IP (R + W). Mice that were given radiation alone received either S-TDCM or saline, 1 hr postirradiation. During the 30-day period of observation, mean survival time was 4.7 days for [R + W], 3.8 days for [R + W + S-TDCM], and 16 days for [R]. Mantel-Cox p-values: 0.0034 ([R + W] versus [R + W + S-TDCM]) and <0.001 ([R] versus [R + S-TDCM]). N = 12. Results are from one of four experiments repeated 3 times.

Because of this effect of daily therapy with ofloxacin, we next treated irradiated/wounded mice (N = 12) with both S-TDCM and ofloxacin. This combined therapy did not significantly increase survival time (10.2 days) compared with ofloxacin therapy alone (11.4 days; $p > 0.05$). Similar results were obtained from mice treated with S-TDCM and oxacillin and mice treated with S-TDCM and gentamicin (data not shown).

Changes in the Number of Survivors after Combination Therapies with Topical and Systemic Antibiotics. Topical and systemic antibiotics can synergize to prevent wound infection (34). To explore this possibility in irradiated/wounded mice, we applied various topical antiseptic and antibiotic preparations to wounds for 5 days postirradiation. The wound sites were cultured to assess the ability of each antibiotic to reduce infection. Survival was monitored. Daily application of gentamicin cream was superior to other preparations tested. (See Materials and Methods.) Gentamicin cream eliminated both Gram-positive and Gram-negative bacteria from the wound site and increased survival time from 4 days (untreated) to 7 days (N = 8) (data not shown).

white blood cells (top panel) and platelets (bottom panel) is shown as determined from individual samples of cardiac blood. No R + W mice survived 10 days. Each point represents the mean ± SEM of data obtained from four mice. Data were normalized with respect to values from control mice using the following equation. $(x_t - x_n) \pm [(SE_t^2 + SE_n^2)]^{1/2}$, where t = test, n = normal. Student's t test p values (* = <0.05, ** = <0.01, *** = <0.001, **** = <0.0001) are relative to daily controls except where indicated by bracket.

Groups of irradiated/wounded mice ($N = 8$) were then treated for 10 days with gentamicin cream alone or gentamicin cream plus systemic oxacillin, gentamicin, or ofloxacin. Therapy with gentamicin cream alone significantly increased survival from 0% (untreated) to 50%. Combination therapy with systemic oxacillin increased survival to 100%, but combination therapy with systemic gentamicin or ofloxacin increased survival only to approximately 40% and 10%, respectively.

Changes in the Number of Survivors after Combination Therapy with S-TDCM together with Topical and Systemic Antibiotics. To illustrate the efficacy of enhancement of nonspecific resistance to infection in this system, mice were administered S-TDCM and the less effective treatment of systemic and topical gentamicin. Groups of mice were irradiated, wounded 1 hr later, and S-TDCM or saline (control) injected IP. Mice were then treated daily for 10 days beginning on day 0 with systemic and topical gentamicin or topical gentamicin alone. Results showed that S-TDCM significantly increased survival compared with antibiotic treatments alone (Fig. 4). The animals that recovered and survived to the end of the 30-day monitoring period were also observed for an additional 30 days. Mice did not show signs of toxicity, infection, or any other deleterious consequences from the treatment protocol.

Serum Concentrations of Antibiotics. A low therapeutic concentration of gentamicin (2.34 ± 0.54 μg/ml) was achieved 1 hr after administration in mice that were treated with both systemic and topical formulations, but not with either alone (0.84 ± 0.07 μg/ml and 0.72 ± 0.04 μg/ml, respectively). Therapeutic concentration of oxacillin (9.56 ± 0.98 μg/ml) was achieved 1 hr after injection, but was not detectable at 6 hr after injection (< 0.5 μg/ml).

DISCUSSION

It is estimated that 10 million patients yearly are treated for traumatic wounds in emergency departments in the United States and that 5% to 30% of these wounds become infected (7). Treatment of these and other life threatening infections is difficult when outpatient therapy fails, systemic toxicity occurs, or the patient is immunocompromised (35).

Development of effective therapies for managing trauma associated infections in these patients is hindered by the lack of suitable animal models. One model that has been used to study the effects of trauma in immunocompromised animals is that of Ledney et al. (15) who showed that survival of B6D2F1 mice exposed to radiation and trauma depends on the type and dose of radiation, the type of skin wound, and the timing of skin wound relative to irradiation (13, 15). Further, irradiation delays skin wound closure compared to closure of wounds in unirradiated mice (15, 16).

Using a similar model of combined injury, we initially found that postirradiation trauma accelerated mortality. Mortality was dependent upon the dose of radiation. These findings support and extend the work of Ledney et al. (13). We next found that postirradiation trauma increased both the onset and severity of leukopenia and thrombocytopenia that correlated with early onset of sepsis. In distinct contrast, trauma in normal mice increased the number of leukocytes and platelets and did not result in sepsis. Importantly, the increase in platelets and leukocytes in wounded mice did not occur until 7 and 10 days post-trauma, respectively. Our previous studies indicated that trauma (4% TBSA) indeed augmented hematopoiesis in both unirradiated and sublethally irradiated mice ((C57Bl/6 × CBA)F1) when given 24 hr before irradiation (16, 17). Following lethal irradiation/trauma, however, mice succumbed to sepsis before augmented hematopoietic regeneration could occur. Nevertheless, antimicrobial therapy with oxacillin and topical gentamicin resulted in 100% survival. Thus it is possible that antimicrobial therapy increased survival by containing the spread of infection until functional hematopoietic elements recovered.

Combination therapy with systemic oxacillin and topical gentamicin may have provided synergistic antistaphylococcal and antienterococcal activity. It seems probable that elimination of *E. coli* from the wound site by topical gentamicin cream contributed significantly to survival. Culture of *S. aureus* from the wound and blood of mice following trauma and the success of combination antibiotic therapies used in this study bring together the findings of several investigators. Kontiainen and Rinne (11) showed that the most common infectious complication of wounds in normal persons is cellulitis caused by *S. aureus* and group A β-hemolytic Streptococci. An antistaphylococcal penicillin such as oxacillin, nafcillin, or a first-generation cephalosporin may be effective in such infections (35). Further, Campos et al. (5) and Steigbigel et al. (32) showed that the antistaphylococcal activity of semisynthetic penicillins is enhanced by adding an aminoglycoside antibiotic, specifically gentamicin, in animals with systemic staphylococcal infection. Oxacillin and gentamicin are also more active together against Enterococci (21).

We have shown further that although S-TDCM, a potent stimulant of hematopoiesis, increased survival of mice exposed to radiation alone (no wound), S-TDCM did not increase survival of irradiated/wounded mice. Nevertheless, S TDCM treatment increased survival of mice given a 10 day course of both topical and systemic gentamicin or topical gentamicin alone. In this regard, it is interesting to note that S TDCM increased survival comparable to systemic oxacillin and topical gentamicin. Nevertheless, for S TDCM to enhance survival in irradiated/wounded mice, it was necessary to provide ancillary antibiotic therapy. We have previously shown that one injection of TDM derived from *M. phlei* increased survival in sublethally irradiated mice challenged with

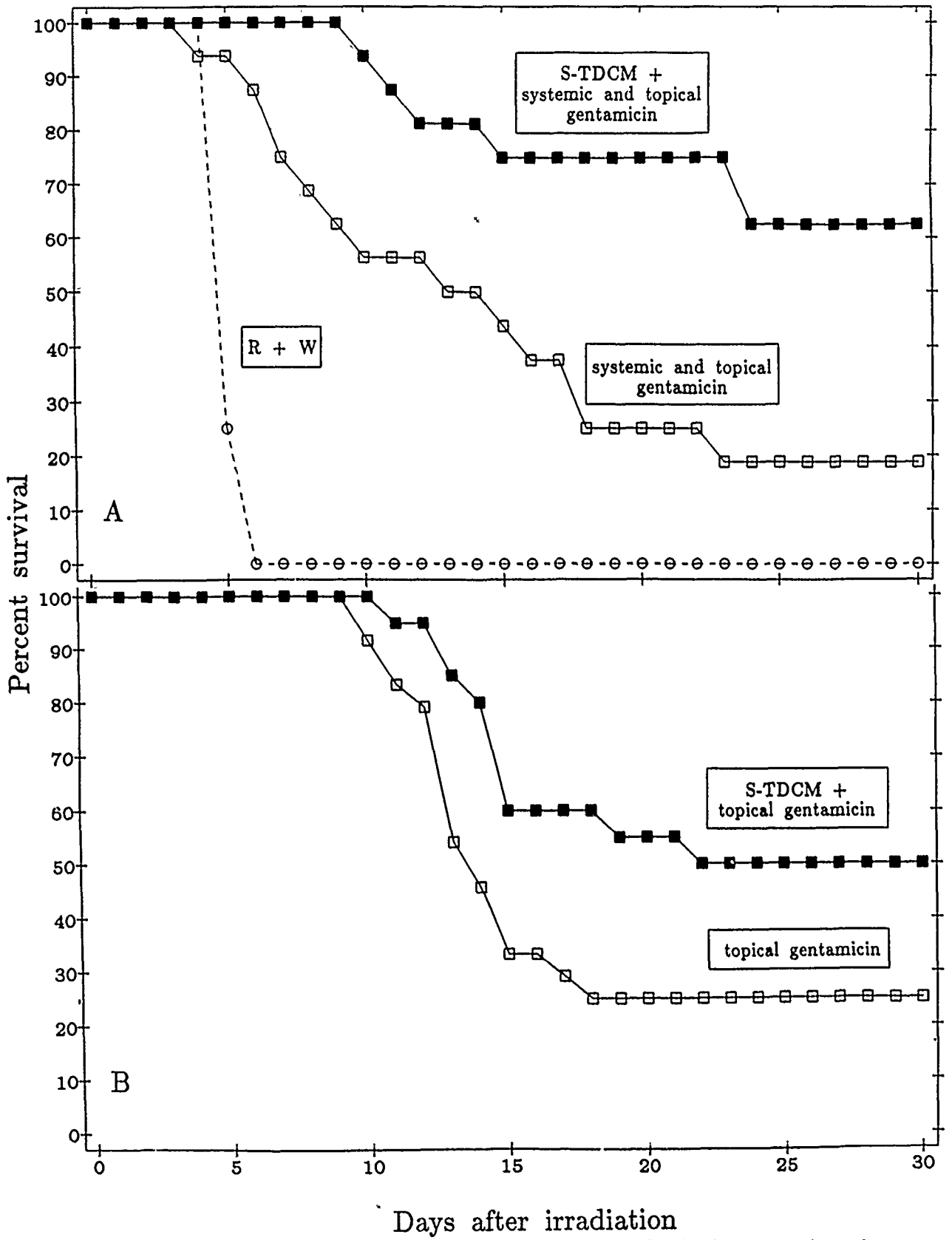

FIG. 4. Survival of irradiated, wounded mice after synthetic trehalose dicorynomycolate combined with systemic and topical gentamicin or topical gentamicin treatment alone. C3H/HeN mice received 8.0 Gy ^{60}Co followed by a 15% total body surface area wound 1 hr postirradiation. Mice were then given either S TDCM (200 μg/mouse) or saline (0.5 ml/mouse) IP. Mice from each group were treated topically with gentamicin cream (once daily) and systemically with gentamicin (7.5 mg/kg/day) (A) or topically with gentamicin cream alone (B). Mantel Cox p values: 0.0044 (A), 0.0328 (B) (S TDCM groups versus antibiotic alone treatment groups). N = (A) 16, (B) 20 (S TDCM), 24 (antibiotic alone). Results of two combined experiments are shown.

10 LD_{50} of *K. pneumoniae* 4 days postirradiation (19). Enhanced antimicrobial activity of radioresistant macrophages probably accounts for this effect (25, 30), because this protective effect was seen before significant marrow regeneration could occur approximately 7–10 days postirradiation (25, 27). Nevertheless, when the challenge dose of *K. pneumoniae* was increased to 5,000 LD_{50}, all mice died. The number of bacteria exceeded the enhancement of resistance augmented by TDM. Survival was possible only with the addition of antibiotic therapy (ceftriaxone). In the present study, mice were lethally irradiated, wounded, and infected by natural, environmental contamination of the wound site. It is possible that colonization and unimpeded growth of both Gram-positive and Gram-negative bacteria exceeded the ability of an immune system stimulated by S-TDCM to contain the spread of infection. Therefore enhanced resistance by S-TDCM in this severe model required augmentation with an antibiotic. The data presented herein demonstrate that irradiated/wounded mice develop leukopenia, thrombocytopenia, and sepsis earlier than mice given lethal radiation alone, and consequently die earlier. S-TDCM treatment alone was not beneficial, but treatment with S-TDCM combined with selected antibiotic therapies increased survival more than antibiotic therapies alone. The data suggest that combined therapies are beneficial following severe compromise of the immune system by irradiation with trauma.

It is known that S-TDCM stimulates hematopoiesis in irradiated mice and concomitantly reduces the number of bacteria that translocate from the gastrointestinal tract (19). Sepsis resulting from the translocation of intestinal bacteria usually does not occur in lethally irradiated mice until 2 weeks postirradiation (36). Although S-TDCM might accelerate hematopoietic recovery in irradiated/wounded mice, this beneficial effect can only be seen when an ancillary antibiotic inhibits bacteria and supports life until marrow regeneration occurs. In support of this hypothesis, Patchen et al. (26) showed that hematopoietic recovery following irradiation is accelerated by treatment with the immunomodulator, glucan, and granulocyte colony-stimulating factor. Thus it is possible that S-TDCM, either alone or combined with the stimulatory effect of wounding, augmented hematopoietic regeneration, which added to final recovery. Further experiments are required to assess these and other possibilities.

S TDCM is unique when compared to other nonspecific immuno-enhancing agents. In addition to the attributes shown in this study, TDM derivatives have the ability to induce long term nonspecific immunity (19, 22) and to synergize with other immunomodulators (22) and antibiotics (19). Toxicity has been largely obviated and administration may soon become more practical as oral formulations are developed. The potential value of S-TDCM clearly argues for further testing and development.

Acknowledgments

We thank Stefanie Vogel and Matthew Pollack for critical review of the manuscript; Santi Datta and Venita Miner for long hours of work and patience in performing blood cell and platelet determinations; John Harrington and the entire staff of the Veterinary Services Division, Armed Forces Radiobiology Research Institute, for commendable animal care; and Laura Lee Lewis-McCullough, Scott Herrity, and Carla Jennings, Diagnostic Services of Comparative Medicine/Clinical Pathology, Uniformed Services University of the Health Sciences, Bethesda, MD, for reliable bacterial identification.

REFERENCES

1. Anhalt, J. P.: Antimicrobial assays. *In* Washington, J. A. (ed): *Laboratory Procedures in Clinical Microbiology.* New York, Springer-Verlag, 1985, Section 12.1.
2. Bond, V. P., Fliedner, T. M., Archambeau, J. O.: Effects of radiation on the hemopoietic system: The bone marrow syndrome. *In* Bond, V., Fliedner, T., Archambeau, J. (eds): *Mammalian Radiation Lethality.* New York, Academic Press, Inc., 1965, pp. 159–230.
3. Brook, I., Elliott, T. B.: Treatment of wound sepsis in irradiated mice. *Int. J. Radiat. Biol.*, **56**: 75-82, 1989.
4. Brook, I., Walker, R. I., MacVittie, T. J.: Effect of antimicrobials on bowel flora and bacterial infection in irradiated mice. *Int. J. Radiat. Biol.*, **53**: 709-716, 1988.
5. Campos, M. E., Rabinovich, S., Smith, I. M.: Therapy of experimental staphylococcal infection with antibiotic combinations. *J. Lab. Clin. Med.*, **83**: 241-248, 1974.
6. Cavanagh, D., Knuppel, R. A., Shepherd, J. H., et al.: Septic shock and the obstetrician/gynecologist. *South. Med. J.*, **75**: 809-813, 1982.
7. Edlich, R. F., Kenney, J. G., Morgan, R. F., et al.: Antimicrobial treatment of minor soft tissue lacerations: A critical review. *Emerg. Med. Clin. No. Amer.*, **4**: 561-580, 1986.
8. Elliott, T. B., Brook, I., Steifel, S. M.: Quantitative study of wound infection in irradiated mice. *Int. J. Radiat. Biol.*, 1990, in press.
9. EORTC International Therapy Project Group. Three antibiotic regimens in the treatment of infection in febrile granulocytopenic patients with cancer. *J. Infect. Dis.*, **137**: 14-97, 1978.
10. Kaplan, H. W., Speck, R. S., Jawetz, F.. Impairment of antimicrobial defenses following total body irradiation in mice. *J. Lab. Clin. Med.*, **40**: 682-691, 1958.
11. Kontiainen, S., Rinne, E.: Bacteria isolated from skin and soft tissue lesions. *Eur. J. Clin. Microbiol.*, **6**: 420-422, 1987.
12 Lederer, E An update on natural and synthetic trehalose diesters. *In* Masihi, K., Lange, W. (eds): *Immunomodulators and Nonspecific Host Defense Mechanisms Against Microbial Infections.* Oxford, Pergamon Press, 1988, pp. 73-83.
13 Ledney, G D., Exum, E. D., Jackson, W. E.. Wound-induced alterations in survival of ^{60}Co irradiated mice: importance of wound timing. *Experientia*, **41**: 614-616, 1985.
14. Ledney, G. D., Exum, E. D., Stewart, D. A., et al.. Survival and hematopoietic recovery in mice after wound trauma and whole body irradiation. *Exp. Hematol.*, **10**: 263-278, 1982.
15. Ledney, G. D., Madonna, G. S., McChesney, D. G., et al.: Complications of combined injury. Radiation damage and skin wound trauma in mouse models. *In* Browne, D., Weiss, J. F., MacVittie, T. J., et al.: *Treatment of Radiation Injuries: Proceedings of the First Consensus Development Conference on Treatment of Radiation Injuries.* New York, Plenum, 1990, in press.
16 Ledney, G D , Stewart, D. A., Exum, E. D., et al.. Skin wound-enhanced survival and myelocytopoiesis in mice after whole-body irradiation. *Acta Radiol. Oncol.*, **20**: 29-38, 1981.
17. Ledney, G. D., Stewart, D. A., Gruber, D. F., et al.. Hematopoietic colony forming cells from mice after wound trauma. *J. Surg. Res.*, **38**: 55-65, 1985.
18. Lemaire, G., Tenu, J. P., Petit, J. F., et al.: Natural and synthetic trehalose diesters as immunomodulators. *Med. Res. Rev.*, **6**: 243-274, 1986.
19 Madonna, G. S., Ledney, G. D., Elliott, T. B., et al.: Trehalose dimycolate enhances resistance to infection in neutropenic animals. *Infect. Immun.*, **57**: 2495-2501, 1989.

20. Madonna, G. S., Ledney, G. D., Funckes, D. C., et al.: Monophosphoral lipid A and trehalose dimycolate therapy enhances survival in sublethally irradiated mice challenged with *Klebsiella pneumoniae*. *In* Masihi, K., Lange, W. (eds): *Immunomodulators and Nonspecific Host Defense Mechanisms Against Microbial Infections*. Oxford, Pergamon Press, 1988, pp. 351–356.
21. Marier, R. L., Joyce, N., Andriole, V. T.: Synergism of oxacillin and gentamicin against enterococci. *Antimicrob. Agents Chemother.*, **8**: 571–573, 1975.
22. Masihi, K. N., Lange, W., Brehmer, W., et al.: Immunological activities of nontoxic lipid A: Enhancement of nonspecific resistance in combination with trehalose dimycolate against viral infection and adjuvant effects. *Int. J. Immunopharmacol.*, **8**: 339–345, 1986.
23. McChesney, D. G., Ledney, G. D., Madonna, G. S.: Trehalose dimycolate enhances survival of fission neutron-irradiated mice and *Klebsiella pneumoniae*-challenged irradiated mice. *Radiat. Res.*, **121**: 71–75, 1990.
24. Numata, F., Nichimura, K., Ishida, H., et al.: Lethal and adjuvant activities of cord factor (trehalose-6,6′-dimycolate) and synthetic analogs in mice. *Chem. Pharm. Bull.*, **33**: 4544–4555, 1985.
25. Patchen, M. L., D'Alesandro, M. M., Brook, I., et al.: Glucan: Mechanisms involved in its radioprotection effect. *J. Leukoc. Biol.*, **42**: 95–105, 1987.
26. Patchen, M. L., MacVittie, T. J., Solberg, B. D.: Survival enhancement and hemopoietic regeneration following radiation exposure: Therapeutic approach using glucan and granulocytye colony stimulating factor. *Exp. Hematol.*, 1990, in press.
27. Patchen, M. L., MacVittie, T. J., Wathen, L. M.: Effects of pre- and post-irradiation glucan treatment on pluripotent stem cells, granulocyte, macrophage and erythroid progenitor cells, and hemopoietic stromal cells. *Experientia*, **40**: 1240–1244, 1984.
28. Pizzo, P. A.: Infectious complications in children with cancer: I. Pathophysiology of the compromised host and initial evaluation and management of the febrile cancer patient. *J. Pediat.*, **98**: 341–354, 1981.
29. Polonsky, J., Lederer, E.: Syntheses de quelques acides mycoliques. *Bull. Soc. Chim. Fr.*, **1954**: 504–510, 1954.
30. Ribi, E.: Structure-function relationship of bacterial adjuvants. *In* Nervig, R., Gough, P., Kaeberle, M., et al. (eds): *Advances in Carriers and Adjuvants for Veterinary Biologics*. Ames, Iowa State University Press, 1986, pp. 35–49.
31. Spector, W. S.: *Handbook of Biologic Data*. Philadelphia, Saunders, 1956, p. 175.
32. Steigbigel, R. T., Greenman, R. L., Remington, J. S.: Antibiotic combinations in the treatment of experimental staphylococcal infections. *J. Infect. Dis.*, **131**: 245–251, 1975.
33. Stewart, D. A., Ledney, G. D., Baker, W. H., et al.: Bone marrow transplantation of mice exposed to a modified fission neutron (N/G-30:1) field. *Radiat. Res.*, **92**: 268–279, 1982.
34. Stringel, G., Bawdon, R., Savrich, M., et al.: Topical and systemic antibiotics in the prevention of wound infection. *J. Pediat. Surg.*, **24**: 1003–1006, 1989.
35. Talan, D. A.: Management of serious wound infections. *Top. Emerg. Med.*, **10**: 33–41, 1989.
36. Walker, R. I., Ledney, G. D., Galley, C. B.. Aseptic endotoxemia in radiation injury and graft-versus-host disease. *Radiat. Res.*, **62**: 242–249, 1975.
37. Zimmerman, J. J., Dietrich, K. A.: Current perspectives on septic shock. *Pediat. Clin. No. Amer.*, **34**: 131–163, 1987.

INT. J. RADIAT. BIOL., 1991, VOL. 59, NO. 4, 941-949

Negative supercoiling increases the sensitivity of plasmid DNA to single-strand break induction by X-rays

J. H. MILLER†, J. M. NELSON†, M. YE†, C. E. SWENBERG‡, J. M. SPEICHER‡ and C. J. BENHAM§

†Biology and Chemistry Department, Pacific Northwest Laboratory, Richland, WA 99352, USA

‡Radiation Biochemistry Department, Armed Forces Radiobiology Research Institute, Bethesda, MD 28014-5145, USA

§Department of Biomathematical Sciences, Mount Sinai School of Medicine, New York, NY 10029, USA

(Received 17 September 1990; revision received 21 November 1990; accepted 28 November 1990)

Negatively supercoiled topoisomers of the plasmid pIBI 30 were irradiated with 250 kV X-rays and assayed for strand scission by agarose gel electrophoresis. The survival of supercoiled molecules (Form I) decreased exponentially with increasing X-ray exposure and the dose required to reduce the fraction of DNA in Form I to 37% of its value in unirradiated controls (D_{37}) decreased with increasing negative superhelicity. This enhanced radiation sensitivity of underwound DNA is tentatively attributed to the transient denaturation of the double helix that increases the susceptibility of individual strands to free radical attack.

1. Introduction

Aqueous solutions of DNA and its components have been the subject of numerous studies of genetic damage by ionizing radiation (for review, see von Sonntag 1987). Supercoiled plasmids are particularly useful for this type of study due to the ease with which the yield of single- and double-strand breaks can be quantitated by gel electrophoresis (Hempel and Mildenberger, 1987). However, the dependence of these yields on the amount of supercoiling and the direction of the torsional stress which supercoiling places on the double helix have not been investigated systematically. Studies of this type are needed because negative supercoiling is a general feature of DNA *in vivo* (for review), see Gellert 1981. An effect of superhelicity of the induction of strand breaks by fission neutrons was recently reported by Swenberg *et al.* (1990). In this paper, the first observations that negative supercoiling increases the yield of single-strand breaks (SSB) in plasmids exposed to X-rays is presented.

Covalently-closed circular duplex DNA is characterized by a linking number defined as the number of times one strand links through the circle defined by the complementary strand. Plasmids which differ only in their linking number are called topoisomers. It is usually most convenient to specify the linking number of topoisomers relative to that of the fully relaxed topoisomer, which is operationally defined by the invariance of its linking number to action of nicking and closing enzymes. The difference in linking number between a topoisomer and the fully relaxed conformation is the linking difference; the ratio of this linking difference to

Table 1. Families of pIBI 30 Topoisomers[a]

Sample number	[EtdBr] (μM)	Linking difference	
		Batch 1	Batch 2
1	9·0	−3·3	−3·8
2	11·7	−4·6	−4·8
3	14·7	−5·9	
4	17·7		−6·9
5	21·3	−8·5	−9·3
6[b]	n.a.	−13·0	−13·0

[a] Details of preparation given under Materials and methods.
[b] Native pIBI 30.

the linking number of the relaxed state is called the specific linking difference or superhelical density. Both prokaryotes and eukaryotes maintain topologically distinct domains in their genomic DNA with defined superhelical densities between −0·03 and −0·09 (Cozzarelli, 1980).

Supercoiled plasmids can accommodate the torsional stresses associated with a non-zero linking difference by assuming a variety of secondary structures (Benham, 1986). In general, torsionally stressed conformations of DNA will involve both twisting and writhing deformations. The latter requires bending energy whereas the former may involve smooth torsional deformation (i.e. a different helicity than that characterizing the unstressed B-form) and/or abrupt conformational changes that are sequence dependent. Cruciform extrusion at inverted repeats (Panayotatos and Wells 1981), local denaturation of regions rich in adenine-thymine (AT) base pairs (Vinograd *et al.* 1968) and B to Z transition (Davies and Zimmerman, 1980) are the most widely studied sequence-specific torsional deformations. At thermodynamic equilibrium, the competition among different secondary structures with the same linking number is influenced by base sequence, domain length and solvent conditions, as well as the linking difference (Benham, 1986). The goal of this research is to understand the effects of this conformational equilibrium on radiation-induced DNA damage.

2. Materials and methods

2.1. *Sample preparation*

The pIBI 30 plasmid was isolated from *Escherichia coli* by alkaline lysis (Ausubel *et al.* 1989). The absorbance ratio A_{260}:A_{280} was approximately 1.85 for all isolates, which is indicative of pure double-stranded DNA preparations without contamination from either protein or RNA (Schleif and Wensink 1981). The proportion of supercoiled DNA was greater than 70% in all samples. Ethidium bromide (EtdBr), purchased for Aldrich, and eukaryotic topoisomerase I (topo I) from Bethesda Research Laboratory were used as received in the procedure of Singleton and Wells (1982) to produce families of topoisomers with superhelical densities less than that of the native plasmid. In this procedure, 38–40 μg of DNA were incubated at 37°C with various amounts of EtdBr and 30 units of topo I in a total volume of 150 μl. Table 1 shows the concentrations of EtdBr used to generate

the families of topoisomers used in this study and their approximate mean linking difference, estimated by the methods discussed below.

If individual members of a family of topoisomers could be separated by the gel electrophoresis conditions, then the mean linking difference of the family was estimated from the relative intensity of EtdBr fluorescence emitted by each topoisomer in the family. This was not the case for samples 4, 5 and 6, which migrated as single bands. The linking difference of sample 6, native pIBI 30, was estimated by counting the number of bands on a gel that resolved all topoisomers produced from the native pIBI 30 by relaxation with topo I. The mean linking difference of samples 4 and 5 was estimated from the approximately logarithmic dependence on linking difference of the separation between supercoiled and nicked-circular DNA on our gels.

After termination of the reactions in the Singleton and Wells (1982) procedure, both EtdBr and topo I were removed by two phenol extractions. Three ethanol extractions were then used to remove the phenol. The DNA was concentrated by ethanol precipitation and samples were resuspended in TE buffer (10 mM Tris, 1 mM EDTA; pH 7·2). The concentration of DNA in each sample was determined by its absorption of 260 nm. Absorption spectra taken over the wavelength range 220–500 nm showed no indication of contamination from EtdBr, topo I, or other chemicals used in sample preparation.

2.2. *Irradiation procedure*

Irradiations were performed using a Norelco MG-300 X-ray generator operated at 250 kV and 10 mA with no additional filtration. Doses were monitored during irradiation by a transmission ion chamber in a fixed position immediately below the exit window of the X-ray tube. The ion chamber was calibrated against a standard Farmer Dosemeter Type 2502/3. The dose-rate in the sample was estimated to be $6{\cdot}0 \pm 0{\cdot}2$ Gy/min and graded doses of X-rays were obtained by varying the exposure time. Samples to be irradiated were placed into the ends of 200 μl Eppendorf pipette tips and the pipette tips were arranged so that 24 samples could be irradiated simultaneously in a field contained within a 3 cm diameter circle. Plasmid DNA was irradiated as 5–10 μl volumes containing DNA in TE buffer at a concentration of 24 ng/μl.

During irradiation, samples were maintained at a constant temperature by airflow over a heat exchanger connected to a temperature controlled (Endocal) circulating bath. The temperature of the samples was monitored by a calibrated thermistor placed in the return airstream 3–4 cm from the pipette tips. By adjusting the temperature of the circulating bath, samples were irradiated as a liquid maintained at $0 \pm 0{\cdot}1$°C.

2.3. *Separation and quantification*

Different topoisomers of supercoiled pIBI 30 (Form I) were separated from each other and from relaxed closed-circular DNA (Form II) by horizontal agarose gel electrophoresis in TBE buffer (89 mM Tris, 89 mM boric acid, 2 mM EDTA; pH $\approx$ 8). All of the irradiated material for a given sample and X-ray dose (typically 0·2 μg of DNA) was loaded into a single well of a 1% agarose gel and subjected to electrophoresis at room temperature. Gels were run submerged under conditions such that the product of voltage and run time was approximately 150 Vhr at a field of 2·5 V/cm. Actual running times and voltage settings were determined by the

progression of tracking dyes. Before staining with a 1·2 μg/ml solution of EtdBr, gels were irradiated with 254 nm ultraviolet light to insure uniform binding of EtdBr to Forms I and II (Hertzberg *et al.* 1989). Excess EtdBr was removed by incubation in 1 mM $MgCl_2$. The relative amount of Form I DNA in each lane of the gel was determined using a Biomed Instruments scanning densitometer in the fluorescence detection mode. Peak areas were demonstrated to be proportional to the amount of DNA in a band by scanning a gel that contained known amounts of HindIII restriction fragments of ϕX174.

3. Results

Figure 1A shows the densitometer trace for the unirradiated control for sample 3 in Table 1. Densitometer traces obtained after this sample was exposed to 40 and 80 Gy of X-rays are shown in Figures 1B and 1C, respectively. The single peak at a small migration distance in each trace is relaxed close-circular DNA (Form II) and the family of peaks at higher migration distances are supercoiled topoisomers (Form I). The presence of linear DNA (Form III), which migrates at a rate between Forms I and II under these conditions, was not detected in either controls or irradiated samples at the exposure levels used in these experiments. As the X-ray dose increases, Form I is progressively converted to Form II due to the induction of SSB that allow supercoiled molecules to relax.

Semi-logarithmic plots of the fraction of DNA in Form I as a function of dose are shown in Figure 2A for samples 1, 5 and 6 of batch 2. The lines were obtained by linear least-squares analysis of the dose–response data with both the slope and y-intercept as adjustable parameters. An estimate of the fraction of supercoiled

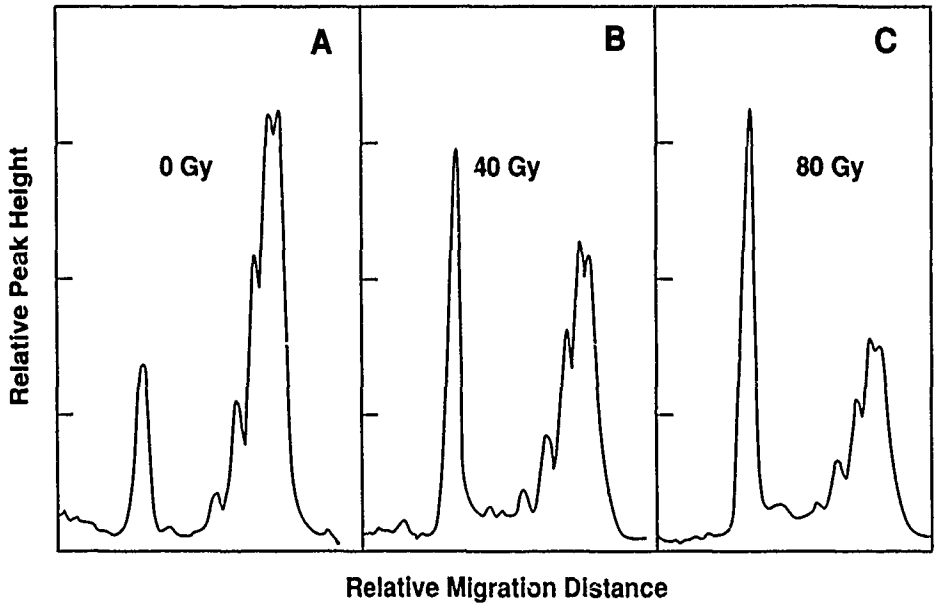

Figure 1. Relative fluoresence intensity as a function of migration distance for plasmid pIBI 30 (sample 3 in Table 1) exposed to X-rays, then subjected to agarose gel electrophoresis and stained with EtdBr. Migration distance increases from left to right.

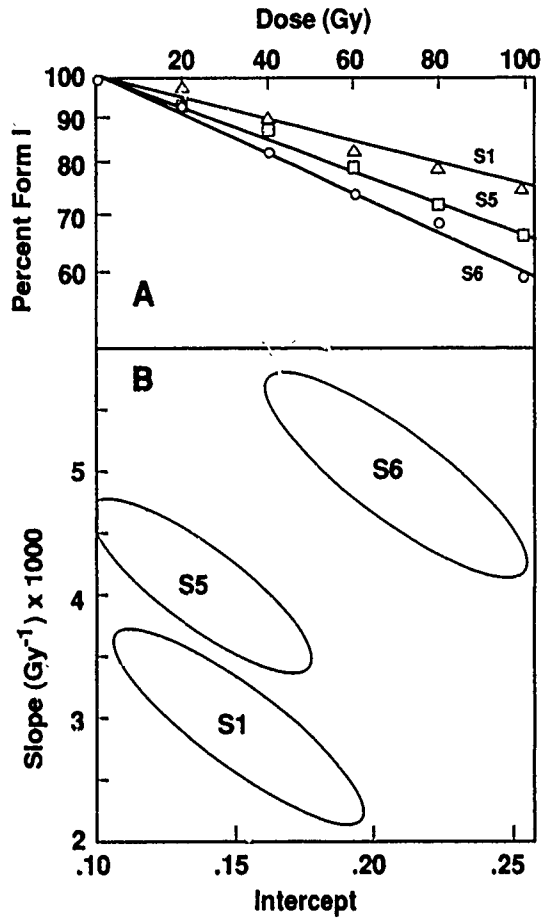

Figure 2. Linear regression analysis of the decrease in Form I (supercoiled DNA) with increasing X-ray dose. (A) Data and fitted lines for samples 1, 5 and 6 of batch 2 . (B) Joint 95% confidence regions for slopes and *y*-intercepts.

DNA in the unirradiated control was obtained from the optimum value of the *y*-intercept. These estimates, 0·86, 0·87 and 0·81 for samples 1, 5 and 6, respectively, were used to normalize the data so that the slopes of the dose responses could be compared more easily. The negative of the slope of each line, which is the reciprocal of D_{37}, is an estimate of the sensitivity of the family of topoisomers to strand scission by X-rays. The coefficient of determination for the regression analysis was greater than 0·98 in all three cases. This indicates that the population of supercoiled molecules decreases exponentially with increasing dose, as expected from the theory of van Touw *et al.* (1985), as the induction of DSB is negligible under our experimental conditions.

Figure 2B shows the joint confidence regions (Mandel and Linning 1957) for the parameters determined by linear regression analysis of the data shown in Figure 2A. The slope and *y*-intercept of the best fit to the dose–response for each sample have a 95% probability of falling within the joint confidence ellipse. As these regions do not overlap, the differences in the slopes of the dose response data

shown in Figure 2A are statistically significant. The magnitude of the slope increases with increasing negative superhelicity of the irradiated sample.

Figure 3 shows the variation with linking difference of the sensitivity to strand scission by X-rays that was observed with families of topoisomers obtained from two separate plasmid preparations. The open and closed symbols refer to batch 1 and 2, respectively. The lines show the best fit of a linear relation between sensitivity and linking difference to each data set. The coefficient of determination for the fit to the data obtained with batch 2 (0·90) is much better than that obtained with batch 1 (0·61) due to the greater scatter in the earlier data. The systematically lower sensitivity of families of topoisomers from batch 2 probably reflects a greater ability of the buffer in this case to scavenge OH radicals. Although batch 1 and 2 are not identical in this respect, both sets of topoisomers show that the sensitivity to strand scission by X-rays increases with increasing negative superhelicity. The slope of a linear relation between sensitivity and linking difference is obviously better determined by the data from the second experiment where a value of $-2{\cdot}1 \pm 0{\cdot}7 \times 10^{-4}$ per Gy per increment of linking difference was obtained. The y-intercept in this case is $2{\cdot}0 \pm 0{\cdot}6 \times 10^{-3}$ per Gy, which is an estimate of the sensitivity of fully relaxed pIBI 30 to induction of SSB by X-rays under the buffering conditions of batch 2. The slope of the best fit to the data obtained with the first batch of topoisomers is not significantly different from that obtained with topoisomers in batch 2.

4. Discussion

Electron micrographs of relaxed and supercoiled DNA (Stryer 1981) suggest that the latter has a more compact secondary structure. Data obtained by van Rijn

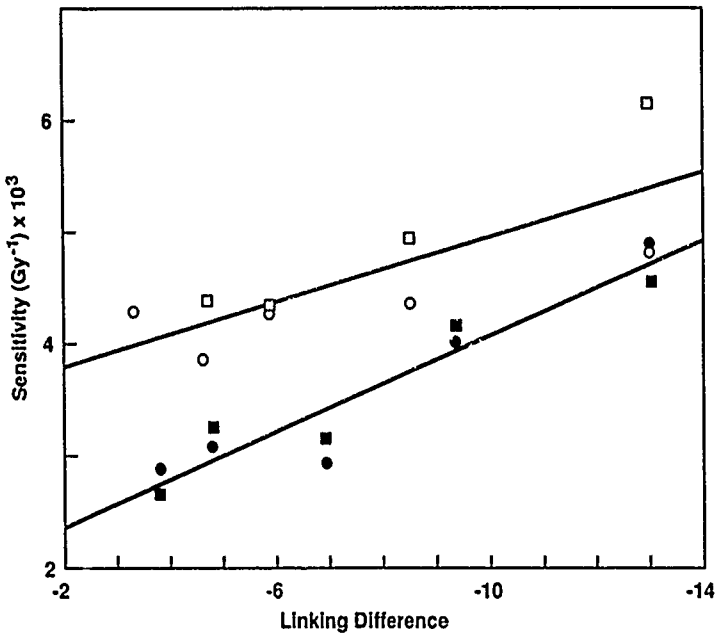

Figure 3. Sensitivity of families of pIBI 30 topoisomers to induction of SSB by X-rays. Data points were obtained by fitting the dose response for survival of Form I DNA (see Figure 2). Open and closed symbols denote results obtained from separate plasmid preparations (see Table 1). Lines show the best fit of a linear relationship between sensitivity and linking difference to th data points.

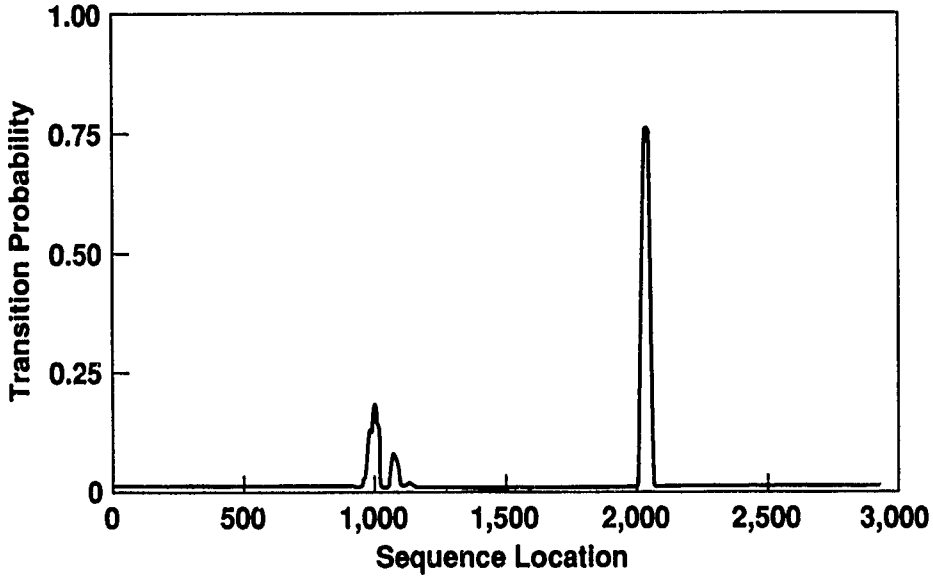

Figure 4. Relative probability for helix-to-random-coil transitions in pIBI 30 calculated at a linking difference of −20, physiological ionic strength and room temperature.

et al. (1985) using single-stranded ϕX174 in buffers with different salt concentrations indicated that the more compact conformations were more radioresistant. However, our observation that negative supercoiling increases the sensitivity of double-stranded DNA to radiation-induced strand scission suggests that another mechanism is operating in our experiments. Some insight into this mechanism may come from the biological function of negative supercoiling which is believed to stimulate the strand separation required for tanscription and replication of double-stranded DNA. Ward (1985) has shown that the preferred sites of OH radical attack on DNA are more accessible to the aqueous environment of the molecule in the unwound conformation than they are in double-stranded DNA mainly due to the greater exposure of DNA bases. This implies that transient stand separation in negatively supercoiled pIBI 30 should cause increased base damage, not strand scission. Hence, if the increase in X-ray induced SSB that is observed with underwound DNA is due to transient strand separation, then a mechanism for conver ' base damage to sugar damage must also be operating in our system. Some evidence for the interaction between base radicals and sugar moieties has been seen in the anoxic irradiation of poly(U) (Deeble *et al.* 1986).

The transient disruptions of base pairing (sometimes called open states) caused by the torsional stress of negative supercoiling are more probable in AT-rich sequences. Hence, if open states are involved in the increased sensitivity to strand scission that is observed with underwound plasmids, then at least a part of that increase should be due to non-random breakage at AT-rich regions. To investigate this mechanism in more detail, computational methods developed by Benham (1990) were used to calculate the probability of helix-to-random-coil transitions as a function of sequence location in pIBI 30. Results obtained at a linking difference of −20, physiological ionic strength and room temperature are shown in Figure 4. Under these conditions, theoretical analysis of the conformational equilibrium predicts that melting of the double helix is most probable near sequence location

2000. Although these preliminary calculations were carried out for higher linking difference and higher temperature than was the case for these experiments, they indicate the sequence locations where non-random breakage due to conformational instability of the double helix is most likely to occur. This information contributes to the design of experiments to detect non-random strand scission by X-rays through the use of restriction enzymes and denaturing gels.

5. Conclusions

Negative supercoiling increases the susceptibility of plasmid pIBI 30 to induction of SSB by ionizing radiation. At a linking difference of −13 (a superhelical density of −0·05 in our 2926 bp plasmid), a sensitivity to strand scission by X-rays that is about twice as large as the estimate of the sensitivity of fully-relaxed pIBI 30 is observed. This phenomenon may contribute to the enhanced yield of SSB in active chromatin observed by Chiu and Oleinick (1982). Although the mechanism for the dependence of X-ray induced strand scission on negative superhelicity is uncertain, it may be related to regions of conformational instability in pIBI 30 that were identified by model calculations. Experiments to test this hypothesis are in progress.

Acknowledgements

The authors gratefully acknowledge support for this work by the Office of Health and Environmental Research (OHER) US Department of Energy under contract DE-AC06-76RLO 1830, the Armed Forces Radiobiology Research Institute, and grant DMB 88-96284 from the National Science Foundation (CJB). We also acknowledge the contributions of Professor E. W. Fleck, Whitman College, Walla Walla, WA, to this work through both helpful discussions and assistance with experimental procedures.

References

Ausubel, F. M., Brent, R., Kingston, R. E., Moore, D. D., Seidman, J. G., Smith, J. A. and Strabl, K., 1989, *Current Protocols in Molecular Biology*, (Wiley Interscience), pp. 1.71–1.74.

Benham, C. J., 1986, Superhelical DNA. *Comments on Molecular and Cellular Biophysics*, **4**, 35–54.

Benham, C. J., 1990, Theoretical analysis of heteropolymeric transitions in superhelical DNA molecules of specified sequence. *Journal of Chemical Physics*, **92**, 6294–6305.

Chiu, S-M. and Oleinick, N. L., 1982, The sensitivity of active and inactive chromatin to ionizing radiation-induced DNA strand breakage. *International Journal of Radiation Biology*, **41**, 71–77.

Cozzarelli, N. R., 1980, DNA gyrase and the supercoiling of DNA. *Science*, **207**, 953–960.

Deeble, D. J., Schulz, D. and von Sonntag, C., 1986, Reaction of OH radicals with poly(U) in deoxygenated solutions: sites of OH radical attack and the kinetics of base release. *International Journal of Radiation Biology*, **49**, 915–926.

Davies, D. R. and Zimmerman, S., 1980, A new twist for DNA? *Nature*, **283**, 11–12.

Gellert, M., 1981, DNA topoisomerases. *Annual Reviews of Biochemistry*, **50**, 879–910.

Hempel, K. and Mildenberger, E., 1987, Determination of G-values for single- and double-strand break induction in plasmid DNA using agarose-gel electrophoresis. *International Journal of Radiation Biology*, **52**, 125–138.

Hertzberg, R. P., Caranfa, M. J. and Hecht, S. M., 1989, On the mechanism of topoisomerase I inhibition by camptothecin: Evidence for binding to an enzyme-DNA complex. *Biochemistry*, **28**, 4629–4638.

MANDEL, J. and LINNIG, F. J., 1957, Study of accuracy in chemical analysis using linear calibration curves. *Analytical Chemistry*, **29**, 743–749.

PANAYOTATOS, N. and WELLS, R. D., 1981, Cruciform structures in supercoiled DNA. *Nature*, **289**, 466–470.

SCHLEIF, R. F. and WENSINK, P. C., 1981, *Practical Methods of Molecular Biology* (Springer-Verlag, New York) p.90.

SINGLETON, C. K and WELLS, R. D., 1982, The facile generation of covalently closed circular DNAs with defined negative superhelical densities. *Analytical Biochemistry*, **122**, 253–257.

STRYER, L., 1981, *Biochemistry*, 2nd ed. (W. H. Freeman, San Francisco), p. 574.

SWENBERG, C. E., HOLWITT, E. A. and SPEICHER, J. M., 1990, Superhelicity and DNA radiation sensitivity, *SAE Technical Paper Series #901349* (Society of Automotive Engineers, Inc., Warrendale, PA), pp. 1–7.

VAN RIJN, K., MAYER, T., BLOK, J., VERBERNE, J. B and LOMAN, H., 1985, Reaction rate of OH radicals with ϕX174 DNA: influence of salt and scavenger. *International Journal of Radiation Biology*, **47**, 309–317.

VAN TOUW, J. H., VERBERNE, J. B., RETÈL, J. and LOMAN, H., 1985, Radiation-induced strand breaks in ϕX174 replicative form DNA: an improved experimental and theoretical approach. *International Journal of Radiation Biology*, **48**, 567–578.

VINOGRAD, J., LEBOWITZ, J. and WATSON, R., 1968, Early and late helix-coil transitions in closed circular DNA. The number of superhelical turns in polyoma DNA. *Journal of Molecular Biology*, **33**, 173–195.

VON SONNTAG, C., 1987, *The Chemical Basis of Radiation Biology* (Taylor & Francis, London).

WARD, J. F. 1985, Biochemistry of DNA Lesions. *Radiation Research*, **104**, S103–S111.

Radical yields in DNA exposed to ionizing radiation: Role of energy and charge transfer

JOHN H. MILLER
Biology and Chemistry Department, Pacific Northwest Laboratory, Richland, WA 99352, U.S.A.
AND
CHARLES E. SWENBERG
Radiation Biochemistry Department, Armed Forces Radiobiology Research Institute, Bethesda, MD 20814, U.S.A.
Received October 7, 1989

Theoretical and experimental studies of free-radical yields in oriented DNA samples exposed to ionizing radiation with high linear energy transfer at 77 K are discussed. The dependence of radical yields on the orientation of DNA chains relative to the particle flux is being investigated to gain insight into the role of intramolecular energy and charge transfer processes in radical production and decay. Model calculations based on a thermal-spike approximation are presented and their limitations for predicting the orientation dependence of radical yields observed after neutron irradiation (see C. M. Arroyo *et al.* Int. J. Radiat. Biol. 50, 789 (1986)) are discussed. A more mechanistic model based on the high mobility of excess electrons in hydrated DNA (D. van Lith *et al.* J. Chem. Soc. Faraday Trans. 1, 82, 2933 (1986)) is outlined.

Les études théoriques et expérimentales sur la production de radicaux libres dans des échantillons orientés d'ADN exposés à un rayonnement ionisant avec un haut transfert d'énergie linéaire à 77 K sont discutées. On examine l'effet sur la production de radicaux de l'orientation des chaînes d'ADN par rapport à la direction du flux de particules, afin de comprendre le rôle du transfert intramoléculaire d'énergie et de charge dans la production et la désintégration des radicaux. Des calculs de modèles basés sur une approximation de pics thermiques sont présentés, et leur limitations pour la prédiction de l'effet de l'orientation sur la production de radicaux observée après irradiation par des neutrons (voir C. M. Arroyo *et al.* Int. J. Radiat. Biol. 50, 789 (1986)) sont discutées. Un modèle plus mécaniste, basé sur la grande mobilité des électrons excédentaires dans l'ADN hydraté (D. van Lith *et al.* J. Chem. Soc. Faraday Trans. 1, 82, 2933 (1986)) est esquissé.

[Traduit par la revue]

Can. J. Phys. 68, 962 (1990)

Introduction

Experiments on oriented DNA exposed to neutrons (1) indicate that free-radical yields depend upon the orientation of DNA molecules relative to the recoil-proton flux. We developed a macroscopic model for this effect (3, 4) based on the assumption that vibrational energy migrates along DNA chains more rapidly than between DNA molecules in the irradiated sample, and approximated this difference by asymmetry in thermal-diffusion coefficients. The model predicts greater conversion of primary-anion radicals to their irreversibly carbon-protonated form when the proton flux is parallel to the molecular orientation than when it is incident perpendicular to the DNA chains. However, a significant difference between radical conversion in the parallel and perpendicular case was calculated only with model parameters that suggest migration of vibrational excitation of the order of 0.2 eV over distances of the order of 100 nm. Since this distance is much larger than is expected for conventional modes of energy transfer in DNA (5), Baverstock and Cundall (6) have suggested that solitary wave motion may be involved. In our response to this suggestion (7), we pointed out that Yomosa's model (8) of the breathing mode of DNA, a transient disruption of base pairing believed to be important in transcription of genetic information, predicts that a solitary wave carrying 0.35 eV of energy will propagate along the double helix with a velocity of 83 nm ns^{-1}. Of course, the similarity between this model of vibrational dynamics in DNA and the conditions, which our thermal-spike calculations suggest must be present for a significant orientation dependence of radical yields, does not prove that either model is correct. Nevertheless, we feel that the effects of DNA structure and dynamics on radiation damage have not yet been investigated sufficiently to dismiss the idea that the special properties of DNA that allow it to perform its biological function may also influence its interaction with ionizing radiation. In this paper we discuss our model of the orientation effect in light of recent experimental data, which indicate that excess electrons in hydrated DNA samples have high mobility and a long lifetime (2), and that cytosine, not thymine as we assumed (3, 4), is probably the main electron-gain center in DNA exposed to low linear energy transfer (LET) radiation at 77 K (9).

Macroscopic model

Since most of the interactions of high-energy protons with matter are glancing collisions that involve small momentum and energy transfer, a proton track is, to a first approximation, a line source of low-energy secondary electrons. Hence, a proton flux that is incident on a sample of oriented DNA molecules in a direction that is nearly parallel to the helical axis will have greater probability of producing multiple excitations in the same DNA chain than a flux that is incident perpendicular to the molecular orientation. In the absence of intramolecular energy or charge transfer, each excitation on a DNA chain should be subject to the same laws that govern the evolution of excitations isolated on different DNA molecules. Conversely, a difference in radical yields induced by proton fluxes incident parallel and perpendicular to the helical axis may reflect the influence of intramolecular energy or charge transfer on free radical production or decay.

Head on collisions produce the most energetic recoil protons in a neutron field, consequently, some of the directional correlation of a neutron flux will be preserved in the secondary proton spectrum. It is therefore reasonable to speculate that the orientation dependence of neutron induced radical yields observed by Arroyo *et al.* (1) is due to intramolecular energy and charge transfer. However, due to the complexity of the ra

Printed in Canada Imprimé au Canada

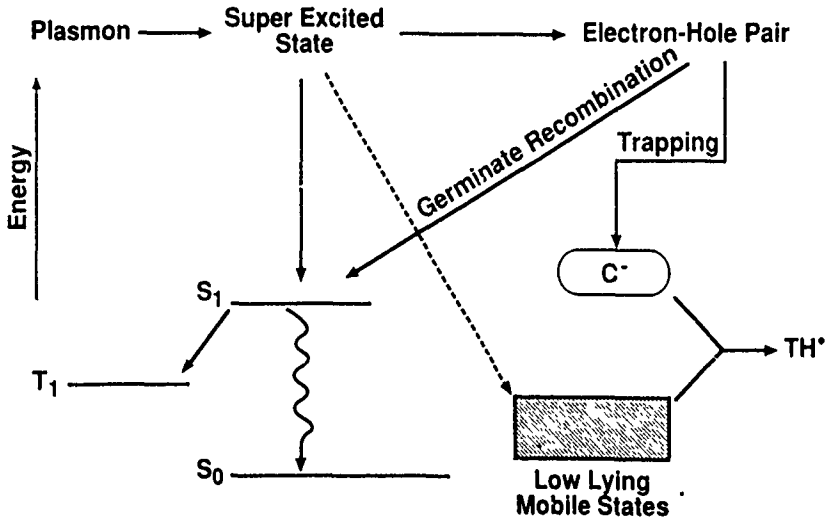

FIG. 1. Schematic of decay modes of energy absorbed from ionizing radiation in hydrated DNA samples.

diation field in that experiment, it is difficult to estimate how much orientation dependence should be expected for a given transfer mechanism. We have, therefore, focused our attention on direct proton irradiation, where the direction and energy of the proton flux can be controlled independently. The main experimental problem with direct proton irradiation is the small penetration of the sample by the beam. We believe that these problems can be solved with thin films of oriented DNA, which we have obtained through collaboration with Professor Allen Rupprecht at the University of Stockholm.

Most of the glancing collisions between fast charged particles and condensed matter produce collective electronic excitations called plasmons (10), which can be viewed as an oscillation of valance electron density relative to ionic cores. Figure 1 illustrates the types of phenomena that are likely to result from the decay of these high-energy (typically 20 to 30 eV) excitations. Plasmons in insulators and semiconductors are expected to decay within five oscillations (10), which corresponds to propagation of a fraction of a nanometer in a few femtoseconds. Nuclear motion on this time scale is negligible. Multiple valence-shell excitations generally satisfy the criteria of large-dipole oscillator strength and resonance needed to be good acceptors of plasmon energy. These localized superexcited states (SES) are not expected to live more than a picosecond and many will decay into particle–hole pairs with some conversion of electronic to vibrational energy. Some SES decay directly to singlet and triplet excitons, but this channel is mainly populated by geminate recombination. In polymeric materials, which are generally characterized by high disorder, ion pairs that escape geminate recombination will rapidly decay to electron-gain and -loss centers that are stable at low temperature. Electron affinity (11) and the ability of shifts in the hydrogen bond between base pairs to compensate for the excess negative charge (12) are believed to be the key factors that determine the relative probability that a given base in DNA will become an electron gain center. By these criteria cytosine should be the dominant electron-gain center. Recent studies with oligonucleotides (9) provide experimental evidence for this mechanism of primary radical-anion production. Since the interstrand proton transfer that stabilizes electron gain centers is reversible (12), warming irradiated samples to temperatures between 160 and 190 K activates electron transfer between stacked bases and opens channels for recombination and irreversible protonation and deprotonation. Protonation of thymine radical anions at C6 to form 5,6-dihydrothymin-5-yl (TH) radicals is the most well established of these channels.

Transfer of energy from electronic to vibrational degrees of freedom is always associated with degradation of plasmon energy. In flexible polymeric materials, this process is believed to involve nonlinear dynamics called "solitary waves" (13). If these mobile low-lying states are produced in a DNA molecule along with localized electron-gain and -loss centers, it is conceivable that they could interact with these centers to produce effects similar to those observed when samples irradiated at 77 K are annealed (14). We feel that the breathing mode of vibrational excitation is currently the most likely candidate for the mobile low-lying state depicted in Fig. 1. In Yomosa's model (8), base pairing is disrupted in this state while base stacking is preserved. This would decouple electron transfer through stacked bases from the interstrand proton transfer that is believed to play a major role in localizing electrons on cytosine (12). At present, there is no direct experimental evidence to support this hypothesis, however, such a detailed mechanism for the conversion of primary radical anions to TH is not an essential part of the thermal-spike model. It avoids these issues by using the macroscopic theory of heat transfer to approximate the underlying microscopic processes. Given our current state of knowledge, this approximation is necessary to obtain quantitative results. This means, of course, that comparing these calculations with experiment data cannot prove or disprove the microscopic mechanisms, nevertheless, the thermal-spike calculations have provided insight on ways to address the problem at a more fundamental level.

Henriksen *et al.* (15) showed that the concept of heavy-ion-induced "heat waves" could be used to calculate conversion of primary radicals in proteins, however, predictions of this model were not confirmed by experiments with carbon, neon, or argon ion beams (15). To address the question of differential radical conversion in the parallel and perpendicular irradiation geometries employed by Arroyo *et al.* (1), we reformulated the thermal spike approximation in terms of track structure rather than simply stopping power. Cylinders with a uniform 1 nm radius were randomly superimposed on proton tracks with a specific orientation relative to the axis of the cylinder. Each inelastic collision in the proton track that fell within the target was treated as a heat source contributing to a radiation induced

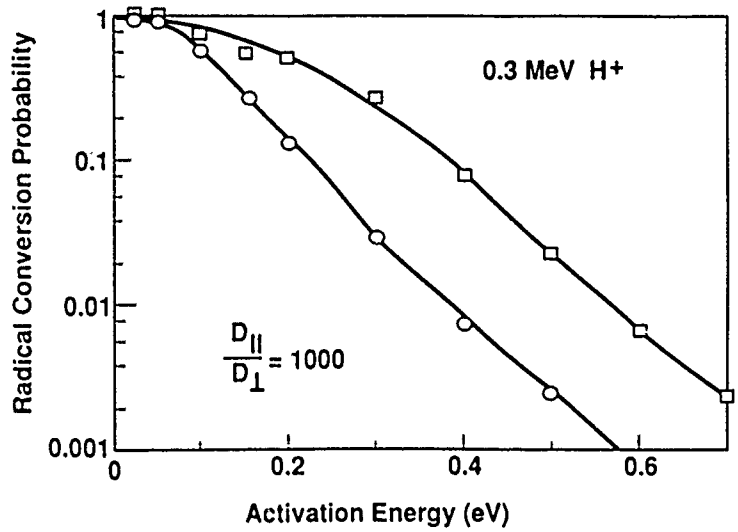

FIG. 2. Model calculations of the probability to convert primary anions to 5,6-dihydrothymin-5-yl (TH) radicals for 0.3 MeV protons incident parallel = or perpendicular ⊥ to oriented DNA samples at 77 K. Thermal diffusion along DNA chains is assumed to be 1000 times greater than diffusion transverse to the helical axis.

temperature

$$[1] \qquad T_k(x,t) = T_{k0}(1 + t/\tau_{\parallel})^{-1/2} \exp\left[\frac{-(x - x_k)^2}{2\Delta^2(1 + t/\tau_{\parallel})}\right]$$

where

$$[2] \qquad T_{k0} = \frac{\epsilon_k}{\sqrt{2\pi^3 b^2 \Delta \rho C}}$$

is the initial excess temperature at position x_k due to the absorption of energy ϵ_k, b is the target radius, Δ is the initial delocalization of plasmon excitations (10), ρ is the mass density, and C is the specific heat. The relaxation time $\tau_{\parallel}$ is related to the parallel diffusion coefficient $D_{\parallel}$ by

$$[3] \qquad \tau_{\parallel} = \frac{\Delta^2}{2D_{\parallel}}$$

The sample temperature at position x at time t after irradiation is then given by

$$[4] \qquad T(x,t) = T_s + \exp\left(-\frac{t}{\tau_{\perp}}\right) \sum_k T_k(x,t)$$

where T_s is ambient temperature and the exponential factor in front of the summation allows for loss of vibrational energy by intermolecular transfer. In an excess of proton donors from water of hydration, we would expect the reaction that converts primary anions to TH to be pseudo-first order; hence, if the rate of reaction is

$$[5] \qquad k(x,t) = A \exp\left[\frac{-Q}{T(x,t)}\right]$$

with A being the collision frequency and Q the activation energy, then the probability of converting a primary anion at position x to TH is

$$[6] \qquad P_{TH}(x) = \int_0^{t_{max}} k(x,t) \exp\left[-\int_0^t k(x,t')\,dt'\right] dt$$

where t_{max} is the duration of the radiation-induced excess temperature. The mean conversion probability is obtained by averaging over the positions of primary anions, which we choose randomly from among the energy deposition events in the target.

Figure 2 shows typical results for the mean probability of converting primary anions to TH as a function of the activation energy for the reaction. These calculations are for 0.3 MeV protons incident on oriented DNA samples either perpendicular or parallel to the DNA fiber axis and the asymmetry of thermal diffusion ($D_{\parallel}/D_{\perp}$) is assumed to be 1000. Complete conversion of primary anions to TH is predicted for both irradiation geometries if the activation energy for irreversible protonation Q is less than 0.05 eV. Differential conversion in the parallel case increases for $0.05 < Q < 0.3$ eV, and the conversion probability is about an order of magnitude greater in the parallel case than the perpendicular case for all $Q > 0.3$ eV. However, for values of Q where the model predicts a large difference between parallel and perpendicular irradiation, the mean radical conversion in the former never exceeds about 30%. If conversion probabilities are further averaged over the distribution of activation energies suggested by the annealing data of Grasslund *et al.* (14), only about 10% of the primary anions produced by a parallel flux of 0.3 MeV protons would be expected to convert to TH. Although this value is an order of magnitude greater than conversion in the perpendicular case for the same model parameters, it cannot explain the predominance of TH radicals observed for neutrons incident parallel to the fiber direction.

Figure 3 shows the variation of the calculated probability to convert primary anions to TH as a function of the asymmetry of diffusion coefficients. The ion energy is 0.3 MeV and the energy barrier to protonation is 0.2 eV. The conversion probability in the parallel case decreases rapidly as the asymmetry of thermal diffusion decreases and approaches the value calculated for perpendicular irradiation, which is only weakly dependent on the ratio of $D_{\parallel}$ to $D_{\perp}$. This behavior is readily understandable in terms of the difference in the patterns of energy deposition for the two irradiation geometries. A high conversion probability is calculated only when a large number of energy deposition events, dispersed over a considerable

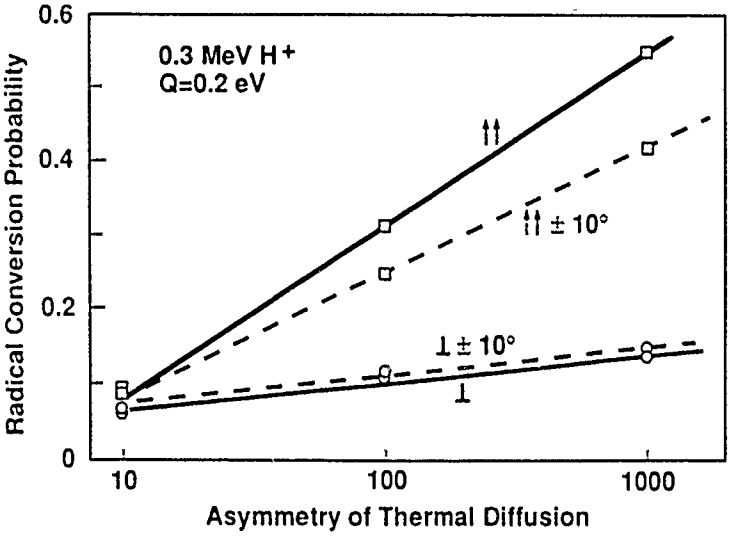

FIG. 3. Dependence on asymmetry of diffusion coefficients of the probability to convert primary anions to TH radicals calculated for 0.3 MeV protons incident parallel □ or perpendicular ○ to oriented DNA fibers at 77 K. Energy barrier to radical conversion is assumed to be 0.2 eV. Broken lines show the effect of ±10° uncertainty in flux alignment.

length of DNA, act cooperatively to overcome the energy barrier to protonation. Intermolecular energy transfer, which we model as thermal diffusion transverse to DNA chains, is very effective in dissipating this pattern of energy deposition.

The trend, shown in Fig. 3, of increasing conversion probability in the parallel case with increasing asymmetry of thermal diffusion saturates but not at unit probability. If $D_\perp = 0$ (i.e., infinite asymmetry) the mean conversion probability is about 70% for 0.3 MeV protons incident parallel to the DNA fibers and assuming an energy barrier of 0.2 eV for protonation of primary-anion radicals. The broken lines in Fig. 3 show the effect on the calculated radical-conversion probabilities of a ±10° uncertainty in alignment of the 0.3 MeV proton flux. Since conversion of primary anions to TH in the perpendicular case depends upon a dense cluster of excitations near the electron-gain center, the small probability of radical conversion calculated in that case is insensitive to uncertainty in the direction of the proton flux. Uncertainty in alignment significantly affects the parallel case because energy deposition patterns favorable to production of TH are less likely. Although we have not attempted to average our model calculations over the energy and directional characteristics of a realistic recoil-proton flux, it is clear from these results that the macroscopic model based on thermal spikes and asymmetry of thermal diffusion predicts that some primary radical anions should be observable in the parallel irradiation geometry. In this regard, the model does not agree with the data of Arroyo *et al.* (1) who observed primary radical anions in the perpendicular case only. We expect that data obtained with direct proton beam irradiation will provide additional criteria for testing the thermal-spike model.

Microscopic model

The thermal spike model, that addresses conversion of primary anions to TH, does not provide a basis for comparing theory and experiment for the orientation dependence of the total radical yield, which probably reflects greater recombination of charged precursors to radical anions and cations in the parallel case. For this reason and the limited success of the macroscopic model in explaining the observations of Arroyo *et al.* (1) regarding TH production, we are attempting to develop a more mechanistic model of the orientation effect. One of the approaches that we are investigating is based on observations by van Lith *et al.* (2) that nanosecond pulses of 3 MeV electrons induce microwave conductivity in hydrated DNA and collagen at low temperature. These observations suggest that electrons ejected by autoionization of SES enter quantum states associated with the hydration layer of macromolecules in which they have mobility comparable with excess electrons in pure ice and a long lifetime. If this interpretation is correct, then oriented DNA samples may be analogous in some respects to quasi-one-dimensional semiconductors (16) and models for photocurrent generation in the latter materials (17) may provide insight into mechanisms for differential radical yields in the parallel and perpendicular irradiation geometries. Figure 4, which was adapted from ref. 17, illustrates a mechanism for the reduction of radical yields and the predominance of TH radicals in the parallel case. The squares in this figure represent preexisting defects in the hydration layer of oriented DNA molecules. If these defects determine the mean free path of mobile electrons in the absence of radiation-induced defects and if scattering from these defects is quickly followed by localization on electron-gain centers, then radical yields in the perpendicular case will be mainly determined by competition between geminate recombination and electron trapping at defects. The broken lines in Fig. 4 represent typical electron trajectories in this process.

In the parallel irradiation geometry, the high-mobility path of excess electrons will contain transient radiation-induced excitations and ionizations in addition to the preexisting defects. These radiation-induced scattering centers are represented in Fig. 4 by circles. Multiple positive ions on the same DNA fiber should reduce the total radical yield in the parallel case because some mobile electrons that escape geminate recombination will undergo nongeminate recombination. Furthermore, the extra energy available in scattering from neutral radiation induced excitations may overcome the barrier to TH production, which we assume rarely occurs in scattering of mobile electrons from preexisting defects. These ideas can be expressed mathematically as coupled rate equations for the decay of mobile electrons and sibling holes in the presence of preexisting and radiation induced traps. We are currently investigating the dependence of radical yields predicted by these

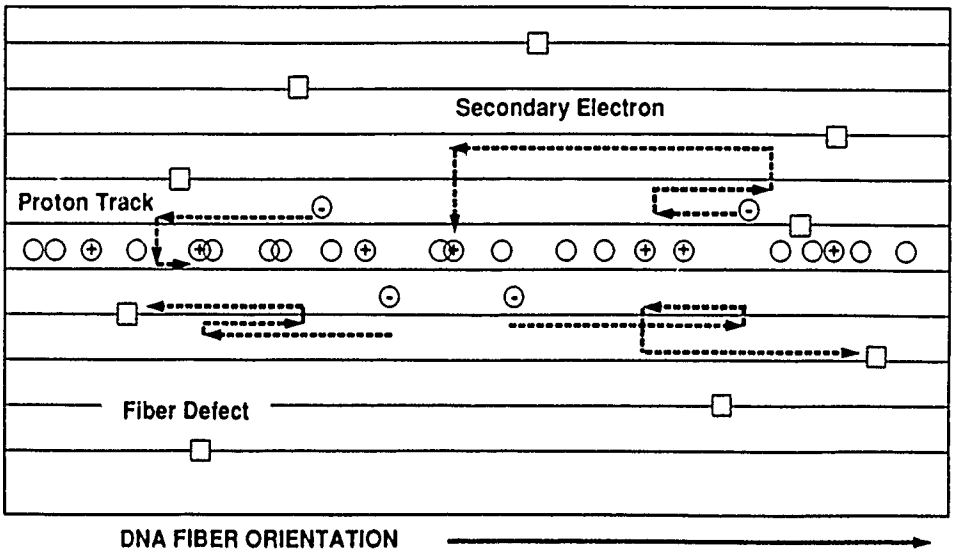

FIG. 4. Schematic diagram of electron recombination and trapping in a quasi-one-dimensional semiconductor. Squares and circles denote preexisting and radiation-induced defects, respectively. Broken lines are typical electron trajectories.

equations on the parameters of the model. For a given proton energy the main degrees of freedom in the model are the lifetime of neutral radiation-induced excitations and the concentration of preexisting defects.

This microscopic model differs from the model based on vibrational energy transfer in several important ways. First, ejected electrons are responsible for the long-range interaction between energy deposition events and the role of vibrational excitation in radical production and decay is local. Second, unlike the model based on vibrational energy transport where the nature of the mobile states was inferred form hydrogen–deuterium exchange rates (8), the electron transport model is based on experimentally observed electron mobility in materials similar to oriented DNA. Finally, calculated total radical yields will provide additional experimental constraints on the electron transport model that are not applicable to the macroscopic model because it could only predict the probability to convert primary anions to TH.

Summary

The observation of an orientation dependence of radical yields in DNA exposed to neutrons (1) has caused renewed interest in the role of energy and charge transfer in radiation damage by ionizing radiation. Both experimental and theoretical investigations are needed to confirm and interpret these findings. We are making progress in the development of methods to calculate the effects of proton energy and beam direction on radicals produced by direct proton irradiation of thin films of oriented DNA. The results obtained thus far suggest that effects like those reported for neutron exposures are possible only if excited states exist within which energy or charge can be transferred over several hundred base pairs on nanosecond time scale; however, we have not yet achieved sufficient agreement between model calculations and radical-yield data to suggest which of several potential transport mechanisms is most likely. The model calculations are, however, beginning to establish links between the data obtained with neutrons and other experimental findings (2) on similar materials. Ultimately these links will be a key factor in determining the significance of the orientation effect for our understanding of the mechanisms of DNA damage by densely ionizing radiation.

Acknowledgements

The authors gratefully acknowlege support for this work by the Office of Health and Environmental Research (OHER) U.S. Department of Energy under contract DE-AC06-76RLO-1830 and the Armed Forces Radiobiology Research Institute.

1. C. M. ARROYO, A. J. CARMICHAEL, C. E. SWENBERG, and L. S. MYERS, JR. Int. J. Radiat. Biol. **50**, 789 (1986).
2. D. VAN LITH, J. M. WARMAN, M. P. DE HAAS, and A. HUMMEL. J. Chem. Soc. Faraday Trans. 1, **82**, 2933 (1986).
3. J. H. MILLER, W. E. WILSON, C. E. SWENBERG, L. S. MYERS, JR., and D. E. CHARLTON. Int. J. Radiat. Biol. **53**, 901 (1988).
4. J. H. MILLER, W. E. WILSON, C. E. SWENBERG, L. S. MYERS, JR., and D. E. CHARLTON. Radiat. Phys. Chem. **32**, 349 (1988).
5. M. GUERON and R. G. SHULMAN. Ann. Rev. Biochem. **37**, 571 (1968).
6. K. F. BAVERSTOCK and R. D. CUNDALL. Int. J. Radiat. Biol. **55**, 151 (1989).
7. C. E. SWENBERG and J. H. MILLER. Int. J. Radiat. Biol. **56**, 383 (1989).
8. S. YOMOSA. Phys. Rev. A: Gen. Phys. **30**, 474 (1984).
9. W. A. BERNHARD. J. Phys. Chem. **93**, 2187 (1989).
10. W. BRANDT and R. H. RITCHIE. *In* Physical mechanisms in radiation biology. *Edited by* R. D. Cooper and R. W. Wood. Technical Information Center, Office of Information Services, U.S.A.E.C. 1974. p. 20.
11. M. D. SEVILLA, R. FAILOR, C. CLARK, R. A. HOLROYD, and M. PETTI. J. Phys. Chem. **80**, 353 (1976).
12. S. STEENKEN. Chem. Rev. **89**, 503 (1989).
13. J. BEDNAR. Int. J. Radiat. Biol. **48**, 147 (1985).
14. A. GRASSLUND, A. EHRENBERG, A. RUPPRECHT, B. TJALLDIN, and G. STROM. Radiat. Res. **61**, 488 (1975).
15. T HENRIKSEN, P. K. HORAN, and W. SNIPES Radiat. Res **43**, 1 (1970).
16. H. J. CANTOW (*Editor*). Advances in polymer science. Vol. 63. Springer-Verlag, Berlin. 1984.
17. E. L. FRANKEVICH, I. A. SOKOLIK, and A. A. LYMAREV. Mol. Cryst. Liq. Cryst. **175**, 41 (1989).

0022-1767/90/1457-2227$02.00/0
THE JOURNAL OF IMMUNOLOGY

Vol. 145, 2227-2234, No. 7, October 1, 1990
Printed in U.S.A.

CHARACTERIZATION OF HUMAN PHAGOCYTIC CELL RECEPTORS FOR C5A AND PLATELET ACTIVATING FACTOR EXPRESSED IN *Xenopus* OOCYTES

PHILIP M. MURPHY,[1]* ELAINE K. GALLIN,† AND H. LEE TIFFANY*

*From the *Bacterial Diseases Section, Laboratory of Clinical Investigation, National Institute of Allergy and Infectious Diseases, National Institutes of Health, and †Department of Physiology, Armed Forces Radiobiology Research Institute, Bethesda, MD 20892*

Platelet activating factor (PAF) and the active cleavage product of the fifth component of complement, C5a, are potent anaphylotoxins and mediators of inflammation. Both substances engage distinct guanine nucleotide binding regulatory protein-coupled receptors on a variety of cell types, thereby activating a signaling cascade that results in the mobilization of intracellular calcium stores, and in functional responses such as neutrophil chemotaxis and smooth muscle contraction. Little is known about the structure of PAF and C5a receptors or about the intracellular signaling pathways used by them. We have used the *Xenopus* oocyte expression system to demonstrate acquired C5a and PAF receptor activity in oocytes injected with mRNA from the promyelocytic leukemia cell line HL60 differentiated with dibutyryl cAMP. Activity was determined by measuring acquired ligand-dependent efflux of intracellular $^{45}Ca^{2+}$ and by measuring ligand-activated transmembrane currents in voltage clamped oocytes. C5a receptor activity was confined to a single sharp peak in sucrose gradient fractionated RNA that corresponded to a transcript size of 2 kb. In contrast, PAF receptor activity was broadly distributed in size fractionated RNA from 3.5 to 6 kb. This suggests that multiple transcripts of different sizes may encode a functional PAF receptor. Both ligands activated their respective receptor in a concentration-dependent and a structure-dependent manner. The acquired C5a-dependent calcium efflux activity was inhibited by pertussis toxin whereas the PAF receptor activity was not, suggesting that the two receptors couple to different G-proteins. These data establish the *Xenopus* oocyte as a model system for studying the molecular and functional properties of the C5a receptor and the PAF receptor(s) of phagocytic cells.

PAF[2] and C5a are important mediators of allergic and inflammatory reactions through their effects on a variety of tissues and cell types (1, 2). In the case of the vascular system, both agonists induce smooth muscle contraction (3, 4) and increase vascular permeability (5, 6), and thus function as anaphylotoxins. In the case of phagocytic cells such as neutrophils, both C5a (7–9) and PAF (10–13) are potent chemoattractants and secretagogues, and are able to activate the respiratory burst. They are therefore thought to play an important role in antimicrobial defense.

As with other chemoattractants, such as the N-formyl peptides of bacteria and leukotriene B_4, C5a, and PAF exert their effects on phagocytic cells by activating high affinity receptors that are coupled to a pertussis toxin sensitive G-protein (14–19). Snyderman et al. (20) have proposed a biochemical model for chemoattractant activation of phagocytic cells based primarily on extensive work with the N-formyl peptides. In these studies, a central signaling role has been defined for a polyphosphoinositide-specific phospholipase C that becomes activated upon stimulation of the receptor-G-protein complex by ligand. Hydrolysis of phosphatidylinositol-1,4-bisphosphate by phospholipase C leads to intracellular accumulation of diacylglycerol and inositol-1,4,5-trisphosphate that activate protein kinase C and mobilize intracellular calcium stores, respectively (20).

The general features of this signaling paradigm apply to the PAF receptor. However, at least one important exception has been identified: whereas all other PAF-dependent responses, including IP_3 accumulation, are pertussis toxin sensitive, PAF-dependent calcium fluxes are resistant to pertussis toxin at concentrations as high as 1 μg/ml (21–23). It has been proposed that this may be due to ionophoretic activity by PAF.

The extent to which the formyl peptide receptor signaling model can be applied to the C5a receptor remains unknown. Although a pertussis toxin sensitive G-protein and cytosolic calcium fluxes are clearly involved (24, 25), there are as yet no studies that have directly examined the effect of C5a on polyphosphoinositide metabolism or on other signaling pathways. Moreover, the pertussis toxin sensitivity of the C5a-dependent calcium flux has not been assessed.

PAF receptor activity has been identified on smooth muscle, endothelium, phagocytes, and platelets by functional and/or radioligand binding criteria and the existence of receptor subtypes has been postulated (26–30). To date, however, the subunit composition and primary structure has not been determined for the putative PAF receptor(s) of any tissue or cell type.

Affinity cross-linking experiments using human neutrophil and eosinophil membranes have indicated that

Received for publication March 22, 1990.
Accepted for publication June 29, 1990.
The costs of publication of this article were defrayed in part by the payment of page charges. This article must therefore be hereby marked *advertisement* in accordance with 18 U.S.C. Section 1734 solely to indicate this fact.

[1] Address correspondence to Dr. Philip M. Murphy, Building 10, Room 11N 110, National Institutes of Health, Bethesda, MD 20892.

[2] Abbreviations used in this paper: PAF, 1-O-octadecyl-2-O-acetyl-sn glycero-3-phosphorylcholine; lyso-PAF, 1-O-octadecyl-sn-glycero-3-phosphorylcholine; enantio-PAF, 3-O-hexadecyl-2-O-acetyl-sn-glycero-1-phosphorylcholine; G protein, guanine nucleotide binding regulatory protein.

the C5a binding site may be formed by a single polypeptide with molecular mass of 40 to 50 kDa (31–34). Additional larger forms of the crosslinked solubilized receptor have been observed, however, and point to the existence of an associated protein (35). The precise nature of this protein is unknown.

Microinjection of heterologous mRNA into oocytes from *Xenopus laevis* has been used to provide important functional and structural information about a large number of secreted, cytosolic and membrane-associated proteins (36, 37). This system has been particularly well suited for the study of that subgroup of G-protein-coupled receptors that is able to mobilize intracellular calcium stores (38–42).

We demonstrate that both C5a receptor and PAF receptor activity are acquired by oocytes from *X. laevis* that have been microinjected with RNA from HL60 granulocytes. The acquired activity is detected by measurement of ligand-dependent transmembrane ion fluxes. The C5a receptor is encoded by a single 2-kb mRNA whereas multiple transcripts of different sizes between 3.5 and 6 kb encode functionally indistinguishable PAF receptors. The preservation of activity for each receptor in size fractionated RNA suggests that the C5a receptor and the PAF receptor(s) may be composed of a single polypeptide chain. Acquired calcium mobilizing activity for C5a in the oocyte is pertussis toxin sensitive whereas that for PAF is not, suggesting that distinct G-proteins may be involved. Finally, PAF did not exhibit ionophoretic activity in this system.

MATERIALS AND METHODS

Reagents. Collagenase type II (131 U/mg) was purchased from Worthington Biochemical Corp., Freehold, NJ. FMLP, diethyl pyrocarbonate, dibutyryl cAMP, ethyl 3-amino benzoate were from Sigma Chemical Co., St. Louis, MO. PAF, lyso-PAF, and enantio-PAF were from Bachem, Philadelphia, PA. Human rC5a was from Sigma. It possessed an EC_{50} of 0.1 nM for human neutrophil chemotaxis. FCS was from HyClone Laboratories, Logan, UT. RPMI 1640 and L-glutamine were from Whitaker M.A. Bioproducts, Walkersville, MD. [α-^{32}P]dCTP (sp. act. >3000 Ci/mmol) and ^{35}S-L-methionine (1200 Ci/mmol) were from Amersham Corp., Arlington Heights, IL. $^{45}CaCl_2$ (25 mCi/mg) was from New England Nuclear, Boston, MA. A random primer labeling kit was from Boehringer-Mannheim, Indianapolis, IN. Pertussis toxin was from List, Campbell, CA. RNA size markers were from Bethesda Research Laboratories, Gaithersburg, MD.

Preparation of polyadenylated RNA. The human promyelocytic leukemia cell line HL60 was expanded at 37°C to log phase in RPMI 1640 medium supplemented with 10% FCS and 2 mM L-glutamine. Differentiation of HL60 cells was accomplished by incubation in supplemented medium containing 0.5 mM dibutyryl cAMP at 37°C for 48 h. Differentiation was confirmed by morphologic inspection and by detection of the formyl peptide receptor by affinity crosslinking with ^{125}I-N-formyl-norleucyl-leucyl-phenylalanyl-norleucyl-tyrosinyl-lysine as previously described (43). Total cellular RNA was prepared from cells stimulated for 24 or 48 h with dibutyryl cAMP by lysis in guanidinium isothiocyanate followed by cesium chloride centrifugation as previously described (44). Polyadenylated RNA was then selected by chromatography on an oligo (dT) cellulose Type 3 column (collaborative Research, Waltham, MA) as previously described (44).

Fractionation of mRNA. An SG series gradient maker (Hoeffer Scientific Instruments, San Francisco, CA), siliconized tubing and a Haake Buchler distributor were washed with 0.2% SDS and then soaked in 0.3% diethyl pyrocarbonate for 12 h to remove RNases. A 5 to 30% sucrose gradient was formed in STE buffer (STE = 10 mM Tris, 10 mM NaCl, 1 mM EDTA, pH 7.4) and was aged at 4°C for 24 h. Pooled poly(A)$^+$ RNA (500 μg) from 24 and 48 h differentiated HL60 cells was heated to 65°C in STE containing 2% sucrose, then applied to the gradient and centrifuged in an SW41 rotor (Beckman Instruments, Inc., Fullerton, CA) at 25,000 rpm for 14 h at 4°C. Fractions were collected manually. fractions 1 7 and 26 34 were 400 μl each, fractions 8 25 were 250 μl each. The sucrose concentration of each fraction was measured by refractometry. The RNA concentration was measured by spotting 1 μl of each fraction on an agarose plate containing ethidium bromide 0.1 μg/ml, by illuminating the plate with UV light and by comparing the observed fluorescence to that emitted by serial dilutions of a standard RNA solution. Each fraction was then precipitated with sodium acetate and ethanol, desalted, lyophilized, and dissolved in water at 1 ng/nl.

RNA analysis. The RNA samples were fractionated on a 1% agarose gel containing 2.2 M formaldehyde, 20 mM 3-(*N* morpholino)propane sulfonic acid 5 mM sodium acetate and 1 mM EDTA, and were also translated with a cell-free reticulocyte lysate system (Promega, Biotec, Madison, WI). The newly synthesized ^{35}S-methionine-labeled proteins were fractionated on a precast SDS 8 to 16% polyacrylamide gel (Novex, Encinitas, CA) and were visualized by autoradiography. The poly(A)$^+$ RNA was structurally intact, enriched in nonribosomal RNA and was capable of generating a broad range of polypeptides (data not shown). Blot hybridization was performed to estimate the size of RNA fractions possessing functional activity. Poly(A)$^+$ RNA (200 ng/fraction) from sucrose gradient fractions 5 through 31 was subjected to denaturing agarose gel electrophoresis in adjacent lanes of a two tier gel. RNA markers run in a parallel lane provided the positions of 1.35, 2.37, 4.4, 7.46, and 9.49 kb. RNA was transferred to nylon membranes (Schleicher & Schuell, Keene, NH) by electroblotting for 3 h at 20 V and then baked in a vacuum oven at 80°C for 45 min. Each of two duplicate blots prepared in this fashion was hybridized to 1 of 2 cDNA probes labeled with [α-^{32}P]dCTP by the random primer method (45). PM1 is a 1.2-kb cDNA that recognizes a 1.2-kb transcript on blots of differentiated HL60 cell RNA (46). H64 (provided by Stuart Orkin, Harvard Medical School, Boston, MA) is a 2.5-kb restriction fragment of the cytochrome b_{558} large subunit cDNA that recognizes a 4.4-kb transcript on blots of differentiated HL60 cell RNA (47). Sp. act. of each probe was approximately 10^9 cpm/μg of DNA. The membranes were prehybridized at 42°C for 2 h in a solution containing 6× SSPE (1× SSPE = 150 mM NaCl, 10 mM NaH_2PO_4 and 1 mM Na_2EDTA, pH 7.4), 5× Denhardt's (1× Denhardt's = 0.02% each of Ficoll, BSA, and polyvinylpyrrolidone), 0.5% SDS, 50 μg/ml herring sperm DNA, and 10 μg/ml tRNA. Hybridization was performed at 42°C for 24 h in a solution containing 50% formamide, 6× SSPE, 1% SDS, 50 μg/ml herring sperm DNA, 10 μg/ml tRNA, and 3×10^6 cpm of labeled probe/ml. Final washing was performed in 0.1× SSPE, 0.4% SDS at 70°C. The relative intensity of specific bands in each RNA fraction of the resulting autoradiographs was quantitated by laser densitometry (Pharmacia LKB, Piscataway, NJ).

Microinjection of RNA into Xenopus oocytes. Adult female laboratory bred *X. laevis* (Nasco, Fort Atkinson, WI) were maintained at 19 to 22°C in a light-dark cycle of 12 h per phase. Frogs were anesthetized with 0.15% ethyl 3-amino benzoate. Ovarian lobes were resected and defolliculated in OR2 solution (82.5 mM NaCl, 1 mM $MgCl_2$, 2.4 mM KCl, 5 mM HEPES, pH 7.5) containing 2 mg/ml collagenase for 2 h on a rotary shaker. individual Dumont stage V-VI oocytes (48) were transferred to ND96 solution (96 mM NaCl, 2 mM KCl, 1.8 mM $CaCl_2$, 1 mM $MgCl_2$, 2.4 mM sodium pyruvate, penicillin 100 U/ml, streptomycin 100 μg/ml, 5 mM HEPES, pH 7.4 to 7.5). After a 12 to 18 h recovery period, oocytes were microinjected at the equator either with 50 nl of diethyl pyrocarbonate-treated water or with a solution of RNA in water using an IM200 microinjector (Narishige USA, Greenvale, NY). Borosilicate glass was pulled on a Kopf pipette puller and the tip was trimmed manually using watchmaker forceps to a diameter of approximately 10 μ. Injection of 50 nl typically required an injection time of 15 ms at 150 kilopascals. Oocytes were then transferred in groups of less than 30 oocytes to 16-mm diameter wells of a 24-well tissue culture plate (Costar, Cambridge, MA) and were incubated in ND96 medium at 20°C. The incubation medium was changed daily. More than 85% of injected oocytes survived this process and were suitable for analysis. The experiments were conducted with oocytes harvested from four different frogs.

Calcium efflux assay. Grouped oocytes were incubated in 500 μl of OR2 medium containing 50 μCi/ml $^{45}Ca^{2+}$ for 3 h at 20°C. They were then washed as groups five times over 60 min with 1 ml exchanges of ND96 medium and were then individually apportioned to replicate 6-mm diameter flat bottomed polystyrene wells containing 100 μl of ND96 medium. Washing was resumed with five 100 μl exchanges of ND96 medium spaced 10 min apart using a multichannel pipette device. After the final wash, 100 μl of ND96 medium with or without ligand was added to the wells. Radioactivity was measured by mixing the extracellular fluid with 3a70b scintillation cocktail (Research Products International, Mt. Prospect, IL) followed by counting in a β counter (Packard Instruments Co., Downers Grove, IL). The baseline unstimulated efflux of $^{45}Ca^{2+}$ was determined for each oocyte without subtraction of environmental background by measuring the cpm in the final 100 μl wash. This was typically less

than 150 cpm. The stimulated calcium efflux was terminated 15 min after the addition of the stimulus, an interval that was determined empirically to be sufficiently long to allow more than 90% of stimulated release of $^{45}Ca^{2+}$ to occur. To demonstrate that the oocytes were adequately and similarly loaded, residual cpm were determined by counting oocyte homogenates after completion of the calcium efflux assay. This ranged from about 1000 to 10,000 cpm per oocyte between experiments, but was quite consistent within each experiment. The stimulus-dependent efflux was calculated in two ways: 1) as the mean ± SEM of the "net $^{45}Ca^{2+}$ efflux," defined as the difference between the cpm detected in the 15-min stimulated extracellular fluid and those detected in the final wash; 2) as the mean ± SEM of the "percent of maximum" defined as (net cpm/(net cpm + residual cpm)) × 100. Both methods of calculating activity gave similar results. These methods are adapted from those previously described by Williams et al. (39).

Whole cell current measurements. Individual oocytes were voltage clamped with an Axoclamp-2 amplifier (Axon Instrument, Foster City, CA) using a standard two electrode voltage clamp configuration. Membrane currents were recorded on a Gould chart recorder. Electrodes were filled with 3 M KCl and had resistances of 5 to 15 megaOhms. Oocytes were clamped at the resting membrane potential, which ranged from −55 to −75 mV. Ligands were added directly to the bath, which contained 3 ml of ND96 medium maintained at 18°C. Added stimuli were removed by bath perfusion, which could be completed within 1 min.

Statistical methods. Differences between means were analyzed with the Student's *t*-test. Results from multiple experiments were pooled and analyzed with the Omnibus test.

RESULTS

Because chemoattractant receptors are able to mobilize intracellularly sequestered calcium in phagocytic cells (20–25), we tested oocytes injected with differentiated HL60 cell RNA for acquired ligand-dependent calcium mobilization by measuring the accelerated efflux of intracellular $^{45}Ca^{2+}$. Figure 1 shows the net $^{45}Ca^{2+}$ efflux from individual oocytes injected with HL60 cell RNA, or with water alone, and then stimulated 4 days later with human rC5a 10 nM (*A*) or PAF 1 μM (*B*). The results indicate ligand-dependent responsiveness suggesting the acquisition of human phagocyte receptors for C5a and PAF by the RNA-injected oocytes. Oocytes injected with water alone did not respond suggesting that they are devoid of native receptors for PAF and human C5a. Oocytes injected with RNA from undifferentiated HL60 cells also failed to respond (not shown), consistent with the observation that chemoattractant receptors are not expressed by immature myeloid cells (49).

The differentiated HL60 cell RNA was fractionated by size on a 5 to 30% sucrose gradient. Figure 2*A* shows that C5a receptor calcium efflux activity was confined to a single sharp RNA containing peak at fractions 10 to 12 of the centrifuged sucrose gradient. We have measured the abundance and established the positions of known HL60 cell transcripts—a 1.2-kb transcript encoding PM1 (46) and a 4.4-kb transcript encoding the large subunit of cytochrome b_{558} (47)—in the sucrose gradient fractions by gel fractionation and blot hybridization analysis. Comparison of the average size of mRNA in the RNA size fractions with commercially obtained RNA size standards gave a similar result and was used to establish the position of the 6-kb marker arrow shown in Figure 2*A* and *B*. Based on the position of the C5a-dependent activity peak relative to these physical size standards, we estimate the size of the transcript encoding the C5a-dependent calcium efflux activity to be 2 kb. This conclusion was supported by separate experiments in which C5a-induced whole cell current activity was found to be confined to the same RNA size fractions as for the calcium efflux activity (not shown).

In contrast to the relatively well-resolved C5a receptor activity seen in Figure 2*A*, PAF receptor activity was found in a broad sucrose gradient peak that contained RNA transcripts ranging from 3.5 to 6 kb in length (Fig. 2*B*). This suggests the possibility of multiple overlapping peaks containing transcripts of different sizes, all of which encode a functional PAF receptor.

Having established that oocyte responsiveness to PAF and C5a requires the injection of RNA of a particular size from differentiated HL60 cells, we next investigated the ligand structural specificity of the observed activity using relevant phospholipid and peptide controls. Figure 3 shows that structural requirements for PAF agonist activity are observed by the acquired PAF receptor expressed in the oocyte as measured by calcium efflux activity. The defined chain length PAF precursor, lyso-PAF, and a defined chain length stereoisomer of PAF, enantio-PAF, are known to lack agonist activity for phagocytic cell responses (1) and failed to increase $^{45}Ca^{2+}$ efflux when applied to RNA-injected oocytes possessing PAF receptor activity. The negative values shown in Figure 3 for lyso-PAF and enantio-PAF indicate that the bath fluid after stimulation actually contained fewer counts than that harvested just before stimulation. No differences were observed when RNA from different positions in the PAF receptor activity peak (see Fig. 2*B*) were tested, for example the smallest active transcripts (a mixture of fractions 14 and 15) and larger active transcripts (a mixture of fractions 24 and 25).

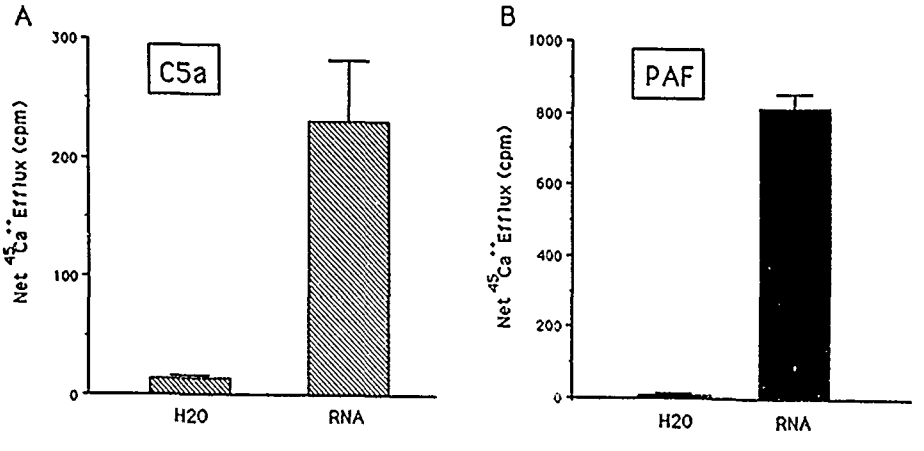

Figure 1. Acquired chemoattractant receptor activity in *Xenopus* oocytes. Oocytes were injected with 50 nl of water or with 50 nl of differentiated HL60 cell poly(A)$^+$ RNA (0.5 ng/nl in *A* and 1 ng/nl in *B*). Four days after injection individual oocytes were stimulated with C5a 10 nM (in triplicate) or with PAF 1 μM (water control in triplicate and RNA injected cells in replicates of five). Responsiveness was calculated as the net $^{45}Ca^{2+}$ efflux as described in *Materials and Methods*. The mean prestimulation $^{45}Ca^{2+}$ efflux was <60 cpm for all conditions and differed by <10% between water and RNA injected oocytes for both *A* and *B*. The mean ± SEM of $^{45}Ca^{2+}$ loaded per oocyte was 1910 ± 47 cpm (n = 14) for the entire experiment: this differed by <10% between RNA and water injected oocytes in both *A* and *B*. Data are from the same experiment which is representative of at least four separate experiments performed for each ligand.

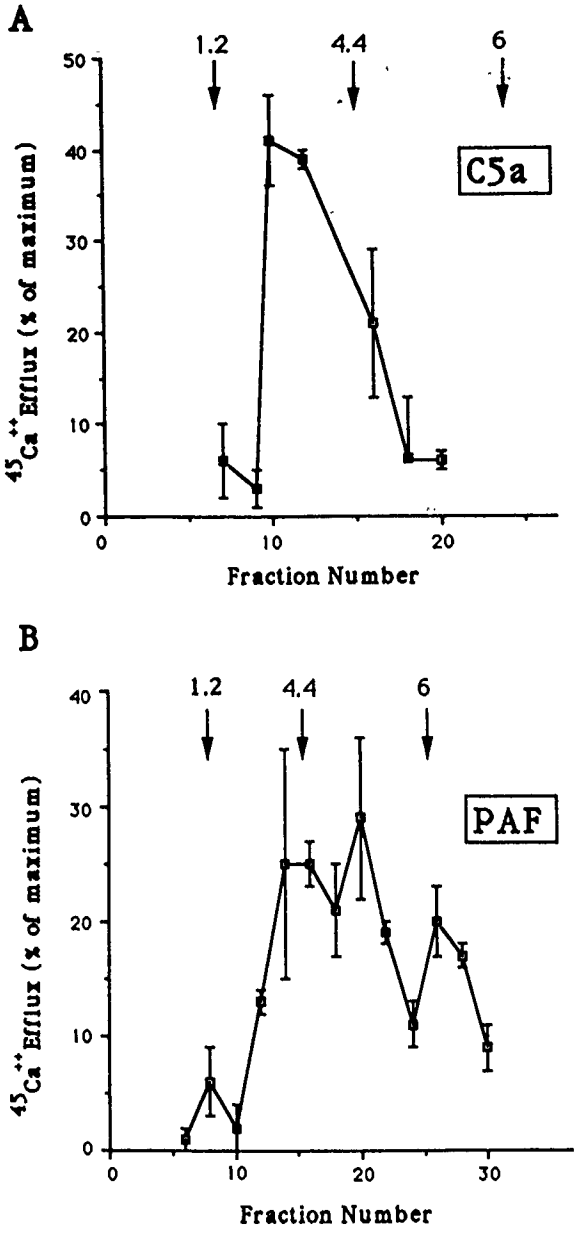

Figure 2. Size estimation of transcripts encoding chemoattractant receptor activity. *A*, Oocytes were injected with 50 ng of RNA from the indicated sucrose gradient fractions. Five days later they were stimulated with C5a 10 nM. For each data point, calcium efflux was measured from individual oocytes in triplicate except for fractions 7 and 12 that are from duplicates. Pools of RNA fractions 20 to 34 possessed no activity (not shown). The activity in fraction 10 represented 22 ± 6-fold that of baseline efflux. The mean ± SEM amount of radiolabel loaded per oocyte was 5077 ± 930 cpm for the entire experiment (n = 19). Data are representative of four separate experiments performed with two independent preparations of RNA. *B*, Oocytes were injected with 50 ng of RNA from a 1:1 mixture of sequential pairs of odd and even numbered sucrose gradient fractions and four days later were stimulated with PAF 1 μM. Data are representative of two independent experiments and derive from four to five replicates per data point, one oocyte per replicate, with the exception of fractions 10/11 and 14/15 which were tested in triplicate and duplicate, respectively. The mean ± SEM baseline efflux and amount of loaded radiolabel per oocyte were 59 ± 9 and 928 + 68 cpm (n = 54) for the entire experiment. In both *A* and *B* the position of RNA size standards in gradient fractions is indicated in kb by the *arrows*.

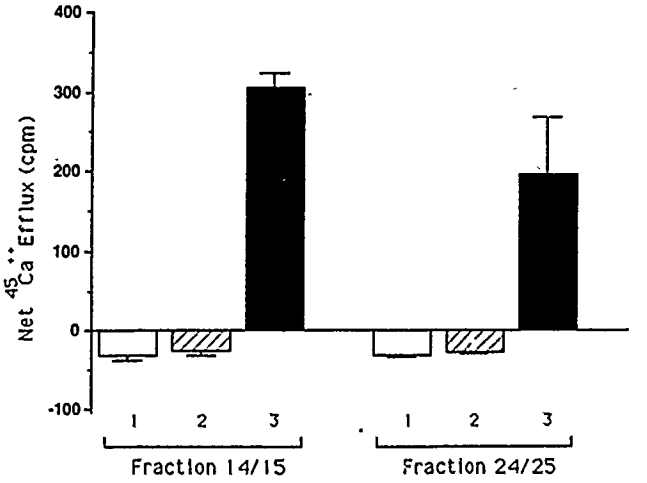

Figure 3. Ligand structural specificity for acquired PAF receptor activity in *Xenopus* oocytes. Oocytes were injected with 50 ng of a 1:1 mixture of sucrose gradient fractions 14 and 15 (*left*) or fractions 24 and 25 (*right*) RNA. Four days later the oocytes were stimulated with lyso-PAF (*lanes 1*), enantio-PAF (*lanes 2*), or PAF (*lanes 3*) at 1 μM. The mean baseline unstimulated calcium efflux was <90 cpm for all conditions and differed by at most 15% between conditions. The mean ± SEM amount of radionuclide loaded per oocyte was 2020 ± 51 cpm (n = 23) for the entire experiment. Data are from four replicates per condition, one oocyte per replicate (with the exception of fraction 14/15, *lane 2* which was tested in triplicate), and are representative of four independent experiments.

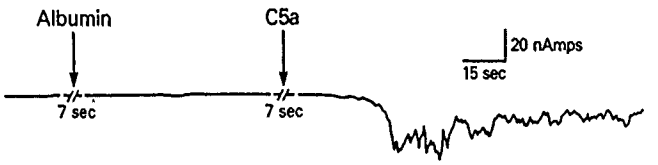

Figure 4. Acquired human C5a receptor expression in *Xenopus* oocytes—detection of ligand-induced currents. Current tracing depicts two electrode voltage clamp data of an oocyte 4 days after injection with 50 nl of unfractionated, differentiated HL60 cell RNA 1 ng/nl. The holding potential was −60 mV. At the indicated times BSA 0.5% or human rC5a 3 nM in 0.5% albumin were added to the bath. Downward deflection indicates inward current. The tracing is representative of four separate experiments using either size fractionated or unfractionated RNA.

Figure 4 shows the first of two controls indicating that the C5a receptor activity is specifically dependent on the C5a polypeptide and cannot be elicited by an irrelevant protein such as albumin. In addition Figure 4 illustrates a second type of functional activity that is subserved by the C5a receptor expressed in the oocyte, namely the activation of transmembrane currents that can be measured in voltage clamped oocytes. A typical tracing is shown of current levels over time in a voltage clamped oocyte before and after stimulation with human rC5a 3nM in media containing 0.5% BSA or with media/BSA alone. A prolonged inward oscillating current is induced only when C5a is present and is not activated by BSA alone. The C5a-induced current is similar to those previously described in the oocyte that are induced by other G-protein coupled receptors that stimulate polyphosphoinositide metabolism, such as the muscarinic acetylcholine receptor. The current that results from activation of this and other calcium mobilizing receptors expressed in the oocyte has been shown to be due to activation of a calcium-dependent chloride conductance (50–52). After injection of 50 ng of RNA from fractions 10 to 12 we have observed C5a stimulated current responses varying in magnitude from 5 to 60 nanoamps in three of four oocytes tested. Oocytes injected with water alone failed to respond to C5a (not shown).

Figure 5 shows a second peptide control indicating that the C5a receptor activity is specifically subserved by the

C5a polypeptide, again determined by measuring C5a-induced whole cell currents in voltage clamped oocytes. We have previously shown that the formyl peptide receptor can be expressed in the *Xenopus* oocyte after injection with 2-kb transcripts from differentiated HL60 cells (52). Figure 5 shows a tracing of current vs time in an oocyte injected with 2-kb RNA. Initial stimulation with 0.5 μM FMLP induced a prolonged inward current (peak current = 50 nanoamps). Baseline current levels were restored by washing the oocyte in buffer alone. Repeat stimulation of the oocyte 6.5 min later with the same concentration of FMLP was ineffective suggesting that homologous desensitization of the formyl peptide receptor had occurred. In contrast, stimulation of the same oocyte 2 min later with 5 nM C5a induced a prolonged inward current response (peak current = 20 nanoamps) that was reversible. These data show that the C5a response is ligand specific and suggest that complete heterologous desensitization of the C5a receptor by stimulation of the formyl peptide receptor in the oocyte does not occur.

Figure 6 shows that both the acquired C5a-induced (*A*) and the acquired PAF-induced (*B*) calcium efflux activity in the oocyte were ligand concentration-dependent. The threshold concentration for C5a responsiveness was approximately 50 pM and the concentration for maximal responsiveness was approximately 10 nM, both of which are in agreement with values for C5a-stimulated changes in quin 2 fluorescence that have been previously determined in bovine and human neutrophils (24, 25). The acquired PAF receptor calcium efflux activity threshold in the oocyte was approximately 100 pM whereas maximal responsiveness was observed at 10 nM PAF. These values are in close agreement with those previously reported for calcium fluxes in human and rabbit neutrophils and human eosinophils (23, 28, 53). At PAF concentrations exceeding 1 μM a decrease in PAF-dependent calcium efflux activity was observed in RNA injected oocytes (not shown). This may be due to exceeding the critical micellar concentration for PAF which is approximately 3 to 5 μM. Others have observed this phenomenon for a variety of PAF responses in phagocytic cells including degranulation and calcium flux (13, 28). Fractions 14/15 and fractions 24/25 RNA, which represent 3.5- and 6-kb RNA transcripts encoding PAF receptor activity in the fractionated RNA (see Fig. 2*B*), subserved receptor

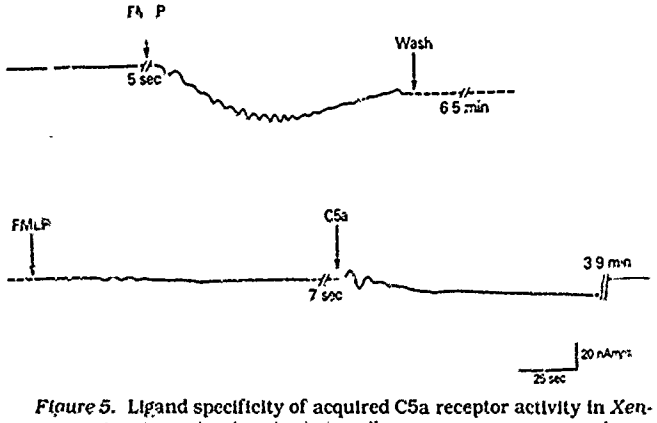

Figure 5. Ligand specificity of acquired C5a receptor activity in *Xenopus* oocytes. Ligand-induced whole cell currents were measured in a voltage clamped oocyte (holding potential = −56 mV) 4 days after injection with 50 nl of unfractionated, differentiated HL60 cell RNA 1 ng/nl. Arrows indicate the times of addition of FMLP 0.5 μM or C5a 5 nM. The tracing is representative of two separate experiments.

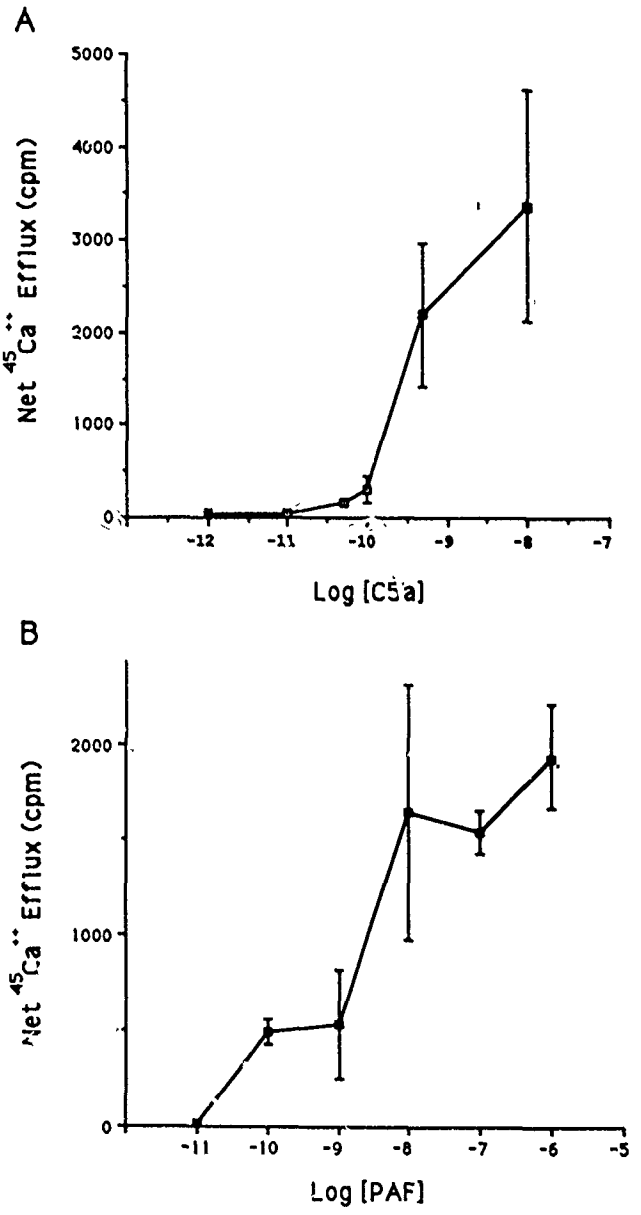

Figure 6. Ligand concentration dependence of acquired chemoattractant receptor activity in *Xenopus* oocytes. Oocytes were injected with 50 ng of a 1:1 mixture of sucrose gradient fractions 12 and 13 (*A*) or fractions 14 and 15 (*B*) and were stimulated 4 days later with the indicated concentration of ligand. Data are representative of two separate experiments performed in replicates of three to five, one oocyte per replicate with the exception of the 10^{-12} M and the 5×10^{-11} M data points of *A* that were not replicated. Baseline efflux was less than 170 cpm per oocyte for all oocytes in both *A* and *B* and did not differ significantly between concentrations. The mean ± SEM amount of radiolabel loaded per oocyte was 5073 ± 1624 cpm (*A*) and 2306 ± 469 cpm (*B*).

activity that possessed an identical ligand concentration dependence (not shown).

It is known that cellular responses to stimulation with C5a are sensitive to pertussis toxin suggesting the involvement of a G-protein-coupled signaling cascade. Figure 7 shows inhibition of acquired C5a-dependent calcium efflux by incubation of RNA-injected oocytes with 2 μg/ml of pertussis holotoxin for 24 h. The inhibitory activity of pertussis toxin was 45 and 85% in 2 separate experiments.

In contrast, oocytes injected with either fraction 14/15 or 24/25—representing the extremes of RNA transcript sizes that encode functional PAF receptors—exhibit PAF receptor activity that is completely insensitive to pertus-

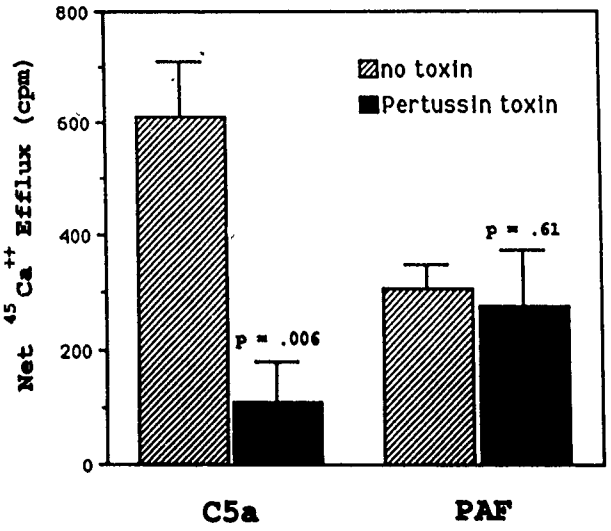

Figure 7. Effect of pertussis toxin on acquired chemoattractant receptor activity in *Xenopus* oocytes. Oocytes were injected with 50 ng of a 1:1 mixture of sucrose gradient RNA fractions 12 and 13 (C5a) or fractions 24 and 25 (PAF). Four days after injection, the RNA injected oocytes were incubated in ND96 with (*black bars*) or without (*diagonal bars*) pertussis toxin 2 μg/ml for an additional 24 h. The oocytes were then loaded with $^{45}Ca^{2+}$ and were stimulated with 10 nM C5a or 1 μM PAF. Control oocytes injected with water alone did not respond to either ligand (not shown). Data are from three to four replicates per condition, one oocyte per replicate and are representative of two separate experiments with C5a and 10 separate experiments with PAF (five each with fractions 14/15 RNA and fractions 24/25 RNA).

sis toxin ($p > 0.5$ for pooled data from five separate experiments each for fractions 14/15 and fractions 24/25 analyzed with the Omnibus test).

Fractions 14/15 and fractions 24/25 were also indistinguishable with respect to the rate at which oocytes injected with each RNA acquired PAF-dependent $^{45}Ca^{2+}$ efflux activity. Expression was detectable as early as 1 day and at least 7 days after injection. Peak activity was observed between 2 and 4 days after injection (data not shown).

DISCUSSION

In summary, we have shown that responsiveness to C5a and PAF can be acquired in the *Xenopus* oocyte after microinjection of mRNA from differentiated HL60 cells. The heterologously expressed activity in each case couples to a signaling cascade that results in transmembrane ion fluxes, probably due to the mobilization of intracellular calcium stores. We have enriched HL60 cell RNA for transcripts encoding C5a receptor activity and have determined that they are confined to a single sharp sucrose gradient peak corresponding to a transcript size of 2 kb. Transcripts of multiple different sizes encode functionally similar PAF receptors when expressed in the oocyte. Finally, although both the C5a and the PAF receptor activate calcium mobilizing elements in the oocyte, they appear to do so by coupling to distinct membrane transducers because the C5a-dependent activity is pertussis toxin sensitive whereas the PAF dependent activity is pertussis toxin resistant.

Although the data from our study do not rule out the possibility of multiple distinct subunits encoded by RNA transcripts of very similar size or of a homomultimeric receptor structure, the existence of receptor activity in small size ranges of size fractionated RNA is consistent with the hypothesis that functional C5a and PAF receptors are composed of a single polypeptide chain as is typical of G-protein-coupled receptors (41, 42). The nicotinic acetylcholine receptor is an example of a heteromultimeric receptor whose functional expression in *Xenopus* oocytes requires the injection of RNA encoding all four polypeptide subunits although only one of them, the α-subunit, contains the ligand binding domain (54).

Affinity cross-linking studies have indicated that the C5a receptor ligand binding subunit has a molecular mass of 40 to 50 kDa (31–34). The core polypeptide M_r may be substantially smaller since this receptor, as with most plasma membrane receptors, is most likely a glycoprotein. No direct studies of the associated carbohydrate content of the receptor have been reported, however. Taking 50 kDa as the upper limit of the molecular mass of the ligand binding polypeptide, it is clear that a transcript 2 kb in length would accommodate approximately 500 bases of 3′- and 5′-untranslated sequences in addition to the coding block.

Affinity cross-linking analysis of the solubilized C5a receptor has also revealed an additional 90-kDa species of unknown structure (35). This could represent dimerization of the receptor-ligand complex, the existence of a distinct monomeric receptor subtype, the existence of an additional receptor subunit, or cross-linking of the receptor to an associated protein. With regard to this last possibility, the activated α-subunit of an associated signal transducing G-protein has been proposed as a candidate to explain the 90-kDa affinity cross-linked species because the 40-kDa difference between the two observed affinity cross-linked forms is similar to the known M_r of G_o-α and G_i-α subunits. Moreover, a precedent exists in the copurification of the formyl peptide receptor and the muscarinic acetylcholine receptor with a G-protein α-subunit (55, 56).

To date there have been no affinity cross-linking methods or antibody reagents generated to study the physical characteristics of the putative PAF receptor of any cell type. In this context, our study firmly establishes that a specific protein from a cell type exhibiting PAF functional and binding activity can be expressed in *Xenopus* oocytes, as assessed by acquired PAF responsiveness in RNA-injected oocytes. An important implication of this result is that precise primary structural information regarding PAF receptors may be obtained by the cloning of cDNA through functional expression in the oocyte, independent of preliminary structural information about the receptor protein. This has been accomplished for two other G-protein-coupled receptors, the substance K receptor (41) and the serotonin 1c receptor (42).

The existence of a broad peak of RNA spanning 3.5 to 6 kb that encodes functional PAF receptors strongly suggests the existence of multiple PAF receptor transcripts of quite different sizes and hints that distinct PAF receptor subtypes may exist in the phagocyte. Based on functional and ligand binding studies, distinct PAF receptor subtypes have been proposed to exist in platelets, neutrophils, and eosinophils (17, 26–28). The existence of multiple receptor subtypes in the neutrophil has been postulated based on the presence of pertussis toxin sensitive and pertussis toxin insensitive PAF dependent activity in this cell type (see *Discussion*). We attempted to identify subtypes by comparing the $^{45}Ca^{2+}$ efflux activity subserved by RNA corresponding to 3.5- and 6-kb transcripts

representing the extremes of transcript sizes that encode PAF receptor activity. However, a similar ligand concentration dependence, ligand structure dependence, pertussis toxin resistance, and kinetics of expression were observed for the PAF receptor calcium efflux activity after injection of these distinct RNA fractions.

Alternatively, these different RNA may be splice variants that encode the same receptor polypeptide due to splicing events in the noncoding regions of a precursor messenger RNA. The larger transcript(s) could represent a nuclear preprocessed RNA derived from a gene containing introns only in the non-protein coding regions. This is quite plausible because many of the G-protein-coupled receptors for which precise genomic structure is known have been shown to derive from genes that are intronless at least through the coding block (57).

Inasmuch as the C5a receptor calcium mobilizing response in the oocyte can be inhibited by pertussis toxin, it is likely that a signal transducing G-protein that is native to the oocyte and that can be ADP-ribosylated by pertussis toxin, such as G_{i2}, is coupled to this receptor. Whether or not the specific coupling proteins supplied by the oocyte are the same isoforms as those in the neutrophil remains to be determined.

Our study confirms previous reports that have shown PAF-dependent calcium fluxes to be pertussis toxin insensitive in phagocytic cells. Interestingly, the PAF-induced calcium response is exceptional in this regard: other cellular responses such as degranulation and chemotaxis, and biochemical responses such as IP_3 accumulation in response to stimulation of phagocytic cells with PAF are exquisitely sensitive to inhibition by pertussis toxin (21, 22). A similar disparity has been observed with another lipid chemoattractant, LTB_4, but has not been found with peptide chemoattractants (21). One potential explanation that has been proposed is that the lipid chemoattractants may possess calcium ionophoretic properties at high concentrations (21, 58). Our study indicates that this is not the case in the oocyte because oocytes that received no RNA clearly do not display augmented calcium efflux in response to 1 μM PAF. Taken together these data suggest the existence of at least two signaling pathways that are used by PAF, one of which is inositol-1,4,5-trisphosphate independent and pertussis toxin insensitive.

In conclusion, these data establish that functional C5a and PAF receptors can be expressed in *Xenopus* oocytes that have been injected with RNA from HL60 granulocytes. Experiments performed with size-fractionated RNA suggest strongly that both receptors are composed of a single polypeptide chain that is encoded by a 2-kb transcript, in the case of the C5a receptor, and multiple transcripts of different sizes ranging from 3.5 to 6 kD, in the case of the PAF receptor. This latter finding suggests that multiple distinct PAF receptor subtypes may exist in phagocytic cells. Differential effects of pertussis toxin indicate that the C5a receptor and the PAF receptor(s) couple to calcium mobilizing effector systems via distinct G-proteins. Lastly, the oocyte expression system has now been identified as a suitable method by which to isolate cDNA clones encoding the C5a receptor and the PAF receptor.

Acknowledgments. We thank Harry Malech for advice and support.

REFERENCES

1. **Pinckard, R. N., J. C. Ludwig, and L. M. McManus.** 1988. Platelet activating factors. In *Inflammation: Basic Principles and Clinical Correlates.* J. I. Gallin, I. M. Goldstein, and R. Snyderman, eds. Raven Press, Ltd., New York, p. 139.
2. **Goldstein, I. M.** 1988. Complement: biologically active products. In *Inflammation: Basic Principles and Clinical Correlates.* J. I. Gallin, I. M. Goldstein, and R. Snyderman, eds. Raven Press, Ltd., New York, p. 55.
3. **Stimler, N. P., and J. T. O'Flaherty.** 1983. Spasmogenic properties of platelet-activating factor: evidence for a direct mechanism in the contractile response of pulmonary tissues. *Am. J. Pathol. 113:75.*
4. **Marceau, F., and T. E. Hugli.** 1984. Effect of C3a and C5a anaphylatoxins on guinea-pig isolated blood vessels. *J. Pharmacol. Exp. Ther. 230:749.*
5. **Humphrey, D. M., L. M. McManus, D. J. Hanahan, and R. N. Pinckard.** 1984. Morphologic basis of increased vascular permeability induced by acetyl glyceryl ether phosphorylcholine. *Lab. Invest. 50:16.*
6. **Hugli, T. E.** 1984. Structure and function of the anaphylatoxins. *Springer Semin. Immunopathol. 7:193.*
7. **Webster, R. O., S. R. Hong, R. B. Johnston Jr., and P. M. Henson.** 1980. Biological effects of the human complement fragments C5a and C5a des Arg on neutrophil function. *Immunopharmacology 2:201.*
8. **Goldstein, I. M., S. Hoffstein, J. I. Gallin, and G. Weissmann.** 1973. Mechanisms of lysosomal enzyme release from human leukocytes: Microtubule assembly and membrane fusion induced by a component of complement. *Proc. Natl. Acad. Sci. USA 70:2916.*
9. **Goetzl, E. J., and K. F. Austen.** 1974. Stimulation of human neutrophil leukocyte aerobic glucose metabolism by purified chemotactic factors. *J. Clin. Invest. 53:591.*
10. **Goetzl, E. J., C. K. Derian, A. I. Tauber, and F. H. Valone.** 1980. Novel effects of 1-O-hexadecyl-2-acyl-sn-glycero-3-phosphorylcholine mediators on human leukocyte function: delineation of the specific roles of the acyl substituents. *Biochem. Biophys. Res. Commun. 94:881.*
11. **O'Flaherty, J. T., C. L. Swendsen, C. J. Lees, and C. E. McCall.** 1981. Role of extracellular calcium in neutrophil degranulation responses to 1-O-alkyl-2-acetyl-sn-glycero-3-phosphorylcholine. *Am. J. Pathol. 105:107.*
12. **Smith, R. J., B. J. Bowman, and S. S. Iden.** 1984. Stimulation of the human neutrophil superoxide anion-generating system with 1-O-hexadecyl/octadecyl-2-acetyl-sn-glyceryl-3-phosphorylcholine. *Biochem. Pharmacol. 33:973.*
13. **Shaw, J. O., R. N. Pinckard, K. S. Ferrigni, L. M. McManus, and D. J. Hanahan.** 1981. Activation of human neutrophils with 1-O-hexadecyl/octadecyl-2-acetyl-sn-glyceryl-3-phosphorylcholine (platelet activating factor). *J. Immunol. 127:1250.*
14. **Wilde, M. W., K. E. Carlson, D. R. Manning, and S. H. Zigmond.** 1989. Chemoattractant-stimulated GTPase activity is decreased on membranes from polymorphonuclear leukocytes incubated in chemoattractant. *J. Biol. Chem. 264:190.*
15. **Huey, R., and T. E. Hugli.** 1985. Characterization of a C5a receptor on human polymorphonuclear leukocytes (PMN). *J. Immunol. 135:2063.*
16. **Feltner, D. E., R. H. Smith, and W. A. Marasco.** 1986. Characterization of the plasma membrane bound GTPase from rabbit neutrophils. I. Evidence for an Ni-like protein coupled to the formyl peptide, C5a, and leukotriene B4 chemotaxis receptors. *J. Immunol. 137.1961.*
17. **Hwang, S-B.** 1988. Identification of a second putative receptor of platelet-activating factor from human polymorphonuclear leukocytes. *J. Biol. Chem. 263:3225.*
18. **Ng, D. S., and K. Wong.** 1986 GTP regulation of platelet-activating factor binding to human neutrophil membranes. *Biochem. Biophys. Res. Commun. 141:353.*
19. **Lad, P. M., C. V. Olson, and I. S. Grewal.** 1985. Platelet activating factor mediated effects on human neutrophil function are inhibited by pertussis toxin. *Biochem. Biophys. Res. Commun. 129:632.*
20. **Snyderman, R., C. D. Smith, and M. W. Verghese.** 1986. Model for leukocyte regulation by chemoattractant receptors. roles of a guanine nucleotide regulatory protein and polypho phoinositide metabolism. *J. Leuk. Biol. 40:785.*
21. **Verghese, M. W., L. Charles, L. Jakoi, S. B. Dillon, and R. Snyderman.** 1987. Role of a guanine nucleotide regulatory protein in the activation of phospholipase C by different chemoattractants. *J. Immunol. 138:4374.*
22. **Naccache, P. H., M. M. Molski, M. Volpi, E. L. Becker, and R. I. Sha'afi.** 1985. Unique inhibitory profile of platelet activating factor induced calcium mobilization, polyphosphoinositide turnover and granule enzyme secretion in rabbit neutrophils towards pertussis toxin and phorbol ester. *Biochem. Biophys. Res. Commun. 130:677.*
23. **Naccache, P. H., M. M. Molski, M. Volpi, J. Shefc, x, T. F. P. Molski,**

L. Loew, E. L. Becker, and R. I. Sha'afi. 1986. Biochemical events associated with the stimulation of rabbit neutrophils by platelet-activating factor. *J. Leuk. Biol. 40:533.*

24. Gennaro, R., T. Pozzan, and D. Romeo. 1984. Monitoring of cytosolic free $^{45}Ca^{++}$ in C5a-stimulated neutrophils: Loss of receptor-modulated $^{45}Ca^{++}$ stores and $^{45}Ca^{++}$ uptake in granule-free cytoplasts. *Proc. Natl. Acad. Sci. USA 81:1416.*
25. Agarwal, S., M. A. Reynolds, L. D. Duckett, and J. B. Suzuki. 1989. Altered free cytosolic calcium changes and neutrophil chemotaxis in patients with juvenile periodontitis. *J. Periodont. Res. 24:149.*
26. Hwang, S-B., and M-H. Lam. 1986. Species difference in the specific receptors of platelet activating factor. *Biochem. Pharmacol. 35:4511.*
27. Stewart, A. G., and G. J. Dusting. 1988. Characterization of receptors for platelet-activating factor on platelets, polymorphonuclear leukocytes and macrophages. *Br. J. Pharmacol. 94:1225.*
28. Kroegel, C., T. Yukawa, J. Westwick, and P. J. Barnes. 1989. Evidence for two platelet activating factor receptors on eosinophils: Dissociation between PAF-induced intracellular calcium mobilization, degranulation and superoxide anion generation in eosinophils. *Biochem. Biophys. Res. Commun. 162:511.*
29. Bussolino, F., M. Aglietta, R. Sanavio, A. Stacchini, D. Lauri, and G. Camussi. 1985. Alkyl-ether phosphoglycerides influence calcium fluxes into human endothelial cells. *J. Immunol. 135:2748.*
30. Doyle, V. M., J. A. Creba, and U. T. Ruegg. 1986. Platelet activating factor mobilizes intracellular calcium in vascular smooth muscle cells. *FEBS Lett. 197:13.*
31. Johnson, R. J., and D. E. Chenoweth. 1985. Labeling the granulocyte C5a receptor with a unique photoreactive probe. *J. Biol. Chem. 260:7161.*
32. Rollins, T. E., and M. S. Springer. 1985. Identification of the polymorphonuclear leukocyte C5a receptor. *J. Biol. Chem. 260:7157.*
33. Barker, M. D., P. J. Jose, T. J. Williams, and D. R. Burton. 1986. The chemoattractant des-Arg^{74}-C5a regulates the expression of its own receptor on a monocyte-like cell line. *Biochem. J. 236:621.*
34. Gerard, N. P., M. K. Hodges, J. M. Drazen, P. F. Weller, and C. Gerard. 1989. Characterization of a receptor for C5a anaphylatoxin on human eosinophils. *J. Biol. Chem. 264:1760.*
35. Rollins, T. E., S. Siciliano, and M. S. Springer. 1988. Solubilization of the functional C5a receptor from human polymorphonuclear leukocytes. *J. Biol. Chem. 263:520.*
36. Gurdon, J. B., C. D. Lane, H. R. Woodland, and G. Marbaix. 1971. Use of frog eggs and oocytes for the study of messenger RNA and its translation in living cells. *Nature 233:177.*
37. Colman, A. 1984. Translation of eukaryotic messenger RNA in *Xenopus* oocytes. In *Transcription and Translation—A Practical Approach*. B. D. Hames and S. J. Higgins, eds. IRL Press Ltd., Oxford, p. 271.
38. Kubo, T., K. Fukuda, A. Mikami, A. Maeda, H. Takahashi, M. Mishina, T. Haga, K. Haga, A. Ichiyama, K. Kangawa, M. Kojima, H. Matsuo, T. Hirose, and S. Numa. 1986. Cloning, sequencing and expression of complementary DNA encoding the muscarinic acetylcholine receptor. *Nature 323:411.*
39. Williams, J. A., D. J. McChesney, M. C. Calayag, V. R. Lingappa, and C. D. Logsdon. 1988. Expression of receptors for cholecystokinin and other Ca^{2+}-mobilizing hormones in *Xenopus* oocytes. *Proc Natl. Acad. Sci. USA 85:4939.*
40. Oron, Y., B. Gillo, R. E. Straub, and M. C. Gershengorn. 1987. Mechanism of membrane electrical responses to thyrotropin-releasing hormone in *Xenopus* oocytes injected with pituitary cell messenger ribonucleic acid. *Mol. Endocrinol. 1:918.*
41. Masu, Y., K. Nakayama, H. Tamaki, Y. Harada, M. Kuno, and S. Nakanishi. 1987. cDNA cloning of bovine substance-K receptor through oocyte expression system. *Nature 329:836.*
42. Julius, D., A. B. MacDermott, R. Axel, and T. M. Jessell. 1988. Molecular characterization of a functional cDNA encoding the serotonin 1c receptor. *Science 241:558.*
43. Malech, H. L., J. P. Gardner, D. F. Heiman, and S. A. Rosenzweig. 1985. Asparagine-linked oligosaccharides on formyl peptide chemotactic receptors of human phagocytic cells. *J. Biol. Chem. 260:2509.*
44. Davis, L. G., M. D. Dibner, and J. F. Battey. 1986. *Basic Methods in Molecular Biology*. Elsevier, Amsterdam, p. 129.
45. Feinberg, A. P., and B. Vogelstein. 1983. A technique for radiolabeling DNA restriction endonuclease fragments to high specific activity. *Anal. Biochem. 132:6.*
46. Murphy, P. M., and H. L. Malech. 1990. Nucleotide sequence of a cDNA encoding a protein with primary structural similarity to G-protein coupled receptors. *Nucleic Acids Res. 18:1896.*
47. Royer-Pokora, B., L. M. Kunkel, A. P. Monaco, S. C. Goff, P. E. Newburger, R. L. Baehner, F. S. Cole, J. T. Curnutte, and S. H. Orkin. 1986. Cloning the gene for an inherited human disorder—chronic granulomatous disease—on the basis of its chromosomal location. *Nature 322:32.*
48. Dumont, J. N. 1972. Oogenesis in *Xenopus laevis* (Daudin). Stages of oocyte development in laboratory maintained animals. *J. Morphol. 136:153.*
49. Harris, P., and P. Ralph. 1985. Human leukemic models of myelomonocytic development: A review of the HL-60 and U937 cell lines. *J. Leuk. Biol. 37:407.*
50. Dascal, N., E. M. Landau, and Y. Lass. 1984. *Xenopus* oocyte resting potential, muscarinic responses and the role of calcium and guanosine 3',5'-cyclic monophosphate. *J. Physiol. 352:551.*
51. Kusando, K., R. Miledi, and J. Stinnakre. 1982. Cholinergic and catecholaminergic receptors in the *Xenopus* oocyte membrane. *J. Physiol. 328:143.*
52. Murphy, P. M., E. K. Gallin, H. L. Tiffany, and H. L. Malech. 1990. The formyl peptide chemoattractant receptor is encoded by a 2 kilobase messenger RNA: expression in *Xenopus* oocytes. *FEBS Lett. 261:353.*
53. Lad, P. M., C. V. Olson, I. S. Grewal, S. J. Scott, D. B. Learn, P. A. Smiley, and M. Lafrance-Fiolich. 1987. Molecular mechanisms in the action of platelet activating factor and other mediators of inflammation. In *New Horizons in Platelet Activating Factor Research*. C. M. Winslow and J. L. Lee, eds. John Wiley and Sons, New York, p. 103.
54. Mishina, M., T. Kurosaki, T. Tobimatsu, Y. Morimoto, M. Noda, T. Yamamoto, M. Terao, J. Lindstrom, T. Takahashi, M. Kuno, and S. Numa. 1984. Expression of functional acetylcholine receptor from cloned cDNAs. *Nature 322:826.*
55. Polakis, P. G., R. J. Uhing, and R. Snyderman. 1988. The formyl-peptide chemoattractant receptor copurifies with a GTP-binding protein containing a distinct 40-kDa pertussis toxin substrate. *J. Biol. Chem 263:4969.*
56. Mates, D. F., D. R. Manning, B. B. Wolfe, and G. R. Luthin. 1989. Pharmacological and biochemical characterization of complexes of muscarinic acetylcholine receptor and guanine nucleotide-binding protein. *J. Biol. Chem. 264:21638.*
57. Kobilka, B. K., T. Frielle, S. Collins, T. Yang-Feng, T. S. Kobilka, U. Francke, R. J. Lefkowitz, and M. G. Caron. 1987. An intronless gene encoding a potential member of the family of receptors coupled to guanine nucleotide regulatory proteins. *Nature 329:75.*
58. Serhan, C. N., J. Fridovich, E. J. Goetzl, P. B. Dunham, and G. Weissmann. 1982. Leukotriene B_4 and phosphatidic acid are calcium ionophores. Studies employing arsenazo III in liposomes. *J. Biol. Chem. 257:4746.*

Role of Cytokines (Interleukin 1, Tumor Necrosis Factor, and Transforming Growth Factor β) in Natural and Lipopolysaccharide-enhanced Radioresistance

By R. Neta,* J. J. Oppenheim,‡ R. D. Schreiber,§ R. Chizzonite,‖ G. D. Ledney,* and T. J. MacVittie*

*From the *Department of Experimental Hematology, Armed Forces Radiobiology Research Institute, Bethesda, Maryland 20814; the ‡Laboratory of Molecular Immunoregulation, Biological Response Modifier Program, National Cancer Institute, Frederick, Maryland 21701; the §Department of Pathology, Washington University School of Medicine, St. Louis, Missouri, 63110; and the ‖Department of Molecular Genetics, Roche Research Center, Hoffmann-La Roche Inc., Nutley, New Jersey 07110*

Summary

Studies of radioresistance and radioprotection provide an excellent in vivo model for dissection of the pathophysiological role of cytokines. The availability of neutralizing antibodies to cytokines has made it possible to assess the contribution of cytokines to host defense and repair processes involved in radioresistance and radioprotection. Administration of anti-interleukin 1 receptor (IL-1R) antibody (35F5) or anti-tumor necrosis factor (TNF) antibody (TN3 19.12) reduced survival of irradiated CD2F1 mice. These results demonstrate conclusively that natural levels of IL-1 and TNF contribute to radioresistance of normal mice. Furthermore, the radioprotective effect of administered IL-1 was blocked not only with anti-IL-1R antibody but also with anti-TNF antibody. Similarly, the radioprotective effect of TNF was reduced with anti-IL-1R antibody. These data suggest that cooperative interaction of both cytokines is necessary to achieve successful radioprotection. Finally, when LPS was used as a radioprotector, the combined administration of anti-IL-1R and anti-TNF not only blocked the radioprotection with LPS, but actually revealed LPS to have a radiosensitizing effect. This effect may be due to induction of TGF-β, since administration of this cytokine results in reduced survival of irradiated mice.

The lethal effects of whole-body exposure to ionizing radiation are due primarily to the destruction of hematopoietic components and subsequent failure of hematopoietic renewal (1, 2). The use of immunostimulatory/inflammatory agents such as LPS before irradiation was shown more than 30 years ago to promote survival from otherwise lethal doses of radiation with subsequent recovery of the hematopoietic system (3, 4). It is now known that many of the pathophysiological in vivo effects of LPS are mediated through the induction of a battery of cytokines, including IL-1 and TNF. We, therefore, hypothesized and established that these two cytokines can confer radioprotection (5, 6). The combined administration of the two cytokines had a synergistic radioprotective effect and was more effective than administration of an optimal dose of LPS (6).

In addition to induction by LPS, IL-1 and TNF are known to be produced in response to stress, infectious agents, and a variety of inflammatory stimuli (7, 8). Most recently, IL-1 and TNF production was shown to be induced after exposure to ionizing radiation (9, 10).

These observations led us to ask several questions. First, do endogenously produced IL-1 and TNF contribute to the enhanced radioresistance of normal mice? Second, do IL-1 and TNF act independently or cooperate in radioprotection? And third, do IL-1 and TNF account for the entire radioprotective effect of LPS? The results reported here provide evidence that IL-1 and TNF are essential for natural as well as for immunomodulator-enhanced radioresistance.

Materials and Methods

Mice. CD2F1 male and C3H/HeN female mice were purchased from the Animal Genetics and Production Branch, National Cancer Institute (Frederick, MD). C3H/HeJ female mice were obtained from The Jackson Laboratory (Bar Harbor, ME). Mice were handled as previously described (6).

Cytokines. Recombinant human IL-1α (rhIL-1α)[1] (117-271 Ro 24-5008; lot IL-1 2/88; sp act 3 × 10^8 U/mg) was kindly provided by Dr. Peter Lomedico, Hoffmann-La Roche Inc. (Nutley, NJ). Recombinant human TNF-α (rhTNF-α) (lot CP4026P08 in PBS; sp act 9.6 × 10^6 U/mg protein) was obtained from Biogen (Cambridge, MA), and recombinant murine TNF-α (rmTNF-α) (lot 4296-17; sp act 2 × 10^8 U/mg, as assayed on L929 cells in our laboratory) was kindly provided by Genentech (San Francisco, CA). TGF-β (lot 8987-53) was kindly provided by Dr. Palladino of Genentech. LPS (protein-free prepared from *Escherichia coli* K235 by the phenol-water extraction method) was kindly provided by Dr. Stefanie Vogel of Uniformed Services University for the Health Sciences (Bethesda, MD).

Antibodies. Anti-IL-1R antibody, mAb 35F5, was raised in rats against cloned IL-1R isolated from EL 4 cells as previously described (11). Anti-murine TNF antibody, mAb TN3.19.12, was raised in Armenian hamsters against murine TNF-α as previously described (12). Rat Ig (Sigma Chemical Co., St. Louis, MO) was used as a control for 35F5 antibody. As controls for TN3.19.12, anti-murine IFN-γ antibody (H22, an antibody raised in hamsters against murine IFN-γ) or hamster IgG (L2.3D9 raised in Armenian hamster against human IL-2, as described [12]) were used.

The antibodies and recombinant cytokines were diluted in pyrogen-free saline on the day of injection. The antibodies were given intraperitoneally 6–20 h before intraperitoneal injection of the cytokines.

Irradiation. Mice were randomized, placed in Plexiglass containers, and were given whole-body irradiation at 40 cGy/min by bilaterally positioned ^{60}Co elements. The number of surviving mice was recorded daily for 30 d.

Statistical Analysis. Statistical evaluation of the results was carried out using χ^2 analysis and Cox Mantel test.

Results

The Role of IL-1 and TNF in Natural Radioresistance. To test whether endogenously produced IL-1 and TNF contribute to the natural radioresistance of normal mice, mice were treated with anti-IL-1R antibody, which blocks the activities of both IL-1α and IL-1β (11), or with anti-TNF antibody (12). Administration of anti-IL-1R antibody (35F5) or anti-TNF antibody (TN3 19.12) to $LD_{40/30}$ irradiated mice reduced their survival (Fig. 1). The apparent radiosensitizing effect observed in normal mice given either antibody 20 h before irradiation was equal to that observed in mice given the antibody 1 h after irradiation. Thus, these antibodies exacerbate radiation damage by blocking the beneficial effects of cytokines even when produced after the completion of radiation exposure.

Do IL-1 and TNF Act Independently or Cooperate in Radioprotection? IL-1 and TNF are well documented to induce one another in vitro (13–16). We examined the interdependence of IL-1 and TNF in radioprotection by testing the effect of neutralization of TNF in IL-1-injected mice and receptor blockage of IL-1 in TNF-injected mice (Fig. 2). Anti-IL-1R antibody, given to mice before TNF administration, reduced the proportion of TNF-radioprotected mice from 60% to 15%. Similarly, anti-TNF antibody reduced IL-1-induced radioprotection from 88% to 40%. These in vivo results show

[1] *Abbreviations used in this paper.* rh, recombinant human, rm, recombinant murine.

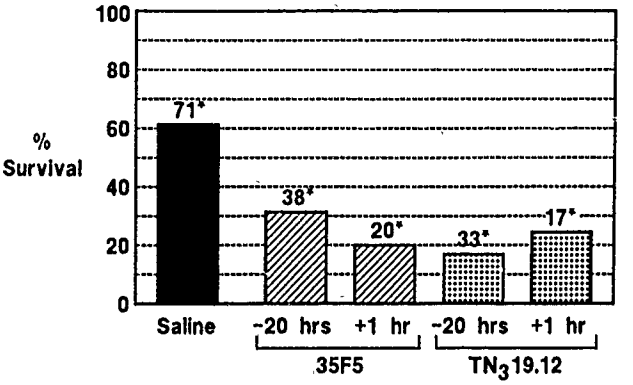

Figure 1. Radiosensitizing effect of anti-IL-1R antibody (35F5) and anti-TNF antibody (TN3 19.12.). CD2F1 male mice 8–10 wk old received intraperitoneal injections of 100 μg 35F5, 20 h before or 1 h after irradiation with 825 cGy ^{60}Co. TN3 19.12 antibody was given at 100 μg 20 h before irradiation or at 50 μg 1 h after irradiation. Groups of control mice were given 100 μg of rat IgG, 100 μg anti-murine IFN-γ, or 100 μg of hamster IgG, or vehicle-saline injection of 0.5 ml per mouse. The survival of mice given 825 cGy was recorded daily for 30 days. The survival time of control mice receiving anti-IFN-γ, rat IgG, or hamster IgG did not differ from mice given saline injections (at 66, 50, and 68%, respectively; not shown in the figure). The survival of mice receiving 35F5 or TN3 19.12 before or after irradiation was significantly different from that of control mice ($p < 0.01$). (*) The number of mice used in the experiments.

that TNF contributes to optimal radioprotection with IL-1, and that IL-1 participates in radioprotection with TNF.

Do IL-1 and TNF Account for the Entire Radioprotective Effect of LPS? The relative contribution of IL-1 and TNF in LPS-

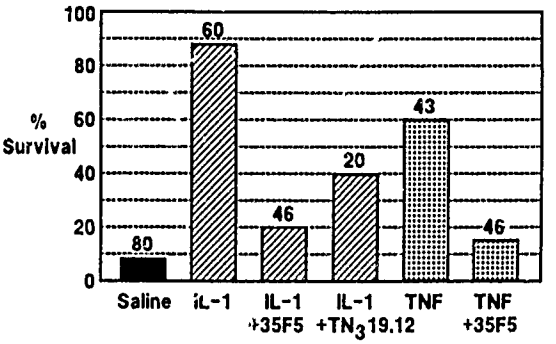

Figure 2. Anti-IL-1R antibody (35F5) reduces TNF-induced radioprotection, and anti-TNF antibody (TN3 19.12) reduces IL-1-induced radioprotection. CD2F1 mice received intraperitoneally 100 μg of 35F5 or 200 μg of TN3 19.12. Groups of control mice received injections of equivalent amounts of rat IgG or hamster IgG (L2.3D9) or saline injections. 20 h later, groups of mice received either 300 ng rhIL-1, 5 μg of rhTNF-α, or 1 μg of rmTNFα. After an additional 20 h, mice received 950 cGy of ^{60}Co radiation. The survival time was recorded for 30 d. The survival of mice receiving rhTNF or rmTNF was similar and the groups were therefore combined. Control mice receiving rat IgG or hamster IgG and IL-1 did not differ significantly in survival from IL-1 only-treated mice (at 80 and 95%, respectively). 65% of mice given hamster IgG before TNF survived. The numbers at the top of the bars indicate the total number of mice used in eight experiments. The survival of mice receiving 35F5 and IL-1 or TN3 19.12 and IL-1 differed significantly ($p < 0.01$) from survival of mice receiving IL-1 alone. Similarly, the survival of mice receiving 35F5 and TNF differed significantly ($p < 0.01$) from that of mice receiving TNF alone.

induced radioprotection was investigated using neutralizing antibodies. Anti-IL-1R antibody given to mice before LPS and lethal irradiation reduced survival from 74% to 20% (Table 1). Similarly, anti-TNF antibody given before LPS reduced survival to 30%. Combined administration of these antibodies completely abolished the radioprotective effect of LPS, demonstrating that this effect is due entirely to the combined effect of IL-1 and TNF. Furthermore, administration of both antibodies actually led to a reduced survival time of LPS-treated mice to less than that of nontreated mice (Figure 3). Thus, inhibition of IL-1- and TNF-mediated effects of LPS revealed LPS to have latent radiosensitizing capabilities.

The Effect of TGF-β on Survival of Irradiated Mice. Based on the above observations, we asked whether some of the cytokines induced by LPS may contribute to increased radiation lethality. LPS induces secretion of TGF-β from human blood monocytes (17). We tested the radiosensitizing effect of TGF-β because of its previously observed activity of inhibiting proliferation of early bone marrow progenitor cells, and of inhibiting many of the biologic effects of IL-1 and TNF (18–22). Indeed, TGF-β given to mice either before or after lethal irradiation resulted in a dose-dependent reduction in survival (Fig. 4).

TGF-β was also radiosensitizing for C3H/HeJ and C3H/HeN mice. 85% (17/20) of control C3H/HeN mice survived 725 cGy radiation, whereas only 10% (1/10) of mice given 10 μg TGF-β 16 h before, and 15% (3/20) given TGF-β 1 h after irradiation, survived. Similarly, none of the C3H/HeJ mice given 10 μg TGF-β 1 h after irradiation with an $LD_{50/30}$ survived. Thus, the sensitizing effect of TGF-β to radiation lethality is not restricted to a particular mouse strain. Combined administration of IL-1 and TGF-β, however, did not result in any reduction of the radioprotective effect of IL-1 (results not shown), indicating that the presence of IL-1 masks the radiosensitizing effects of TGF-β.

Table 1. *Effect of Anti-IL-1 Antibody and Anti-TNF Antibody on LPS-induced Radioprotection*

Group	Treatment		Dead/ total	Percent survival
	LPS	Antibody		
1	–	Saline	56/59	5
2	+	Saline	16/61	74
3	+	Rat IgG	12/36	67
4	+	Hamster IgG	3/18	83
5	+	Anti-IL-1R	24/30	20
6	+	Anti-TNF	14/20	30
7	+	Anti-IL-1R – anti-TNF	20/20	0

CD2F1 mice received intraperitoneally 200 μg anti-IL-1R, 200 μg anti-TNF, or both. Groups of control mice received 200 μg hamster IgG, rat IgG, or saline injections. 20 h later, mice received 1 μg *E. Coli* LPS intraperitoneally, and 1 d later were given 950 cGy gamma radiation. The survival time was recorded for 30 d. The survival of mice in groups 5 and 6 was significantly reduced ($p < 0.01$) compared with survival of mice in groups 2, 3, and 4. There was no significant difference in the survival of groups 2, 3, and 4.

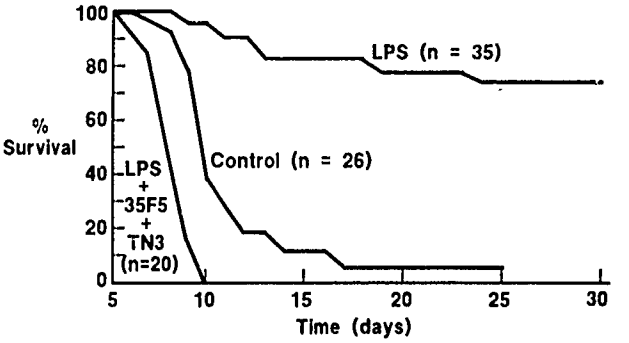

Figure 3. Effect of anti-IL-1R antibody and anti-TNF antibody on LPS-induced radioprotection. Groups of mice received treatment as described in Table 1. The daily record of survival of mice given a combination of 200 μg of 35F5 and 200 μg of TN3 19.12 antibody and LPS, LPS alone, or saline control and 950 cGy irradiation is presented. The mean survival time of LPS- and antibody-treated mice was significantly reduced as compared with the control mice ($p < 0.001$ using Cox Mantel test).

Discussion

Cytokines have been shown to have so many complex effects that it has become virtually impossible to predict their relevant role from the in vitro models. Consequently, it is more imperative than ever to evaluate their pathophysiological role in vivo. Studies of the role of cytokines in counteracting the lethal effects of radiation provide a useful model for evaluating the in vivo role of these cytokines in promoting the restoration of hematopoiesis and consequent enhancement of host resistance to infections. Our results showing that greater number of mice receiving anti-IL-1R antibody or anti-TNF antibody die after exposure to ionizing radiation indicate that endogenously produced IL-1 and TNF play an important role in the host's ability to recover from lethal radiation. The specificity of anti-IL-1R antibody was previously demonstrated

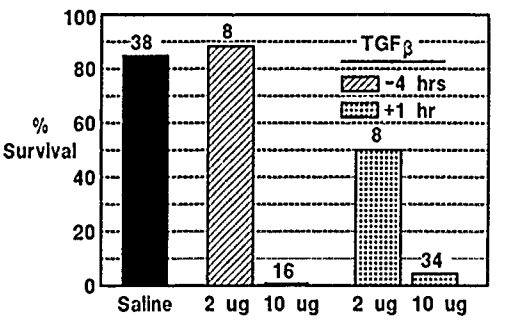

Figure 4. Radiosensitizing effect of TGF-β. CD2F1 mice received intraperitoneal injections of rhTGF β at times before and after irradiation in quantities as indicated, or saline injection. The results are a summary of three experiments. The survival of mice receiving 10 μg TGF-β before or after irradiation differ significantly ($p < 0.001$) from that of saline-treated mice.

since passive immunization of mice with 35F5 antibody reduced IL-1-induced radioprotection, and also reduced IL-1-induced serum levels of IL-6, CSF, and serum amyloid P (23, 24). Similarly, administration of anti-TNF antibody, TN3-19.12, to mice subsequently treated with LPS specifically prevented the appearance of TNF in the circulation (12). Serum levels of 35F5 and TN3 19.12 were previously shown to plateau within 6–8 h and to remain elevated for 2–7 d after injection (11, 12). Thus, the data showing that administration of antibody after irradiation has an effect similar to antibody given before irradiation suggest that radiation-induced IL-1 and TNF confer radioresistance by promoting repair and restoring host defenses after lethal radiation damage. This effect of endogenously produced IL-1 and TNF is augmented by administration of an exogenous supply of these cytokines, as previously observed (5, 6, 25).

Our observation that anti-IL-1R antibody largely blocks TNF-induced radioprotection whereas anti-TNF antibody partially blocks IL-1-induced radioprotection suggests that mutual induction of IL-1 by TNF and TNF by IL-1 occurs in vivo as well as in vitro (13–16), and their subsequent interaction is necessary to achieve optimal radioprotection. This is in agreement with a report by Dinarello et al. (26) demonstrating that the second pyrogenic phase induced by supernatants from TNF-stimulated mononuclear cells could be neutralized by anti-IL-1 antibody. We have also observed that the levels of CSF induced in circulation after challenge with IL-1 can be reduced by anti-TNF antibody, whereas TNF-induced CSF is reduced by anti-IL-1R antibody (Neta et al., unpublished results). Consequently, mutual induction of TNF and IL-1 may be required not only for achieving in vivo radioprotection, but also for other in vivo effects. The generally observed overlapping activities of IL-1 and TNF (27, 28) may reflect a cellular requirement for triggering by both signals, and administration of either IL-1 or TNF alone would result in the production of the necessary second signal; thus accounting for their apparent ability to act by themselves.

LPS is known to induce a battery of cytokines, including IL-1, TNF, CSF, IL-6, IL-8, IFN, and TGF-β (29–33). We have previously shown that granulocyte CSF, granulocyte/macrophage CSF, and IL-6, when administered together with suboptimal doses of IL-1, synergize in radioprotection (6, 36). However, the present results indicate that neutralization of TNF and IL-1 not only completely blocks the radioprotective effect of LPS but also unexpectedly reveals LPS to have radiosensitizing properties. Since administration of TGF-β results in greatly enhanced mortality of irradiated mice, and LPS is a known inducer of TGF-β, we assume that in the absence of IL-1 and TNF, other LPS-induced cytokines, IL-6, granulocyte CSF, or granulocyte/macrophage CSF, cannot prevent radiation induced lethality. The finding that when given with IL-1, TGF-β does not reduce IL-1-induced radioprotection, provides further support that IL-1 is critical for radioprotection. Whether the enhanced lethality observed due to TGF-β is the direct result of: (*a*) inhibiting proliferation of early progenitor cells; (*b*) impairment of IL-1 and TNF synthesis, as previously shown (34); or (*c*) reduction of IL-1R expression (35) remains to be established. It is possible that other cytokines induced with LPS, in addition to TGF-β, may also contribute to radiosensitization. Indeed, we have previously shown that IL-6 given alone before irradiation acts also as a radiosensitizer (36).

In conclusion, the present results provide the first demonstration that: (*a*) the endogenously produced cytokines, IL-1 and TNF, contribute to natural radioresistance; (*b*) IL-1 and TNF, even when given separately, interact with one another to produce radioprotection; (*c*) radioprotection with LPS depends on induction of IL-1 and TNF, since blocking the activities of these two cytokines completely abolishes the radioprotective effect of LPS; (*d*) in the absence of IL-1 and TNF, LPS exerts a radiosensitizing effect; and (*e*) TGF-β renders mice more sensitive to radiation. Thus, LPS induces a mixture of radioprotective and radiosensitizing cytokines. These cytokines also mediate the immunomodulating effects of LPS. Consequently, therapeutic use of selected cytokines may be preferable to the use of exogenous immunomodulators such as LPS, which induce mixtures of cytokines capable of counteracting each other's effects.

We thank Mr. Marshall Pilcher for technical assistance and Drs. John Ainsworth, Ira Green, Scott Durum, and Gideon Strassman for critical review of this manuscript.

This work was supported by the Armed Forces Radiobiology Research Institute, Defense Nuclear Agency, under work unit 00129. Views presented in this paper are those of the authors; no endorsement by the Defense Nuclear Agency or the Department of Defense has been given or should be inferred. Research was conducted according to the principles enunciated in the Guide for the Care and Use of Laboratory Animals, prepared by the Institute of Laboratory Animal Resources, National Research Council.

Address correspondence to Ruth Neta, Department of Experimental Hematology, Armed Forces Radiobiology Research Institute, Bethesda, MD 20814.

Received for publication 19 November 1990 and in revised form 11 February 1991.

References

1. Bond, V.P., T.M. Fliedner, and J.O. Archambeau. 1965. Mammalian Radiation Lethality. A Disturbance in Cellular Kinetics. Academic Press, New York. 340 pp.
2. Van Bekkum, D.W. 1969. Bone marrow transplantation and partial body shielding for estimating cell survival and repopulation. *In* Comparative Cellular and Species Radiosensitivity. V.P. Bond and T. Sugahara, editors. Igaku-Shoin Ltd., Tokyo. 175–192.
3. Ainsworth, E.J., and H.B. Chase. 1959. Effect of microbial antigens on irradiation mortality in mice. *Proc. Natl. Exp. Biol. Med.* 102:483.
4. Smith, W.W., I.M. Alderman, and R.I. Gillespie. 1957. Increased survival in irradiated animals treated with bacterial endotoxins. *Am. J. Physiol.* 191:124.
5. Neta, R., S.D. Douches, and J.J. Oppenheim. 1986. Interleukin-1 is a radioprotector. *J. Immunol.* 136:2483.
6. Neta, R., J.J. Oppenheim, and S.D. Douches. 1988. Interdependence of the radioprotective effects of human recombinant IL-1, TNF, G-CSF, and murine recombinant G-CSF. *J. Immunol.* 140:108.
7. Dinarello, C.A. 1989. Interleukin-1 and its biologically related cytokines. *Adv. Immunol.* 44:153.
8. Durum, S., J.J. Oppenheim, and R. Neta. 1990. Immunophysiological role of interleukin-1. *In* Immunophysiology: Role of Cells and Cytokines in Immunity and Inflammation. J.J. Oppenheim and E. Shevach, editors. Oxford University Press, Oxford. 210–225.
9. Hallahan, D.E., D.R. Spriggs, M.A. Beckett, D.W. Kufe, and R.R. Weichselbaum. 1989. Increased tumor necrosis factor α mRNA after cellular exposure to ionizing radiation. *Proc. Natl. Acad. Sci. USA.* 86:10104.
10. Woloschak, G.E., C.-M. Chang-Liu, P.S. Jones, and C.A. Jones. 1990. Modulation of gene expression in syrian hamster embryo cells following ionizing radiation. *Cancer Res.* 50:339.
11. Chizzonite, R., T. Truitt, P.L. Kilian, A.S. Stern, P. Nunes, K.P. Parker, K.L. Kaffka, A.O. Chua, D.K. Lugg, and U. Gubler. 1989. Two high-affinity interleukin-1 receptors represent separate gene products. *Proc. Natl. Acad. Sci. USA.* 86:8029.
12. Sheehan, K.C.F., N.H. Ruddle, and R.D. Schreiber. 1989. Generation of hamster monoclonal antibodies that neutralize tumor necrosis factors. *J. Immunol.* 142:3884.
13. Bachwich, P.R., S.W. Chensue, J.W. Larrick, and S.L. Kunkel. 1986. Tumor necrosis factor stimulates interleukin-1 and prostaglandin E_2 production in resting macrophages. *Biochem. Biophys. Res. Commun.* 136:94.
14. Le, J., D. Weinstein, U. Gubler, and J. Vilcek. 1987. Induction of membrane associated interleukin 1 by tumor necrosis factor in human fibroblasts. *J. Immunol.* 138:2137.
15. Nawroth, P.P., I. Bank, D. Handley, J. Cassimeris, L. Chess, and D. Stern. 1986. Tumor necrosis factor/cachectin interacts with endothelial cell receptors to induce release of interleukin 1. *J. Exp. Med.* 163:1363.
16. Phillip, R., and L.B. Epstein. 1986. Tumor necrosis factor as immunomodulator and mediator of monocyte cytotoxicity induced by itself, γ-interferon, and interleukin 1. *Nature (Lond.).* 323:86.
17. Assoian, R.K., B.E. Fleurdelys, H.C. Stevenson, P.J. Miller, D.K. Madtes, E.W. Raines, R. Ross, and M.B. Sporn. 1987. Expression and secretion of type b transforming growth factor by activated human macrophages. *Proc. Natl. Acad. Sci. USA* 84:6020.
18. Espevik, T., I.S. Figari, M.R. Shalaby, G.A. Lackides, G.D. Lewis, H.M. Shepard, and M.A. Palladino. 1987. Inhibition of cytokine production by cyclosporin A and transforming growth factor β. *J. Exp. Med.* 166:571.
19. Ellingsworth, L.R., D. Nakayama, P. Segarini, J. Dasch, P. Carillo, and W. Waegell. 1988. Transforming growth factor-βs are equipotent growth inhibitors of interleukin-1-induced thymocyte proliferation. *Cell. Immunol.* 114:41.
20. Wahl, S.M., D.A. Hunt, H.L. Wong, S. Dougherty, N. McCartney-Francis, L.M. Wahl, L. Ellingsworth, J.A. Schmidt, G. Hall, A.B. Roberts, and M.B. Sporn. 1988. Transforming growth factor-β is a potent immunosuppressive agent that inhibits IL-1-dependent lymphocyte proliferation. *J. Immunol.* 140:3026.
21. Keller, J.R., C. Mantel, G.K. Sing, L.R. Ellingsworth, S.R. Ruscetti, and F.W. Ruscetti. 1988. Transforming growth factor β1 selectively regulates early hematopoietic progenitors and inhibits the growth of interleukin 3-dependent myeloid leukemia cell lines. *J. Exp. Med.* 168:737.
22. Keller, J.R., I.K. Mcniece, L.R. Ellingsworth, P.J. Quesenberry, G.K. Sing, and F.W. Ruscetti. 1991. Transforming growth factor β directly regulates primitive murine hematopoietic cell proliferation. *Blood.* 75:596.
23. Gershenwald, J.E., Y. Fong, and T.J. Fahey. 1990. Interleukin 1 receptor blockade attenuates the host inflammatory response. *Proc. Natl. Acad. Sci. USA.* 87:4966.
24. Neta, R., S.N. Vogel, J.M. Plocinski, N.S. Tare, W. Benjamin, R. Chizzonite, and M. Pilcher. 1990. In vivo modulation with anti-interleukin 1 (IL 1) receptor (p80) antibody 35F5 of the response to IL 1. The relationship of radioprotection, colony stimulating factor, and IL 6. *Blood.* 76:57.
25. Neta, R., and J.J. Oppenheim. 1988. Cytokines in therapy of radiation injury. *Blood.* 72:1093.
26. Dinarello, C.A., J.G. Cannon, S.M. Wolff, H.A. Berheim, B. Beutler, A. Cerami, I.S. Figari, M.A. Palladino, Jr., and J.V. O'Connor. 1986. Tumor necrosis factor (cachectin) is an endogenous pyrogen and induces production of interleukin 1. *J. Exp. Med.* 163:1433.
27. Le, J., and J. Vilcek. 1987. TNF and IL 1: cytokines with multiple overlapping biological activities. *Lab. Invest.* 56:234.
28. Neta, R., T. Sayers, and J.J. Oppenheim. 1991. Relationship of tumor necrosis factor to interleukins. *In* Tumor Necrosis Factor. J. Vilcek and B.B. Aggarwal, editors. Marcel Dekker, Inc., New York. In press.
29. Carswell, E.A., L.J. Old, and R.L. Kassel. 1975. An endotoxin induced serum factor that causes necrosis of tumors. *Proc. Natl. Acad. Sci. USA.* 72:3666.
30. Beutler, B., I.W. Milsark, and A.C. Cerami. 1985. Cachectin/tumor necrosis factor: production, distribution, and metabolic fate in vivo. *J. Immunol.* 135:2972.
31. Metcalf, D. 1971. Acute antigen-induced elevation of serum colony stimulating factor (CSF) levels. *Immunology.* 21:427.
32. Youngner, J.S., and W.R. Stinebring. 1965. Interferon appearance stimulated by endotoxin, bacteria, or viruses in mice pretreated with Escherischia coli endotoxin or infected with Mycobacterium tuberculosis. *Nature (Lond.).* 208:456.
33. Vogel, S.N., and M.M. Hogan. 1990. Role of cytokines in endotoxin-mediated host responses. *In* Immunophysiology, Role of Cells and Cytokines in Immunity and Inflammation. J.J. Oppenheim and E.N. Shevach, editors Oxford University Press, Oxford. 238–258.

34. Chantry, D., M. Turner, E. Abney, and M. Feldmann. 1989. Modulation of cytokine production by transforming growth factor β. *J. Immunol.* 142:4295.
35. Dubois, C.M., F.W. Ruscetti, E.W. Palaszynski, L.A. Falk, J.J. Oppenheim, and J.R. Keller. 1990. Transforming growth factor β is a potent inhibitor of interleukin 1 (IL-1) receptor expression. Proposed mechanism of inhibition of IL-1 action. *J. Exp. Med.* 172:737.
36. Neta, R., S.N. Vogel, J.D. Sipe, G.G. Wong, and R.P. Nordan. 1988. Comparison of in vivo effects of human recombinant IL 1 and human recombinant IL 6 in mice. *Lymphokine Res.* 7:403.

Administration of Interleukin-6 Stimulates Multilineage Hematopoiesis and Accelerates Recovery From Radiation-Induced Hematopoietic Depression

By M.L. Patchen, T.J. MacVittie, J.L. Williams, G.N. Schwartz, and L.M. Souza

Hematopoietic depression and subsequent susceptibility to potentially lethal opportunistic infections are well-documented phenomena following radiotherapy. Methods to therapeutically mitigate radiation-induced myelosuppression could offer great clinical value. In vivo studies in our laboratory have demonstrated that interleukin-6 (IL-6) stimulates pluripotent hematopoietic stem cell (CFU-s), granulocyte-macrophage progenitor cell (GM-CFC), and erythroid progenitor cell (CFU-e) proliferation in normal mice. Based on these results, the ability of IL-6 to stimulate hematopoietic regeneration following radiation-induced hematopoietic injury was also evaluated. C3H/HeN female mice were exposed to 6.5 Gy ^{60}Co radiation and subcutaneously administered either saline or IL-6 (1,000 μg/kg) on days 1 through 3 or 1 through 6 postexposure. On days 7, 10, 14, 17, and 22, femoral and splenic CFU-s, GM-CFC, and CFU-e contents and peripheral blood white cell, red cell, and platelet counts were determined. Compared with saline treatment, both 3-day and 6-day IL-6 treatments accelerated hematopoietic recovery; 6-day treatment produced the greater effects. For example, compared with normal control values (N), femoral and splenic CFU-s numbers in IL-6–treated mice 17 days postirradiation were 27% N and 136% N versus 2% N and 10% N in saline-treated mice. At the same time, bone marrow and splenic GM-CFC values were 58% N and 473% N versus 6% N and 196% N in saline-treated mice; bone marrow and splenic CFU-e numbers were 91% N and 250% N versus 31% N and 130% N in saline-treated mice; and peripheral blood white cell, red cell, and platelet values were 210% N, 60% N, and 24% N versus 18% N, 39% N, and 7% N in saline-treated mice. These studies demonstrate that therapeutically administered IL-6 can effectively accelerate multilineage hematopoietic recovery following radiation-induced hematopoietic injury.

NEUTROPENIA and thrombocytopenia are major factors contributing to morbidity and mortality after radiation exposure. Agents capable of enhancing host resistance to infection and/or regenerating hematopoietic elements necessary for efficient host defense mechanisms and hematopoietic hemostasis could be useful in treating myelosuppression caused by radiotherapy or accidental radiation exposures, such as those occurring recently in Chernobyl (USSR), Goiania (Brazil), and El Salvador (San Salvador).

Hematopoietic proliferation and differentiation are regulated by a variety of hematopoietic colony-stimulating factors (CSFs) and interleukins (ILs).[1,2] IL-6 is a pleiotropic cytokine that has been ascribed a variety of biologic activities including antiviral activity,[3,4] ability to stimulate B-cell differentiation and Ig secretion,[5,6] ability to stimulate hybridoma/plasmacytoma growth,[7] ability to activate T cells[8,9] and induce cytolytic T-cell differentiation,[10] and the ability to induce the production of acute-phase proteins.[11] In addition, IL-6 has recently been demonstrated to play a role in hematopoiesis.

Hematopoietic effects of IL-6 were first described by Ikebuchi et al[12] who reported that, in vitro, IL-6 acted synergistically with IL-3 to hasten the appearance of multilineage blast cell colonies grown from murine spleen cells. A similar synergy between IL-6 and IL-3 was shown using purified human bone marrow progenitors.[13] IL-6 has also been demonstrated to augment IL-3–induced megakaryocytopoiesis in vitro.[14] Furthermore, additional murine studies have demonstrated that incubating marrow cells in liquid cultures supplemented with IL-6 and IL-3 increases exogenous spleen colony-forming units (CFU-s) numbers and enhances the ability of the cultured cells to rescue lethally irradiated recipient mice.[15] Ikebuchi et al[12] proposed that IL-6 shifted hematopoietic stem cells from the G_0 to the G_1 stage of the cell cycle where they became more responsive to the effects of additional hematopoietic factors. This hypothesis has recently been substantiated by data of Rennick et al,[16] who demonstrated the ability of IL-6 to interact with IL-4, granulocyte CSF (G-CSF), macrophage CSF (M-CSF), and GM CSF to selectively enhance the clonal growth of progenitor cells at specific stages of lineage commitment and maturation. When used alone, IL-6 has been shown to directly support the in vitro proliferation of murine GM progenitors,[17,18] as well as to directly promote megakaryocyte maturation in vitro.[19] Furthermore, IL-6 can enhance the function of mature neutrophils.[20]

Compared with in vitro studies, in vivo experience with IL-6 has been rather limited. Suzuki et al[21] showed that continuous perfusion of IL-6 into normal mice increased splenic CFU-s numbers. Additionally, Okano et al[22] demonstrated that bone marrow transplanted mice which were subsequently treated with IL-6 exhibited both enhanced hematopoietic repopulation and enhanced survival. Dose-dependent increases in platelet counts have also been demonstrated in mice[23] and primates[24] receiving in vivo treatment with IL-6.

From the Department of Experimental Hematology, Armed Forces Radiobiology Research Institute, Bethesda, the American Red Cross, Rockville, MD, and AMGen, Thousand Oaks, CA

Submitted April 26, 1990; accepted October 2, 1990.

Supported by the Armed Forces Radiobiology Research Institute, Defense Nuclear Agency, under Research Work Unit 00132. Views presented in this report are those of the authors; no endorsement by the Defense Nuclear Agency has been given or should be inferred. Research was conducted according to the principles enunciated in the Guide for the Care and Use of Laboratory Animals prepared by the Institute of Laboratory Animal Resources, National Research Council.

Address reprint requests to Myra L. Patchen, PhD, Department of Experimental Hematology, Armed Forces Radiobiology Research Institute, Building 42 NNMC, Bethesda, MD 20889-5145

The publication costs of this article were defrayed in part by page charge payment. This article must therefore be hereby marked "advertisement" in accordance with 18 U.S.C. section 1734 solely to indicate this fact.

0006-4971/91/7703-0004$0.00/0

We have further evaluated the in vivo effects of IL-6. In this article we report that IL-6 is capable of stimulating the proliferation of multiple lineages of hematopoietic progenitor cells in normal mice, and is also capable of accelerating multiple lineage hematopoietic regeneration following radiation-induced hematopoietic depression.

MATERIALS AND METHODS

Mice. C3H/HeN female mice (~20 g) were purchased from Charles River Laboratories (Raleigh, NC). Mice were maintained in an AAALAC (American Association for Accreditation of Laboratory Animal Care) accredited facility in Micro-Isolator cages (Lab Products, Maywood, IL) on hardwood-chip, contact bedding and were provided commercial rodent chow and acidified water (pH 2.5) ad libitum. Animal rooms were equipped with full-spectrum light from 6 AM to 6 PM and were maintained at 70°F ± 2°F with 50% ± 10% relative humidity using at least 10 air changes per hour of 100% conditioned fresh air. On arrival, all mice were tested for Pseudomonas and quarantined until test results were obtained. Only healthy mice were released for experimentation. All animal experiments were approved by the Institute Animal Care and Use Committee before performance.

IL-6. IL-6 was provided by AMGen (Thousand Oaks, CA). This IL-6 (lot no. 012789) had a specific activity of 1.52×10^7 U/mg. One unit of IL-6 was defined as the amount required to stimulate the production of IgM by the SKW6.4 cell line to half maximal level. Endotoxin contamination was less than 0.5 ng/mg protein based on the limulus amebocyte lysate assay. IL-6 was administered subcutaneously (s.c.) in a 0.1-mL vol at the doses and times specified for individual experiments. Control mice were injected with an equal volume of sterile saline.

Irradiation. The Theratron-80 source at the Armed Forces Radiobiology Research Institute was used to administer unilateral total-body ^{60}Co γ radiation. Mice were placed in ventilated Plexiglas containers and irradiated at a dose rate of 0.4 Gy/min. Dosimetry was performed using ionization chambers with calibration factors traceable to the National Institute of Standards and Technology.

Cell suspensions. The cell suspensions used for each assay represented tissues from three normal, irradiated, or treated and irradiated mice at each time point. Cells were flushed from femurs with 3 mL of McCoy's 5A medium (Flow Labs, McLean, VA) containing 10% heat-inactivated fetal bovine serum (Hyclone Labs, Logan, UT). Spleens were pressed through a stainless steel mesh screen, and the cells were washed from the screen with 6 mL medium. The number of nucleated cells in the suspensions was determined by Coulter counter (Coulter, Hialeah, FL). Femurs and spleens were removed from mice killed by cervical dislocation.

Spleen colony-forming unit (CFU) assays. Spleen CFU have been shown to arise from the clonal proliferation of pluripotent hematopoietic stem cells. Exogenous CFU (CFU-s) were evaluated by the method of Till and McCulloch.[24] Recipient mice were exposed to 9 Gy of total body radiation to completely eradicate endogenous hematopoietic stem cells. Three to 5 hours later, 5×10^4 bone marrow or 5×10^5 spleen cells were intravenously (i.v.) injected into the irradiated recipients. Twelve days after transplantation, the recipients were killed by cervical dislocation and their spleens were removed. The spleens were fixed in Bouin's solution, and the number of grossly visible spleen colonies was counted. Endogenous spleen colony-forming units (E-CFU) were also evaluated by a method of Till and McCulloch.[26] Mice were exposed to 6.5 Gy of total body radiation to only partially ablate endogenous hematopoietic stem cells. Twelve days after irradiation, the spleens were removed, fixed in Bouin's solution, and the spleen colonies formed by the proliferation of surviving endogenous hematopoietic cells were counted. Each treatment group consisted of five mice and experiments were repeated twice.

Granulocyte-macrophage colony-forming cell (GM-CFC) assay. Hematopoietic progenitor cells committed to granulocyte and/or macrophage development were assayed using a double-layer agar GM-CFC assay.[27] Mouse endotoxin serum (5% vol/vol) was added to feeder layers as a source of CSF. Colonies (>50 cells) were counted after 10 days of incubation in a 37°C humidified environment containing 5% CO_2. Triplicate plates were cultured for each cell suspension, and experiments were repeated twice.

Erythroid colony-forming unit (CFU-e) assay. Bone marrow and splenic CFU-e were assayed by a modification[28] of the original plasma clot technique described by Stephenson et al.[29] Cells were plated in 0.4 mL plasma clots in 4-well Nunclon (Roskilde, Denmark) culture dishes with step III anemic sheep plasma (Connaught Labs, Swiftwater, PA) as the erythropoietin (Ep) source. Bone marrow and splenic CFU-e clot suspensions contained 0.25 and 0.50 U of Ep per milliliter, respectively. After incubation at 37°C in a humidified atmosphere containing 5% CO_2 in air for 2.5 days, plasma clots were harvested, fixed with 5% glutaraldehyde, and stained with benzidine and Giemsa. A CFU-e was defined as an individual aggregate of eight or more benzidine-positive cells.

Peripheral blood cell counts. Blood was obtained from halothane-anesthetized mice by cardiac puncture using a heparinized syringe attached to a 20-gauge needle. White blood cell (WBC), red blood cell (RBC), and platelet (PLT) counts were performed using a Coulter counter. In addition, blood smears were prepared and stained with Diff-Quik (Bayer Healthcare Corp, McGaw Park, IL) to perform WBC differential counts.

Statistics. Results of replicate experiments were pooled and are represented as the mean ± standard deviation of pooled data. The Student's *t*-test was used to determine statistical differences. Significance level was set at $P < .05$.

Experimental design. Cytokine responses can vary significantly in different strains of mice.[30,31] Because of this, the first phase of this study was to identify an IL-6 dose capable of maximally stimulating hematopoietic proliferation in the C3H/HeN mouse strain used in our studies. IL-6 doses bracketing those previously reported to stimulate murine hematopoiesis in vivo[21,23,31] were evaluated using stimulation of endogenous spleen colony formation as a hematopoietic indicator. The second phase of this study was to determine the spectrum of hematopoietic progenitors (eg, CFU s, GM CFC, CFU e) and mature peripheral blood cells (eg, WBC, RBC, PLT) capable of responding to IL 6, as well as to evaluate the duration of IL 6 induced hematopoietic responses. These studies were performed in normal (ie, nonirradiated) mice. Based on the multilineage hematopoietic effects induced by IL 6 in normal mice, the third phase of this study was initiated to evaluate the ability of IL 6 to stimulate multilineage hematopoiesis and to accelerate hematopoietic regeneration following radiation induced hematopoietic injury. Because of the apparent ability of IL 6 to enhance stem cell lineage commitment and maturation,[12,14,16-19] we were concerned that prolonged in vivo IL 6 administration may induce stem cell "burn out." For this reason, both long (6 day) and short (3 day) IL 6 treatment modalities were evaluated.

RESULTS

Hematopoietic stimulation is IL-6 dose dependent. The endogenous spleen colony assay was used to determine the dose of IL 6 required to obtain optimal hematopoietic stimulation in C3H/HeN mice. In these studies, IL 6 in doses of 50 μg/kg/d, 500 μg/kg/d, or 1,000 μg/kg/d was

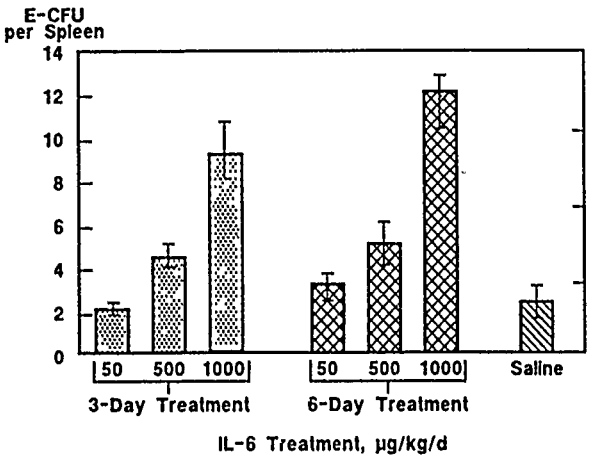

Fig 1. Effect of IL-6 dose and injection schedule on endogenous spleen colony formation in C3H/HeN mice exposed to 6.5 Gy ^{60}Co radiation. Data represent mean the ± standard deviation of values obtained from the spleens of 10 mice. A direct dose-dependent increase in E-CFU numbers was observed following both 3-day and 6-day IL-6 treatment. In both treatment groups IL-6 doses of 500 µg/kg/d and 1,000 µg/kg/d significantly increased ($P < .05$) E-CFU numbers with respect to saline control values. In addition, in both treatment groups the 1,000 µg/kg/d IL-6 dose increased E-CFU numbers to a significantly ($P < .05$) greater extent than the 500 µg/kg/d IL-6 dose.

injected s.c. into mice for either 3 days or 6 days. IL-6 doses were split such that one half of the dose was administered at 6 AM and one half of the dose at 6 PM. Twelve hours after the final IL-6 injection, mice were exposed to 6.5 Gy ^{60}Co and E-CFU numbers were determined 12 days later. Figure 1 illustrates that IL-6 produced a direct dose-dependent increase in E-CFU numbers and that the 6-day treatment was slightly more effective than the 3-day treatment. Based on these results, the 1,000 µg/kg/d IL-6 dose was chosen for subsequent experiments.

IL-6 stimulates multilineage hematopoiesis in normal mice. Normal mice were used to further characterize the hematopoietic response induced following a 3-day or 6-day treatment with IL-6 at the 1,000 µg/kg/d dose. On days 1, 4, 7, 10, 14, 17, and 22 after initiation of IL-6 treatment, bone marrow and splenic cellularity, CFU-s, GM-CFC and CFU-e numbers, as well as peripheral blood WBC, RBC, and PLT numbers were evaluated. Both 3-day and 6-day IL-6 treatment induced multilineage hematopoiesis as evidenced by changes in bone marrow (Table 1) and splenic (Table 2) stem and progenitor cell contents. Increases in splenic stem and progenitor cell numbers became evident as early as 4 days after initiation of IL-6 treatment (Table 2), while increases in bone marrow stem and progenitor cell numbers did not become evident until 10 days after initiation of IL-6 treatment (Table 1). The 6-day IL-6 treatment generally produced more dramatic and prolonged effects than the 3-day treatment. Interestingly, marrow contents on days 1, 4, and 7 following initiation of IL-6 treatment actually decreased, suggesting that IL-6 may induce bone marrow cell mobilization. Compared with the significant IL-6–induced responses observed at the stem and progenitor cell levels, peripheral blood WBC and RBC values remained relatively unchanged (Table 3). However, peripheral blood PLT values did slightly increase after both 3-day and 6-day IL-6 treatment (Table 3).

IL-6 therapy accelerates multilineage hematopoietic recovery following radiation injury. To evaluate the therapeutic potential of IL-6 in treating radiation-induced hematopoietic damage, mice were exposed to 6.5 Gy ^{60}Co radiation and subsequently administered IL-6 (1,000 µg/kg/d) for either 3 days or 6 days. On days 7, 10, 14, 17, and 22 following radiation exposure, bone marrow and splenic cellularity and CFU-s, GM-CFC, and CFU-e contents were evaluated. As shown in Table 4, both 3-day and 6-day IL-6 treatment accelerated recovery of femoral and splenic cellularity compared with irradiated saline controls. Recovery of femoral CFU-s (Fig 2), GM-CFC (Fig 3), and CFU-e (Fig 4) was also accelerated in irradiated mice by both 3-day and 6-day IL-6 treatment. Greater recovery was observed after 6-day IL-6 treatment, however, even with this treatment, femoral CFU-s numbers were only ~30% normal, GM-

Table 1. Effects of IL-6 on Bone Marrow Cellularity, CFU-s, GM-CFC, and CFU-e Contents in Normal Mice

	Treatment								
	Saline*	IL-6† Day After Initiation of IL-6 Injection							
			1	4	7	10	14	17	22
Cells per femur (×10^6)	5.4 ± 0.2	IL-6 × 3 d	4.7 ± 0.2	4.1 ± 0.3§	3.9 ± 0.2§	4.8 ± 0.4	6.3 ± 0.3§	6.3 ± 0.5	5.9 ± 0.5
		IL-6 × 6 d			4.1 ± 0.2§	4.3 ± 0.4§	6.8 ± 0.3§	5.8 ± 0.4	5.7 ± 0.3
CFU-s per femur (×10^3)	2.1 ± 0.3	IL-6 × 3 d	1.4 ± 0.1§	1.7 ± 0.1	2.3 ± 0.3	2.4 ± 0.2	3.2 ± 0.3§	1.7 ± 0.2	1.6 ± 0.1§
		IL-6 × 6 d			2.1 ± 0.1	3.1 ± 0.1§‖	4.7 ± 0.3§‖	3.1 ± 0.1§‖	1.7 ± 0.1
GM-GFC per femur (×10^3)	3.4 ± 0.3	IL-6 × 3 d	2.7 ± 0.2§	2.2 ± 0.1§	2.5 ± 0.1§	4.2 ± 0.1§	4.6 ± 0.2§	2.9 ± 0.2	3.5 ± 0.2
		IL-6 × 6 d			3.2 ± 0.1‖	4.5 ± 0.1§	5.5 ± 0.2§‖	3.9 ± 0.1‖	3.6 ± 0.1
CFU-e per femur (×10^3)‡	9.8 ± 1.3	IL-6 × 3 d	8.9 ± 0.5	8.0 ± 0.2	6.6 ± 0.5§	13.2 ± 1.0	18.5 ± 2.2§	15.2 ± 2.0§	11.6 ± 1.3
		IL-6 × 6 d			7.8 ± 0.8	8.7 ± 1.4‖	15.0 ± 1.8§	12.4 ± 0.5	14.3 ± 1.5§

Pooled results from two experiments.

*Values from mice treated for 3 days did not differ from values from mice treated for 6 days with saline. Therefore, all saline data were pooled.

†1,000 µg/kg/d of IL-6 administered s.c.

‡Mean results obtained from only one experiment.

§$P < .05$, with respect to saline values.

‖$P < .05$, with respect to values obtained from mice receiving IL-6 for 3 days.

Table 2. Effects of IL-6 on Splenic Cellularity, CFU-s, GM-CFC, and CFU-e Contents in Normal Mice

	Treatment								
	Saline*	IL-6† Day After Initiation of IL-6 Injection							
			1	4	7	10	14	17	22
Cells per spleen ($\times 10^8$)	1.1 ± 0.1	IL-6 × 3 d	1.5 ± 0.1§	2.2 ± 0.2§	1.4 ± 0.1§	1.2 ± 0.1	1.0 ± 0.1	1.5 ± 0.2§	1.8 ± 0.1§
		IL-6 × 6 d			1.6 ± 0.1§	1.2 ± 0.1	0.9 ± 0.1	1.5 ± 0.1§	2.0 ± 0.2§
CFU-s per spleen ($\times 10^3$)	7.3 ± 0.7	IL-6 × 3 d	6.1 ± 0.6	26.1 ± 1.8§	12.8 ± 0.9§	11.6 ± 1.2§	9.7 ± 0.7§	8.1 ± 0.7	7.9 ± 0.8
		IL-6 × 6 d			21.8 ± 0.4§‖	20.7 ± 1.0§‖	13.4 ± 0.4§‖	11.9 ± 1.3§‖	7.8 ± 0.8
GM-GFC per spleen ($\times 10^3$)	4.4 ± 0.5	IL-6 × 3 d	3.4 ± 0.4	31.6 ± 2.2§	8.7 ± 0.3§	6.8 ± 0.3§	6.5 ± 0.4§	6.3 ± 0.1§	4.0 ± 0.4
		IL-6 × 6 d			14.7 ± 0.6§‖	10.2 ± 0.4§‖	9.6 ± 0.5§‖	6.4 ± 0.3§	5.4 ± 0.2§‖
CFU-e per spleen ($\times 10^5$)‡	1.0 ± 0.1	IL-6 × 3 d	1.0 ± 0.2	2.3 ± 0.7	1.3 ± 0.1	0.9 ± 0.1	1.1 ± 0.2	0.7 ± 0.1	1.1 ± 0.1
		IL-6 × 6 d			3.3 ± 0.2§‖	1.5 ± 0.1§‖	0.9 ± 0.1	1.2 ± 0.1‖	1.3 ± 0.2

Pooled results from two experiments.

*Values from mice treated for 3 days did not differ from values from mice treated for 6 days with saline. Therefore, all saline data were pooled.

†1,000 μg/kg/d of IL-6 administered s.c.

‡Mean results obtained from only one experiment.

§$P < .05$, with respect to saline values.

‖$P < .05$, with respect to values obtained from mice receiving IL-6 for 3 days.

CFC numbers were only ~40% normal, and CFU-e numbers were ~80% normal at 22 days postirradiation. In the spleen, a much more dramatic hematopoietic response was observed (Figs 5 through 7). Even in saline-treated mice, explosive splenic hematopoietic recovery occurred approximately 2 weeks postirradiation, with progenitor cell numbers often overshooting control values before normalizing. Both 3-day and 6-day IL-6 treatment accelerated splenic CFU-s (Fig 5), GM-CFC (Fig 6), and CFU-e (Fig 7) recovery in irradiated mice. GM-CFC recovery was enhanced to a significantly greater extent than either CFU-s or CFU-e recovery. In mice treated with IL-6 for 6 days, peak splenic GM-CFC numbers reached 630% of normal values (Fig 6), compared with peak CFU-s numbers that reached only 210% of normal values (Fig 5), and peak CFU-e numbers that reached only 250% of normal values (Fig 7). In addition to intensifying the magnitude of the GM-CFC recovery, IL-6 treatment also intensified the duration of the overshoot phenomenon (Fig 6). The stimulation induced by IL-6 at the bone marrow and splenic stem and progenitor cell levels also ultimately influenced the mature blood cell levels as indicated by an accelerated reappearance of mature WBC (Fig 8), RBC (Fig 9), and PLT (Fig 10) in the peripheral blood. With regard to WBC, not only did IL-6 accelerate the recovery of total WBC numbers, but WBC differentials also returned to normal more rapidly in IL-6–treated mice. WBC in nonirradiated mice typically consisted of 27% ± 4% neutrophils, 69% ± 6% lymphocytes, and 4% ± 1% monocytes. On day 17 postirradiation, WBC in IL-6–treated mice consisted of 25% ± 5% neutrophils, 73% ± 4% lymphocytes, and 3% ± 1% monocytes, compared with 9% ± 2% neutrophils, 86% ± 5% lymphocytes, and 5% ± 2% monocytes in saline-treated mice. It was also noted that although 6-day versus 3-day IL-6 treatment produced different effects on bone marrow and splenic stem and progenitor cell recovery, very little difference between these two treatments was observed at the peripheral blood cell level.

DISCUSSION

Morbidity and mortality associated with high-level radiation exposures can be directly attributed to infectious and hemorrhagic complications resulting from radiation-induced neutropenia and thrombocytopenia. In recent years, several immunomodulators and hematopoietic growth factors have been evaluated for the ability to stimulate hematopoietic regeneration after radiation or chemotherapy induced myelosuppression. Of these, the immunomod

Table 3. Effects of IL-6 on Peripheral Blood Cellularity in Normal Mice

	Treatment								
	Saline*	IL-6† Day After Initiation of IL-6 Injection							
			1	4	7	10	14	17	22
WBC per mL ($\times 10^6$)	7.3 ± 0.3	IL-6 × 3 d	6.5 ± 0.5	6.6 ± 0.5	6.7 ± 0.6	6.9 ± 0.6	7.3 ± 0.5	7.4 ± 0.6	6.8 ± 0.6
		IL-6 × 6 d			7.4 ± 0.6	7.5 ± 0.7	7.9 ± 0.8	7.7 ± 0.6	7.9 ± 0.6
RBC per mL ($\times 10^9$)	6.5 ± 0.2	IL-6 × 3 d	6.6 ± 0.6	6.7 ± 0.5	6.9 ± 0.6	7.2 ± 0.5	7.4 ± 0.7	6.4 ± 0.4	6.9 ± 0.5
		IL-6 × 6 d			7.2 ± 0.5	7.3 ± 0.5	7.5 ± 0.6	6.9 ± 0.6	6.6 ± 0.5
PLT per mL ($\times 10^8$)	11.5 ± 0.6	IL-6 × 3 d	9.9 ± 0.6‡	13.7 ± 0.8‡	14.6 ± 1.0‡	10.7 ± 0.9	10.4 ± 0.9	10.0 ± 0.9	10.0 ± 0.7
		IL-6 × 6 d			13.6 ± 1.0‡	11.0 ± 0.6	10.3 ± 0.7	10.0 ± 0.4	10.0 ± 0.5

Pooled results from two experiments.

*Values from mice treated for 3 days did not differ from values from mice treated for 6 days with saline. Therefore, all saline data were pooled.

†1,000 μg/kg/d of IL-6 administered s.c.

‡$P < .05$, with respect to values.

Table 4. Effects of IL-6 on Bone Marrow and Splenic Cellularity in Irradiated Mice

	Day Postirradiation				
	7	10	14	17	22
Cells per femur ($\times 10^6$)*					
Saline†	1.8 ± 0.2	1.3 ± 0.3	1.8 ± 0.2	2.0 ± 0.1	2.5 ± 0.2
IL-6 × 3 d‡	1.2 ± 0.1‖	1.2 ± 0.2	1.9 ± 0.2	3.3 ± 0.2‖	3.3 ± 0.2‖
IL-6 × 6 d‡	1.1 ± 0.1‖	0.9 ± 0.3	1.5 ± 0.2	1.9 ± 0.2¶	3.7 ± 0.4‖
Cells per spleen ($\times 10^7$)§					
Saline†	1.3 ± 0.1	1.3 ± 0.1	1.9 ± 0.2	8.9 ± 0.9	20.7 ± 0.9
IL-6 × 3 d‡	1.1 ± 0.1	1.5 ± 0.1	2.4 ± 0.2	20.6 ± 0.9‖	8.7 ± 0.6‖
IL-6 × 6 d‡	1.2 ± 0.1	1.3 ± 0.1	4.6 ± 0.5‖¶	26.4 ± 0.9‖¶	14.8 ± 0.8‖¶

C_3H/HeN mice were exposed to 6.5 Gy ^{60}Co radiation on day 0; pooled results from two experiments.

*Cellularity per femur in nonirradiated control mice was $5.4 \pm 0.2 \times 10^6$.

†Values from mice treated for 3 days did not differ from values from mice treated for 6 days with saline. Therefore, all saline data were pooled.

‡1,000 μg/kg/d of IL-6 administered s.c. beginning 1 day after irradiation.

§Cellularity per spleen in nonirradiated control mice was $11.0 \simeq 1.0 \times 10^7$.

‖$P < .05$, with respect to saline values.

¶$P < .05$, with respect to values obtained from mice receiving IL-6 for 3 days.

ulator glucan[27,32] and the hematopoietic growth factors granulocyte CSF (G-CSF;[33-36]) and granulocyte-macrophage CSF (GM-CSF;[34,37,38]) have shown promise. G-CSF and GM-CSF selectively enhance granulocyte regeneration through their ability to both amplify GM-CFC progenitor cell pools and accelerate granulocyte maturation.[39,40] As a result of accelerating granulocyte reconstitution, these cytokines enhance survival in irradiated animals by reducing susceptibility to life-threatening opportunistic infections. However, preclinical studies involving large animals have demonstrated that, even with enhanced granulocyte regeneration, hemorrhage due to radiation induced loss of platelets remains a life-threatening problem.[36,38] In addition, hemorrhage exacerbates anemia, which also occurs following radiation-induced hematopoietic injury. Currently these problems are only controlled by PLT and RBC transfusions.[36,37]

In view of these complications, agents capable of stimulating multiple lineage (especially granuloid, platelet, and erythroid) hematopoietic reconstitution would be extremely useful for the treatment of radiation-induced hematopoietic injury. Our studies in normal mice confirmed the ability of IL-6 to enhance CFU-s, GM-CFC, and PLT production.[21,23] In addition, we demonstrated the ability of IL-6 to increase CFU-e numbers. Because of these multilineage hematopoietic effects, IL-6 appeared to be an especially appropriate cytokine to evaluate for usefulness in the treatment of radiation-induced hematopoietic depression. Results obtained from our murine model of radiation

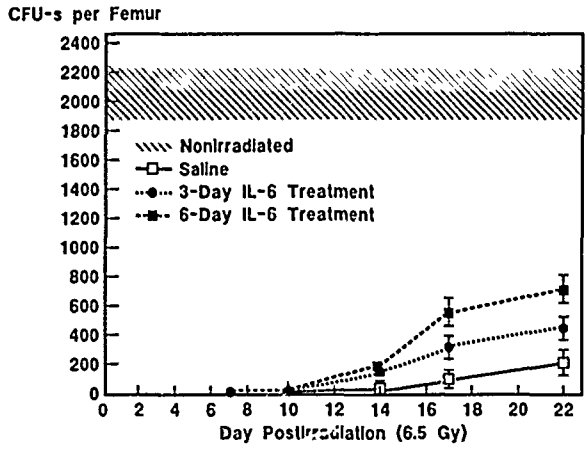

Fig 2. Effect of IL-6 on bone marrow CFU-s recovery in irradiated C3H/HeN mice. Mice were exposed to 6.5 Gy ^{60}Co and administered IL-6 (1,000 μg/kg/d, s.c.) for either 3 days or 6 days. Data represent the mean ± standard deviation of pooled values obtained from two separate experiments. In comparison with saline controls, CFU-s numbers in both 3-day and 6-day IL-6–treated mice were significantly ($P < .05$) increased on days 14, 17 and 22, 6-day IL-6 treatment produced a greater response, with 6-day IL-6 values being significantly ($P < .05$) increased above 3-day IL-6 values on days 17 and 22.

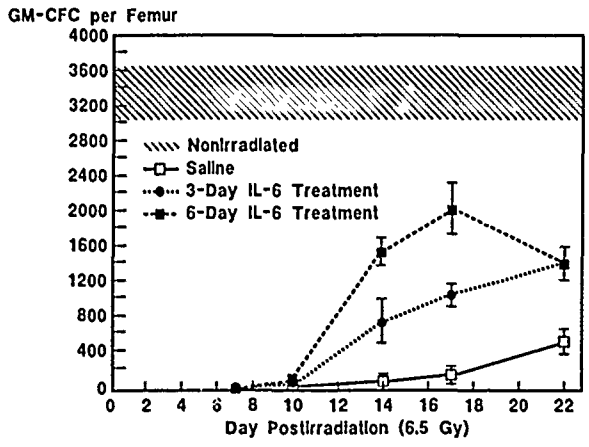

Fig 3. Effect of IL-6 on bone marrow GM-CFC recovery in irradiated C3H/HeN mice. Mice were exposed to 6.5 Gy ^{60}Co and administered IL-6 (1,000 μg/kg/d, s.c.) for either 3 days or 6 days. Data represent the mean ± standard deviation of pooled values obtained from two separate experiments. In comparison with saline controls, GM-CFC numbers in both 3 day and 6 day IL-6 treated mice were significantly ($P < .05$) increased on days 10, 14, 17, and 22, 6 day IL-6 treatment produced a greater response, with 6 day IL-6 values being significantly ($P < .05$) increased over 3 day IL-6 values on days 14 and 17.

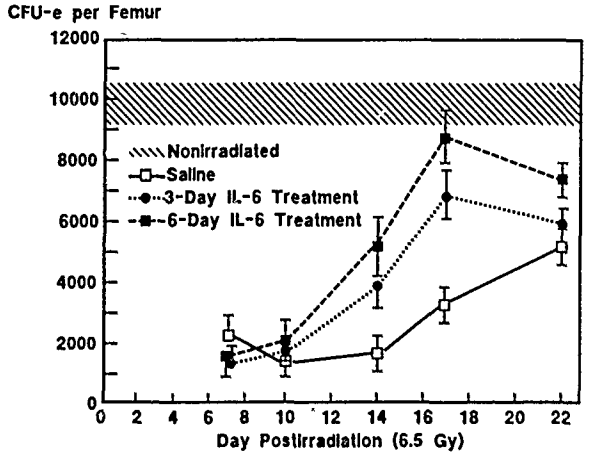

Fig 4. Effect of IL-6 on bone marrow CFU-e recovery in irradiated C3H/HeN mice. Mice were exposed to 6.5 Gy ^{60}Co and administered IL-6 (1,000 μg/kg/d, s.c.) for 3 days or 6 days. Data for 6-day IL-6 treatment represent the mean ± standard deviation of pooled values obtained from two separate experiments. Data for 3-day IL-6 treatment represent the mean ± standard deviation of values obtained from one experiment. In comparison with saline controls, CFU-e numbers in both 3-day and 6-day IL-6–treated mice were significantly ($P < .05$) increased on days 14 and 17. On day 22, CFU-e numbers in 6-day IL-6–treated mice were also significantly ($P < .05$) higher than either saline or 3-day IL-6 values.

induced hematopoietic depression clearly showed that IL-6 also stimulates multiple lineage hematopoietic regeneration after radiation injury. IL-6–treated mice exhibited accelerated bone marrow and splenic CFU-s, GM-CFC, and CFU-e regeneration, as well as accelerated recovery of mature peripheral WBC, RBC, and PLT. The 6-day IL-6

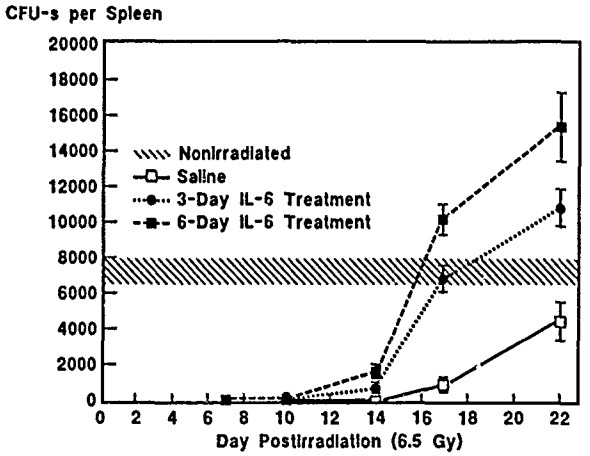

Fig 5. Effect of IL-6 on splenic CFU-s recovery in irradiated C3H/HeN mice. Mice were exposed to 6.5 Gy ^{60}Co and administered IL-6 (1,000 μg/kg/d, s.c.) for either 3 days or 6 days. Data represent the mean ± standard deviation of pooled values obtained from two separate experiments. In comparison with saline controls, CFU-s numbers in both 3-day and 6-day IL-6–treated mice were significantly ($P < .05$) increased on days 14, 17, and 22. In addition, 6-day IL-6 treatment produced a greater response, with 6-day IL-6 values being significantly ($P < .05$) increased above 3-day IL-6 values on days 10, 14, 17, and 22.

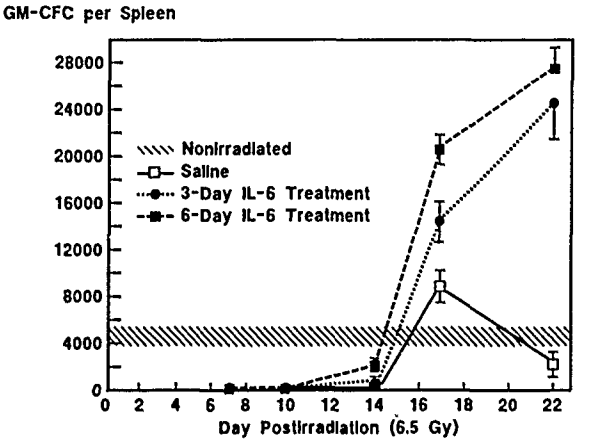

Fig 6. Effect of IL-6 on splenic GM-CFC recovery in irradiated C3H/HeN mice. Mice were exposed to 6.5 Gy ^{60}Co and administered IL-6 (1,000 μg/kg/d, s.c.) for either 3 days or 6 days. Data represent the mean ± standard deviation of pooled values obtained form two separate experiments. In comparison with saline controls, GM-CFC numbers in both 3-day and 6-day IL-6–treated mice were significantly ($P < .05$) increased on days 14, 17, and 22. Six-day IL-6 treatment produced a greater response, with 6-day IL-6 values being significantly ($P < .05$) increased above 3-day IL-6 values on days 14 and 17.

treatment induced the greatest recovery, with no evidence of stem cell "burn out." Recently Takatsuki et al[41] have also reported the ability of IL-6 to accelerate CFU-s, GM-CFC, and PLT recovery following chemotherapy-induced hematopoietic depression.

The IL-6 dose used (1,000 μg/kg/d) to produce our reported hematopoietic effects may seem high with respect to doses of cytokines such as G-CSF or GM-CSF. However, to obtain good hematopoietic stimulation with these cyto-

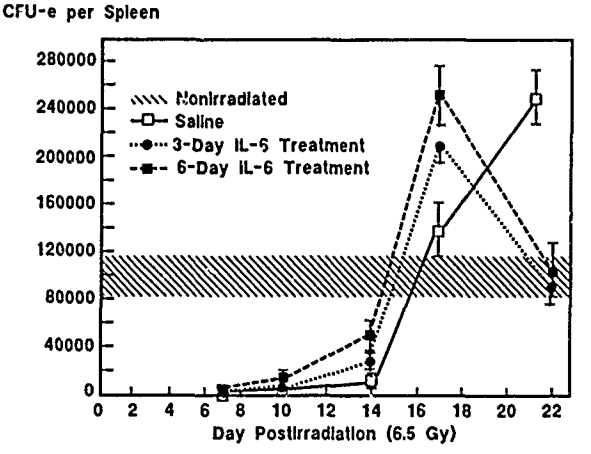

Fig 7. Effect of IL-6 on splenic CFU-e recovery in irradiated C3H, HeN mice. Mice were exposed to 6.5 Gy ^{60}Co and administered IL-6 (1,000 μg/kg/d, s.c.) for 3 days or 6 days. Data for 6-day IL-6 treatment represent the mean ± standard deviation of pooled values obtained from two separate experiments. Data for 3 day IL 6 treatment represent the mean ± standard deviation of values obtained from one experiment. In comparison with saline controls, CFU e numbers in both 3 day and 6 day IL 6 treated mice were significantly ($P < .05$) increased on days 10, 14, and 17.

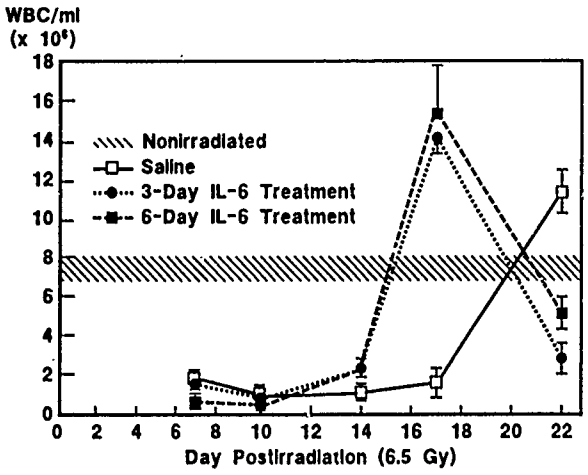

Fig 8. Effect of IL-6 on WBC recovery in irradiated C3H/HeN mice. Mice were exposed to 6.5 Gy ^{60}Co and administered IL-6 (1,000 μg/kg/d, s.c.) for either 3 days or 6 days. Data represent the mean ± standard deviation of pooled values obtained from two separate experiments. In comparison with saline controls, WBC numbers in both 3-day and 6-day IL-6–treated mice were significantly ($P < .05$) increased on days 14 and 17.

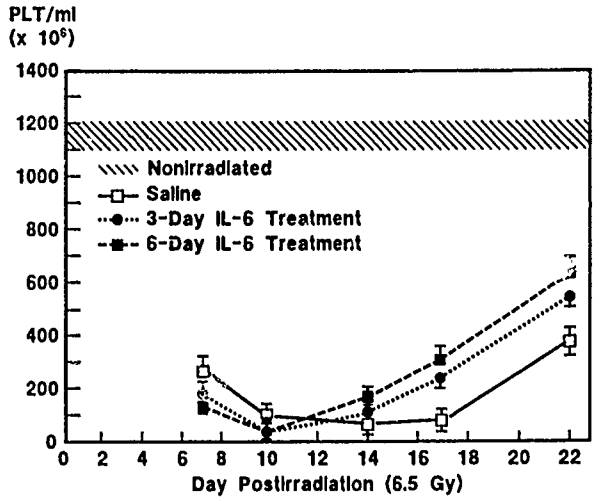

Fig 10. Effect of IL-6 on peripheral blood platelet recovery in irradiated C3H/HeN mice. Mice were exposed to 6.5 Gy ^{60}Co and administered IL-6 (1,000 μg/kg/d, s.c.) for either 3 days or 6 days. Data represent the mean ± standard deviation of pooled values obtained from two separate experiments. In comparison with saline controls, PLT numbers in both 3-day and 6-day IL-6–treated mice were significantly ($P < .05$) increased on days 14, 17, and 22.

kines, extended therapy is generally required and we observed good hematopoietic stimulation with as few as 3 days of IL-6 treatment. In reality, valid comparisons of cytokine effectiveness are difficult to make because of differences in cytokine-specific activities, as well as routes of cytokine administration (s.c., i.p., i.v.), administration schedules (continuous infusion, once a day, twice a day, etc), and durations of treatment (ranging from 1 to 22 days) used in various published studies.

IL-6 has been hypothesized to mediate its multilineage hematopoietic effects by shifting stem cells from the G_0 to the G_1 stage of the cell cycle where they become more responsive to additional hematopoietic growth factors such as IL-3, IL-4, G-CSF, M-CSF, or GM-CSF.[12,16] The effect of radiation exposure alone on the endogenous production of such cytokines has not been fully determined. However, ultraviolet (UV) radiation has been shown to increase the synthesis and release of IL-1 and GM-CSF by epidermal cells,[42,43] and sublethal γ radiation has been shown to increase IL-1 and tumor necrosis factor (TNF) production by peritoneal macrophages.[44] Thus, in the sublethal radiation model used in our studies, it seems likely that some macrophages and accessory cells capable of producing cytokines would survive radiation exposure, and that these cytokines would be present to interact with IL-6 in influencing stem cell proliferation and commitment.

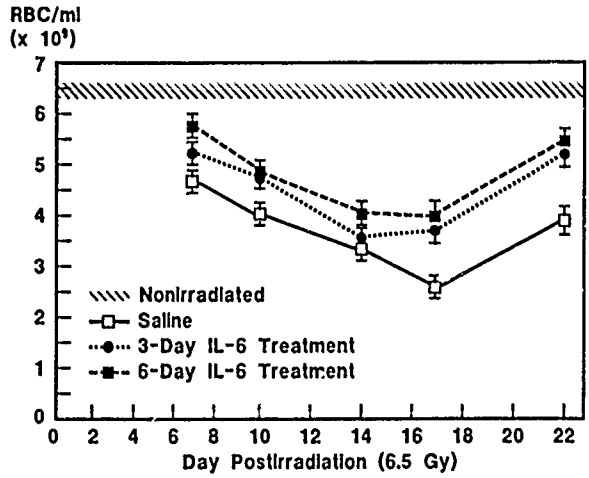

Fig 9. Effect of IL-6 on RBC recovery in irradiated C3H/HeN mice. Mice were exposed to 6.5 Gy ^{60}Co and administered IL-6 (1,000 μg/kg/d, s.c.) for either 3 days or 6 days. Data represent the mean ± standard deviation of pooled values obtained from two separate experiments. In comparison with saline controls, RBC numbers in both 3-day and 6-day IL-6–treated mice were significantly ($P < .05$) increased on days 7, 10, 17, and 22; 6-day IL-6 values were also significantly ($P < .05$) increased on day 14.

The fact that IL-1 and TNF have been reported to increase in mice after a sublethal radiation exposure such as that used in our studies is especially interesting.[44] Both IL-1 and TNF have been demonstrated to be potent inducers of IL-6.[45,46] Hence, the hematopoietic regeneration that ultimately does occur following sublethal radiation injury (as illustrated in Figs 2 through 10 by our data obtained from saline-treated mice) may be partially mediated by the induction of endogenous IL-6 by endogenous IL-1 and TNF released after radiation exposure. Clearly, however, our studies show that augmenting endogenous IL-6 levels further accelerates hematopoietic regeneration. Exogenous administration of IL-1 to myelosuppressed mice has also been shown to enhance hematopoietic regeneration[47-49]; induction of IL-6 may likewise play a role in this phenomenon. Interestingly, as observed with IL-1,[47] administration of IL-6 to sublethally irradiated mice delays splenic and thymic lymphoid recovery (Williams JL, Patchen ML, Darden J. unpublished results, August 1990). These prelim-

inary results further suggest that many of IL-1's effects on lymphopoiesis may involve the induction of IL-6.

In conclusion, we have demonstrated the ability of IL-6 to induce multilineage hematopoietic stimulation in vivo capable of accelerating the regeneration of mature WBC, PLT, and RBC in radiation-injured mice. Whether these effects are directly mediated by IL-6 or mediated by secondary hematopoietic growth factors induced following in vivo IL-6 administration remains to be determined. Nevertheless, these results suggest that IL-6 may be therapeutically useful in the treatment of radiation- or chemotherapy-induced myelosuppression requiring multilineage repopulation.

ACKNOWLEDGMENT

The authors are grateful to Brian Solberg, Barbara Calabro, Sheryl Reilly, and Roxanne Fischer for technical assistance and to Catherine Sund for editorial assistance.

REFERENCES

1. Quesenberry P, Souza L, Krantz S. Growth Factors. Hematology 1989: Educational Program of the American Society of Hematology. Philadelphia, PA, Saunders, 1989, p 98

2. Laver J, Moore MA: Clinical use of recombinant human hematopoietic growth factors. J Natl Cancer Inst 81.1370, 1989

3. Weissenbach J, Chernajovsky Y, Zeevi M, Shulman L, Soreq H, Nir H, Wallach D, Perricaudet M, Tiollais P, Revel M: Two interferon mRNAs in human fibroblasts: In vitro translation and Escherichia coli cloning studies. Proc Natl Acad Sci USA 77:7152, 1980

4. Sehgal PB, Sagar AD: Heterogeneity of poly(I)poly(C)-induced human fibroblast interferon mRNA species. Nature 288: 95, 1980

5. Muraguchi A, Kishimoto T, Miki Y, Kuritani T, Kaieda T, Yoshizaki K, Yamamura Y: T-cell replacing factor- (TRF) induced IgG secretion in human B blastoid cell line and demonstration of acceptors for TRF. J Immunol 127:412, 1981

6. Hirano T, Yasukawa K, Harada H, Taga T, Watanabe Y, Matsuda T, Kashiwamura S, Nakajima K, Koyama K, Iwamatsu A, Tsunasawa S, Sakiyama F, Matsui H, Takahara Y, Taniguchi T, Kishimoto T: Complimentary DNA for a novel human interleukin (BSF-2) that induces B lymphocytes to produce immunoglobulin. Nature 324:73, 1986

7. VanDamme J, Opdenakker G, Simpson RJ, Rubira MR, Cayphas S, Vink A, Billiau A, VanSnick J: Identification of the human 26-kd protein, interferon $beta_2$, as a B-cell hybridoma/plasmacytoma growth factor induced by interleukin-1 and tumor necrosis factor. J Exp Med 165:914, 1987

8. Garman RD, Jacobs KA, Clark SC, Raulet DH: B-cell stimulating factor 2 ($beta_2$ interferon) functions as a second signal for interleukin-2 production by mature murine T-cells. Proc Natl Acad Sci USA 84:7629, 1987

9. Lotz M, Jirik F, Kabouridis R, Tsoukas C, Hirano T, Kishimoto T, Carson DA: BSF-2/IL-6 is costimulant for human thymocytes and T-lymphocytes. J Exp Med 167:1253, 1988

10. Takai Y, Wong GG, Clark SC, Burakoff SJ, Herrman.. SH: B-cell stimulatory factor 2 is involved in the differentiation of cytotoxic T-lymphocytes. J Immunol 140:508, 1988

11. Gauldie J, Richards C, Harnish D, Lansdorf P, Baumann H Interferon $beta_2$/B-cell stimulatory factor type 2 shares identity with monocyte derived hepatocyte stimulatory factor and regulates the major acute phase protein response in liver cells. Proc Natl Acad Sci USA 84:7251, 1987

12. Ikebuchi K, Wong GG, Clark SC, Ihle JN, Hirai Y, Ogawa M: Interleukin 6 enhancement of interleukin 3-dependent proliferation of multipotential hemopoietic progenitors. Proc Natl Acad Sci USA 84:9035, 1987

13. Leary AG, Ikebuchi K, Hirai Y, Wong GG, Yang YC, Clark SC, Ogawa M. Synergism between interleukin 6 and interleukin 3 in supporting proliferation of human hematopoietic stem cells: Comparison with interleukin-1 alpha. Blood 71.1759, 1988

14. Bruno E, Hoffman R. Effect of interleukin-6 on in vitro human megakaryocytopoiesis. Its interaction with other cytokines. Exp Hematol 17:1038, 1989

15. Okano A, Suzuki C, Takatsuki F, Akiyama Y, Koike K, Ozawa K, Hirano T, Kishimoto T, Nakahata T, Asano S: In vitro expansion of the murine pluripotent hemopoietic stem cell population in response to interleukin 3 and interleukin 6. Application to bone marrow transplantation. Transplantation 48:495, 1989

16. Rennick D, Jackson J, Yang G, Wideman J, Lee F, Hudak S: Interleukin-6 interacts with interleukin-4 and other hematopoietic growth factors to selectively enhance the growth of megakaryocytic, erythroid, myeloid, and multipotential progenitor cells. Blood 73:1828, 1989

17. Wong GG, Witek-Giannotti JS, Temple PA, Kriz R, Ferenz C, Hewick RM, Clark SC, Ikebuchi K, Ogawa M: Stimulation of murine hemopoietic colony formation by human IL-6. J Immunol 140:3040, 1988

18. Suda T, Yamaguchi Y, Suda J, Miura Y, Okano A, Akiyama Y: Effect of interleukin-6 (IL-6) on the differentiation and proliferation of murine and human hemopoietic progenitors. Exp Hematol 16:891, 1988

19. Ishibashi T, Kimura H, Uchida T, Kariyone S, Friese P, Burstein SA: Human interleukin 6 is a direct promoter of maturation of megakaryocytes in vitro. Proc Natl Acad Sci USA 86:5953, 1989

20. Burish L, Rosenbaum R, Albury L, Clark, S: Activation of neutrophils by recombinant interleukin-6. Cell Immunol 121:280, 1989

21. Suzuki C, Okano A, Takatsuki F, Miyasaka Y, Hirano T, Kishimoto T, Ejima D, Akiyama Y: Continuous perfusion with interleukin 6 (IL-6) enhances production of hematopoietic stem cells (CFU-s). Biochem Biophys Res Commun 159:933, 1989

22. Okano A, Suzuki C, Takatsuki F, Akiyama Y, Koike K, Nakahata T, Hirano T, Kishimoto T, Ozawa K, Asano S: Effects of interleukin-6 on hematopoiesis in bone marrow-transplanted mice. Transplantation 47:738, 1989

23. Ishibashi T, Kimura H, Shikama Y, Uchida T, Kariyone S, Hirano T, Kishimoto T, Takatsuki F, Akiyama Y. Interleukin-6 is a potent thrombopoietic factor in vivo in mice. Blood 74.1241, 1989

24. Asano S, Okano A, Ozawa K, Nakahata T, Ishibashi T, Koike K, Kimura H, Tanioka Y, Shibuya A, Hirano T, Kishimoto T, Takaku F, Akiyama Y. In vivo effects of recombinant human interleukin-6 in primates. Stimulated production of platelets. Blood 75:1602, 1990

25. Till JE, McCulloch EA: A direct measurement of the radiation sensitivity of normal mouse bone marrow cells. Radiat Res 14:213, 1961

26. Till JE, McCulloch EA. Early repair processes in marrow cells irradiated and proliferating in vivo. Radiat Res 18:96, 1963

27. Patchen ML, MacVittie TJ. Hemopoietic effects of intravenous soluble glucan administration. J Immunopharmacol 8.407, 1986

28. Schwartz GN, Patchen ML, Neta R, MacVittie TJ. Radioprotection of mice with interleukin 1. Relationship to the number of

erythroid and granulocyte-macrophage colony-forming cells. Radiat Res 121:220, 1990

29. Stephenson JR, Axelrad AA, McLeod DL, Shreeve MM: Induction of colonies of hemoglobin-synthesizing cells by erythropoietin in vitro. Proc Natl Acad Sci USA 68:1542, 1971

30. Neta R, Vogel SN, Oppenheim JJ, Douches SD. Cytokines in radioprotection: Comparison of the radioprotective effects of IL-1, IL-2, GM-CSF and IFN gamma. Lymphokine Res 5:105, 1986

31. Neta R, Vogel SN, Sipe J, Wong GG, Nardau RP: Comparison of in vivo effects of human recombinant IL-1 and human recombinant IL-6 in mice. Lymphokine Res 7:403, 1988

32. Patchen ML, MacVittie TJ, Solberg BD, Souza LM: Survival enhancement and hemopoietic regeneration following radiation exposure: Therapeutic approach using glucan and granulocyte colony-stimulating factor. Exp Hematol 18:1042, 1990

33. Patchen ML, MacVittie TJ, Solberg BD, Souza LM: Therapeutic administration of recombinant human granulocyte colony-stimulating factor accelerates hemopoietic regeneration and enhances survival in a murine model of radiation-induced myelosuppression. Int J Cell Cloning 8:107, 1990

34. Talmadge JE, Tribble H, Pennington R: Protective, restorative, and therapeutic properties of recombinant colony-stimulating factors. Blood 73:2093, 1989

35. Kobayashi Y, Okabe T, Urabe A, Suzuki N, Takaku F: Human granulocyte colony-stimulating factor produced by *Escherichia coli* shortens the period of granulocytopenia induced by irradiation in mice. Jpn J Cancer Res 78:763, 1987

36. MacVittie TJ, Monroy RL, Patchen ML, Souza LM: Therapeutic use of recombinant human G-CSF (rhG-CSF) in a canine model of sublethal and lethal whole-body irradiation. Int J Radiat Biol 57:723, 1990

37. MacVittie TJ, Monroy RL: Potential improvement in the management of seriously irradiated persons, in Ricks RC, Fry SA (eds): The Medical Basis for Radiation Acident Preparedness. Clinical Experiences and Follow-Up Since 1979. Elsevier Science, New York, NY (in press)

38. MacVittie TJ, Vriesendorp H, Monroy RL, Souza L, Donahue RE, Patchen ML, Brandenburg R, Konradi L. Rescue of lethally irradiated canines using therapeutic administration of either recombinant human G-CSF or GM-CSF. Exp Hematol 17:579, 1989 (abstr)

39. Groopman JE, Molina JM, Scadden DT: Hemopoietic growth factors: Biology and clinical applications. N Engl J Med 321:1449, 1989

40. Peters WP: The effect of recombinant human colony-stimulating factors on hematopoietic reconstitution following autologous bone marrow transplantation. Semin Hematol 26:18, 1989

41. Takatsuki F, Okano A, Suzuki C, Miyasaka Y, Hirano T, Kishimoto T, Ejima D, Akiyama Y: Interleukin 6 perfusion stimulates reconstitution of the immune and hemopoietic systems after 5-fluorouracil treatment. Cancer Res 50:2885, 1990

42. Kupper TS, Chua AO, Flood P, McGuire J, Gubler U: Interleukin-1 gene expression in cultured human keratinocytes is augmented by ultraviolet irradiation. J Clin Invest 80:430, 1987

43. Ansel JC, Perry P: Modulation of GM-CSF expression in epidermal cells. Clin Res 36:374A, 1988 (abstr)

44. McChesney DG, Holobaugh PA, Briggs R, Beal K: Effect of whole body irradiation and threhalose dimycolate on TNF and IL-1 production by murine macrophages. J Leukoc Biol 46:325, 1989 (abstr)

45. McIntosh JK, Jablons DM, Mule JJ, Nardan RP, Rudikoff S, Lotze MT, Rosenberg SA: In vivo induction of IL-6 by administration of exogenous cytokines and detection of de novo serum levels of IL-6 in tumor-bearing mice. J Immunol 143:162, 1989

46. Brouckaert P, Spriggs DR, Demetri G, Kufe DW, Fries W: Circulating interleukin 6 during a continuous infusion of tumor necrosis factor and interferon gamma. J Exp Med 169:2257, 1989

47. Morrissey P, Charrier K, Bressler L, Alpert A: The influence of IL-1 treatment on the reconstitution of the hemopoietic and immune systems after sublethal radiation. J Immunol 140:4204, 1988

48. Benjamin WR, Tare NS, Hayes TJ, Becker JM, Anderson TD. Regulation of hemopoiesis in myelosuppressed mice by human recombinant IL-1 alpha. J Immunol 142:792, 1989

49. Moore MAS, Warren DJ: Synergy of interleukin-1 and granulocyte colony stimulating factor. In vivo stimulation of stem cell recovery and hematopoietic regeneration following 5-fluorouracil treatment of mice. Proc Natl Acad Sci USA 84.7134, 1987

RADIATION RESEARCH 125, 41–47 (1991)

The Influence of Exogenous Eicosanoids on the Radiation Response of Cultured Bovine Aortic Endothelial Cells

D. B. RUBIN,*† E. A. DRAB,† A. M. STONE,* T. L. WALDEN, JR.,‡ AND W. R. HANSON§

*Department of Medicine and †Department of Therapeutic Radiology, Rush-Presbyterian-St. Luke's Medical Center, Chicago, Illinois 60612, ‡The Armed Forces Radiobiology Research Institute, and §The Loyola–Hines Department of Radiotherapy, Loyola University and Hines VA Medical Center, Chicago, Illinois 60611

RUBIN, D. B., DRAB, E. A., STONE, A. M., WALDEN, T. L., JR., AND HANSON, W. R. The Influence of Exogenous Eicosanoids on the Radiation Response of Cultured Bovine Aortic Endothelial Cells. *Radiat. Res.* 125, 41–47 (1991).

The radioprotection by several eicosanoids was investigated in cultures of bovine aortic endothelial cells. One hour before irradiation (0–500 cGy, ^{137}Cs γ rays) 10 μg/ml of PGD_2, PGE_1, PGI_2, misoprostol (PGE_1-analog), 16,16-dimethyl PGE_2, PGA_2, or 1 μg/ml LTC_4 was added. Radiation decreased incorporation of [^{3}H]thymidine at 4 h, cell number/culture at 24 h, and cell survival as measured by colony formation. Under these conditions the eicosanoids were not radioprotective. Two eicosanoids, PGD_2 and PGA_2, appeared to be toxic. Because receptors might mediate eicosanoid-induced radioprotection, radioligand binding of PGE_2 and LTC_4 and levels of adenosine 3', 5'-cyclic monophosphate (cAMP) were measured. Evidence for a receptor was equivocal; there was nonspecific binding and metabolism of LTC_4. The level of cAMP was elevated by 16-16-dimethyl-PGE_2 in the presence of isobutyl methylxanthine; however, this combination of the prostaglandin and the methylxanthine was not radioprotective. These investigations suggest that an elevated cAMP level alone does not lead to eicosanoid-induced radioprotection of bovine aortic endothelial cell monolayers *in vitro*.

INTRODUCTION

Many eicosanoids protect the cells of the gastric and intestinal mucosa from exposure to acid, ethanol, heat, and other forms of chemical injury (*1*) In addition, several eicosanoids consistently have been shown to protect the cell renewal systems of the intestine (*2, 3*) and bone marrow (*3, 4*) from radiation damage *in vivo* Pretreatment with some eicosanoids has enhanced survival of irradiated mice (*2, 3, 5–7*). Although evidence suggests that the eicosanoids protect by first binding to specific receptors (*8*), subsequent events leading to radiation protection are not known.

Reports of radiation protection by prostaglandins *in vitro* have been less consistent in their results and conclusions than those *in vivo*. Both Prasad (*9*) and Lehnert (*10*) reported *in vitro* radiation protection of CHO cells and V79 cells, respectively, by PGE_1. These investigators associated elevated levels of adenosine 3',5'-cyclic monophosphate (cAMP) with the radioprotection. PGE_1 is the one prostaglandin that has been shown to have no radioprotective activity *in vivo* in the mouse intestine (*11*). In contrast to the work of Prasad (*9*) and Lehnert (*10*), Millar and Jinks (*12*) were unable to demonstrate radiation protection in V79 cell lines using PGE_1 and eicosanoids of the A series and were also unable to modify radiation sensitivity of V79 and mouse fibrosarcoma cells with nonsteroidal anti-inflammatory agents (*13*). Likewise, Holahan and co-workers (*14*) failed to find radiation protection induced by PGE_2 in V79 cells. Walden *et al.* (*15*) reported slight radiation protection by pretreating V79 cells with leukotriene C_4 (LTC_4). However, their later investigations with PGE_2[1] failed to demonstrate radioprotection *in vitro* in cell lines from transformed rat granulosa and mouse fibrosarcoma. Cells from both lines did not bind radiolabeled PGE_2, which suggests that these cells lacked receptors for this eicosanoid. Lastly, Hanson and DeLaurentiis found (*16*) that M-1 melanoma cells were protected *in vitro* from radiation by 16,16-dimethyl PGE_2 but only when cells were grown as spheroids and not as cell monolayers. Their observations implicate the possible role of cell–cell contact, cell shape, or cell interaction with growth media in prostaglandin-induced radioprotection.

The lack of consistency in results using cultured cell lines reported in the literature prompted the investigations into eicosanoid-induced radioprotection *in vitro* reported here. We compared these results to those obtained using the aminothiol radioprotector WR-1065. Bovine aortic endothelial cells were chosen for these studies for a variety of reasons: (1) The radiation response of endothelial cells is important in the pathogenesis of radiation-induced destruc-

[1] N. K. Farzaneh, J. M. Speicher, T. Fitz, and T. L. Walden, Jr., Absence of prostaglandin E2-induced radioprotection in two cell lines lacking specific PGE2-binding sites. Presented at the 37th Annual Meeting, Radiation Research Society, Seattle, WA, 1989.

0033-7587/91 $3.00

tion of normal tissue (*17, 18*) and tumors (*19, 20*). (2) Cultures of endothelial cells from bovine aorta have been irradiated and their cytotoxic and biochemical responses have been characterized in our laboratory (*21–25*). (3) Endothelial cells from a culture strain that maintain differentiated endothelial function could be compared to freshly harvested cells (*23*). Specifically, the endothelial cells in this study had angiotensin-converting enzyme activity, von Willebrand factor-related antigen, a cobblestone appearance at confluency, and predominantly a G_1/G_0-phase cell cycle distribution without aneuploidy, and were not immortalized in culture. (4) The interaction of the eicosanoids and the endothelium is an important area of investigation considering that the most prominent endothelial eicosanoids, PGI_2 and PGE_2, help regulate vasoreactivity, thrombosis, and aspects of the inflammatory response. (5) Changes in the levels of PGI_2 production have been associated with endothelial cell damage after irradiation (*25–27*).

MATERIALS AND METHODS

Cell Culture

Endothelial cells were from thoracic aortas of freshly slaughtered 2-year-old steers. The cells were isolated, grown (*21–23*), and identified (*28–30*) as reported previously. Each observation, "*n*", represents a vial of cells that were thawed, plated at a density of 2×10^5/dish (35 mm), and grown simultaneously in 70–100 dishes When the cells reached visual confluence 3–4 days after plating, they were tested.

Addition of Eicosanoids

Prostaglandins (PGs) A_2, D_2, E_1, I_2, and 16,16-dimethyl PGE_2 were gifts from the Upjohn Company (Kalamazoo, MI). A PGE_1 analog, misoprostol, was a gift from G. D. Searle and Company (Skokie, IL). The LTC_4 was obtained from Biomol Research Laboratories (Philadelphia, PA). Stock solutions were made in ethanol to a concentration of 1 mg/ml and final concentration of the PGs in the cultures was 10 μg/ml. The LTC_4 was supplied in a solvent mixture of methanol:water:acetic acid:ammonium hydroxide (65.35.0.08.0.04) and final culture concentration was 1 μg/ml. The PGs and LTC_4 were stored at −70°C prior to use. When cell confluence was reached, the culture medium was changed to 2% FBS (v/v) to reproduce experimental conditions in previous investigations of irradiated bovine aortic endothelial cells (*21–25*) and to minimize the eicosanoid degradation induced by albumin and the enzymes present in serum (*31*). After the change in medium, each PG or LTC_4 was added. The vehicle for each eicosanoid was added to control cultures.

For "positive" control experiments, the widely studied aminothiol radioprotector WR-1065 (*32*) (1 m*M* final concentration) was added to separate cultures to determine that the endothelial cells in this study could be protected by classical methods.

Irradiation

Eicosanoids were added 1 h prior to irradiation The radiation protocols were similar to those reported previously (*21–25*). Cells were exposed to ^{137}Cs (GammaCell 40R, Atomic Energy of Canada, Ltd.) at a rate of 104 cGy/min under ambient conditions. Most experiments tested the effects of 500 cGy and a smaller number tested a range of radiation dose from 0 to 1000 cGy. Control cultures were sham-irradiated (0 Gy).

Assays of Cytotoxicity

Cells were returned to the incubator and analyzed for number of adherent cells at 4 and 24 h after irradiation as described previously (*21–25*). Cultures were rinsed with Hanks Balanced Salt Solution (HBSS, calcium/magnesium-free, GIBCO, Grand Island, NY) and the cells were removed with trypsin (0.05% w/v) and EDTA (0.02% w/v) (GIBCO) for measurement of cell number using a Coulter counter (Coulter Electronics, Hialeah, FL).

In experiments to measure cell survival leading to colony formation, cells were removed with trypsin/EDTA immediately after irradiation and replated onto culture dishes (100 mm). Cell density for plating was 5×10^3/dish at 0 Gy and was increased in graded numbers for higher radiation doses. Cultures were incubated under routine conditions for 7–10 days and the resulting colonies were stained and fixed *in situ* with cold methylene blue (0.5% w/v) in EtOH (70% v/v) for 20 min. Colonies were counted manually and survival parameters were calculated as described (*33*).

Assays of DNA Synthesis and cAMP

DNA synthesis was determined by measuring incorporation of [^{3}H]TdR into cultured cells. One microcurie [^{3}H]TdR (18.2 μCi/mmol, Dupont-New England Nuclear, Boston, MA) was added to the cultures for 1 h beginning 3 h after irradiation as described previously (*25*). Cells were removed with trypsin and their contents precipitated in a 10% (w/v) solution of trichloroacetic acid (TCA). The precipitate was solubilized in a solution of 1 *N* NH_4OH. Radioactivity in the TCA precipitate was counted by liquid scintillation (MARK III, TM Analytic, Elk Grove, IL) and the amount of [^{3}H]TdR incorporated per dish was corrected for the number of adherent cells.

Levels of cAMP were determined by radioimmunoassay (kit from Amersham, Arlington Heights, IL) in samples that were extracted in acetic ethanol as described (*34*). Approximately 15×10^6 cells were sampled for each assay and the level of cAMP was corrected for cell number. Pilot studies demonstrated that isobutylmethylxanthine (IBMX, 10^{-5} *M*, an inhibitor of phosphodiesterase) enhanced the elevation of cAMP in the cultured endothelial cells. Therefore, a change in the level of cAMP after eicosanoid treatment was examined with and without the addition of IBMX.

Binding of LTC_4 and PGE_2

Radiolabeled LTC_4 and PGE_2 were added to endothelial cells that were prepared in the following ways. (1) scraped directly from a thoracic aorta of a recently slaughtered steer, (2) removed from the aorta by use of collagenase, (3) scraped from a subculture, and (4) removed with trypsin/EDTA from a subculture. The endothelial cells were stored at −40°C prior to the binding assays.

Assays for specific binding of LTC_4 were conducted as described previously (*35*). Briefly, assays contained 1×10^6 endothelial cells, 25 m*M* HEPES, pH 7.35, 78 fmol [^{3}H]LTC_4 [14,15(N)^{3}H] leukotriene C_4, sp act 38.4 Ci/mmol, DuPont New England Nuclear, Boston, MA) and 10 m*M* serine borate in 100 μl of HBSS (containing calcium and magnesium) (*36*). Binding studies were done on ice over a 30-min incubation to minimize the enzymatic degradation of LTC_4. Nonspecific binding was determined in a parallel series of assay tubes to which unlabeled LTC_4, LTD_4, or LTE_4 was added to a final concentration of 2.56 pmol. After incubation, cells were pelleted by centrifugation and the radioactivity in the pellet was counted by liquid scintillation. All assays were performed in triplicate or quadruplicate. Twelve- to 16-point Scatchard analyses were performed using a fixed amount of radiolabeled LTC_4 and varying the concentration of unlabeled LTC_4. Data thus obtained were fitted by linear regression to one-site binding models using the LIGAND binding analysis program.

The same binding assay protocols used for LTC_4 were used for studying PGE_2 binding by substituting radiolabeled PGE_2 [5,6,8,11,12,14,15(N)-^{3}H]PGE_2, sp act 200 Ci/mmol, DuPont–New England Nuclear) and unlabeled PGE_2 for the LTC_4. Serine-borate was not present in the PGE_2 binding assays.

Metabolism of LTC_4

The [^{3}H]LTC_4 was incubated with tissue culture medium (FBS, 10% v/v) or with approximately 1×10^6 endothelial cells that had been scraped from cultures and stored at −40°C. Before storage, the cells were washed with HBSS and pelleted by centrifugation three times to remove the FBS, which is a source of γ-glutamyl transpeptidase, an enzyme capable of metabolizing LTC_4 to LTD_4. As a further precaution, incubations with the leukotriene were conducted in the presence of serine-borate, a transition state inhibitor of γ-glutamyl transpeptidase (*37*). For analysis of the cellular metabolism, the cells were thawed and resuspended in 400 μl of HBSS containing 25 m*M* HEPES buffer, pH 7.35, and 30 nCi of [^{3}H]LTC_4 adjusted to 1 μg of LTC_4/ml. For analysis of the metabolism by the media, 400 μl of the media was buffered as indicated and was incubated with labeled and unlabeled LTC_4. The leukotriene was incubated with the cells or the media for 30 min at either 4 or 37°C. After the incubations the samples were extracted by the addition of 40 μl of formic acid, 75 μl of isopropyl alcohol, and 800 μl of ethyl acetate. The upper organic fraction containing the leukotrienes was removed and evaporated to dryness under nitrogen. The evaporated samples were resuspended in 35 μl of the high-pressure liquid chromatography (HPLC) solvent (see below) and injected into the HPLC system for analysis. The recovery efficiency for labeled leukotrienes using this extraction procedure is approximately 95%.

High-Pressure Liquid Chromatography (HPLC)

Analyses by HPLC were performed as described previously (*15*) using an IBM Model 9560 Ternary Gradient Liquid Chromatography System (IBM Instruments, Orchard Park, CT). Samples were chromatographed on a narrow-bore Altech C-18 column, 250 × 2 mm, containing 5-μm particles, and eluted with an isocratic solvent system consisting of acetonitrile (Burdick Jackson, Muskegon, MI) and 5 m*M* KH_2PO_4 in water (pH 4.2), in a 1:2 ratio, at a flow rate of 1 ml/min (*15*). The eluant was automatically mixed with liquid scintillation solvent (Tru-Count, IN/US Instruments, Fairfield, NJ) and the labeled leukotriene metabolites were detected using a RAMONA-D radiation flow through monitor (IN/US Instruments) attached to the HPLC system.

Statistical Analysis

All observations were made on duplicate or triplicate culture dishes chosen from a set of 20 to 60 replicate cultures that were plated and grown simultaneously. The number of total observations, *n*, is indicated where appropriate for the different experimental conditions. Statistical analysis was based on Student's paired *t* test when comparing simultaneously prepared control and experimental cultures. MANOVA techniques (SPSS and SYSTAT computer programs) were used to test for significant differences between multiple parameters such as changes over time or interaction between two drugs.

RESULTS

Radiation-Induced Endothelial Cytotoxicity

The number of adherent cells was not changed at 4 h after 5 Gy but at 24 h the cell number was reduced by approximately 25% (Table I). This reduction in cell number was preceded by a 25% reduction in [^{3}H]TdR incorporation per cell at 4 h after 5 Gy irradiation (Table I). Surviving fraction of irradiated cells was approximately 0.08 after 5 Gy based on colony formation. These findings are similar to our previous observations in irradiated endothelial cells (*22–26*).

In the irradiated cultures, pretreatment with the exogenous eicosanoids did not prevent loss of the number of adherent cells (Table I) or [^{3}H]TdR incorporation (Table I). Also after 5 Gy, colony formation was not affected by the following compounds: PGD_2, PGE_1, PGI_2, misoprostol, 16-16-dimethyl PGE_2, and LTC_4. In contrast to a protective effect, PGD_2 appeared to be cytotoxic. In the control nonirradiated cultures there were fewer cells after 24 h than in cultures that were not exposed to PGD_2 (Table I). In three of four experiments, PGA_2 also decreased the number of adherent cells at 24 h by approximately 25% ([mean ± SEM, × 10^6 cells] control = 2.6 ± 0.3 versus PGA_2 = 1.9 ± 0.4).

In contrast to the lack of radioprotection with the eicosanoids, WR-1065 enhanced survival after irradiation as measured by colony formation (control D_0 = 125 cGy versus 190 cGy for WR-1065-treated cells). However, WR-1065 did not consistently attenuate acute cell loss (data not shown).

Metabolism of LTC_4 by Endothelial Cells and Tissue Culture Medium

The LTC_4 was rapidly metabolized by both the tissue culture medium (10% FBS, v/v) and the endothelial cells. The unconditioned medium metabolized the LTC_4 to LTD_4 and LTE_4 (Fig. 1). Incubation of LTC_4 with the unconditioned medium at 37°C for 30 min resulted in 26% conversion to LTD_4, and 16% to LTE_4 with 58% remaining unmetabolized. This conversion does not take place in the presence of 10 m*M* serine-borate (data not shown) when the incubation was conducted on ice. Endothelial cells were scraped from the culture dish, rinsed of their medium containing serum, and stored at −40°C. When thawed, the endothelial cell samples metabolized LTC_4 to LTD_4, but did not further convert the LTD_4 to LTE_4 (Fig. 1). Thirty minutes after incubation of LTC_4 with the endothelial cells, 34% of the compound remained unmetabolized and 66% was converted to LTD_4.

Binding of LTC_4 and PGE_2

Endothelial cells have binding sites for [^{3}H]LTC_4 that were blocked entirely by unlabeled LTC_4. However, the specificity of this binding for LTC_4 is in question since the binding is reduced to approximately 85% of control when unlabeled LTD_4 was added (Table II). Unlabeled LTE_4 displaced approximately 15% of the LTC_4. The association

TABLE I
Number of Endothelial Cells and Incorporation of [^{3}H]TdR after Irradiation and Eicosanoid Treatment

Treatment	Time after irradiation (hours)	Cell adherence (1×10^6) 0 Gy	5 Gy	(*n*)	Incorporation of [^{3}H]TdR 0 Gy	5 Gy	(*n*)
Control	4	2.9 ± 0.2	2.5 ± 0.3	(7)	17.6 ± 3.0	13.3 ± 2.4*	(8)
	24	2.6 ± 0.3	1.6 ± 0.2*	(12)	—	—	
PGD_2	4	2.8 ± 0.2	2.8 ± 0.2	(4)	16.6 ± 2.9	12.1 ± 2.4*	(8)
	24	1.9 ± 0.3†	1.5 ± 0.2	(12)	—	—	
PGE_1	4	3.0 ± 0.2	3.0 ± 0.4	(4)	16.1 ± 3.3	12.4 ± 2.7*	(8)
	24	2.7 ± 0.3	1.7 ± 0.2*	(13)	—	—	
PGI_2	4	3.0 ± 0.3	3.1 ± 0.4	(4)	17.9 ± 3.4	13.3 ± 3.3**	(4)
	24	2.6 ± 0.3	1.7 ± 0.2*	(12)	—	—	
MISO	4	3.0 ± 0.2	2.7 ± 0.3	(4)	15.5 ± 2.5	13.4 ± 2.6‡	(8)
	24	3.1 ± 0.4	2.0 ± 0.3*	(7)	—	—	
16-16PGE_2	4	2.9 ± 0.1	2.6 ± 0.1	(6)	17.5 ± 5.3	13.7 ± 4.2‡	(7)
	24	2.9 ± 0.4	1.8 ± 0.3‡	(6)	—	—	
LTC_4	4	2.3 ± 0.3	2.2 ± 0.2	(4)	15.0 ± 0.6	10.6 ± 0.1*	(5)
	24	2.5 ± 0.2	1.4 ± 0.1*	(6)	—	—	

Note. Data are means ± SEM, significance of radiation effect (0 Gy versus 5 Gy). *$P < 0.005$, **$P < 0.001$, ‡$P < 0.025$, significance of eicosanoid effect (0 Gy versus 0 Gy): †$P < 0.001$.

rate for LTC_4 binding by the endothelial cells was very rapid and binding reached a plateau within 3 min following the addition of [^{3}H]LTC_4.

The bovine aortic endothelial cells tested directly from the vessel and from subcultures (8 passages, approximately 20 doublings after primary culture) possessed binding sites for [^{3}H]LTC_4. Expressed as percentage binding per 10^6 cells (mean ± SEM, $n = 3$, background binding = 2.18 ± 0.17, 5 nCi [^{3}H]LTC_4 per assay tube) endothelial cells scraped from subcultures bound three times more radiolabeled LTC_4 (34.62 ± 3.22) than the cells scraped directly from the vessel (11.84 ± 0.10). Harvesting the endothelial cells from the aorta by use of collagenase reduced the binding (3.44 ± 0.21). However, harvesting the subcultured cells by use of trypsin did not appear to alter the binding (36.72 ± 5.22).

The data obtained by Scatchard analysis are best fitted by a one-site binding model using the LIGAND binding analysis program. The K_D for the binding site is $1 \times 10^{-7} \pm 3 \times 10^{-8}$ *M* ($n = 6$), with a $B_{max} = 5 \times 10^{-8} \pm 2 \times 10^{-6}$ *M*. From this analysis it is estimated that there are 30,000 ± 12,000 binding sites per cell. Scatchard analysis and other binding studies indicated that [^{3}H]PGE_2 did not bind to endothelial cells isolated directly from aortas or removed from culture (data not shown).

cAMP

The endothelial cells had elevated cAMP levels after brief treatments with IBMX and eicosanoids (Fig. 2). Without drug exposure the average value of cAMP was 1.33 pg/10^6 cells (based on an analysis of 60 cultures). With methylxanthine, the levels rose two- to threefold within 5 min ($P < 0.001$ by Student's paired *t* test and $P < 0.025$ by MANOVA). Mean values for the cAMP levels dropped over the 30 min following methylxanthine administration, but this change was not statistically significant.

When the eicosanoids were added without IBMX, cAMP levels were not elevated under the experimental conditions reported here. Misoprostol (10 μg/ml and 100 μg/ml), 16, 16-dimethyl PGE_2 (10 μg/ml), or LTC_4 (1 μg/ml) did not increase the level of cAMP measured at 5, 15, 30, and 60 min after the drugs were added. Data for 10 μg/ml concentrations of misoprostol and 16-16 dimethyl PGE_2 are shown in Fig. 2. Five minutes after the addition of 100 μg/ml misoprostol or of LTC_4, cAMP levels were 1.1 pmol/10^6 cell for both treatments (average of $n = 2$ for each). The highest cAMP levels were seen after cotreatments with 16,16-dimethyl PGE_2 and IBMX that elevated the levels nearly five times the baseline values (Fig. 2). Student's paired *t* test indicated that the combination of IBMX and 16,16-dimethyl PGE_2 had a greater effect than IBMX alone ($P < 0.01$) or 16,16-dimethyl PGE_2 alone ($P < 0.001$); however, a Bonforoni adjustment after MANOVA testing did not demonstrate a significant difference ($0.05 \leq P < 0.1$) between IBMX alone and IBMX with the 16,16-dimethyl PGE_2. Misoprostol did not enhance the IBMX effect on the levels of cAMP.

Despite the elevated levels of cAMP, IBMX alone and IBMX plus 16,16-dimethyl PGE_2 did not modify the radiation induced reduction of colony formation, number of adherent cells, or [^{3}H]TdR incorporation (data not shown).

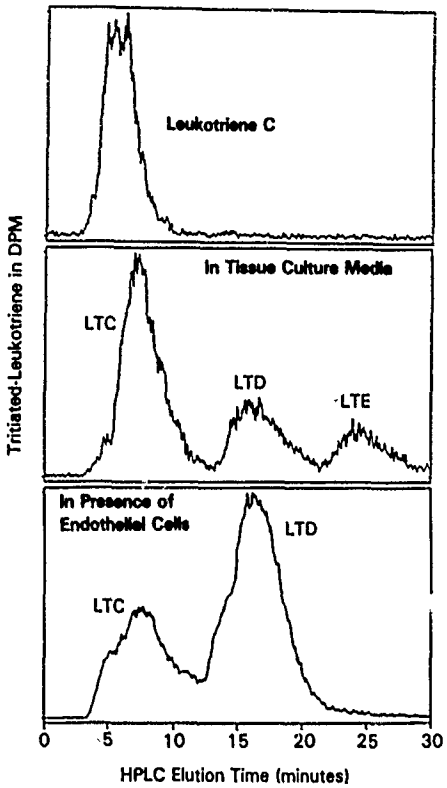

FIG. 1. Leukotriene C_4 metabolism by medium and by endothelial cells. [^{3}H]LTC_4 was incubated in the presence of RPMI-1640 culture medium with or without the addition of fetal bovine serum. Three HPLC chromatograms are shown in this figure. The top chromatogram shows an unmetabolized standard of LTC_4, and the middle shows the metabolism of LTC_4 by culture medium containing 10% (v/v) serum. The bottom chromatogram shows metabolism of LTC_4 by endothelial cells in the absence of serum.

Again, the significance of the radiation-induced changes in thymidine incorporation was $P < 0.001$ for all conditions.

DISCUSSION

Contrary to results found *in vivo*, the eicosanoids did not protect cultured vascular endothelial cells from radiation injury. This absence of eicosanoid-induced protection appears to be unrelated to the classic mechanism of thiol radioprotection since WR-1065 protected the endothelial cells from some degree of radiation injury. Likewise, eicosanoid-induced increases in cAMP levels alone were not sufficient to produce radiation protection. Unlike cultured bovine aortic endothelial cells in one other report (*37*), the endothelial cells used in this investigation did not have a high degree of specific binding for LTC_4. PGE_2 binding was also absent in these endothelial cells, a deficiency that in other cells is associated with a lack of radioprotection by eicosanoids.[1]

The implications of these results are twofold. First, cytoprotection *in vivo* by the eicosanoids may require a physiological system that cannot easily be duplicated with isolated cells *in vitro*. Second, it may not be possible to induce radioprotection with eicosanoids in every cell type, particularly in the endothelial cells from bovine aorta.

We speculate that the inability to demonstrate radioprotection in the vascular endothelial cell strains is linked to the absence of specific ligand–receptor binding for PGE_2 and LTC_4. That receptors for eicosanoids are important for

TABLE II
Time Course and Specificity of Leukotriene C_4 Binding by Endothelial Cells

Incubation time (s)/ Conditions	Amount [^{3}H]LTC_4 bound (dpm) minus background binding
0	0
20	156 ± 1
30	334 ± 68
60	588 ± 47
90	659 ± 64
120	715 ± 3
150	811 ± 57
150 + unlabeled LTC_4	0
+ unlabeled LTD	126 ± 25
+ unlabeled LTE_4	621 ± 123
Total [^{3}H]LTC_4 (dpm/assay)	6900 ± 412

Note. Data are means ± SEM, $n = 6$.

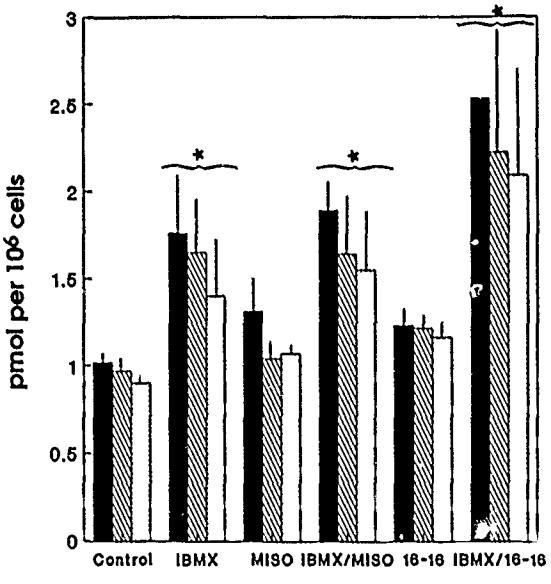

FIG. 2. Levels of cAMP in control cultures of endothelial cells or in cultures treated with misoprostol (designated MISO in figure) or 16, 16-dimethyl PGE_2 (designated 16-16) alone or with IBMX. Values are presented as pmol per 10^6 cells at three different times after administration (solid = 5 min, hatched = 15 min, dotted = 30 min). Data are the means ± SEM, $n = 5$. *Significantly increased levels after addition of IBMX with or without the prostaglandin analog ($P < 0.001$).

radioprotection is based on evidence that different isomeric forms of PGs impart different degrees of radioprotection *in vivo* (*8*). One cannot rule out the possibility that the effect of eicosanoids is independent of receptors. The previous report on LTC_4 binding to bovine aortic endothelial cells demonstrated a binding two orders of magnitude higher than reported here (*37*), but the earlier study was conducted on membrane preparations rather than on whole cells. Perhaps the membrane preparation unmasks receptors not measured by our techniques. It is not clear at this time whether the binding site we have observed is, in part, a specific receptor or another protein capable of binding LTC_4. For example, glutathione S-transferase (*41*) and several other proteins have been reported to bind LTC_4 through recognition of the glutathione moiety. The displacement of LTC_4 binding by LTD_4 suggests this possibility and strongly mitigates against specific LTC_4 receptors (*42*) associated with our endothelial cells grown under the stated conditions. In addition, our evidence of endothelial cell conversion of LTC_4 to LTD_4 and the inhibition of this conversion by serine borate indicates that these cells probably possess γ-glutamyl-transpeptidase, another candidate for the LTC_4-binding protein. The lack of LTC_4-induced radioprotection could be attributed to an absence of or reduced number of specific receptors, or to the inactivation of LTC_4 at the endothelial cell surface before it can induce radioprotection.

Protection of blood vessels *in vivo* by eicosanoids is found in studies of gastrointestinal ethanol toxicity and is not directly comparable to radiation-induced cytotoxicity. The microvasculature, and presumably the endothelium of the microvasculature, in the stomach of rats is protected from ethanol-induced destruction by a prostaglandin E_2 analog (*38*). Since eicosanoids protect a variety of cells *in vivo* from radiation and other toxic conditions, we still suspect that eicosanoids can also protect endothelial cells; but, if eicosanoid receptors are required for radioprotection and if endothelial cells isolated directly from the bovine aorta bind less LTC_4 than they do in culture, perhaps only endothelial cells of certain vessels can be protected by eicosanoids.

As suggested from work by Hanson and co-workers (*5, 39*), the mechanism of radioprotection by thiol compounds such as WR-2721 is different from that of eicosanoids. As a cell monolayer, the endothelial cells were protected by WR-1065 (the dephosphorylated form of WR-2721) but not by the various eicosanoids. Therefore, the *in vitro* results reported here also suggest that the mechanism of protection by eicosanoids and the thiol WR-1065 are different from one another.

Contrary to the reports by Prasad (*9*) and Lehnert (*10*), our observations do not support the hypothesis that elevation of cAMP plays a principal role in eicosanoid-induced radiation protection. Others have noted effects of eicosanoids that appear independent of cAMP. For example, Hughes-Fulford and colleagues reported (*41*) that DNA synthesis and cell cycle progression are inhibited by prostaglandins in nonendothelial cells through mechanisms not dependent on changes in cAMP.

A significant finding in the studies reported here was the loss of adherent endothelial cells after PGD_2 and PGA_2 treatments, a loss that was not apparent after treatment with the other eicosanoids. Evidence suggests that these two cyclopentenone PGs inhibit cell proliferation in nonendothelial cells (*43, 44*). One putative mechanism for this effect is that PGD_2 is converted to δ-12-PGJ_2 that binds to membranes and nuclei, stimulates production of heat-shock proteins, inhibits expression of c-myc, and blocks entry of G_1-phase cells into S phase (*44*). If this phenomenon were to occur in a cell monolayer where cell renewal is active (*23, 45*), a reduced number of adherent cells would be noted after one cell cycle as it was in these experiments. Under conditions where endothelial cell proliferation is active, such as in tumors, transplanted organs, or chronic inflammation, selective inhibition of endothelial cell division by eicosanoids might be useful therapeutically.

ACKNOWLEDGMENTS

This work was supported by, NIH HL-41155-02, The American Cancer Society, Illinois Division, Inc., The Upjohn Company, Rush University, Department of Defense Contract #DNA001-86-0038 (W.R.H.), and by the Armed Forces Radiobiology Research Institute, Defense Nuclear Agency, under Research Work Unit 00152 (T.W.). No endorsement by the Defense Nuclear Agency has been given or should be inferred. We thank Mary Grover for her technical assistance, Dr. Marija Norusis, Biostatician, Department of Preventive Medicine (RPSLMC) for assistance with statistical analysis, and Soledad S. Callejas, Medical Science Liaison of The Upjohn Company.

RECEIVED: February 13, 1990; ACCEPTED. August 3, 1990

REFERENCES

1 A. ROBERT, J. E. NEZAMIS, C. LANCASTER, and A. J. HANCHAR, Cytoprotection by prostaglandins in rats: Prevention of gastric necrosis produced by alcohol, HCl, NaOH, hypertonic NaCl and thermal injury. *Gastroenterology* 77, 433–443 (1979).

2. W. R. HANSON and C. THOMAS, 16-16 Dimethyl prostaglandin E_2 increases survival of murine intestinal stem cells when given before photon irradiation. *Radiat. Res.* 96, 393–398 (1983).

3 W. R. HANSON and L. J. AINSWORTH, 16,16-Dimethyl prostaglandin E_2 induces radioprotection in murine intestinal and hematopoietic stem cells. *Radiat. Res.* 103, 196–203 (1985).

4 T. L. WALDEN, JR., M. L. PATCHEN, and T. J. MACVITTIE, Leukotriene-induced radioprotection of hematopoietic stem cells. *Radiat. Res.* 113, 388–395 (1988).

5. W. R. HANSON, K. HOUSEMAN, and P. W. COLLINS, *In vivo* radiation protection by prostaglandins and related compounds of the arachidonic acid cascade. *Pharmacol. Ther.* 39, 347–356 (1988).

6 T. L. WALDEN, JR., L. PATCHEN, and S. L. SNYDER, 16 16-Dimethyl prostaglandin E_2 increases survival in mice following irradiation *Radiat. Res.* 109, 440–448 (1987).

7 T. L. WALDEN, JR., Pretreatment with leukotriene C_4 enhances the whole-animal survival of mice exposed to ionizing radiation. *Ann. NY Acad. Sci.* 524, 431–433.

8. W. R. HANSON, K. A. HOUSEMAN, A. K. NELSON, and P. W. COL-

LINS, Radiation protection of the murine intestine by misoprostol, a prostaglandin E_1 analogue, given alone or with WR-2721, is stereospecific. *Prostaglandins Leukotrienes Essential Fatty Acids* **32**, 101–105 (1988).

9. K. N. PRASAD, Radioprotective effect of prostaglandin and an inhibitor of cyclic nucleotide phosphodiesterase on mammalian cells in culture. *Int. J. Radiat. Biol.* **22**, 187–189 (1972).
10. S. LEHNERT, Modification of postirradiation survival of mammalian cells by intracellular cAMP. *Radiat. Res.* **62**, 107–116 (1975).
11. W. R. HANSON and K. DELAURENTIIS, Comparison of *in vivo* murine intestinal radiation protection by E-prostaglandins. *Prostaglandins* **33**, Suppl., 93–104 (1987).
12. B. C. MILLAR and S. JINKS, Do prostaglandins affect cellular radiosensitivity? *Int. J. Radiat. Biol.* **46**, 367–373 (1984).
13. B. C. MILLAR, S. JINKS, and T. J. POWLES, Flurbiprofen, a nonsteroidal anti-inflammatory agent, protects cells against hypoxic cell radiosensitizers *in vitro*. *Br. J. Cancer* **44**, 733–740 (1981).
14. E. V. HOLAHAN, JR., W. F. BLAKELY, and T. L. WALDEN, JR., Effect of PGI_2 on radiation response of Chinese hamster V-79 cells *in vitro*. In *Prostaglandin and Lipid Metabolism in Radiation Injury* (T. L. Walden, Jr., and H. N. Hughes, Eds.), pp. 253–262. Plenum, New York, 1987.
15. T. L. WALDEN, JR., E. V. HOLAHAN, and G. N. CATRAVAS, Development of a model system to study leukotriene-induced modification of radiation sensitivity in mammalian cells. *Prog. Lipid Res.* **25**, 587–590 (1986).
16. W. R. HANSON and K. DELAURENTIIS, Human melanoma spheroids are protected from radiation injury by 16,16-dimethyl PGE_2. *Proc. Am. Assoc. Cancer Res.* **26**, 68a (1985). [Abstract]
17. J. W. HOPEWELL, The importance of vascular damage in development of late radiation effects in normal tissues. In *Radiation Biology in Cancer Research* (R. E. Meyn and H. R. Withers, Eds.), pp. 449–459. Raven Press, New York, 1980.
18. M. P. LAW, Radiation-induced vascular injury and its relation to late effects in normal tissues. *Adv. Radiat. Biol.* **9**, 37–73 (1981).
19. J. DENEKAMP, Changes in the rate of proliferation in normal tissues after irradiation. In *Radiation Research: Biomedical, Chemical, and Physical Perspectives* (O. F. Nygaard, H. I. Adler, and W. K. Sinclair, Eds.), pp. 810–825. Academic Press, New York, 1975.
20. J. DENEKAMP, Endothelial cell proliferation as a novel approach to targeting tumor therapy. *Br J Cancer* **45**, 136–139 (1982).
21. D. B. RUBIN, E. A. DRAB, W. F. WARD, L. J. SMITH, and S. M. FOWELL, Enzymatic responses to radiation in cultured vascular endothelial and smooth muscle cells. *Radiat. Res.* **99**, 420–432 (1984).
22. T. T. LAM, D. B. RUBIN, and E. A. DRAB, The effect of dexamethasone on the cytotoxic and enzymatic response of cultured endothelial cells to radiation. *Radiat. Res.* **103**, 240–250 (1985).
23. D. B. RUBIN, E. A. DRAB, W. F. WARD, and K. D. BAUER, Cell cycle changes and cytotoxicity in irradiated cultures of bovine aortic endothelial cells. *Radiat. Res.* **108**, 206–214 (1986).
24 D. B. RUBIN, E. A. DRAB, W. F. WARD, and K. D. BAUER, Cell cycle progression in irradiated endothelial cells cultured from bovine aorta. *Radiat. Res.* **116**, 364–371 (1988).
25 D. B. RUBIN, E. A. DRAB, C. TS'AO, D. GARDNER, and W. F. WARD, Prostacyclin synthesis in irradiated endothelial cells cultured from bovine aorta. *J. Appl Physiol.* **58**, 592–597 (1985).
26 A. ELDOR, I. VLODAVSKY, E. HYAM, R. ATZMON, and Z. FUKS, The effect of radiation on prostacyclin (PGI_2) production by cultured endothelial cells. *Prostaglandins* **25**, 263–279 (1983).
27. G. L. HAHN, M. J. MENCONI, M. CAHILL, and P. POLGAR, The influence of gamma radiation on arachidonic acid release and prostacyclin synthesis. *Prostaglandins* **25**, 783–791 (1983).
28. M. A. GIMBRONE, JR., Culture of vascular endothelium. *Prog. Hemostasis* **3**, 1–28 (1976).
29. J. W. RYAN, A. CHUNG, L. C. MARTIN, and U. S. RYAN, New substrates for the radioassay of angiotensin converting enzyme of endothelial cells in culture. *Tissue Cell* **10**, 555–562 (1978).
30. E. A. JAFFE, R. L. NACHMAN, C. G. BECKER, and R. MINICK, Culture of human endothelial cells derived from umbilical veins. Identification by morphologic and immunologic criteria. *J. Clin. Invest.* **52**, 2745–2757 (1973).
31. F. A. FITZPATRICK and M. A. WYNALDA, Albumin-lipid interactions: Prostaglandin stability as a probe for characterizing binding sites on vertebrate albumins. *Biochemistry* **20**, 6129–6134 (1981).
32. C. P. SIGDESTAD, S. H. TREACY, L. A. KNAPP, and D. J. GRDINA, The effect of 2-[(aminopropyl)-amino] ethanethiol (WR-1065) on radiation induced DNA double strand damage and repair in V79 cells. *Br. J. Cancer* **55**, 477–482 (1987).
33. E. J. HALL, Cell survival curves. In *Radiobiology for the Radiologist*, 2nd ed., pp. 30–38. Harper and Row, Hagerstown, MD, 1978.
34. B. L. BROWN, J. D. M. ALBANO, R. P. EKINS, and A. M. SGHERZI, A simple and sensitive saturation assay method for the measurement of adenosine 3',5'-cyclic monophosphate. *Biochem. J.* **121**, 561–562 (1971).
35. T. L. WALDEN, JR., N. K. FARZANEH, and L. RICHARDS, Lipoxygenase products in radiation injury and radioprotection. In *Leukotrienes and Prostanoids in Health and Disease* (U. Zor, Z. Naor, and A. Danon, Eds.), Vol. 3, pp. 154–160. Karger, Basel, 1989.
36. S. S. TATE and A. MEISTER, Serine-borate complex as a transition state inhibitor of gamma-glutamyl transpeptidase. *Proc. Natl. Acad. Sci. USA* **75**, 4806–4809 (1978).
37 A. MULLER, C. GHIGHERI-BERTEZ, G. MODAT, and C. BONNE, Specific binding of leukotriene C_4 to endothelial cell membranes. *Prostaglandins Leukotrienes Med.* **26**, 233–240 (1987).
38. P. O'BRIEN, C. SCHULTZ, B. GANNON, and J. BROWNING, Protective effects of the synthetic prostaglandin enprostil on the gastric microvasculature after ethanol injury in the rat. *Am. J. Med.* **81**, Suppl. 2A, 12–17 (1986).
39. W. R. HANSON, Radioprotection of murine intestine by WR-2721, 16,16-dimethyl prostaglandin E_2 and the combination of both agents. *Radiat. Res.* **111**, 361–373 (1987).
40. M. HUGHES-FULFORD, J. WU, T. KATO, and M. FUKUSHIMA, Inhibition of DNA synthesis and cell cycle by prostaglandins independent of cAMP. In *Advances in Prostaglandin, Thromboxane and Leukotriene Research*, Vol. 15, pp. 401–404. Raven Press, New York, 1985.
41 F F. SUN, L.-Y CHAU, B. SPUR, E. J. COREY, R. A. LEWIS, and K. F. AUSTIN, Identification of a high affinity leukotriene C_4 binding protein in rat liver cytosol as glutathione-S-transferase. *J. Biol. Chem.* **261**, 8540–8546 (1986).
42 R P ROBERTSON, Characterization and regulation of prostaglandin and leukotriene receptors: An overview. *Prostaglandins* **31**, 395–412 (1986).
43 K IKAI, M UJIHARA, M KASHIWARA, and M. FUKUSHIMA, Inhibition of the proliferation of transformed epidermal cells in culture by various prostaglandins. *J. Invest. Dermatol.* **89**, 69–72 (1987).
44 K OHNO, M FUKUSHIMA, M FUJIWARA, and S. NARUMIYA, Induction of 68,000-dalton heat shock proteins by cyclopentenone prostaglandins. Its association with prostaglandin-induced G_1 block in cell cycle progression. *J. Biol. Chem.* **263**, 19764–19770 (1988).
45 G. M HAHN and J. B. LITTLE, Plateau-phase cultures of mammalian cells: An *in vitro* model for human cancer. *Curr. Top. Radiat. Res. Q.* **8**, 39–83 (1972).

Journal of Biomolecular Structure & Dynamics, ISSN 0739-1102
Volume 8, Issue Number 5 (1991), ©Adenine Press (1991).

Synthesis and Characterization of Stereoisomers of 5,6-Dihydro-5,6-Dihydroxythymidine

Y. Vaishnav[1], E. Holwitt[1†], C. Swenberg[1],
H.-C. Lee[2‡] and L.-S. Kan[2*]
[1]Radiation Biochemistry Department
Armed Forces Radiobiology Research Institute
Bethesda, MD 20889-5145

[2]Department of Biochemistry, School of Hygiene and Public Health
The Johns Hopkins University
615 North Wolfe Street, Baltimore, MD 21205

Abstract

Six products were isolated by reverse phase HPLC from the reaction of thymidine with osmium tetroxide. Four of the products were identified as stereoisomers of 5,6-dihydro-5,6-dihydroxythymidine (TG). The absolute configurations of these four compounds (from the shortest to the longest HPLC retention times) were determined by two-dimensional nuclear magnetic resonance spectroscopy to be (−)-*trans*-5S,6S-, (+)-*trans*-5R,6R-, (−)-*cis*-5R,6S-, and (+)-*cis*-5S,6R-5,6-dihydro-5,6-dihydroxythymidine. The other two products were dimers with unknown linking sites. Parameters of the mass and nuclear magnetic resonance spectra are reported and discussed.

Introduction

The base thymine in DNA may convert either to *cis*- or *trans*-5,6-dihydro-5,6-dihydroxy-thymidine, otherwise known as thymidine glycol (TG) (Figure 1), by oxidation and/or ionizing radiation *in vivo* and *in vitro* (1). Formation of the TG lesion is known to cause distortions in DNA local conformation, disrupting base pairing with the complementary nucleic acid strand (2-4). In an earlier investigation TG was positioned at a unique site in the single stranded genome of a bacteriophage M13mp19 derivative. From this alteration the replication of the genome in *E. Coli.* yielded targeted mutations at a frequency of 0.3%; these mutations were exclusively thymine to cytosine (5). The lethal effect of putative TG in M13mp8 phage DNA has been extensively examined and the phage survival probability as a function of TG dose has been determined (6). *In vitro*, TG lesion in DNA strongly inhibits DNA elongation. In all these investigations the identity of the particular TG stereoisomer

†Current address: USAF School of Aerospace Medicine, Brooks Air Force Base, TX 78235.
‡Current address: Georgetown Medical School, Washington, D.C.
*Author to whom correspondence should be addressed.

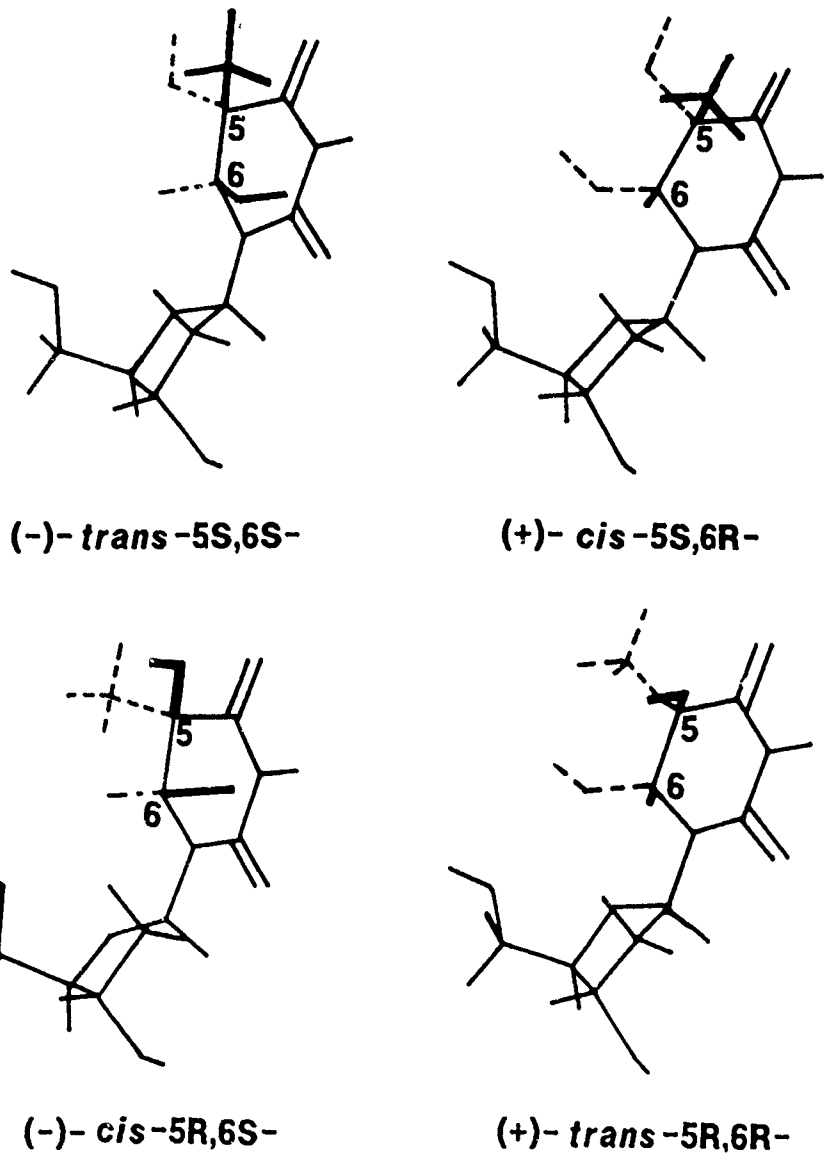

Figure 1: Molecular structure of all four stereoisomers of thymidine glycol produced by Alchemy II program (Tripos Associates, St. Louis, MO) on an IBM P/C-50 personal computer.

(or stereoisomers (Figure 1)) involved is unclear. Modeling studies suggest, however, that the isomer *in vivo* is (−)-*cis*-5R,6S-5,6-dihydro-5,6-dihydroxy-thymidine (5). As a preliminary step towards future investigation concerned with the incorporation of a specific isomer in a known oligomer, we report here a complete characterization of all four TG stereoisomers by the techniques of mass spectrometry (MS) and nuclear magnetic resonance spectroscopy (NMR). The four isomers (shown as Figure 1) were initially separated by HPLC after the oxidation reaction of thymidine with osmium tetroxide. The reported synthesis and partial characterization of the TG

stereoisomers were first reported in the late seventies (7,8). The synthetic protocol introduced here is easy and efficient. Most researchers produce TG by the permanganate oxidation of thymidine (1,9-12). However, the reaction conditions for the permanganate oxidation of thymidine must be strictly controlled to maximize the production of TG and prevent formation of 5-hydroxy-5-methylbarbituric acid deoxyriboside (12) and other products (1). Furthermore, to obtain TG, it is essential to purify it from the other products by column chromatography. While Howgate and co-workers (1) did prepare TG using osmium tetroxide, their procedure required three weeks and paper chromatography to separate the glycol from an impurity before obtaining pure TG. The protocol presented here does not require any chromatography and only yields TG crystals, consisting in excess of 60% of one stereoisomer, (−)-*cis*-5R,6S-5,6-dihydro-5,6-dihydroxythymidine.

Materials and Methods

Chemicals: Thymidine and osmium tetroxide were obtained from Chemical Dynamics Corp. (S. Plainfield, NJ) and Colonial Metals, Inc. (Elkton, MD), respectively. Potassium chlorate was purchased from Mallinckrodt, Inc. (St. Louis, MO). Bis(trimethlsilyl)trifluoroacetamide (BSTFA) and acetonitrile were purchased from Pierce Chemical Co. (Rockford, IL). All other solvents used in this report were from Fisher Co. (Pittsburgh, PA) and used without further purification.

The Oxidation Reaction: 0.8 gram of thymidine was dissolved in 50 mL of water and 1.0 gram of osmium tetroxide was then added. The solution was stirred for four days at room temperature during which the color of the reaction mixture darkened. Afterward 1.67 grams of potassium chlorate ($KClO_3$) was added and the solution was stirred for an additional hour or until the solution became transparent with a slight yellow color. The solution was then extracted three times with 50 mL of chloroform each time to remove osmium tetroxide and the organic phase was discarded. The aqueous phase was collected and lyophilized. The dry powder was resuspended in 50 mL of boiling methanol. The suspension was filtered while still hot. The undissolved material, which was mostly potassium chlorate, was discarded. The filtrate was gradually cooled to room temperature then filtered again to remove any additional precipitate. The methanol solution was then evaporated to dryness. The powder was resuspended in 50 mL of boiling 2-propanol and again filtered to remove precipitates. The filtrate was refrigerated for two to three days during which the products crystallized from solution. At this point, the supernatant may still contain some products. The crystals were collected and washed with 3 to 4 mL of methanol and dried. A final product of 270 mg was obtained with this procedure which corresponds to a total yield of approximately 34%. HPLC was performed with both analytical and preparative reverse phase columns. The HPLC-graded water was used to elute the column and the collector was monitored by ultraviolet absorption at 200, 210, 220, and 240 nm.

The melting temperature of the crude products was measured by a Fisher-Johns Apparatus. The elemental analysis was determined by Galbraith Laboratories, Inc. (Knoxville, TN).

Mass Spectral Analysis: Mass spectra were obtained by a Kratos Analytical 25RFA Mass Spectrometer Systems. Samples were analyzed using a direct insertion probe (DIP) at 70 eV in an electron impact mode. Samples were also transformed into their corresponding trimethylsilyl ethers and injected into the gas chromatographic column (13,14). The trimethylsilyl ether derivatives were prepared in hypovials by dissolving 25 μg of each HPLC-purified material into 20 μL of BSTFA and allowed to react and equilibrate at room temperature for 24 hours before analysis. A Carlo Erba HR/GC was interfaced with the mass spectrometer. The GC/MS analysis was carried out using a fused silica capillary column (50 m × 0.32 mm i.d.) coated with 5% cross linked phenyl methysilicone gum phase (film thickness 0.17 μm). The injection port and the ion source were monitored at 260°C and the GC/MS interphase at 280°C. Helium was used for carrier gas at an inlet pressure of 10 kPA and the split mode was used for the GC/MS analysis. The mass spectrometer was calibrated using perfluorokerosenes (PFK) for the mass range of 1,000 AMU.

^{1}HNMR: NMR spectra were obtained on a Bruker WM-300 spectrometer. The probe temperature was regulated by a BVT-1000 temperature regulator. The 1-D spectra were recorded using quardrature detection mode at a 16 K data point file with spectral width 2400 Hz, which has a digital resolution equivalent to 0.29 Hz/pt. A total of 128 scans were accumulated for each spectrum. In the 2-D COSY and NOESY NMR spectroscopy (15), the pulse sequences used were 90, t_1, 45, and 90, t_1, 90, τ_m, 90, (where t_1 and τ_m (0.6 second) are the incremental and mixing times), respectively. Afterward, the FIDs were collected following the last pulse of each sequence. A total of 512 t_1 spectra were collected for 2-D COSY and 256 t_1 for 2-D NOESY, both were processed by a 1K × 1K 2D FT. 256 and 1024 scans were accumulated in each t_1 dimension in 2-D COSY and 2-D NOESY, respectively.

NMR spectral simulation was performed on an ASPECT 3000 microcomputer with Bruker software PANIC. The chemical shift and coupling constant values were determined accurately by spectral simulation. The molecular modeling of TG stereoisomers used Alchemy II Program (Tripos Associates, St. Louis, MO) on an IBM P/S-2 60 computer with energy minimization.

Results and Discussion

The Monomeric Products Separation and Analysis By:

a. HPLC

A typical HPLC chromatograph of the reaction mixtures eluted by water is shown in Figure 2. There are five products designated as 1, 2, 3, 4, and 5'. The product 5' can be further separated by 5% acetonitrile solution into two products, 5 and 6 (Figure 2). There was no absorption at 260 nm for all products. For this reason, we can conclude that there is complete oxidation of thymidine, i.e., there is no thymidine left in the solution. In addition, the yields of these products are quite different; product 5, a major product (>50%), $\gg 6 \gg 3 > 1 > 4 \gg 2$. Thus the reaction protocol described in the previous section is an efficient met^{L} od for generation of one pure thymidine glycol isomer (product 5).

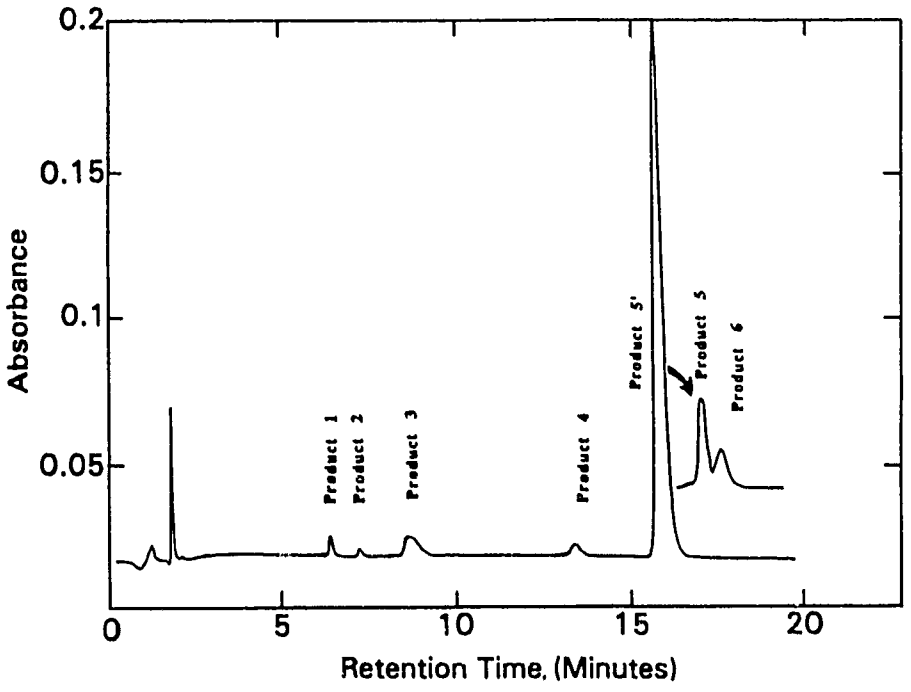

Figure 2: HPLC profiles of thymidine glycol after the oxidation reaction. The eluent solution is water. The flow rate is 2 mL/min., and the column is a Whatman preparative octadecylsilyl silica gel ODS-3 (M20 10/50). Products 1, 2, 3, 4, and 5' can be separated and collected. Product 5' was then flow through the column eluted with 5% acetonitrile to give products 5 and 6 (please note the scales are not justified).

b. The Elemental Analysis

The element analysis was performed on product 5. Results are as follows:

	%C	%H	%N	%O	%Cl
1st trial	43.62	5.98	9.98	38.49	trace
2nd trial	43.33	6.12	9.96	38.43	trace
average	43.48	6.05	9.97	38.46	~0
calculated	43.48	5.84	10.14	40.54	0

The calculated data were based on $C_{10}H_{16}O_7N_2$ (mol. wt. 276.25), the elemental formula for TG.

c. The Melting Temperature

The melting temperature of the crude product is 190-192°C. A narrow range is observed because the primary component in the crude product is product 5.

d. Mass Spectra

All four underivatized solid samples were analyzed by DIP/MS and their trimethyl-

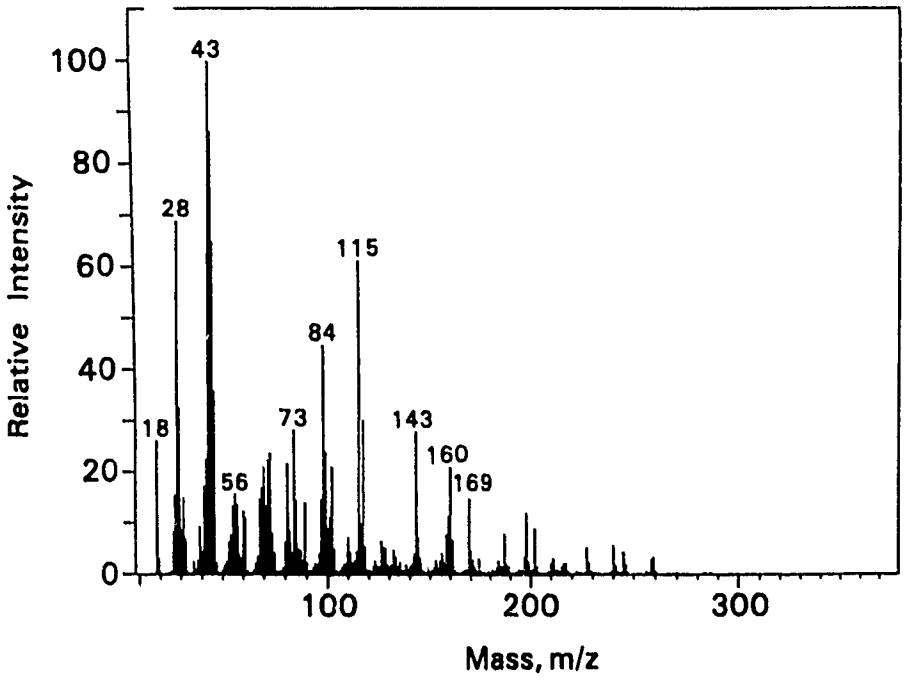

Figure 3: Mass spectrum of product 5.

silyl derivatives were analyzed by GC/MS systems. The structural elucidation was made as follows:

The product 5 which is the major component of the HPLC analysis showed the following major fragments upon DIP/MS (Figure 3).

m/z	258	259	159	160	161	117
fragment	$M-H_2O$	M-OH	B	B+H	B+2H	S

where the M, B, and S are TG molecule, base, and deoxyribose ions, respectively.

It has been well-recognized that the most important fragmentation process in nucleoside mass spectra involves the cleavage of the glycosidic bond resulting in either B and/or S ion depending upon which half retains the positive charge. The base ion occurs predominantly with one H and two H's rearranged from the sugar, primarily from the hydroxyl group (16). The ion at 117 is clearly from the sugar ion. Although DIP/MS provides extensive fragmentation and reveals many structural features, it failed to show an appreciable molecular ion due to thermal dehydration. Therefore, all purified isomers were further subjected to trimethylsilylation and analyzed by GC/MS (17,18,and 19).

The GC/MS experiments were performed on TMS derivatized TG. All isomers except product 3 of the HPLC showed two peaks on total ion chromatograph (TIC) after the trimethylsilylation. The MS of product 5 is shown in Figure 4 and the

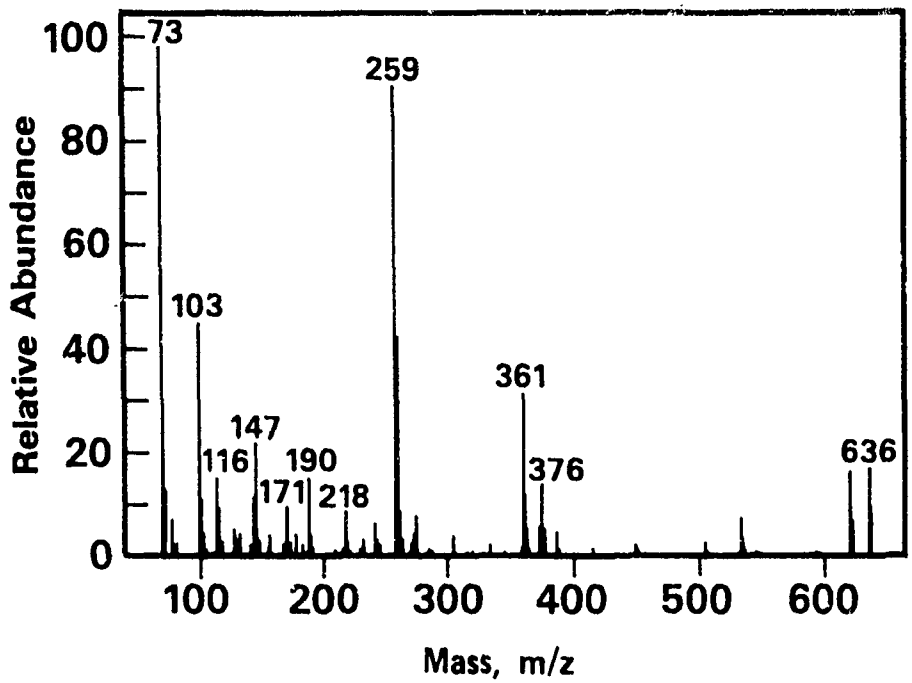

Figure 4: Mass spectrum of the trimethylsilyl derivative TG(TMS)$_5$. The molecular ion [M · $^+$] at m/z 636, m/z 621 [M$^+$ − · CH$_3$], 361 [M · $^+$ − · CH$_3$ − ((TMS)$_2$S + H)], and 259 [M$^+$ − · CH$_3$ − ((TMS)$_3$B + 2H)], where B represents base and S represents deoxyribose moieties. The minor peak (19.04 minutes) from the total ion chromatogram was identified as (TMS)$_4$TG (not shown here) had following major m/z values: 564, 549, 304 and 260.

remaining data including the other isomers are collected in Table I. Examination of the mass spectrum of the first peak (shorter GC retention time) suggests that it corresponds to TG(TMS)5, while the second peak (longer GC retention time) corresponds to TG(TMS)$_4$ (see Table I). No further attempts were made to drive the silylation reaction towards completion since both the TMS derivatives of TG are equally useful for structural elucidation.

The mass spectrum of the TG(TMS)$_4$ clearly showed the molecular ion at m/z 564 and fragment ions at 549 [M · $^+$ − · CH$_3$], 304 [M · $^+$ − ((TMS)$_2$S − H)], 260 [M · $^+$ − ((TMS)$_2$B + H)], 259 [M · $^+$ − ((TMS)$_2$B + 2H)]. On the other hand, the mass spectrum of TG(TMS)$_5$ showed the molecular ion at m/z 636 and fragments at m/z 621 [M · $^+$ − · CH$_3$], 361 [M · $^+$ − · CH$_3$ − ((TMS)$_2$S − H)], 260 [M · $^+$ − ((TMS)$_3$B + H)], and 259 [M · $^+$ − ((TMS)$_3$B + 2H)]. There are two ions from TMS itself, namely, 147: [Si(CH$_3$)$_3$OSi(CH$_3$)$_2$]+ and 73 [Si(CH$_3$)$_3$]+, which appeared in most samples, are characteristic and diagnostic ions for the presence of oxygen in the base (17).

Under identical conditions, all isomers showed similar fragmentation patterns (Table I) upon DIP/MS and GC/MS analyses although with different peak intensities (Table I). In addition, the retention times of TG(TMS)$_4$ and TG(TMS)$_5$ are similar for all four isomers. These results strongly support identities of products 1, 3,

Table I
Identification and Characterization of TMS Derivatives of Thymidine Glycol Isomers by Gas Chromatography-Mass Spectrometry

TG products #	TG TMS Derivative	GC RT, min.	Prominent Ions (m/z) vs. Ion-Intensity, %
	$(TMS)_5$	18.1 (18.00)	636 (28.6), 621 (28.0), 361 (42.0), 304 (28.56), 259 (100.0), 147 (22.0), 73 (64.26)
1			
	$(TMS)_4$	19.1 (19.10)	564 (1.5), 549 (15.0), 304 (100.0), 259 (50.2), 147 (25.5)
	$(TMS)_5$	--*--	-*-
3			
	$(TMS)_4$	16.5 (16.50)	564 (5.2), 549 (20.2), 304 (100.0), 259 (50.1), 147 (25.3)
	$(TMS)_5$	17.5 (17.49)	636 (50.2), 621 (33.3), 533 (10.2), 361 (33.3), 259 (100.0), 147 (18.1), 73 (62.5)
5			
	$(TMS)_4$	19.0 (19.04)	564 (3.3), 549 (20.1), 461 (8.1), 304 (100.0), 259 (60.3)
	$(TMS)_5$	18.4 (18.43)	636 (18.1), 621 (17.5), 533 (7.7), 361 (28.8), 259 (90.5), 147 (22.3), 73 (100.0)
6			
	$(TMS)_4$	19.1 (19.12)	564 (3.2), 549 (15.5), 304 (85.8), 259 (48.8), 147 (25.3), 73 (100.0)

TG isomers (1, 3, 5, and 6) were purified by HPLC analysis from the reaction product mixture obtained from the osmium tetroxide-induced oxidation of thymidine. Individual products were freeze dried, treated with BSTFA and analyzed by capillary column/gas chromatography-mass spectrometry as was shown in Figures 3 and 4. Except for product 3, which did not form $(TMS)_5$ derivative all other products gave rise to $(TMS)_5$ as well as $(TMS)_4$ derivatives.

5, and 6 from HPLC as structural isomers of TG. The absolute configurations of all four isomers were determined by NMR spectroscopy as shown below.

e. ^1H NMR

A typical ^1H NMR spectrum of TG (product 5) is shown in Figure 5. The sample contained a trace amount of product 6 marked by "x", which does not affect the NMR, nor MS analyses.

The assignment of furanose ^1H NMR resonances of product 5 was accomplished by determining their coupling patterns and by 2-D COSY analysis as shown in Figure 5B (lower half of the 2D map). The H_1, (6.19 ppm) is clearly coupled to H_2 and H_2 (2.38 and 2.18 ppm, respectively). In turn, these hydrogen are coupled to H_3 (4.40 ppm), then to H_4, (3.91 ppm) and finally H_4, couples to H_5, and H_5,, (3.72 and 3.75 ppm). Base protons H_6 and CH_3 resonances were recognized by their long range couplings (the long-range coupling 2D COSY data are not shown). Furthermore,

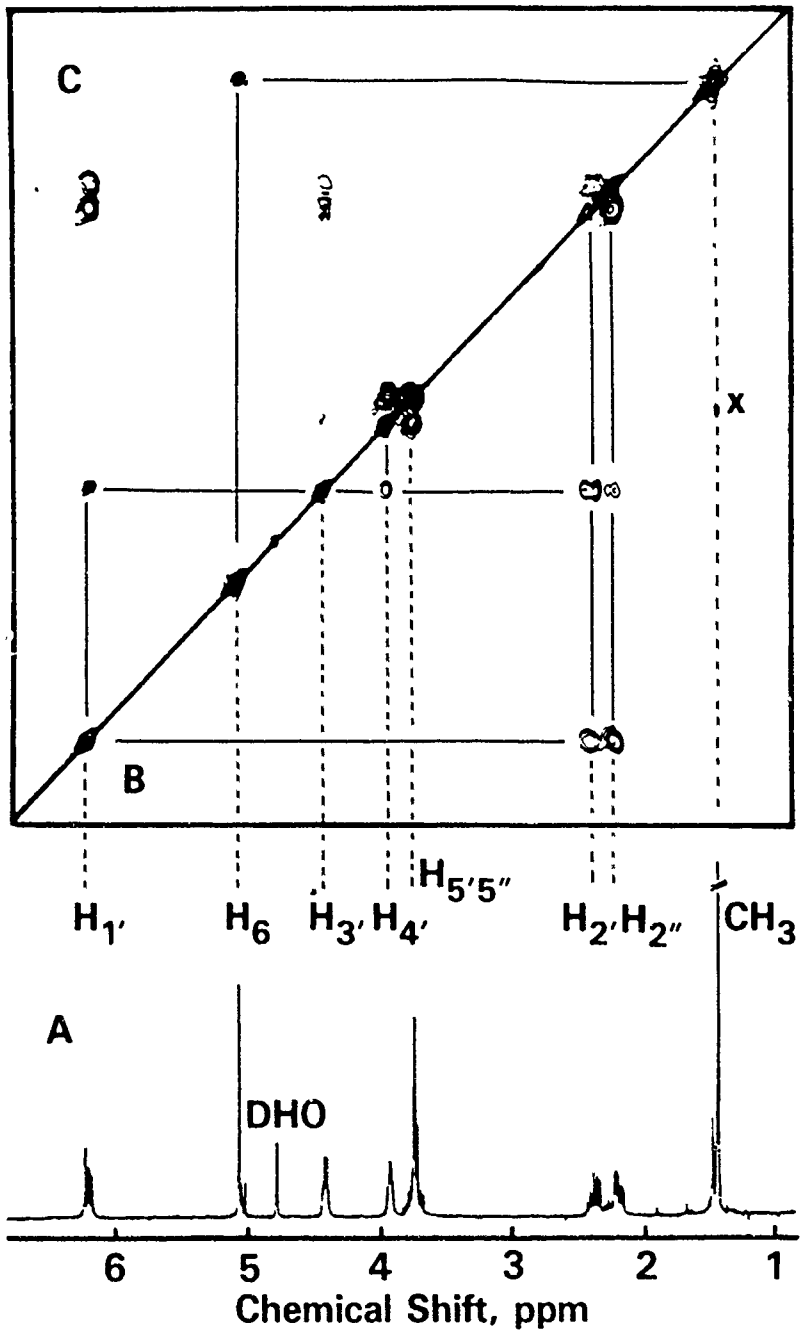

Figure 5: 2-D COSY (B) and NOESY (C) ^{1}H NMR spectra of product 5. the 1-D spectrum (A) is also recorded at the bottom for reference. Impurities are marked with "x".

Table II
The Chemical Shift and Coupling Constant Values ^{1}H NMR Resonances of Thymidine Glycol Isomers in Aqueous Solution (no buffer) at 25°C

Atom # product	δ (ppm) 1	3	5	6
6	5.69	5.11	5.04	5.03
CH_3	1.48	1.43	1.42	1.44
1′	6.32	6.25	6.19	6.15
2′	2.21	2.37	2.38	2.28
2″	2.16	2.18	2.18	2.23
3′	4.60	4.54	4.40	4.40
4′	4.25	3.80	3.91	3.91
5′	a	5.06	3.72	3.72
5″	a	5.04	3.75	3.77
	$J_{C\text{-}H}$ (Hz)			
$J_{1'\text{-}2'}$	9.5	9.6	8.4	7.0
$J_{1'\text{-}2''}$	5.8	5.9	6.0	6.7
$J_{2'\text{-}2''}$	−14.1	−14.1	−13.9	−14.1
$J_{2'\text{-}3'}$	4.8	5.9	6.0	7.0
$J_{2''\text{-}3'}$	1.8	1.9	2.8	4.2
$J_{3'\text{-}4'}$	~1	1.8	3.8	3.6
$J_{4'\text{-}5'}$	~1	4.8	4.6	4.4
$J_{4'\text{-}5''}$	~1	0	3.7	3.7
$J_{5'\text{-}5''}$	a	−12.1	−12.0	−12.3

a under water peak, can not be measured.

Atom # product	δ (ppm) 2		4	
	A	B	A	B
6	5.69	5.11	5.10	5.05
CH_3	1.48	1.43	1.46	1.46
1′	6.18	6.07	6.20	6.17
2′	2.30	2.66	2.31	2.27
2″	2.22	2.27	2.24	2.25
3′	4.50	4.41	4.51	4.42
4′	3.82	4.13	3.83	3.93
5′	5.10	3.69	5.12	3.74
5″	5.08	3.63	5.12	3.77

the CH_3 signal was easily identified by its large signal intensity. These spectral assignments are identical to those reported by Cadet and co-workers (8). The assignments of all isomers can be and have been done in a similar manner (2D-COSY). The chemical shift values, collected in Table II, of all four isomers were obtained by spectral simulation. We found the ^{1}H NMR chemical shift values of products 5 and 6 are almost identical whereas those of product 1 are similar to those of product 3. It is worthwhile to note that the chemical shifts of $H_{5'}$ and $H_{5''}$ of products 1 and 3 have been moved to downfield about 1.5 ppm. This can be verified by the 2D-COSY of product 3 (Figure 6B). It is clearly the coupling pattern: $H_{1'}$ (6.25 ppm) to $H_{2',2''}$ (2.37, 2.18 ppm) to $H_{3'}$ (4.54 ppm) to $H_{4'}$ (3.80 ppm) then to $H_{5',5''}$ (5.06, 5.04 ppm). These observations allow us to subdivide these four isomers into two sub-groups, *cis* and *trans*.

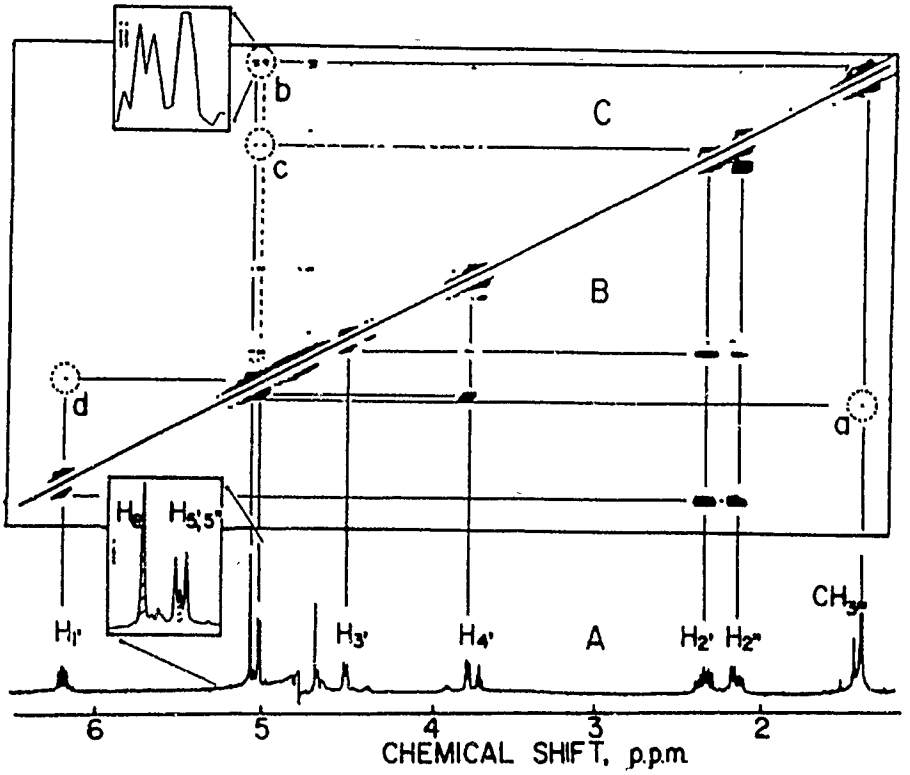

Figure 6: 2-D COSY (B) and NOESY (C) ^{1}H NMR spectra of product 3. The 1-D spectrum (A) is also recorded at the bottom for reference. The small box at the bottom is an enlarged view of H_6 and $H_{5',5''}$. The small box at the top contains the profile of the weak NOE between H_6 and CH_3 group.

The stereochemical structures (i.e., *cis* and *trans*) associated with saturation of the C_5-C_6 double bond and the glycosidic bond can be determined by the ^{1}H-^{1}H spatial relations between C_6-H and C_5-CH_3, between C_6-H and $C_{1'}$-H and between C_6-H and $C_{2'}$-H. The distances between these protons were examined by 2-D NOESY for all four stereoisomers. A 2-D NOESY spectrum of product 5 is shown in Figure 5C (upper half of the 2-D map). The result of these key NOE's are summarized as follows:

products	NOE			designated isomers
	H_6-CH_3	H_6-$H_{2'}$	H_6-$H_{1'}$	
1	weak	weak	un-observable	(−)-*trans*-5S,6S
3	weak	strong	un-observable	(+)-*trans*-5R,6R
5	strong	weak	un-observable	(−)-*cis*-5R,6S
6	strong	strong	un-observable	(+)-*cis*-5S,6R

There should be a strong NOE observed in 2-D NOESY (Figure 5C) if C_6-H and C_5-CH_3 are in the *cis* orientation because the distance between C_6-H and C_5-CH_3 is shorter in *cis* than in *trans* (Figure 6C). Similarly, the NOE between C_6-H and $C_{2'}$-H should be stronger than those between C_6-H and $C_{1'}$-H if the glycosidic bond of a

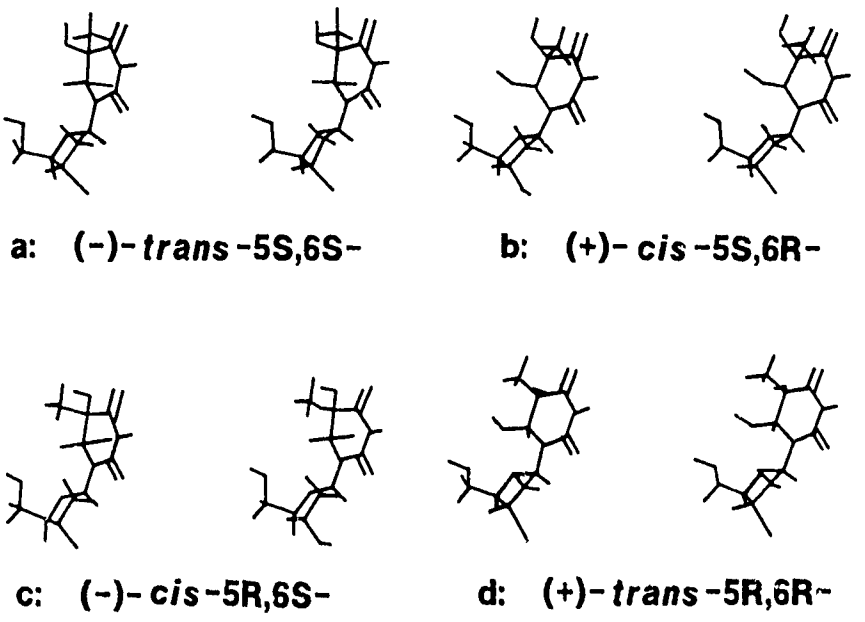

Figure 7: The absolute configurations of product 1: (−)-*trans*-5S,6S, product 3: (+)-*trans*-5R,6R, product 5: (−)-*cis*-5R,6S, and product 6: (+)-*cis*-5S,6R, in steric drawing. These structures were also produced by Alchemy II program (Tripos Associates, St. Louis, MO) on an IBM P/S personal computer, based on NMR results and molecular structure and energy minimization.

nucleoside is in an *anti* configuration. Again this is because the distance in the former pair (around 2 Å) is shorter than in the latter pair (about 3.5 Å) as inferred from modeling studies. In our case we detected no NOE at the giving mixing time (τ_m = 0.6 second) between C_6-H and $C_{1'}$-H for all four isomers. From this we concluded that all four isomers are in the *anti* configuration around the glycosidic bond. In addition, the size of the NOE between C_6-H and $C_{2'}$-H can also be used to determine the absolute configuration around C_6. The distances measured between C_6-H and $C_{2'}$-H are 1.9 Å and 2.1 Å in [6R] and [6S], respectively. Accordingly the NOE's between C_6-H and $C_{2'}$-H in products 3 and 6 are larger than those associated with the other two isomers and thus can be assigned to [6R]. Together with the information of NOE's between C_6-H and C_5-CH_3, the absolute configurations of the four stereoisomers can be determined at both of the two chiral centers, i.e., at C_5 and C_6, and along the glycosidic bond (Figure 7). The results are listed in the table above and their energy minimized three dimensional structures are shown in Figure 7.

We furthermore noted that the sugar conformation for all four TG isomers can be determined by coupling constants of the sugar proton resonances. All ^{1}H-^{1}H (proton-to-proton) coupling constants were obtained directly from the coupling pattern of each assigned peak (Figures 8, 9A, and 9B). The result was further confirmed by spectral simulation and are collected in Table II. The sum of $J_{1'-2'}$ and $J_{3'-4'}$ of all four isomers are equal to the typical value (10.8 ± 0.4) of deoxynucleosides (20). Thus, the % of ^{2}E can be estimated by $J_{1'-2'}/(J_{1'-2'} + J_{3'-4'})$ and are indicated as follows. The conforms of exocyclic $C_{4'}$-C_5 bond can be determined by the values of $J_{4'-5'}$ and $J_{4'-5''}$ as

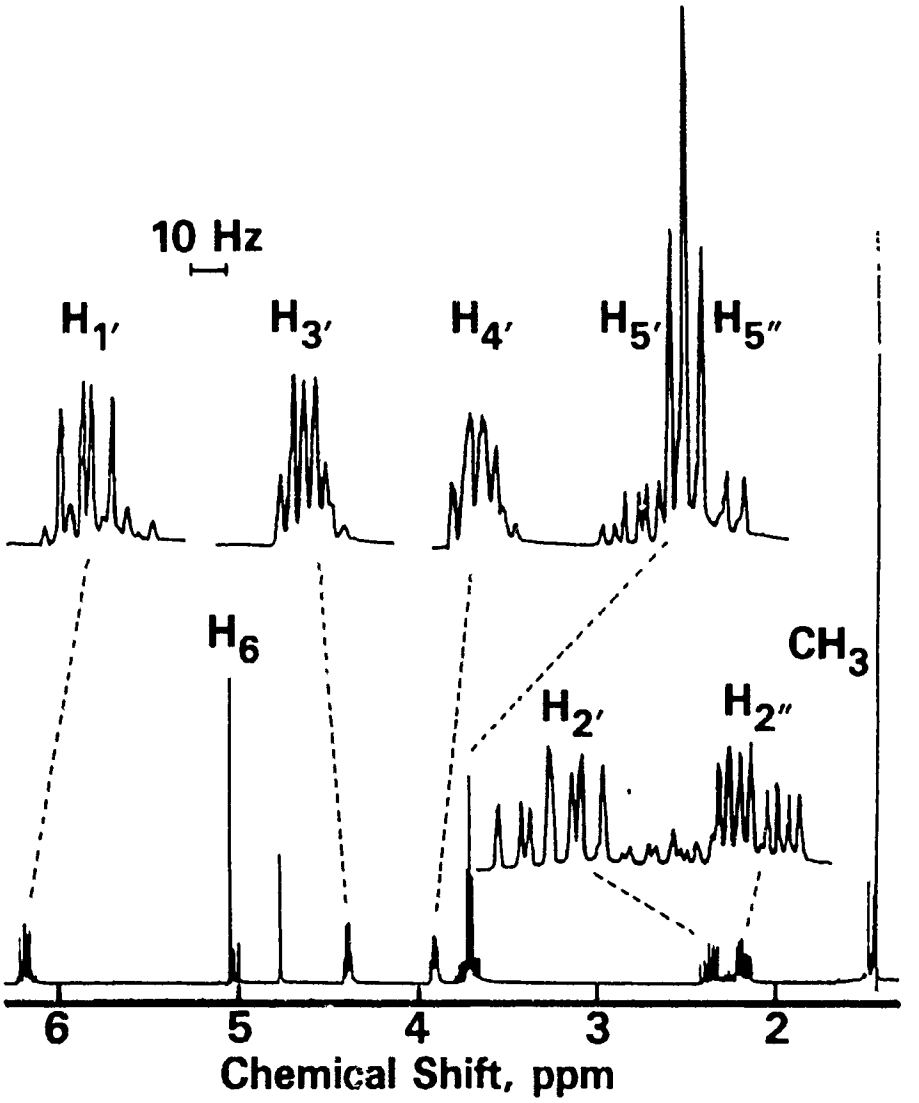

Figure 8: A detailed 1-D ^{1}H NMR spectra of product 5 at 300 MHz. The entire spectrum is on the bottom. The expanded patterns of each functional group are on top. The chemical shift and coupling constant values were obtained by spectral simulation (spectra not shown).

gg = $(13 - J_{4'\text{-}5'} - J_{4'\text{-}5''})/10$ and the results are also listed as follows (20,21)

products	isomers	% of ^{2}E	% of gg ($C_{4'}$-$C_{5'}$)
1	(−)-*trans*-5S,6S	90	100
3	(+)-*trans*-5R,6R	90	100
5	(−)-*cis*-5R,6S	69	47
6	(+)-*cis*-5S,6R	73	42
	Thymidine	62	44

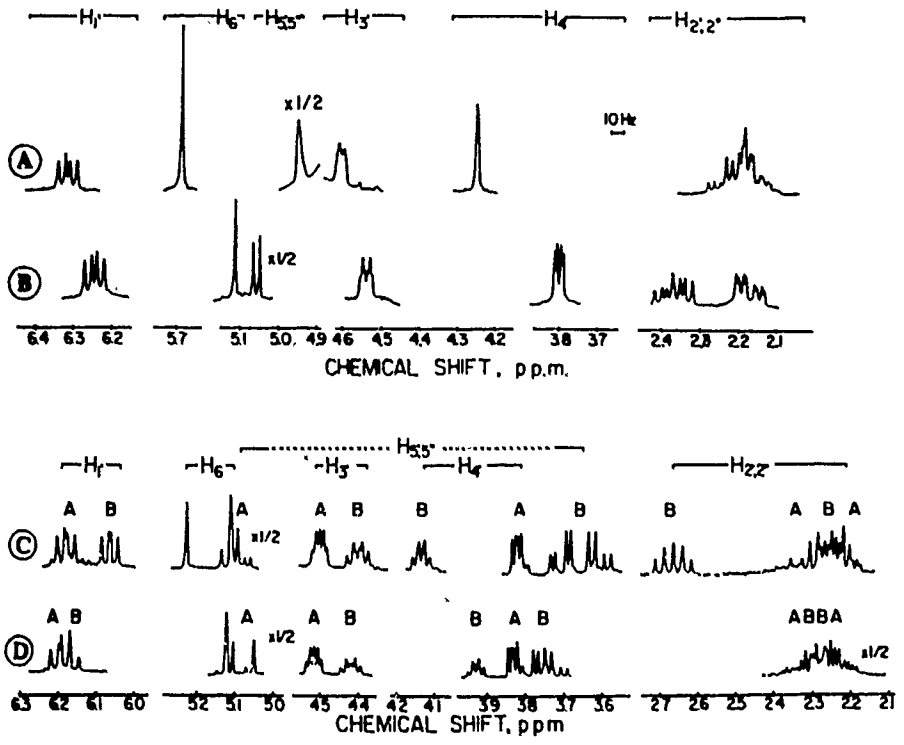

Figure 9: A, B, C, and D are the detailed 1-D ^{1}H NMR spectra of products 1, 3, 2, and 4 at 300 MHz, respectively.

We find that the furanose ring is in ^{2}E (2′-endo) for *trans* and ^{2}E (2′-endo)/^{3}E (3′-endo) equilibrium (or ^{4}E (4′-endo)) for *cis*. It is interesting to note that an NOE is indeed observed between $C_{1'}$-H and $C_{4'}$-H (Figure 5C) indicating an ^{4}E conformation for product 5. It is evident that the sugar conformations in *cis* isomers, but not the *trans* isomers, are very similar to their parent nucleoside: thymidine.

The Dimeric Products

The ^{1}H NMR spectra of products 2 and 4 clearly show a dimeric pattern (Figures 9C, 9D, 10, and 11). All peaks can be assigned by 2D-COSY (Figures 10 and 11). There are two kinds $H_{5',5''}$ chemical shifts. Therefore, these dimers may composed by a *trans* and a *cis* TG. 2D-NOESY is difficult to be performed due to two reasons. First, the sample quantities are small and second, these two products are relatively unstable. They are soon converted to product 5 in room temperature. However, the identities of these two dimers can be revealed by chemical shifts (Table II) as composed by a *trans* (the A part of 2 and 4)and a *cis* (the B part of 2 and 4) isomers.

Conclusion

The synthetic protocol introduced is simple and efficient. There was one major product, namely, (−)-*cis*-5R,6S 5,6-dihydro-5,6-dihydroxythymidine, which is more than

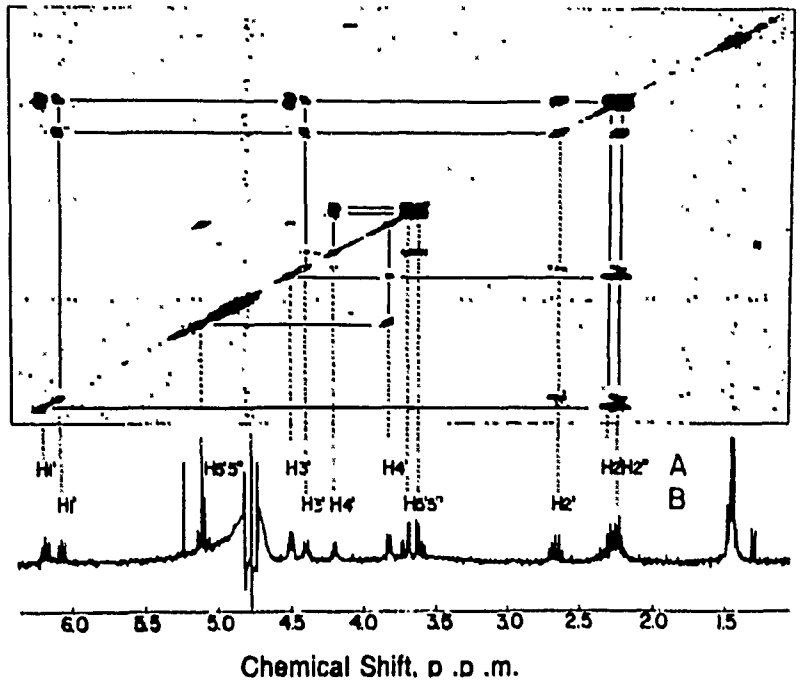

Figure 10: 2-D COSY ^{1}H NMR spectrum of product 2.

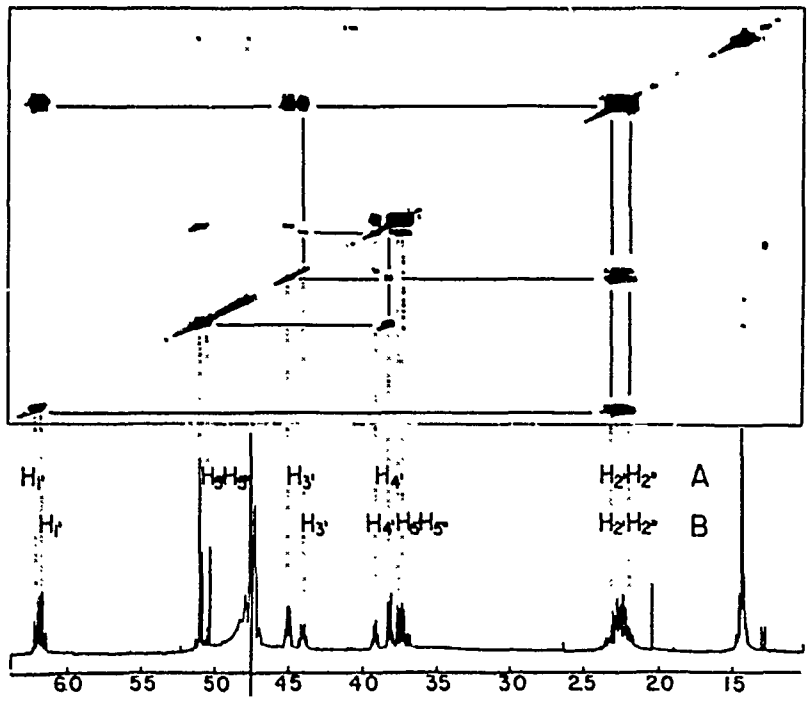

Figure 11: 2-D COSY ^{1}H NMR spectrum of product 4.

60% by weight. The minor products found were stereoisomers of TG and two dimers in trace amounts. There is no unreacted thymidine left. The total yield was 34%. However, this can be improved by evaporating the 2-propanol above the TG crystals. Furthermore, sizable amount of products may have been discarded with the chloroform. Even so, our synthetic method is worthy of reporting since TG was produced by the permanganate oxidation of thymidine is more difficult (1, 9-12) as described in the *Introduction*. Furthermore, all four stereoisomers of TG can be purified by a reverse phase HPLC column eluted by water. The separation procedures are simple and inexpensive which are opposite to the report from Howgate and co-workers (1).

We were able to determine the structures of all four stereoisomers of TG. Highly sensitive analytical methods of MS and NMR were used for the structural determinations. Data obtained from elemental analysis and MS revealed that these four products have the same molecular weight and share the same chemical formula.

Finally we note that the *trans* products are unstable. They slowly convert into the *cis* isomers at room temperature. Therefore, the mechanism and efficiency of converting *cis* to *trans* may be somewhat different from that already reported in the literature (7). Investigations addressing the conformation changes are currently in progress.

Acknowledgments

We acknowledge The Biophysical NMR Facility Center (established by NIH grant GM-27512) for using the Bruker WM-300 NMR spectrometer. This work is partially supported by NIH grants PO1 ES 03841-03 and PO1 ES 03819-03; by DOE grant DE-FG02-88ER 60636; and by Armed Forces Radiobiology Research Institute. Finally, we thank Dr. J. Cadet for helpful discussions.

References and Footnotes

1. Howgate, P., Jones, A.S. and Tittensor, J.R., *J. Chem. Soc., Sec. C*, 275-279 (1968).
2. Rycyna, R.E. and Alderfer, A.L., *Nucleic Acids Res. 13*, 5949-5963 (1985).
3. Kan, L.-S., Voituriez, L. and Cadet, J., *Biochemistry 27*, 5796-5803 (1988).
4. Taylor, S.-J., Garrett, D.S. and Cohrs, M.P., *Biochemistry 27*, 7206-7215 (1988).
5. Basu, A.K., Loechler, E.L., Leadon, S.A. and Essigmann, J.M., *Proc. Natl. Acad. Soc. 86*, 7677-7681 (1989).
6. Rouet, P. and Essigman, J.M., *J. Cancer Res. 45*, 6113-6118 (1985).
7. Cadet, J., Ulrich, J. and Teoule, R., *Tetrahedron 31*, 2057-2061 (1975).
8. Cadet, J., Ducolomb, R. and Hruska, F.E., *Biochim. Biophys. Acta 563*, 206-215 (1979).
9. Frenkel, K., Goldstein, M.S., Duker, N.J. and Teebor, G.W., *Biochemistry 20*, 750-754 (1981).
10. Furlong, E.A., Jorgensen, T.J. and Henner, W.D., *Biochemistry 25*, 4344-4349 (1986).
11. Ide, H., Melamede, R.J. and Wallace, S.S., *Biochemistry 27*, 964-969 (1987).
12. Iida, S. and Hayatsu, *Biochem. Biophy. Acta 228*, 1-8 (1971).
13. M. Dizdaroglu, E. Holwitt, M. Hagan and W. Blakely, *Biochemistry J. 235*, 591-536 (1986).
14. Dizdaroglu, M., *Biotechniques 4*, 536-546 (1986).
15. Ernst, R.R., Bodenhausen, G. and Wohaun, A., *Principles of Nuclear Magnetic Resonance in One and Two Dimensions*, Clarendon Press, Oxford, England.
16. Hettich, R.L., Buchanan, M.V. and Ho, C.-H., *Biomed. Environ. Mass Spec. 19*, 55-62 (1990).
17. McCloskey, J.A. and Krahmer, V.I., *Advd. Mass Spectrometry 7*, 1485 (1977).
18. Biemann, K. and McCloskey, J.A., *J. Am. Chem. Soc. 84*, 2005 (1962).

19. Maneuso, N.R., Tsunakawa, S. and Biemann, K., *Anal. Chem. 38*, 1775 (1966).
20. Cheng, D.M. and Sarma, R.H., *J. Am. Chem. Soc. 99*, 7333-7348 (1977).
21. Cheng, D., Kan, L.-S., Frechet, D., Ts'o, P.O.P., Uesuge, S., Shida, T. and Ikehara, M., *Biopolymers 23*, 775-795 (1984).

Date Received: July 20, 1990

Communicated by the Editor R.H. Sarma

AFRRI TECHNICAL REPORT

Maximum Temperature Calculation and Operational Characteristics of Fuel Follower Control Rods for the AFRRI TRIGA Reactor Facility

M. Forsbacka

M. Moore

AFRRI TR91-1

DEFENSE NUCLEAR AGENCY

ARMED FORCES RADIOBIOLOGY RESEARCH INSTITUTE

BETHESDA, MARYLAND 20889-5145

REVIEWED AND APPROVED

MARK MOORE
Reactor Facility Director

GEORGE W. IRVING, III
Colonel, USAF, BSC
Director

Contents

INTRODUCTION

Operational requirements of the Armed Forces Radiobiology Research Institute (AFRRI) TRIGA reactor facility necessitate the implementation of fuel follower control rods (FFCR's). Fuel follower control rods are like the standard TRIGA control rods as described in section 4.10.1 of the AFRRI TRIGA Safety Analysis Report (SAR) except that they have a fuel-filled follower rather than an air or aluminum follower. The primary purpose of the FFCR's is to offset the long-term effects of fuel burnup.

The Code of Federal Regulations (CFR; Title 10, Part 50.59) requires that modifications of a portion(s) of a licensed facility, as described in the facility SAR, be documented with a written safety analysis. The SAR ensures that all safety issues associated with the implementation of FFCR's have been reviewed. This technical report will show that implementing FFCR's will allow the standard control rods to function in their intended purpose and will restore core reactivity economically. FFCR's have been implemented in approximately a dozen TRIGA reactors and have been used for over 20 years without reported failure.

This report has been submitted to the AFRRI Radiation Facility Safety Committee to ensure that all safety questions have been reviewed before submission to the U.S. Nuclear Regulatory Commission (NRC), as required under 10 CFR 50.59.

GENERAL DESCRIPTION OF FUEL FOLLOWER CONTROL RODS

The current AFRRI TRIGA standard control rods were installed in 1964. The standard control rod consists of a sealed aluminum tube (0.065 inch thick) approximately 1.25 inches in diameter and 31 inches long. The upper 15.25 inches of the tube contain a compacted borated graphite rod (B_4C with 25-percent free boron or other boron compounds), which functions as a neutron absorber or poison. The lower end of the tube contains a 15.25-inch long and 1.125-inch diameter solid aluminum rod called the aluminum follower. The follower functions as a mechanical guide for the control rod as it is withdrawn from or inserted into the reactor core.

The proposed FFCR's differ from the current standard control rods in the following respects:

- The aluminum cladding is replaced by smooth stainless steel (SS304) cladding with a wall thickness of 0.020 inch. The inner and outer diameters are 1.085 inches and 1.125 inches, respectively.
- The length of the control rod is increased to 37.75 inches; the absorber and fuel follower section are both nominally 15 inches long.
- The outer diameter of the absorber section and the fuel follower are both 1.085 inches.
- The fuel follower has a solid zirconium rod as its central core with an outer diameter of 0.225 inch.

The absorber or poison material of the proposed FFCR's is, however, identical to the standard control rods presently installed.

The fuel contained in the FFCR consists of a fuel-moderator element in which zirconium hydride is homogeneously mixed with partially enriched uranium. The FFCR fuel element contains 12 percent uranium by weight and has a nominal enrichment of 20 percent in the ^{235}U isotope. The FFCR fuel element contains about 30.0 grams of ^{235}U--this is 79% of the ^{235}U loading of a standard AFRRI TRIGA fuel element. The nominal hydrogen-to-zirconium ratio in the FFCR fuel element is 1.7 with a range between 1.6 and 1.7. The FFCR fuel element contains no burnable poison. The stainless steel cladding on the FFCR fuel element has a hardness greater than the aluminum control rod guide tubes, so wearing will occur on the guide tubes rather than on the FFCR fuel elements.

FFCR MAXIMUM FUEL TEMPERATURE CALCULATION

A thermal-hydraulic analysis of the FFCR fuel element to determine the maximum fuel temperature uses the following model:

- The neutron mean free path for neutrons of all energies is smaller than the diameter of the TRIGA fuel rods, so the reactor must be treated as a heterogeneous reactor. Thus, the active volume of the core is taken to be the volume of fuel contained within the reactor core.
- The ratio of power in a fuel element with 12 wt-% uranium versus 8.5 wt-% uranium is 1.21. This is determined by General Atomics design calculations.[1]
- The reactor is operating at a steady-state power level of 1.0 MW, and the heat flux across the fuel element is described by Fourier's law of thermal conduction:[2]

$$q''(r) = -k\nabla T(r) \qquad (1)$$

where
$q''(r)$ = heat flux at position r
k = thermal conductivity
$T(r)$ = temperature at position r

For steady-state heat transport, the heat production rate and the rate of energy loss due to heat transport are equal. This can be generally expressed as

$$q'''(r) = \nabla \cdot q''(r) \qquad (2)$$

where
$q'''(r)$ = volumetric heat rate (heat production rate) at position r.

Substituting equation (1) into equation (2) yields the time-independent equation of thermal conduction:

$$q'''(r) = -\nabla \cdot k\nabla T(r) \qquad (3)$$

Equation (3) is, thus, the second-order ordinary differential equation that must be solved to determine the maximum temperature attained in the fuel portion of the FFCR.

Using this model to determine the maximum fuel temperature divides the analysis into two separate tasks: determining the power density in the FFCR in a D-ring grid position and solving equation (3) for the given power density.

Power Density in FFCR Fuel Element

The anticipated fuel loading for the AFRRI TRIGA reactor core with FFCR's installed will consist of 77 standard TRIGA fuel elements and the three FFCR fuel elements. Presuming that the control rods are fully withdrawn to achieve a power level of 1.1 MW, the total active fuel volume will be 30,597.9 cm^3. Thus, the average power density at 1.1 MW will be 36.0 W/cm^3.

The maximum fuel temperature is the important parameter, so only the radial variation of the core centerline power density is considered. To determine the maximum power density in the D-ring location of the FFCR fuel element, the following calculations are made:

For the AFRRI TRIGA, the radial and axial peak-to-average power ratios are 1.55 and 1.30, respectively.[3] Thus the maximum power density (heat rate) will be

$$q'''_{max} = (1.55)(1.30)q'''_{ave} = 72.4 \text{ W/cm}^3 \quad (4)$$

To determine $q'''_{D\text{-ring}}$ relative to q'''_{max}, it is useful to compute a scaling factor from the gross variation of thermal neutron flux in the radial direction (thermal flux and power density are directly proportional). The normalized radial flux distribution for the AFRRI TRIGA core is best represented by a Bessel function of the first kind of order zero:

$$\phi_{therm} = J_0\left(\frac{2.405r}{R_e}\right) \quad (5)$$

where
R_e = 21.78 cm, the extrapolated core radius
r = 11.99 cm, radial position of D-ring element

and the Bessel function scaling factor is J_o (1.3240) = 0.6074.

The power density for the D-ring is thus computed to be

$$q'''_{D\text{-ring}} = (0.6074)\ q'''_{max} = 44.0 \text{ W/cm}^3 \quad (6)$$

Because the FFCR fuel element differs from the standard fuel element in concentration of uranium, the power density in an FFCR fuel element is

greater than the power density in a standard fuel element by a factor of 1.21.[1]

Taking the above scaling factor into account, the power density of an FFCR fuel element is found to be

$$q'''_{FFCR} = (1.21)q'''_{D\text{-}ring} \qquad (7)$$
$$= 53.2\ W/cm^3$$

Note that the calculation of q'''_{FFCR} takes into account the most limiting condition for power peaking in a 12 w/o fuel element versus an 8.5 w/o fuel element. As developed in equation (7), q'''_{FFCR} is still considerably less than the theoretical maximum q''' as determined in equation (4). A less conservative approach would have also accounted for the reduced volume in an FFCR fuel element.

Maximum Temperature in FFCR Fuel Element

Equation (3) takes the following form for cylindrical geometry with axial and azimuthal symmetry (see Figure 1):

$$\frac{1}{r}\left[\frac{d}{dr}kr\frac{dT}{dr}\right] + q''' = 0 \qquad (8)$$

The boundary conditions required that constrain equation (8) are as follows:

$$\frac{dT}{dr} = 0 \text{ at } r = R_i \text{ and } T = T_i \text{ at } r = R_i \qquad (9)$$

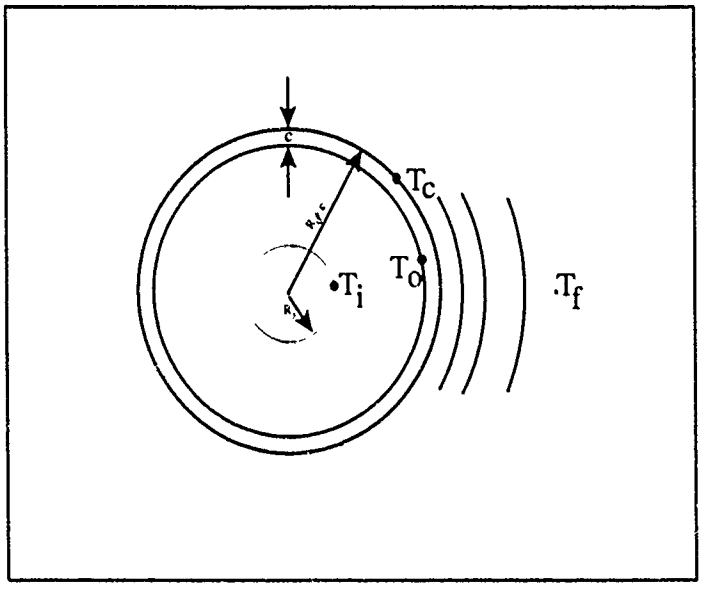

Figure 1. Cross-section of FFCR fuel element.

Integrating equation (8) twice yields a general solution of the form

$$T(r) = -q''' \frac{r^2}{4k_f} + C_1 \ln(r) + C_2 \tag{10}$$

Applying the boundary conditions to solve for the temperature difference between the outer edge of the zirconium rod and the inner surface of the cladding,

$$C_1 = \frac{q'''R_i^2}{2k_f} \tag{11}$$

$$C_2 = T_i - \frac{q'''R_i^2}{2k_f}\left(\ln(R_i) - \frac{1}{2}\right)$$

$$T_i - T_o = \frac{q'''R_i^2}{4k_f}\left[\left(\frac{R_o}{R_i}\right)^2 - 2\ln\left(\frac{R_o}{R_i}\right) - 1\right] \tag{12}$$

To account for the transfer of heat from the fuel through the cladding to the coolant, we must consider the heat conduction between the inner and outer surfaces of the cladding, q_{clad}, and the heat conduction from the outer surface of the cladding to the coolant, q_{fluid}. We make the assumption that no heat is produced in the cladding or the coolant, so the heat conduction from the outer surface of the fuel, q_{fuel}, must be equal to q_{clad} and q_{fluid}. The heat conduction leaving the fuel is given by

$$q_{fuel} = \pi(R_o^2 - R_i^2)Lq''' = \pi((R_o/R_i)^2 - 1)LR_i^2 q''' \tag{13}$$

where
L = length of fuel element

$$q_{clad} = -k_c A \left.\frac{dT}{dr}\right|_{clad} = \frac{2\pi k_c L(T_o - T_c)}{\ln\left(\frac{R_o + c}{R_o}\right)} \tag{14}$$

$$q_{fluid} = hA(T_c - T_f) = 2\pi(R_o + c)Lh(T_c - T_f)$$

Note that the area, A, used in computing q_{clad} is the logarithmic mean area of the cladding. Recall that

$$q_{fuel} = q_{clad} = q_{fluid} \tag{15}$$

So we can solve for the temperature differences in the above equations in terms of q''':

$$T_o - T_c = \ln\left(\frac{R_o + c}{R_o}\right)\left[\left(\frac{R_o}{R_i}\right)^2 - 1\right]\frac{R_i^2}{2}\,q'''$$

$$T_c - T_f = \frac{1}{(R_o+c)h}\left[\left(\frac{R_o}{R_i}\right)^2 - 1\right]\frac{R_i^2}{2}\,q''' \qquad (16)$$

Adding equations (16) with equation (12) and solving for T_i gives us the expression for the maximum temperature in the FFCR.

$$T_i = T_f + \frac{q'''R_i^2}{4k_f}\left[\left(\frac{R_o}{R_i}\right)^2 - 2\ln\left(\frac{R_o}{R_i}\right) - 1\right] + \frac{q'''R_i^2}{2}\left[\left[\left(\frac{R_o}{R_i}\right)^2 - 1\right]\left[\frac{1}{k_c}\ln\left(\frac{R_o + c}{R_o}\right) + \frac{1}{h(R_o + c)}\right]\right] \qquad (17)$$

where
T_i = maximum fuel temperature
T_f = bulk coolant temperature
R_o = 1.38 cm (radius of FFCR fuel element)
R_i = 0.286 cm (radius of Zr rod)
c = 0.051 cm (cladding thickness)
k_f = 0.18 W/cm-°C (thermal conductivity of UZrH)[4]
k_c = 0.138 W/cm-°C (thermal conductivity of SS304)[2]
h = 1.339 W/cm^2-°C (free convective heat transfer coefficient of water)
q''' = 53.2 W/cm^3 (from equation (7))

Note that the free convective heat transfer coefficient, h, was an experimentally derived quantity. The method by which h was determined is presented in Appendix A. Solving equation (17) using a volumetric heat rate of 53.2 W/cm^3 and a bulk water temperature of 48.6°C (the conditions at which h was determined) yields a maximum fuel temperature of 210.2°C. The maximum temperature achieved in the FFCR is nearly 180°C less than the normal temperature of 390°C in a standard fuel element in the B-ring during a 1.0 MW steady-state power operation.

Fuel Temperature in Pulse Mode Operation

The Nordheim-Fuchs model predicts the maximum fuel temperature achieved in a pulse mode operation.[5] The fundamental assumptions of this model are as follows:

- The neutron flux in the reactor is separated into a spatial component (shape factor) and a time-dependent component (amplitude factor), such that

$$\Phi(r,t) = vn(t)\Psi(r) \qquad (18)$$

where
v = neutron velocity
n(t) = neutron density (amplitude factor), proportional to power
$\Psi(r)$ = shape factor

The shape factor is assumed to remain constant during a pulse. This is called the point-reactor model.

- The production of delayed neutrons and the effects of source neutrons are neglected.

- The pulse from a thermodynamic standpoint is adiabatic, so

$$\frac{dT}{dt} = Kn(t) \tag{19}$$

where
T = fuel temperature
K = reciprocal of heat capacity

From the first and second assumptions we can write the time-dependent neutron density as

$$\frac{dn}{dt} = \frac{\rho - \beta}{\ell} n \tag{20}$$

where
ℓ = mean lifetime of neutrons in the reactor
β = delayed neutron fraction
ρ = reactivity

To account for a step insertion of reactivity, we can write

$$\rho = \rho_o - \alpha \Delta T \tag{21}$$

where
α = negative of the temperature coefficient of reactivity
ρ_o = step insertion of reactivity

Taking the derivative with respect to time of the above equation and substituting the result from equation (18),

$$\frac{d\rho}{dt} = -\alpha Kn \tag{22}$$

Applying the chain rule to equation (20) yields

$$\frac{dn}{d\rho} = -\frac{(\rho - \beta)}{\alpha K \ell} \tag{23}$$

Integrating equation (23) and solving for the constant of integration gives us the result

$$n = \frac{1}{2\alpha K1} [(\rho_o - \beta)^2 - (\rho - \beta)^2] \quad (24)$$

The pulse is terminated when n becomes negligibly small. This occurs when

$$\rho = 2\beta - \rho_o \quad (25)$$

Equation (25) gives us the condition for the total energy release from the pulse, which manifests itself as a temperature rise in the fuel element when it is substituted into equation (21).

$$\Delta T_{core,ave} = \frac{2(\rho_o - \beta)}{\alpha} \quad (26)$$

Calculations by General Atomics show that a complete core of 12 w/o fuel would have a temperature coefficient of reactivity, α, that is 75% of the value for an 8.5 w/o fueled core.[1] The value for $\alpha_{8.5\ w/o}$ is taken to be -\$0.0118/°C. (This value was experimentally verified with a series of 23 pulses ranging from \$1.30 to \$2.00 that resulted in an average $\alpha_{8.5\ w/o}$ of -\$0.0128/°C--within 8.5% of the published value.) The effect of adding three 12 w/o FFCR's would, however, have a negligible effect on the overall temperature coefficient of reactivity for the entire core.[1]

Applying the Nordheim-Fuchs model for self-limiting power excursions, we can determine the maximum average increase in temperature for the entire core using equation (26). For a maximum allowed reactor pulse with a \$4.00 step insertion of reactivity, the maximum attained average temperature rise is calculated to be 333°C. Applying the power-peaking factors from the previous section, the maximum calculated temperature rise in an FFCR would be $1.48 \cdot \Delta T_{core,ave}$; the temperature rise for an FFCR for a \$4.00 pulse is calculated to be 493°C. Assuming an initial temperature of 25°C, the maximum temperature value would be 518°C. Note that even in the limiting case, neither the technical specification safety limit of 1000°C nor the limiting safety systems setting of 600°C is violated.

FFCR OPERATIONAL CHARACTERISTICS

FFCR's are a standard design offered as a stock item by General Atomics and have been used in several TRIGA reactors for over 20 years. FFCR's are currently implemented in approximately a dozen TRIGA reactors. There has been no reported evidence of fuel failure as a result of FFCR use in the United States. The operational issues to be resolved are the effects of burnup on the FFCR and the influence of FFCR's on the temperature coefficients of reactivity, shut-down margin, and rod worth.

FFCR control rod worth curves will be generated the same way that standard control rod worth curves are. Since the poison section of the FFCR will be the same as that of the currently installed standard control

rods, the worth of the poison section of the FFCR will be that of the currently installed control rods. Measurements made by AFRRI reactor staff of control rod worth of the currently installed standard control rods yielded a nominal rod worth of $1.90. The fuel follower is expected to add at least $0.70 of reactivity[6] when the control rod is fully withdrawn, so the total rod worth for an FFCR is estimated to be $2.60. The transient control rod and its follower have been measured and have a total nominal worth of $4.01. The shutdown margin, as established by ANS/ANSI 15.1, is computed as follows:

Total rod worth		$11.81
k_{excess} (maximum)	-	$ 5.00
		$ 6.81
Worth of TRANS rod	-	$ 4.01
Shutdown margin		$ 2.80

The shutdown margin with the most reactive control rod removed from the reactor is $2.80--well in excess of $0.50 minimum allowed value.

Once operational rod worth curves are established and power monitoring channels have been calibrated by the thermal power calibration method, power coefficient of reactivity curves will be generated. The issues regarding the measurement of shut-down margin and excess reactivity are addressed in Appendix B, Reactor Core Loading and Unloading.

Structural changes in the FFCR's will be monitored on an annual basis as part of the annual shutdown and maintenance. Specific effects to be monitored are the elongation and lateral bending of the fuel. FFCR fuel elements that have an elongation greater than 0.100 inch or a lateral bend greater than 0.0625 inch will be removed from service.

CONCLUSION

The analysis in this report shows that installing FFCR's in the AFRRI TRIGA reactor core will not result in an unsafe condition or violation of technical specifications. The primary parameter of interest, the maximum fuel temperature, was computed to be 210°C in the limiting case for steady-state operation and 518°C in the limiting case for pulse operation. Operational issues regarding maximum excess reactivity, shutdown margin, and burnup have also been addressed, and it has been determined that sufficient surveillance capabilities exist to prevent any unsafe or illegal condition.

REFERENCES

1. General Atomics, letter to M. Moore on fuel follower control rods, 28 October 1988.

2. El-Wakil, M. M., *Nuclear Heat Transport*, The American Nuclear Society, Lagrange Park, IL, 1978.

3. Defense Atomic Support Agency, *AFRRI/USAEC Facility License R-84, Complete with Applications and Amendments*, Bethesda, MD, 1962.

4. Wallace, W. P., and Simnad, M. T., *Metallurgy of TRIGA Fuel Elements*, GA-1949, General Atomics, San Diego, CA, 1961.

5. Hetrick, D. L., *Dynamics of Nuclear Reactors*, The University of Chicago Press, 1971.

6. DNA Contract DNA001-89-R-0030 to General Atomics for fuel follower control rod construction.

7. Jaluria, Y., *Natural Convection Heat and Mass Transfer*, Pergamon Press, 1980.

APPENDIX A: DETERMINATION OF FREE CONVECTIVE HEAT TRANSFER COEFFICIENT

Introduction

We can measure the bulk water temperature within the AFRRI TRIGA core to determine the average free convective heat transfer coefficient of the cooling water. This experiment involves inserting a temperature-measuring probe between the B- and C-ring fuel elements while the reactor is operating at a steady-state power level of 1.0 MW and measuring the water temperature at various axial positions. Once the bulk water temperature has been determined, Newton's law of cooling can be used to calculate the average free convective heat transfer coefficient.

Experimental Apparatus and Procedure

The equipment used in this experiment consists of two approximately 18-foot lengths of chromal-alumel thermocouple wires fused together at one end, encased in a 16-foot-long, 0.375-inch-diameter aluminum (Al) tube, and the thermocouple display readout on the AFRRI computerized reactor control console (Figure A-1).

The potential difference generated at the thermocouple junction as the water is heated by the reactor is amplified and displayed by the thermocouple circuitry in the AFRRI computerized reactor control console. The thermocouple is initially inserted into the core to correspond to position I. The thermocouple resides in each region for several minutes to allow it to attain thermal equilibrium. Once thermal equilibrium is attained, ten temperature readings are taken at 10-second intervals. After each temperature measurement, the thermocouple is withdrawn to the next position, and the temperature measuring procedure is repeated.

Figure A-2 shows that the temperature is measured in five axial positions: (I) 3 inches below midpoint (14 inches of thermocouple wire inserted into the core); (II) midpoint in axial dimension; (III) halfway between midpoint and bottom of graphite slug; (IV) at top of fuel region; (V) 1.5 inches above top of fuel region.

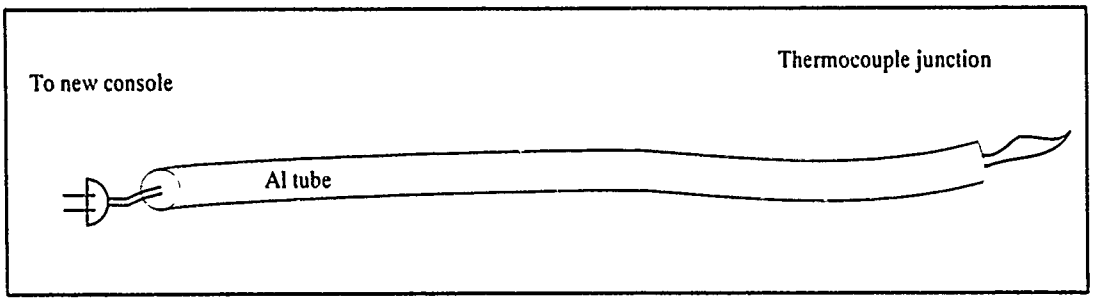

Figure A-1. Experimental apparatus.

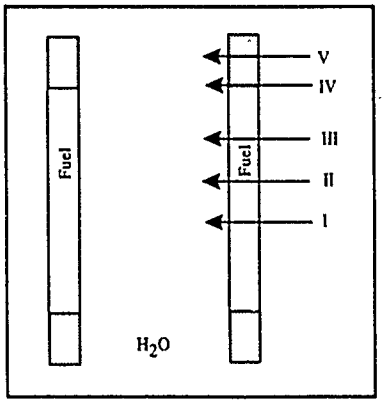

Figure A-2. Axial measuring points.

Safety Considerations

There are two safety considerations associated with this experiment: radiation streaming and an unintentional positive change in reactivity if the thermocouple wires are rapidly withdrawn from the reactor core while it is at power. Radiation streaming is avoided by flooding the aluminum tube with water and bending the tube so that it is at an angle not normal to the top of the core. The thermocouple wire displaces only 0.043 $inch^3$ of water when it is fully inserted in the core, so using the void coefficient of reactivity, the thermocouple wire represents a negative reactivity insertion of only 0.001 cents. If we were to estimate conservatively that the thermocouple wire had the same neutron-absorbing properties of a control rod, the maximum negative reactivity would be only 0.01 cents. Thus, there is no possibility of a reactivity accident associated with the apparatus used in this experiment.

Data

Table A-1 summarizes the data gathered during a 1.0 MW steady-state run of the AFRRI TRIGA reactor. The variation in the temperature measurements is most likely due to variance in the radial position of the temperature probe in the channel.

Table A-1. Bulk Water Temperature at Each Axial Position in the AFRRI TRIGA Reactor Core

Axial position	Inlet temp (°C)	Measured core bulk water temp (°C)
I	22	72.9
II	24	65.0
III	25	48.6
IV	26	51.6
V	27	59.7

Analysis and Conclusion

The purpose of this experiment is to determine the bulk water temperature within the core shroud; thus, it is the lowest measured value of the water temperature that is sought. Figure A-3 illustrates the temperature variation within a cooling channel.

Table A-1 shows that the measured value that most closely represents the bulk water temperature within the core shroud is 48.6°C.

The free convective heat transfer coefficient, h, is found by solving equation (8) for boundary conditions given by a standard TRIGA fuel element. Equation (A-1) gives the solution in terms of h.

$$h = \left(\frac{1}{r_o + c_o}\right)\left[\frac{(T_i - T_f) - \frac{q'''r_i^2}{4k_f}\left[\left(\frac{r_o}{r_i}\right)^2 - 2\ln\left(\frac{r_o}{r_i}\right) - 1\right]}{\frac{q'''r_i^2}{2}\left[\left(\frac{r_o}{r_i}\right)^2 - 1\right]} - \frac{1}{k_c}\ln\left(\frac{r_o + c_o}{r_o}\right)\right]^{-1} \quad \text{(A-1)}$$

where
T_i = measured fuel temperature at 1.0 MW
T_f = measured bulk coolant temperature in the core
r_o = fuel outer radius, 1.816 cm
r_i = fuel inner radius, 0.229 cm
c_o = cladding thickness, 0.051 cm
k_f = thermal conductivity of fuel, 0.18 W/cm-°C
k_c = thermal conductivity of clad, 0.138 W/cm-°C
q''' = volumetric heat rate.

The measured fuel temperature in the B-ring at 1.0 MW steady-state power level is 390°C, and the calculated volumetric heat rate is 65.9 W/cm^3. Using the measured value of the bulk coolant temperature of 48.6°C yields a value of 1.339 W/C°-cm^2 for the free convective heat transfer coefficient.

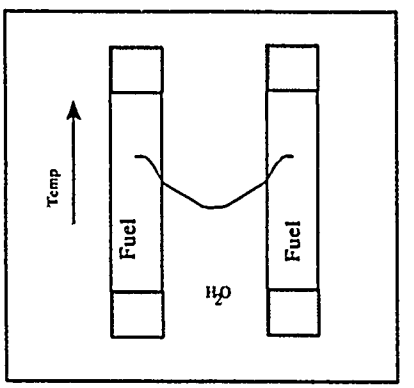

Figure A-3. Temperature variation within a cooling channel.

Newton's law of cooling expresses the linear relationship between the heat transfer rate, Q, and the temperature difference between the clad surface temperature, T_c, and the bulk water temperature, T_f, as

$$Q = hA(T_f - T_c)$$

where h is the overall convective heat transfer coefficient and A is the area of the fuel element.[7] The value of h determined for the AFRRI TRIGA is unique in that it takes into account the flow configuration, fluid properties, and the dimensions of the fuel elements. Assuming that the dependence of Q on the temperature difference $T_f - T_c$ is roughly linear, then the value of h, computed using data from B-ring elements with their higher heat transfer rate and local temperature difference, will be close to the value for h for D-ring positions.

APPENDIX B: REACTOR CORE LOADING AND UNLOADING

General

Loading and unloading of the reactor core shall be performed under the supervision of the Reactor Facility Director or the Reactor Operations Supervisor.

Specific

1. Setup

   a. Ensure that at least one nuclear instrumentation channel is operational.

   b. Ensure that the source is in the core.

   c. Ensure that an operator monitors the reactor console during all fuel movements.

   d. Check new FFCR's before insertion into the core; this includes cleaning, visual inspection, and length and bow measurements.

   e. Install all control rods.

   f. If irradiated fuel elements are to be removed unshielded from the pool, obtain a Special Work Permit (SWP) from the Safety and Health Department (SHD); do not remove fuel elements with a power history (greater than 1 KW) in the previous 2 weeks from the reactor pool.

2. Core Loading

   a. After each step of fuel movement perform the following:

      (1) Record detector readings.

      (2) Withdraw control rods 50%; record readings.

      (3) Withdraw control rods 100%; record readings.

      (4) Calculate 1/M.

      (5) Plot 1/M versus number of elements (and total mass of ^{235}U).

      (6) Predict critical loading.

      (7) Insert ALL rods; continue to next step.

   b. Load elements in the following order:

      (1) Load the B-ring and C-ring thermocouple elements.

(2) Connect thermocouple outputs to reactor control console display.

(3) Install any other thermocouple elements.

(4) Complete loading of B- and C-ring elements (total of 18 standard elements plus 3 FFCR's).

(5) Load D-ring (total of 33 standard elements plus 3 FFCR's).

(6) Load the following E-ring elements in order:

16, 17, 18, 20, 6, 8, 9, 10 (total of 41 standard elements plus 3 FFCR's).

(7) Complete the E-ring by loading the following elements in order:

15, 21, 11, 5, 14, 22, 4, 12, 13, 1 (total of 51 standard elements plus 3 FFCR's).

(8) Load the following F-ring elements in two elements per step until criticality is achieved, using the following loading order:

22, 23, 24, 21, 20, 25, 26, 27, 28, 29, 30, 1, 2, 3, 4, 5, 19, 18, 17, 16, 15, 14, 13, 6, 12, 7, 11, 8, 10, 9.

Once criticality has been achieved, perform control rod worth measurements at core position 500 by rod drop technique. Calculate shutdown margin (SDM):

SDM = total control rod worth - K_{excess} - TRANS rod worth

(9) Load core to \$2.00 excess reactivity by loading two elements per step using the loading order in instruction 8.

(10) Verify control rod worth using rod drop techniques; calculate SDM.

(11) Load the core to achieve a K_{excess} that will allow calibration of the TRANS rod based on the last available worth curve of the TRANS rod (approximately \$4.00). Calculate the reactivity value of each element as it is added.

(12) Calibrate all control rods.

(13) Calculate SDM.

(14) Estimate K_{excess} with a fully loaded core (must not exceed \$5.00).

(15) Load core to fully operational load using loading order in instruction 8, and recalibrate all control rods. Calculate SDM.

(16) Adjust the core loading pattern to meet operations requirements if necessary. Recalibrate all control rods. Calculate SDM.

3. Core Unloading

a. Unload the reactor core starting with the F-ring and ending with the B-ring.

b. Remove the fuel elements individually from the reactor core, identify them by serial number, and place them in the fuel storage racks or a shipping cask.

c. If elements are to be loaded into a shipping cask, clean the cask completely, and check for radiological contamination before placing the cask in or near the pool. Load cask in accordance with procedures specific to the cask.

d. Once the cask is loaded, perform an air sample and survey; check temperature and pressure inside cask, if necessary.

e. If elements are placed in temporary storage away from core monitoring, ensure that criticality monitoring in accordance with 10 CFR 70 is in place.

DISTRIBUTION LIST

DEPARTMENT OF DEFENSE

ARMED FORCES INSTITUTE OF PATHOLOGY
ATTN: RADIOLOGIC PATHOLOGY DEPARTMENT

ARMED FORCES RADIOBIOLOGY RESEARCH INSTITUTE
ATTN: PUBLICATIONS DIVISION

ARMY/AIR FORCE JOINT MEDICAL LIBRARY
ATTN: DASG-AAFJML

ASSISTANT TO SECRETARY OF DEFENSE
ATTN: AE
ATTN: HA(IA)

DEFENSE NUCLEAR AGENCY
ATTN: TITL
ATTN: DDIR

DEFENSE TECHNICAL INFORMATION CENTER
ATTN: DTIC-DDAC
ATTN: DTIC-FDAC

FIELD COMMAND DEFENSE NUCLEAR AGENCY
ATTN: FCFS

INTERSERVICE NUCLEAR WEAPONS SCHOOL
ATTN: RH

LAWRENCE LIVERMORE NATIONAL LABORATORY
ATTN: LIBRARY

UNDER SECRETARY OF DEFENSE (ACQUISITION)
ATTN: OUSD(A)/R&AT

DEPARTMENT OF THE ARMY

HARRY DIAMOND LABORATORIES
ATTN: SLCHD-NW
ATTN: SLCSM-SE

LETTERMAN ARMY INSTITUTE OF RESEARCH
ATTN: SGRD-UL-B1-R

SURGEON GENERAL OF THE ARMY
ATTN: MEDDH-N

U.S. ARMY AEROMEDICAL RESEARCH LABORATORY
ATTN: SCIENTIFIC INFORMATION CENTER

U.S. ARMY ACADEMY OF HEALTH SCIENCES
ATTN: HSHA-CDF

U.S. ARMY CHEMICAL RESEARCH, DEVELOPMENT, AND ENGINEERING CENTER
ATTN: DIRECTOR OF RESEARCH

U.S. ARMY INSTITUTE OF SURGICAL RESEARCH
ATTN: DIRECTOR OF RESEARCH

U.S. ARMY MEDICAL RESEARCH INSTITUTE OF CHEMICAL DEFENSE
ATTN: SGRD-UV-R

U.S. ARMY NUCLEAR AND CHEMICAL AGENCY
ATTN: MONA-NU

U.S. ARMY RESEARCH INSTITUTE OF ENVIRONMENTAL MEDICINE
ATTN: DIRECTOR OF RESEARCH

U.S. ARMY RESEARCH OFFICE
ATTN: BIOLOGICAL SCIENCES PROGRAM

WALTER REED ARMY INSTITUTE OF RESEARCH
ATTN: DIVISION OF EXPERIMENTAL THERAPEUTICS

DEPARTMENT OF THE NAVY

NAVAL AEROSPACE MEDICAL RESEARCH LABORATORY
ATTN: COMMANDING OFFICER

NAVAL MEDICAL COMMAND
ATTN: MEDCOM-21

NAVAL MEDICAL RESEARCH AND DEVELOPMENT COMMAND
ATTN: CODE 40C

OFFICE OF NAVAL RESEARCH
ATTN: BIOLOGICAL SCIENCES DIVISION

DEPARTMENT OF THE AIR FORCE

BOLLING AIR FORCE BASE
ATTN: AFOSR

BROOKS AIR FORCE BASE
ATTN: USAFOEHL/RZ
ATTN: USAFSAM/RZ
ATTN: USAFSAM/RZB

NUCLEAR CRITERIA GROUP, SECRETARIAT
ATTN: WL/NTN

SURGEON GENERAL OF THE AIR FORCE
ATTN: HQ USAF/SGPT
ATTN: HQ USAF/SGES

U.S. AIR FORCE ACADEMY
ATTN: HQ USAFA/DFBL

OTHER FEDERAL GOVERNMENT

BROOKHAVEN NATIONAL LABORATORY
ATTN: RESEARCH LIBRARY, REPORTS SECTION

CENTER FOR DEVICES AND RADIOLOGICAL HEALTH
ATTN: HFZ-110

DEPARTMENT OF ENERGY
ATTN: ER-72 GTN

GOVERNMENT PRINTING OFFICE
ATTN: DEPOSITORY RECEIVING SECTION
ATTN: CONSIGNED BRANCH

LIBRARY OF CONGRESS
ATTN: UNIT X

LOS ALAMOS NATIONAL LABORATORY
ATTN: REPORT LIBRARY/P364

NATIONAL AERONAUTICS AND SPACE ADMINISTRATION
ATTN: RADLAB

NATIONAL AERONAUTICS AND SPACE ADMINISTRATION,
GODDARD SPACE FLIGHT CENTER
ATTN: LIBRARY

NATIONAL CANCER INSTITUTE
ATTN: RADIATION RESEARCH PROGRAM

NATIONAL LIBRARY OF MEDICINE
ATTN: OPI

U.S. ATOMIC ENERGY COMMISSION
ATTN: BETHESDA TECHNICAL LIBRARY

U.S. FOOD AND DRUG ADMINISTRATION
ATTN: WINCHESTER ENGINEERING AND
ANALYTICAL CENTER

U.S. NUCLEAR REGULATORY COMMISSION
ATTN: LIBRARY

RESEARCH AND OTHER ORGANIZATIONS

BRITISH LIBRARY (SERIAL ACQUISITIONS)
ATTN: DOCUMENT SUPPLY CENTRE

CENTRE DE RECHERCHES DU SERVICE DE SANTE DES
ARMEES
ATTN: DIRECTOR

INHALATION TOXICOLOGY RESEARCH INSTITUTE
ATTN: LIBRARY

INSTITUT FUR RADIOBIOLOGIE
ACADEMIE DES SANITATS UND GESUNHEITSWESESNS DER
BW (WEST GERMANY)
ATTN: DIRECTOR

KAMAN TEMPO
ATTN: DASIAC

NBC DEFENSE RESEARCH AND DEVELOPMENT CENTER OF
THE FEDERAL ARMED FORCES (WEST GERMANY)
ATTN: WWDBW ABC-SCHUTZ

NCTR-ASSOCIATED UNIVERSITIES
ATTN: EXECUTIVE DIRECTOR

RUTGERS UNIVERSITY
ATTN: LIBRARY OF SCIENCE AND MEDICINE

UNIVERSITY OF CALIFORNIA
ATTN: LABORATORY FOR ENERGY-RELATED
HEALTH RESEARCH
ATTN: LAWRENCE BERKELEY LABORATORY

UNIVERSITY OF CINCINNATI
ATTN: UNIVERSITY HOSPITAL, RADIOISOTOPE
LABORATORY